Abstract

Integrated control and process design (ICPD) was implemented for circulating fluidized bed power plants (CFB) in this thesis to obtain fast electrical power load changes. The need to reduce global emissions has resulted in new design requirements for CFB boilers: Combustion power plants are needed for fast load changes due to renewable power variations, and process modifications like oxy-combustion have to be implemented for CFB boilers. This thesis addressed the new requirements by integrating control design with process design for CFB boilers, which was done now for the first time.

The work defined an ICPD procedure for closed-loop CFB processes that focuses on load change performance. This was done by reviewing and classifying ICPD literature to select suitable design and analysis methods. The new ICPD procedure consisted of process analysis based on dynamic simulation and state estimation, control structure selection based on relative gain methods, and simultaneous dynamic optimization of process and controller parameters.

The design stages were validated through industrial case studies. In the process analysis stage, CFB combustion and flue gas dynamics were studied to define how the boiler should be modified for oxy-combustion. In the control design stage, the relative gain methods were used to identify feasible control structures and performance-limiting interactions in a once-through CFB boiler. In the ICPD optimization stage, the CFB steam path mass storage parameters and controllers were optimized for simulated load change ramps. The goal was to achieve tight output electrical power control and satisfy selected secondary control objectives.

The results show how faster load changes and a better flexibility for process modifications are obtained through ICPD compared to sequential process and control design. The design guidelines presented in this thesis thus enable more sustainable power generation in the grid.

Keywords: integrated control and process design, process control, process optimization, relative gain array, state estimation, circulating fluidized bed boiler, oxy-combustion

Hultgren, Matias, Säätösuunnittelu CFB-kattiloille yhdistettynä prosessisuunnitteluun.
Oulun yliopiston tutkijakoulu; Oulun yliopisto, Teknillinen tiedekunta, Systeemitekniikka.

Tiivistelmä

Tässä väitöstutkimuksessa sovellettiin integroitua säätö- ja prosessisuunnittelua (ICPD) kiertoleijupetivoimalaitoksiin (CFB) nopeiden sähkön kuormanmuutosten saavuttamiseksi. Globaalien päästöjen vähentämisen tarve on asettanut uusia suunnitteluvaatimuksia CFB-kattiloille: Uusiutuvan energiantuotannon vaihteluiden vuoksi polttovoimalaitoksia tarvitaan nopeita kuormanmuutoksia varten ja happipolton kaltaisia prosessimuunnoksia on sovellettava CFB-kattiloille. Uusista vaatimuksista johtuviin haasteisiin väitöstutkimus vastasi integroimalla säätö- ja prosessisuunnittelua CFB-kattiloille. Näin tehtiin nyt ensimmäistä kertaa.

Työssä määritettiin suljetun piirin CFB-prosesseille kuormanmuutosten suorituskykyä painottava ICPD-suunnittelumalli. Tämä suoritettiin tarkastelemalla ja luokittelemalla ICPD-kirjallisuutta sopivien suunnittelu- ja analyysimenetelmien valitsemiseksi. ICPD-suunnittelumalli koostui dynaamiseen simulointiin ja tilaestimointiin perustuvasta prosessianalyysista, suhteellisen vahvistuksen menetelmiin ("relative gain") perustuvasta säätörakenteen valinnasta sekä prosessin ja säädinten parametrien yhtäaikaisesta dynaamisesta optimoinnista.

Suunnitteluvaiheet validoitiin teollisten tutkimusesimerkkien kautta. CFB:n poltto- ja savukaasundynamiikkaa tutkittiin prosessianalyysivaiheessa, tarkoituksena määrittää, kuinka kattilaa tulisi muuntaa happipolttoa varten. Säätörakenteen valintavaiheessa suhteellisen vahvistuksen menetelmiä käytettiin läpivirtaus-CFB-kattilalle soveltuvien säätörakenteiden ja suorituskykyä rajoittavien vuorovaikutusten määrittämiseen. CFB:n höyrypuolen massavarantoparametrit ja säätimet optimoitiin simuloiduille kuormarampeille ICPD-optimointivaiheessa. Tavoitteena oli saavuttaa tarkka tuotettavan sähkön säätö sekä valitut toissijaiset säätötavoitteet.

Tulokset osoittavat, miten ICPD:n kautta saavutetaan nopeampia kuormanmuutoksia ja parempi joustavuus prosessimuutosten osalta vaiheittaiseen prosessi- ja säätösuunnitteluun verrattuna. Työssä esitetyt CFB-kattiloiden suunnittelukäytännöt mahdollistavat täten ympäristöystävällisemmän voimantuotannon verkossa.

Asiasanat: integroitu prosessi- ja säätösuunnittelu, prosessin säätö, prosessin optimointi, relative gain array, tilaestimointi, kiertoleijupetikattila, happipoltto

Et veritas liberabit vos

Acknowledgements

I would like to express my gratitude to my supervisors, Professor Enso Ikonen and Docent Jenő Kovács, for their guidance throughout my doctoral studies. Thank you for the doctoral work opportunity and for introducing me to the exciting world of power plant control. My warm thanks go to Professor Sigurd Skogestad and Associate Professor Pál Szentannai for their efforts and valuable comments during the pre-examination of my thesis. I also wish to thank my follow-up group for doctoral training: Professor Juha Tanskanen and Dr. István Selek from the University of Oulu, and Dr. Jouni Ritvanen from LUT University.

From the Systems Engineering group, I wish to acknowledge all the colleagues that I had the pleasure to work with during my doctoral training. These include Jukka Hiltunen, Lic. Tech., for the numerous inspiring discussions and helpful assistance, Dr. Laura Niva for the scientific-academic collaboration and peer support, as well as Dr. Seppo Honkanen, Antti Yli-Korpela, M.Sc., and Harri Aaltonen, Lic. Tech., for shared ideas, projects, and discussions. In general, I wish to acknowledge the numerous colleagues and friends that I have made over the years from the other research groups of Process and Environmental Engineering at the University of Oulu, as well as the national GSCE community.

From industry, I would like to thank Sumitomo SHI FW in Varkaus for providing me with the resources and expertise to study the most cutting-edge developments in fluidized bed power generation. In addition to my supervisor, Principal Research Engineer Jenő Kovács, I would like to express my sincere gratitude to Dr. Edgardo Coda Zabetta, Ari Kettunen, and Mikko Salo for their support. For my participation in the oxy-fired pilot boiler experimental testing at the VTT Technical Research Centre of Finland in Jyväskylä in 2011, special thanks

List of abbreviations and symbols

Abbreviations

ASU   air separation unit
CCS   carbon capture and storage
CCU   carbon compression unit
CDOF   control degrees of freedom
CFB   circulating fluidized bed
CHP   combined heat and power plant
CLDG   closed-loop disturbance gain
CPU   carbon purification unit
CV   controlled variable
DOF   degrees of freedom
DRGA   dynamic relative gain array
DSH   desuperheater water spray
ECO   economizer preheater
EVAP   evaporator
FG   flue gas
FW   feedwater
G   generator
HE   heat exchanger
HP   high-pressure turbine section
ICI   integral controllability with integrity
ICI PRG   ICI analysis with the PRG for all partially controlled subsystems
ICPD   integrated control and process design
ISE   integral square error
kW_{th} kilowatts, thermal
LP   low-pressure turbine section
LTI   linear time-invariant
MIDO   mixed-integer dynamic optimization
MIMO   multiple-input-multiple-output
MILP   mixed-integer linear programming
MINLP   mixed-integer nonlinear programming
MPC   model predictive control
MV   manipulated variable

MW_e	megawatts, electrical
MW_{th}	megawatts, thermal
NI	Niederlinski index
norm.	normalized
NO_X	nitrogen oxides, generic expression
OTU	once-through steam path
OTU-CFB	once-through circulating fluidized bed boiler
oxy-CFB	oxy-fired circulating fluidized bed boiler
PID	proportional-integral-derivative controller
PRG	partial relative gain
PRG_{mn}	PRG matrix for partially controlled subsystem, loops m–n closed
PRGA	performance relative gain array
PSE	process systems engineering
prim.	primary
RFG	recirculated flue gas
RGA	relative gain array
RH	reheater heat exchanger
RHvalve	reheater bypass valve
sec.	secondary
SH	superheater heat exchanger
SO_X	sulfur oxides, generic expression
SP	setpoint
TPM	throughput manipulator
tot.	total
T.valve	turbine valve
UKF	unscented Kalman filter
vol%	volume percentage

Latin symbols

a_{yu}	real term of the DRGA element between output y and input u ($a_{\lambda yu}$ in Publication IV)
A	process state matrix in the state-space model state equation
b_{yu}	complex term of the DRGA element between output y and input u ($b_{\lambda yu}$ in Publication IV)
B	thermodynamic irreversibility rate [W]
B	process input matrix in the state-space model state equation

13

$c(s)$	controller transfer function
c_{ss}	state noise vector (v in Publication II)
C	covariance (P in Publication II)
$\mathbf{C}$	process state matrix in the state-space model measurement equation
d	process disturbance variable
d_{ss}	measurement noise vector (w in Publication II)
D_i	PID controller derivative gain for controlled variable i
$\mathbf{D}$	process input matrix in the state-space model measurement equation
E	output electrical power [MW]
f_{des}	process and control performance equations
f_{proc}	process, control, and measurement physical equations; "0" subscript denotes initial conditions
f_{ss}	state equation in the state-space model (f in Publication II)
g_{yu}	static gain between process output y and input u
$\mathbf{G}$	process static gain matrix between CV and MV variables
$\hat{\mathbf{G}}$	diagonal $\mathbf{G}$ that only contains control connection MV–CV gains
$\bar{\mathbf{G}}_{mn}$	gain matrix for partially controlled subsystem of $\mathbf{G}$, loops m–n closed
$\mathbf{G}(s)$	process transfer function matrix between CV and MV variables
$\hat{\mathbf{G}}(s)$	diagonal scaled $\mathbf{G}(s)$ that only contains control connection MV–CV transfer functions
$\bar{\mathbf{G}}(s)$	scaled $\mathbf{G}(s)$ matrix
$\mathbf{G}_d(s)$	disturbance transfer function matrix between CVs and disturbances
$\hat{\mathbf{G}}_d(s)$	process CLDG matrix
$\bar{\mathbf{G}}_d(s)$	scaled $\mathbf{G}_d(s)$ matrix
h_w	specific enthalpy of a stream [J/kg]
$h_{yu}(s)$	transfer function between process output y and input u
$\mathbf{H}(j\omega)$	frequency response matrix of $\mathbf{G}(s)$ at frequencies ω
I_i	PID controller integral gain for controlled variable i
$\mathbf{I}$	identity matrix
J	ICPD optimization objective function
j_i	individual ICPD design objective i
j_{ni}	value of objective i with nominal process/control parameters
k	sampling instance
K	UKF Kalman gain
L	firing power [kg/s]
m	amount of matrix rows

14

n	amount of matrix columns
n_i	amount of variable, stream, or component i (N_i in Publication IV)
N_i	PID controller derivative filter for controlled variable i
$nDRGA$	dynamic relative gain number
$nRGA$	relative gain number
p	pressure [bar]
P_i	PID controller proportional gain for controlled variable i
$p(i|j)$	probability density function for event i, given j
Q	heat transfer rate [W]
q_E	parameter for evaporator storage percentage of total storage [%]
q_{S1}	parameter for SH storage percentage before DSH cooling [%]
s	Laplace s-plane operator [rad/s]
s_w	specific entropy of a stream [J/(kg·K)]
T	temperature [°C]
T_K	temperature [K]
t	time, "0" subscript denotes initial time [s]
t_I	thermal inertia delay [s]
u	process input variable or input variable vector
U	vector of controller design parameters
u_c	closed-loop input variable in partial control
u_{ci}	input variable that is used to control output variable i
u_o	open-loop input variable in partial control
$\tilde{u}_i$	scaled process input variable i (u_i in Publication V)
v	turbine valve position
$\bar{v}$	nominal turbine valve position
v_{max}	maximum bound of the turbine valve signal
v_{min}	minimum bound of the turbine valve signal
w	mass flow (m in Publications III, V) [kg/s]
w_{des}	process and control performance inequality constraints
w_{proc}	process and control physical inequality constraints
w_{ss}	measurement equation in the state-space model (h in Publication II)
W	output work [W]
x	process state variable or state variable vector
$\bar{x}$	process state vector mean
$x(t; x_0)$	differential equation system solution with initial condition x_0
X	vector of process design parameters
y	process output variable or output variable vector

$\bar{y}$	process output vector mean
y_c	closed-loop output variable in partial control
y_o	open-loop output variable in partial control
$\tilde{y}_i$	scaled process output variable i (y_i in Publication V)
$\mathbf{Y}_k$	matrix with measurements up to instance k ($\tilde{Y}_k$ in Publication II)
z_i	reference signal for controlled variable i (i_{SP} in Publication V)

Greek and Cyrillic symbols

α	scaling parameter in the scaled unscented transform
$\mathbf{\Gamma}(s)$	process PRGA matrix
δ	process inequality constraints in CFB steam path ICPD (n in Publication V)
ε	flow exergy [W]
$\varepsilon_{ch,w}$	specific chemical exergy of a stream [J/kg]
η_{ex}	exergy efficiency [%]
η_{th}	energy efficiency [%]
Θ	simulated time range upper limit (T in Publication V) [s]
κ	scaling parameter in the scaled unscented transform
λ	parameter equation in the scaled unscented transform
λ_{yu}	relative gain between output y and input u
μ	measurement equations in CFB steam path ICPD
ξ	process open-loop equations in CFB steam path ICPD (m in Publication V), "0" subscript denotes initial conditions
σ	controllability equations in CFB steam path ICPD
τ_{TOT}	total steam path storage coefficient [m·s^2]
Υ	UKF transformed measurement ($\mathbf{Y}$ in Publication II)
υ	solution distance in Lyapunov stability definition
φ	controller equations in CFB steam path ICPD
ψ	initial condition distance in Lyapunov stability definition
Ω	analyzed frequency range upper limit [rad/s] (F in Publication V)
ω	radial frequency [rad/s]
Ҳ	UKF sigma point ($\mathbf{X}$ in Publication II)

Original publications

This thesis is based on the following publications, which are referred throughout the text by their Roman numerals:

I   Hultgren, M., Ikonen, E., & Kovács, J. (2014). Oxidant control and air-oxy switching concepts for CFB furnace operation. *Computers & Chemical Engineering, 61*, 203–219. https://doi.org/10.1016/j.compchemeng.2013.10.018

II Hultgren, M., Ikonen, E., & Kovács, J. (2014). Circulating fluidized bed boiler state estimation with an unscented Kalman filter tool. In *2014 IEEE Conference on Control Applications (CCA)* (pp. 310–315). Antibes: Institute of Electrical and Electronics Engineers (IEEE). https://doi.org/10.1109/CCA.2014.6981364

III Hultgren, M., Ikonen, E., & Kovács, J. (2017). Integrated control and process design in CFB boiler design and control – Application possibilities. In D. Dochain, D. Henrion, & D. Peaucelle (Eds.), *20th IFAC World Congress, IFAC-PapersOnLine 50*(1) (pp. 1997–2004). https://doi.org/10.1016/j.ifacol.2017.08.180

IV Hultgren, M., Ikonen, E., & Kovács, J. (2017). Once-through circulating fluidized bed boiler control design with the dynamic relative gain array and partial relative gain. *Industrial & Engineering Chemistry Research, 56*(48), 14290–14303. https://doi.org/10.1021/acs.iecr.7b03259

V   Hultgren, M., Ikonen, E., & Kovács, J. (2019). Integrated control and process design for improved load changes in fluidized bed boiler steam path. *Chemical Engineering Science, 199*, 164–178. https://doi.org/10.1016/j.ces.2019.01.025

All of the publications listed above were written by the author of the thesis. The main responsibilities of the author were research design, modeling for control design, implementation of design and control tools, conduction of simulations, data analysis, and reporting of the results. Experimental data and industrial power plant simulators were obtained from the industrial research partners of this work, and the author participated in experimental testing related to Publications I and II.

Other related publications by the author:

Hultgren, M., Kovács, J., & Ikonen, E. (2015). Combustion control in oxy-fired circulating fluidized bed combustion. In D. Bankiewicz, M. Mäkinen, & P. Yrjas (Eds.), *Proceedings of the 22nd International Conference on Fluidized Bed Conversion: Vol. 2* (pp. 1195–1205). Turku: Åbo Akademi.

Contents

1   Introduction

The thesis investigates the integration of control and process design in circulating fluidized bed (CFB) boilers. In integrated control and process design (ICPD), the process and its control system are designed simultaneously to obtain improved dynamics and control performance. ICPD thus differs from conventional sequential design, where the process is synthesized first based on steady-state specifications, and the control design is performed for the resulting flowsheet to satisfy dynamic performance and stability criteria. The thesis claims that ICPD tools based on first-principles simulation, relative gain analysis, and closed-loop process optimization provide a means for enhanced load change performance in a CFB power plant.

Systematic ICPD design has rarely been applied in scientific literature to large-scale conventional power plants. Dynamic optimization of process and controller parameters has been discussed in a series of works on a residential-scale combined heat and power (CHP) system (Burnak, Diangelakis, Katz, & Pistikopoulos, 2019a; Diangelakis, Burnak, & Pistikopoulos, 2017; Diangelakis & Pistikopoulos, 2017a, 2017b; Pistikopoulos & Diangelakis, 2016; Pistikopoulos et al., 2015), where the latest papers also encompassed operational scheduling. Cao, Fuentes-Cortes, Chen, and Zavala (2017) applied multi-objective stochastic programming for minimizing the cost, emissions, and water consumption of a residential-scale CHP system. Teichgraeber, Brodrick, and Brandt (2017) optimized process parameters together with time-variant setpoints for an oxy-fired combined cycle, but with no explicit closed-loop ICPD considerations. Chen and Bollas (2017) applied simultaneous optimization to a combined cycle power plant and Capra and Martelli (2015) to an organic Rankine cycle plant. Powell, Hedengren, and Edgar (2014) investigated the operational flexibility of a hybrid solar-fossil fuel power plant through dynamic optimization. Interestingly, ICPD design has been employed more frequently for improving the load flexibility of the post-combustion capture process for carbon capture and storage (CCS), which is used to separate CO_2 from boiler flue gases (e.g., Sharifzadeh, Bumb, & Shah, 2016; Sharifzadeh & Shah, 2019).

ICPD design has been applied to the fluidized bed boiler for the first time in this thesis and its related publications. ICPD has also never been considered as a solution for improving the performance of industrial load-following boilers prior to the thesis, as this problem has previously only been addressed in a sequential manner through improved control design or new boiler operational modes (Kovács, Kettunen, Ikonen, Hultgren, & Niva, 2015; Zhao et al., 2018a; Zhao, Wang, Liu, Chong, & Yan, 2018b). Improving load changes in combustion power plants is an

essential prerequisite for quickly building a more sustainable energy market with a high percentage of renewables, as flexible generation is a more promising short- to medium-term option for this purpose than demand response or energy storage technologies (Gonzalez-Salazar, Kirsten, & Prchlik, 2018). At the same time, boiler design continuously needs to contribute to the lowering of emissions and increased profitability. These challenges make this thesis a significant contribution to the power generation field and a platform for continued fluidized bed boiler research.

1.1 Research context

Combustion power plants are facing significant challenges in modern power generation, where reducing greenhouse gas emissions has become a priority. Most importantly, boilers are required to perform fast, frequent, and large transitions between load levels (International Energy Agency [IEA], 2011; Kovács et al., 2015). As the portion of renewable energy sources with output power variations increases in the grid (e.g., wind and solar), conventional power plants increasingly need to adjust their own power output to maintain the network balance. The resulting load ramp size and speed requirements can be very challenging for a large industrial power plant (e.g., a 60% to 100% load ramp with a 5%/min speed), which greatly increases the importance of dynamics and control in boiler design.

The new focus on load transitions has had a significant effect on boiler design goals and constraints. Solid fuel power plants were previously mainly operated at full load with the focus on maximum efficiency. Control design centered on fast disturbance rejection, and processes were designed to decrease the effects of disturbances on the power output. In load transition-oriented operation, setpoint tracking is emphasized instead, as the boiler should be able to follow the output electrical power (MW_e) demand trajectory accurately. Boilers are also required to operate at partial loads for long time periods and recover from load changes quickly. Process solutions that contribute to increased MW_e control reserves are essentially favorable for both operational modes, but units with a large thermal storage can also reduce the ability of the process to move rapidly between operating points in load-following mode. Control reserves also typically result in increased capital costs for the power plant due to increased equipment size.

In addition to the load change performance, adequate power generation efficiency should also preferably be maintained in load-following boilers to maximize profits. As higher efficiencies are typically achieved through extreme operating conditions, disturbances caused by large load changes require tight state

variable control due to material safety constraints. Moreover, higher efficiencies have been achieved through large greenfield CFB boiler sizes and interconnected flowsheets, which has resulted in novel and challenging process dynamics.

The second major effect of sustainable power generation on combustion power plants is that the plants themselves should contribute to the lowering of emissions, with the main emission components being CO_2, especially for fossil fuels, as well as SO_X and NO_X. This emphasizes active combustion control, which is complicated further by the current focus on biofuels and waste combustion, mainly because of fuel quality variations and high fuel moisture content. Emission reduction technologies may require extensive changes to the boiler flowsheet and its control system. One prominent example is the oxy-combustion configuration for CCS, where fuel is combusted with a mixture of pure oxygen and recirculated flue gas instead of air in order to concentrate and capture CO_2 emissions.

The new sustainability requirements for solid fuel boilers call for advanced control methods and a plant-wide focus for control design. However, as the open-loop dynamics are fully determined by the process design, the consequent control design has limited possibilities for improving the overall dynamic performance. Clearly, the decision-making domains of process and control design overlap, yet they are usually treated as separate steps. By combining the process and control design stages through ICPD, dynamic aspects and control requirements can affect the process flowsheet design, and process specific dynamics can become more effectively incorporated into the control solution (Fig. 1). This has the potential to improve closed-loop responses, and design decisions with a negative influence on control performance can be avoided. This is the motivation for introducing an integrated design approach for combustion power plants, as described in this thesis.
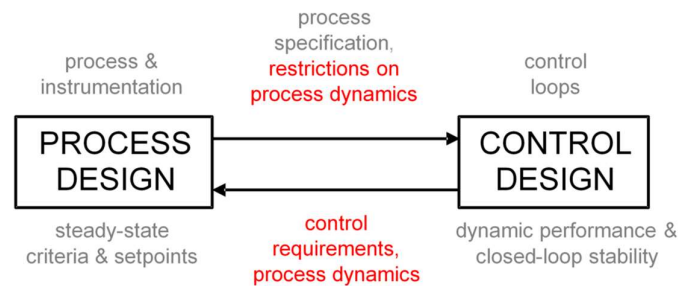
Fig. 1. The ICPD design principle. The red markings illustrate the interaction between the design stages (Publication III, reprinted with permission from IFAC).

24

Improving CFB load changes through ICPD allows an increased use of renewable energy, while maintaining network balance. An improved disturbance rejection in boiler state variables enables the use of more extreme operating conditions through control squeeze and shift, leading to increased efficiency and reduced emissions. Lastly, a flexible design approach facilitates the adaptation of existing closed-loop CFB designs to new technologies that offer the potential for emission reduction or improved efficiency, such as oxy-combustion or large supercritical boiler units.

The choice of the CFB as the target boiler for ICPD research was motivated by the current state of solid fuel power generation. CFB technology contributes to reduced SO_X and NO_X emissions and enables the effective combustion of difficult fuels; however, it is also a complex process with turbulent flow conditions, solid material recycle dynamics, and tight furnace temperature constraints. For the water-steam cycle, the thesis focuses on once-through (OTU) boiler control. The OTU setup enables high efficiencies, but is also challenging to control. Together, these aspects create a challenging load-following boiler design problem that would benefit from process and control design integration. Moreover, while the CFB and OTU technologies are well-known separately, the first full-scale supercritical OTU-CFB was only constructed in 2009 (Kovács, Kettunen, & Ojala, 2012).

1.2 Objectives and contributions

ICPD was applied to the industrial-scale CFB boiler process in the work described in this thesis. The main objective was to obtain closed-loop CFB designs with improved load change performance. The secondary objective was to form guidelines for modifying existing CFB designs for process configurations that aim at reduced emissions. Therefore, the goal was ultimately to enable a more sustainable electrical power generation in a grid of both conventional and renewable power plants.

Both objectives were addressed successfully in the thesis and its publications. Faster and more accurate load changes were obtained through an ICPD approach compared to sequential design, and the air-fired CFB boiler was successfully modified for oxy mode. The results showed for the first time that CFB power plant design practices can be improved by forming a link between process and control design. Overall, the contributions of the thesis can be summarized as follows:

1. Control-oriented process analysis based on dynamic simulation was applied to the CFB combustion side. The approach resulted in a detailed comparison of

air- and oxy-combustion for the CFB, as well as the novel application of advanced state estimation for CFB model analysis (Publications I and II).

2. A novel characterization of the ICPD research field was formed through an extensive literature review. ICPD design implementation was evaluated for the CFB boiler problem for the first time (Publication III).

3. A relative gain procedure was defined for CFB control design, combining multiple relative gain methods and stepwise variable analysis. It was used to define a zero-level control structure for the OTU-CFB boiler, which is the first extensive plant-wide relative gain application for the CFB boiler (Publication IV).

4. A novel hierarchical ICPD design procedure was formed from established process and control design methods (Publications III, IV, and V).

5. Integrated control and process design was applied to the fluidized bed boiler for the first time through the defined ICPD approach (Publication V).

6. The work showed that improved overall load changes can be obtained for the CFB boiler through ICPD (Publication V).

7. The work established design guidelines for improved load-following performance and effective operation in CFB boilers (Publications I and V).

Publication I showed how control design aspects can be included in CFB process design through first-principles parameter analysis and dynamic simulation. The work resulted in guidelines for modifying the CFB hotloop (furnace, gas-solid separator, solids return leg) for oxy-combustion, including schemes for performing transitions between air and oxy mode. The design integration was promoted for the oxy-CFB by connecting the chemical, physical, operational, and structural properties of the boiler to its control performance, verified through simulations with an industrial hotloop simulator. Publication I differed from much of the prior oxy-CFB process design research through this control-oriented focus. The control design outcomes were further tested through closed-loop simulations by Hultgren, Kovács, and Ikonen (2015).

Publication II demonstrated how unscented Kalman filter (UKF) estimation can be used in ICPD as an offline model analysis tool. This application area differs from the conventional role of state estimation in monitoring and filtering. This publication extended the research described in Publication I by applying a UKF tool to the oxy-CFB hotloop simulator. The tool was used for obtaining accurate estimates of time-variant process states, inputs, and parameters based on experimental data. The UKF was successfully validated as a suitable tool for CFB

26

process timeseries analysis. This outcome is important, as the performance of the UKF compared to linearized methods is known to be application specific (Daum, 2005). The estimated states can be used to improve process model accuracy and to enable more informed process design decisions.

Publication III formulated a novel characterization of the ICPD research field, where the focus was on reoccurring properties of ICPD methodologies that can be used to select suitable design methods for new process applications. An extensive ICPD literature review was conducted for this purpose, and ICPD was reviewed for power plants for the first time. Two ICPD design examples were also presented for a simple CFB steam path model, constituting the first CFB boiler ICPD case studies. The first example illustrated the effect of steam storage parameters on the dynamic relative gain array (DRGA) and how DRGA changes were reflected in the electrical power control. In the second example, the superheater mass storage was optimized together with the main steam pressure controller for simulated load ramps.

In Publication IV, an extensive controllability and interaction analysis procedure was formulated for the CFB boiler, based on the steady-state partial relative gain (PRG) and the DRGA. While these methods are established in the literature, their combination into a detailed procedure that examines control loop sets of increasing complexity is a novel contribution. The procedure was applied to an industrial OTU-CFB simulator, resulting in a zero-level control structure that supports fast load changes. This work was supported by Hultgren et al. (2015), who used the PRG for the oxy-CFB hotloop. Publication IV also validated the feasibility of using relative gain methods as controllability measures, as the defined procedure was able to highlight the main performance-limiting variable interactions in the OTU-CFB. Control interactions had not been analyzed for the CFB power plant to this extent in earlier literature.

The work carried out in Publications III and IV was expanded in Publication V by defining a novel ICPD procedure for the CFB boiler, with a focus on fast load changes. This was also the first systematic application of ICPD design to a CFB power plant. The publication forms the basis for the ICPD approach of this thesis, by combining closed-loop dynamic process/controller parameter optimization with control structure analysis based on the performance relative gain array (PRGA), and closed-loop disturbance gain (CLDG). Publication V showed how using the procedure for an industrial CFB steam path resulted in improved load changes compared to sequential process design and controller tuning. It was also stated in this publication that CFB load change performance can be quantified in terms of

electrical power tracking, steam pressure control, disturbance rejection capacity, first-principles efficiency, and controllability based on the PRGA and the CLDG.

The research publications and their contributions to the overall research aim are summarized in Table 1. The thesis outline is structured as follows. Chapter 2 describes the CFB power plant and its main control tasks. Chapter 3 presents the ICPD review, and performance evaluation is discussed separately in Chapter 4. Chapter 5 describes the analysis and design methods that are used in the ICPD procedure, and the chapter also summarizes the industrial CFB boiler case studies that were used in Publications I–V to validate the individual methods. Chapter 6 discusses the design results of the case studies and their significance for CFB boiler ICPD development. Finally, Chapter 7 presents the conclusions of the thesis.

Table 1. Introduction of the research papers and their contribution to the research aim.

Original publication	Contribution
Publication I	
Oxidant control and air-oxy switching concepts for CFB furnace operation	Control aspects were integrated into CFB process design through model analysis and dynamic simulation. Guidelines for modifying the CFB for oxy-combustion and performing air to oxy transitions were provided.
Publication II	
Circulating fluidized bed boiler state estimation with an unscented Kalman filter tool	ICPD model analysis was extended with an unscented Kalman filter tool. Estimation of time-variant parameters and states for control-oriented process design was demonstrated for the oxy-CFB.
Publication III	
Integrated control and process design in CFB boiler design and control – application possibilities	A novel ICPD research characterization was made, and ICPD was reviewed for power plants. Relative gain analysis guided process design and ICPD optimization were implemented for the CFB boiler for the first time.
Publication IV	
Once-through circulating fluidized bed boiler control design with the dynamic relative gain array and partial relative gain	An extensive relative gain procedure was defined for CFB control design and interaction analysis in ICPD. Plant-wide control structure selection guidelines were created for the OTU-CFB boiler based on the procedure.
Publication V	
Integrated control and process design for improved load changes in fluidized bed boiler steam path	A novel ICPD procedure was defined for the CFB boiler, combining dynamic ICPD optimization with relative gain control design. Improved load changes were gained for the CFB steam path based on the procedure.

2   CFB boiler process & control

The work carried out for this thesis examined load changes in the circulating fluidized bed (CFB) boiler, depicted in Fig. 2 with a once-through (OTU) steam path. The CFB and the bubbling fluidized bed boiler are fluidized bed processes, and like other solid fuel boilers they consist of the combustion/flue gas side and the water-steam cycle subsystems. Section 2.1 discusses the CFB combustion side, which was the focus of Publications I and II. Section 2.2 deals with the water-steam cycle, which was the target process in Publications III and V. The control tasks of the boiler are presented in section 2.3; this topic was investigated in Publication IV.
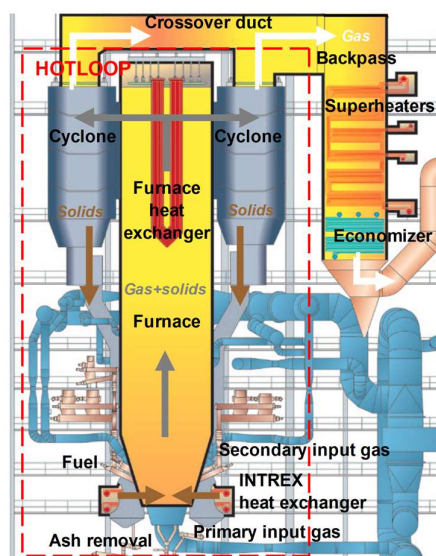
Fig. 2. Operational schematic figure of a CFB boiler (Publication IV, adapted with permission. Copyright 2017 American Chemical Society).

2.1   Combustion & flue gas side

In fluidized bed boilers, fuel is combusted in a bed of incombustible material (e.g., sand or ash), which is fluidized in the furnace with the input oxidant gas flows. In the CFB setup, the particles are entrained with the oxidant gas and leave the furnace from the top. The solids are separated from the flue gas in cyclones and the gas is directed to the flue gas duct (Basu, 2006; Sarkar, 2015). The solids are circulated

back to the furnace through the return leg, which often contains solid material heat exchangers (HE) such as Intrex™ fluidized bed units. The furnace temperature is maintained within an 800–900 °C range, and limestone is commonly fed into the bed for SO_X gas capture. The input oxidant gas is heated in LUVO preheaters and fed as the fluidizing primary gas flow (prim.) from the bottom of the furnace, and as secondary gas flows higher up in the riser (sec.).

The input oxidant gas is typically air, and it provides the necessary oxygen for combustion. The oxidant can also be formed in other ways, such as in oxy-combustion carbon capture and storage (CCS). In oxy-combustion (Stanger et al., 2015), fuel is combusted with a mixture of high purity oxygen (typically from an air separation unit, ASU) and recirculated flue gas (RFG), so that the flue gas CO_2 content is elevated to 70–98 vol% (dry). This enables the recovery of CO_2 in carbon compression and purification units (CCU + CPU), see Fig. 3. Aside from greenfield oxy boilers or retrofits to existing power plants, CFB boilers can be constructed as dual-fired units that can operate flexibly in both air and oxy mode. ASU, CCU, and CPU units were considered beyond the scope of this work.
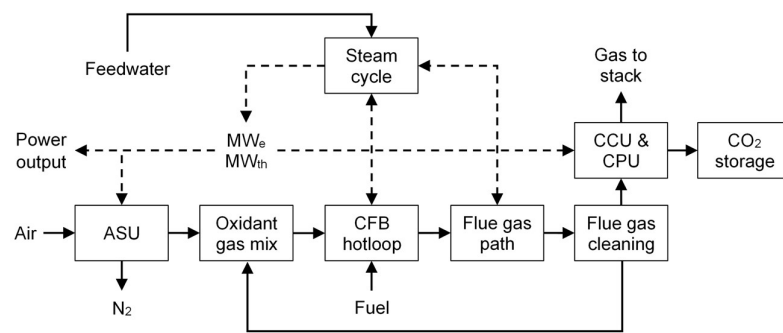
Fig. 3. Oxy-CFB schematic figure, material streams (solid lines), heat (dashed lines).

Oxy-combustion findings from the literature were discussed for both pulverized fuel and fluidized bed boilers in Publication I, and the design aspects explored in Publication I have been discussed in several references since. The fundamentals of fluidized bed oxy-firing were reviewed by Anthony and Hack (2013), Singh and Kumar (2016), and Stanger et al. (2015). The different design requirements for retrofit, dual-fired, and greenfield oxy-CFB boilers were addressed through theory and simulations by Leckner and Gómez-Barea (2014), and Seddighi (2017), similarly to Publication I. Seddighi, Clough, Anthony, Hughes, and Lu (2018) also

examined oxy-CFB scale-up issues. Similarly to the simulations in Publication I, Lappalainen, Tourunen, Mikkonen, Hänninen, and Kovács (2014) performed CFB simulations for transitions between air and oxy mode. Effects of oxy-combustion on solid material heat exchangers (e.g., Intrex units) were omitted from Publication I, and Bolea, Romeo, and Pallarés (2012), and Seddighi, Pallarès, Normann, and Johnsson (2015) concluded that oxy-firing at high O_2 percentages would increase the external heat exchanger material load. With regard to the control design results of Publication I, Niva, Hultgren, Ikonen, and Kovács (2017) carried out plant-wide control synthesis for the oxy-CFB hotloop based on self-optimizing control and relative gain analysis. Liu, Shi, Zhong, and Yu (2019) reviewed the experimental work and the numerical modeling of oxy-CFB coal and biomass co-firing.

Together, the furnace, gas-solid cyclones, and the return leg form the CFB hotloop (Fig. 2). The hotloop and the flue gas path contain heat exchangers, where heat is transferred to the water-steam side to generate steam. The positioning of the heat exchangers on the combustion side is boiler specific, although the evaporator is usually implemented as furnace water-wall tubes, and water and air preheaters are often located as the last heat exchangers of the flue gas path (Joronen, Kovács, & Majanne, 2007). The resulting interconnected process structure and the case-by-case design are the central motivators for studying ICPD for CFB power plants.

2.2   Water-steam cycle

In the water-steam cycle (Joronen et al., 2007; Sarkar, 2015), feedwater (FW) is pumped to a high pressure (pump + valve) and preheated, with the economizer (ECO) as the final preheater before evaporation. Saturated steam is formed in the evaporator (EVAP), and the steam temperature is elevated further in the superheating section, which typically consists of several superheaters (SH) and cooling desuperheater (DSH) water sprays. The pressure and temperature of the resulting superheated main steam (live steam) are the boiler steam parameters.

The main steam expands in the turbine high-pressure (HP) and low-pressure (LP) sections to generate electrical power (MW_e), with possible reheating of the steam between the sections (reheater, RH). The expanded steam is condensed back to water in the condenser. In CHP plants, a portion of the main steam bypasses the turbine and is fed to a CHP heat exchanger to generate heating power. In this work, only condensing plants with electrical power generation are considered.

Based on their evaporator setup, boilers are classified into drum and OTU units (Fig. 4). In drum boilers, water is separated from steam after evaporation and

recirculated back to the evaporator. In OTU boilers, feedwater transforms into main steam in a "once-through" pass without separation, and the boundaries between preheating, evaporation, and superheating may shift depending on the boiler operation. OTU steam generation enables the construction of large CFB boilers with fast changes in the evaporation rate, as well as high efficiencies resulting from the supercritical steam parameters that are enabled by this steam cycle setup. The OTU steam path was investigated in Publication IV.
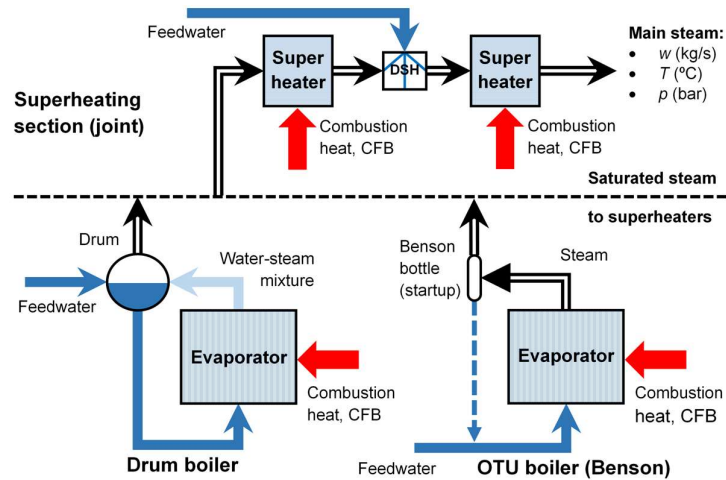
Fig. 4. Basic water-steam paths for generating main steam: the drum boiler and the OTU (Benson) boiler. A two-stage superheating block with one DSH spray is shown.

The steam cycle can either be operated with a constant main steam pressure at all load levels (constant-pressure mode) or with load-dependent main steam pressures (sliding-pressure mode). The steam pressure is maintained with the turbine throttle valve, which enables the use of fast stored steam control reserves. Due to its steam path structure, sliding-pressure operation can more readily be implemented for the OTU boiler than for drum boilers. ICPD design outcomes were compared for constant- and sliding-pressure load changes in Publication V.

The OTU steam path presents challenges for load-following electrical power control. The steam control reserves are limited due to the small evaporator storage capacity, which also causes combustion disturbances to be carried over to the steam quality more easily than in drum boilers. The flow conditions are complex, and the configuration results in a direct connection between the feedwater flow and the

32

main steam properties (Fig. 5). The resulting interactions have the potential to reduce MW_e control performance, and they were explored in Publication IV.
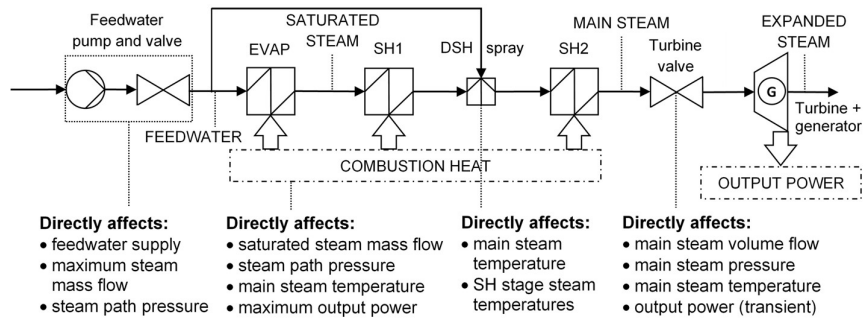
Fig. 5. Effects of manipulated variables on generated power and steam properties.

2.3 Main control tasks

The control objectives of a condensing power plant can be divided between those related to power output and those related to state variables (Doležal & Varcop, 1970; Joronen et al., 2007; Klefenz, 1986). The main control task is to maintain the output electrical power at its setpoint. CHP plants have a separate control target for the generated heat. State variables are controlled to maintain output power quality, high plant efficiency, and operational safety. CFB control tasks and typical control setups from industry were outlined in Publications I and IV:

– **Output MW_e control:** determined by turbine or combustion control.
– **Main steam pressure control:** determined by turbine or combustion control.
– **Turbine-generator unit control:** output MW_e adjusted with the turbine valve; also frequency and voltage for boilers that participate in grid frequency control.
– **Feedwater control:** the feedwater flow should match the generated steam and combustion heat, typically implemented as drum level control (drum boiler) or evaporator output steam enthalpy control (OTU boiler).
– **Steam temperature control:** control of main steam temperature and SH stage intermediate temperatures; most commonly adjusted with DSH sprays.
– **Combustion control:** coordination of fuel and oxidant flows to generate the required heat for steam formation, maintain fluidization, and ensure complete combustion; usually includes separate flue gas O_2 percentage control.

- **Furnace pressure control:** can be adjusted with induced draft flue gas fans.
- **CHP heat control:** can be adjusted using the turbine HP and LP bypass flows.
- **Supporting units:** coordination of boiler with flue gas cleaning, ASU, etc.

The focus of this thesis is on electrical power control during load setpoint changes. This control task is basically a 2×2 variable problem between the generated power at the turbine and the generated steam in the boiler. The MW_e output is altered by adjusting the steam flow with the turbine throttle valve or by increasing the firing power (fuel + oxidant flows). As these actions also affect the main steam pressure, output MW_e control and steam pressure control are coordinated with the upper-level unit master control strategy (Fig. 6). In boiler-following control, the MW_e is controlled with the turbine valve and the main steam pressure with the firing power. In turbine-following control, the opposite control connections are applied. Boiler-following mode enables fast output MW_e changes using the turbine valve, but the new load level can only be maintained permanently by changing the firing power.
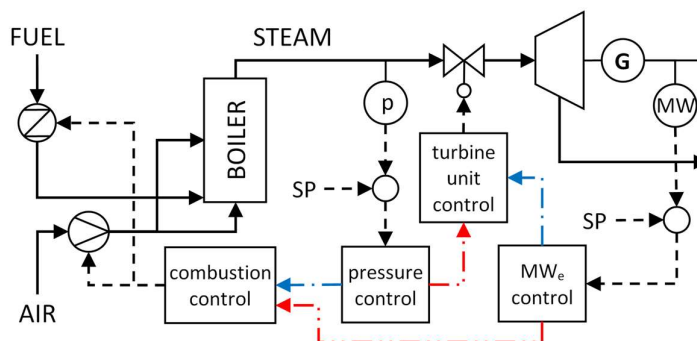
Fig. 6. Boiler-following (blue) and turbine-following (red) control (Publication IV, reprinted with permission. Copyright 2017 American Chemical Society).

Multi-loop PID control was used for all CFB control tasks in Publications I–V. This approach was chosen due to the prevalence of PID control even in modern steam power plants, as ICPD control design should preferably be suitable for current industrial practices. Nevertheless, much research has also been conducted for improving MW_e control through advanced control methods. Several references of advanced and model-based load-following control were listed in Publication V, and some recent studies on centralized multiple-input-multiple-output (MIMO) model predictive control (MPC) are mentioned for the CFB boiler in section 3.2.

3 Integrated control and process design

This chapter describes the integrated control and process design (ICPD) literature review of Publication III. ICPD or "simultaneous design" aims at improving closed-loop performance by increasing the interaction between process and control design. Publication III focused on power plant ICPD applications, and two major outcomes were derived. Firstly, formal ICPD was introduced, which has never been reported for CFB boilers before, and rarely for power plants in general (cf. Chapter 1). Secondly, a novel ICPD classification was formulated, focusing on individual methodology characteristics. The purpose of this chapter is to explain how this characterization influenced the selection of ICPD design methods in the thesis. References were presented for each methodology type in Publication III, and recent reference lists have also been provided by Burnak, Diangelakis, and Pistikopoulos (2019b), Rafiei and Ricardez-Sandoval (2020b), Sharifzadeh (2013), Swartz and Kawajiri (2019), and Vega, Lamanna de Rocco, Revollar, and Francisco (2014).

This chapter is structured according to the formulated ICPD characterization, with performance evaluation discussed separately in Chapter 4. Section 3.1 outlines the characterization and compares it with other literature reviews. Section 3.2 deals with the scope and structure of an ICPD methodology. Sections 3.3–3.4 deal with process knowledge oriented ICPD and mathematical programming ICPD. Section 3.5 summarizes the ICPD procedure that was formed based on the literature review.

3.1 ICPD classifications in the literature

The need to integrate control and process design has been recognized for a long time in chemical process engineering. As a result, ICPD is currently a wide research field with numerous approaches for different design needs. Ziegler and Nichols (1943) first stated that control performance depends on both the process and its control system, which summarizes the basic concept of ICPD. Other works that are often cited as pioneering in the field (e.g., Grossmann & Harjunkoski, 2019; Luyben, 2004; Pistikopoulos & Diangelakis, 2016) were provided by Buckley (1964), Sargent (1967), and Lee, Koppel, and Lim (1972).

For systematic ICPD, the first major research direction focused on designing processes that are easy to control, where concepts like controllability and flexibility (cf. section 4.5) were defined as a bridge between process and control design (Morari, 1992; Perkins, 1989). The second advancement was to formulate process and control design into a simultaneous optimization problem (Perkins & Walsh,

1996). The development of ICPD optimization progressed rapidly (cf. Burnak et al., 2019b; Kookos & Perkins, 2004; Sakizlis, Perkins, & Pistikopoulos, 2004) from simpler approaches such as economic back-off evaluation (Narraway, Perkins, & Barton, 1991) to the dynamic optimization of structural and continuous parameters in the closed-loop system (Bahri, Bandoni, & Romagnoli, 1996; Mohideen, Perkins, & Pistikopoulos, 1996; Schweiger & Floudas, 1998). This mathematical programming approach to ICPD has largely dominated contemporary research.

The most recent development in ICPD research is the inclusion of scheduling and operational optimization into the problem (e.g., Burnak et al., 2019a; Koller & Ricardez-Sandoval, 2017). Model-based control is also increasingly used in ICPD (e.g., Gutierrez, Ricardez-Sandoval, Budman, & Prada, 2014; Sakizlis et al., 2004), which coincides with the increased interest in MPC control in industry. Rafiei and Ricardez-Sandoval (2020b) summarized the current challenges for ICPD research: the need for suitable disturbance and uncertainty descriptions, problem size inflation, multi-objective nature of the problem, tendency for local optima, and the added complexity caused by discrete decision variables. On the whole, despite the extensive research history of ICPD, the challenge of fast load changes in large power plants has never been addressed through formal ICPD prior to this thesis.

ICPD approaches were characterized in Publication III according to Table 2, which is a novel contribution of the thesis. The characterization differs from most other reviews, as it highlights individual characteristics that occur in ICPD methodologies rather than defining rigid methodology classes.

Table 2. Basic ICPD characteristics (Publication III, adapted with permission from IFAC).

Problem definition	Design structure	Methodology basis
Performance evaluation	Degree of interaction	Process knowledge ICPD
Economic & environmental	Anticipating sequential	Heuristics
Thermodynamic analysis	Partially integrated	Phenomenon based
Dynamic control performance	Fully integrated	System analysis based
System properties for control		
Purpose	Decomposition	Mathematical programming ICPD
Attain achievable performance	Hierarchy of design steps	Controllability optimization
Improve dynamics with design	Decomposition methods	Dynamic optimization, MIDO
Form process + control system	Closed design framework	Embedded control optimization
Scope	Control design	Robust optimization
Continuous/discrete decisions	Adapt default control structure	Back-off optimization
Dynamic/static operation	Plant-wide control design	Multi-objective search
Process/control design basis	Model-based control ICPD	Stochastic/probabilistic search

This thesis posits that the novel characterization facilitates the selection of ICPD methods for a new application area like the CFB. Three main groups were defined in Table 2: "problem definition", "decision-making structure", and "methodology basis". The first group outlines how the design problem is set up. The second group concerns how process and control design interact. The third group consists of process knowledge and mathematical programming ICPD.

The main connection between Publication III and other reviews comes from the separation between process knowledge and mathematical programming ICPD. Vega et al. (2014) distinguished between dynamic integrated optimization and "projecting methods", where dynamics are incorporated into the design through controllability and multiplicity methods, recycle dynamics, and first-principles analysis. Burnak et al. (2019b) outlined three ICPD classes: static flexibility analysis, dynamic controllability and resiliency analysis, and the full integration of process and control design in one framework. Similar separations between linear controllability index methods and optimization-based ICPD were described by Engell, Trierweiler, Völker, and Pegel (2004), and Jørgensen, Gani, and Andersen (1999), who also considered passivity-based methods (cf. subsection 4.5.1) as a separate class. Mencarelli, Chen, Pagot, and Grossmann (2020) grouped process superstructure design methods (cf. section 3.4) into chemical/physical "targeting techniques", hierarchical decomposition methods, and superstructure optimization.

The characterization in Table 2 differs from most prominent ICPD reviews, as far as process knowledge ICPD is concerned. Firstly, it is considered to be proper ICPD design in the thesis, while many works only label mathematical programming ICPD as "integrated" (e.g., Sharifzadeh, 2013). Secondly, "process knowledge" includes both first-principles and system analysis in Table 2, whereas many authors simply divide ICPD between system analysis approaches and simultaneous optimization (e.g., Burnak et al., 2019b; Sakizlis et al., 2004; Yuan, Chen, Sin, & Gani, 2012). Lastly, the thesis suggests that the difference between heuristics (e.g., Martín & Adams, 2019) and process characterization should be emphasized more in the literature, especially for detailed multi-stage methodologies.

The subclasses of mathematical programming ICPD in Table 2 were inspired by the review of Yuan et al. (2012). The classification focused on solution strategies, while a more property-oriented approach was presented by Vega et al. (2014). Sharifzadeh (2013) outlined a somewhat different classification, containing multi-objective controllability methods, model reduction methods (including robust and embedded control optimization), nonlinearity analysis, geometric operability analysis, flexibility methods, simulator-based dynamic optimization, back-off

methods, and the perfect control approach. Gutierrez et al. (2014), Ricardez-Sandoval, Budman, and Douglas (2009), and Huusom (2015) listed classes for controllability index methods, dynamic optimization, and robust optimization. A common general classification (e.g., Sakizlis et al., 2004) considers multi-objective optimization for economically optimal processes with feasible dynamics around nominal operating points, and approaches that use a single economic objective in a dynamic optimization framework with operability constraints.

Here, the ICPD scope was limited to the process (flowsheet, equipment sizing, operating conditions) and its control system (structure, controllers). As such, integrated scheduling and control was considered beyond the scope of this thesis. ICPD was also separated from the broader topic of "process systems engineering" (PSE), which encompasses process simulation, synthesis, control, operations, and optimization (Grossmann & Harjunkoski, 2019), but does not emphasize the interaction between process and control design. Despite this, many design methods are similar in ICPD and PSE, especially for process optimization (e.g., Martín & Adams, 2019; Mitsos et al., 2018). Lastly, ICPD is often connected to process integration and intensification in the literature (Daoutidis, Zachar, & Jogwar, 2016), which are also beyond the scope. For reference, Nikačević, Huesman, Van den Hof, and Stankiewicz (2012) reviewed the effects of process intensification on control and presented a conceptual ICPD approach that focused on intensified processes.

3.2 Problem definition & design structure

The features used for defining the ICPD problem (Table 2, first column) are the purpose, scope, and performance goals of the methodology, as described in Publication III. Three general purposes can be defined. Firstly, the design can map the achievable dynamic performance, which gives ICPD a benchmarking role. Secondly, the design can suggest modifications for improving control performance and reveal causes for poor open- and closed-loop dynamics. Thirdly, the closed-loop process can be fully generated by the ICPD approach. The ICPD procedure of this thesis considers the latter two approaches in Publications III–V, although the achievable performance was also mapped for oxy-combustion in Publication I.

Regarding scope, ICPD is primarily based on either process or control design, and either static or dynamic operation. Huusom (2015) highlighted how the control problem is always restricted by the process, whereas operational measures from control design must be included separately in the process synthesis problem. The thesis focused on the CFB dynamic operation and relied on control design tools.

38

Available design scopes in ICPD are shown in Fig. 7. Most of the listed continuous variables for process and control design, as well as discrete control connection variables, were considered in Publications I–V. As boiler flowsheets were based on in-house data, discrete variables were not used for the process design.

	Process design	Control design	Process scheduling
Discrete	∗Flowsheet: units & connections ∗Unit design, e.g. heat exchanger pipe count	∗MV/CV/ measurement selection ∗MV–CV control connections ∗Controller algorithm	∗Sequence operations & order ∗Production decisions ∗Process start-ups & shut-downs
Continuous	∗Unit sizing ∗Material & energy stream sizing ∗Static states & setpoints	∗Controller parameters ∗Buffer control reserve sizing ∗State & setpoint trajectories	∗Batch schedule time stamps & durations ∗Plant-wide schedule time stamps & durations

Fig. 7. Decision domains of ICPD, separated into discrete and continuous design.

ICPD is structured (Table 2, second column) based on the degree of process–control interaction, the methodology decomposition, and the control design framework. The most comprehensive methodologies are fully integrated for all process and control design activities. In partial integration, some design decisions are made outside the main ICPD steps. In anticipating sequential approaches, control aspects are only taken into account during the process design. The ICPD procedure of the thesis is partially integrated, as it consists of two distinct stages: control structure selection (Publications III and IV), and integrated process/controller optimization (Publications III and V). Moreover, Publications I and II represent an anticipating sequential approach, as the goal was to achieve improved CFB dynamic operation in the oxy-fired mode based on knowledge from the air-fired mode.

ICPD methodologies are decomposed as closed frameworks, sets of individual tools, or hierarchies of design steps. Common hierarchical decomposition strategies for control tasks have been discussed by Larsson and Skogestad (2000),

Sharifzadeh (2013), Stephanopoulos and Ng (2000), and Vasbinder, Hoo, and Mann (2004). The ICPD procedure of this thesis is a hierarchy of connected design steps, although the ICPD optimization (Publication V) is a fully closed framework.

For the control design framework, Publication III stated how MPC control and especially plant-wide control are important for ICPD. Plant-wide control defines the control strategy for an entire plant, with a particular focus on variable selections and the control system topology. The design is cast as a multi-objective MIMO problem, subject to process dynamics, disturbances, constraints, and control law (Larsson & Skogestad, 2000; Luyben, Tyréus, & Luyben, 1999; Stephanopoulos & Ng, 2000). Many plant-wide control design frameworks contribute to process and control design integration, such as self-optimizing control (Skogestad, 2004) and the eigenvalue-based analytical hierarchical procedure (Vasbinder et al., 2004).

Plant-wide control design tools were used in Publication IV for defining the control structure between pre-selected manipulated variables (MV) and controlled variables (CV) of the CFB boiler. The selection of MVs and CVs was based on design experience (cf. section 2.3), but formal selection criteria are also available in the literature (Larsson & Skogestad, 2000; Skogestad & Postlethwaite, 2005; van de Wal & de Jager, 2001). Generally speaking, few results are available in the literature regarding plant-wide control in conventional power plants. Aside from the references listed in Publication IV, Niva et al. (2017) and Zotică, Nord, Kovács, and Skogestad (2020) recently applied self-optimizing control to solid fuel boilers.

Several advantages have been presented in the literature for using MPC control in ICPD (Huusom, 2015; Rafiei & Ricardez-Sandoval, 2020b): The controller model can be linked to process parameters, process and controller optimization can be combined, optimal control action is ensured, and effective constraint handling is possible. Economic-MPC is seen as especially promising for enabling flexible control design during early process design stages (Oyama & Durand, 2020). A centralized MPC can also bypass the need for a separate control structure design step in the ICPD procedure. However, a plant-wide MIMO controller is often challenging to implement in practice (Sharifzadeh, 2013; Skogestad, 2004).

The main question regarding the use of MPC control in CFB boiler ICPD is the availability of suitable controller models for the desired load range. In addition, the models would need to be re-identified for each process structure during the ICPD iteration (Gutierrez et al., 2014; Huusom, 2015). While MPC was not used in the thesis for these reasons, previous CFB boiler MPC applications are available in the literature, with recent papers from Zimmerman, Kyprianidis, and Lindberg (2018) on furnace and steam temperature control, and Zhang, Gao, Hong, Liu, and

Wang (2019) on load-following performance, for example. These studies indicate the potential feasibility of MPC-based ICPD for CFB boiler problems in the future.

3.3 Process knowledge oriented ICPD

Process knowledge ICPD relies on modeling and operational knowledge of the process and its control system. The process is examined using first-principles theory, simulation, and system analysis to determine how design decisions affect dynamics and control performance. Closed-loop operation is thus improved through an increased qualitative understanding of the process (Luyben, 2004). Process knowledge ICPD was classified according to Fig. 8 in Publication III.
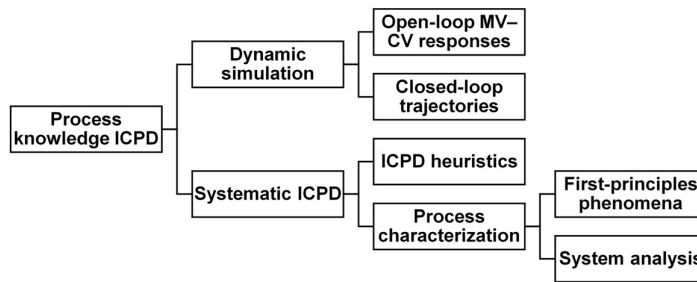
Fig. 8. Classification of process knowledge oriented ICPD methodologies.

The simplest way to implement ICPD is to examine open- or closed-loop dynamics with a simulator during the process design to verify that design decisions do not lead to dynamic limitations (Lyman & Luyben, 1994). This approach was used for power plants by e.g., Majanne and Maasalo (2009) for analyzing the control system operation, by Mertens, Alobaid, Starkloff, Epple, and Kim (2015) for comparing drum and OTU steam cycle start-up dynamics, and by Zhao et al. (2018a, 2018b) for analyzing different steam extraction modes, as well as by Sharifzadeh and Shah (2019) for post-combustion capture dynamic sensitivity analysis. More systematic ICPD approaches are divided here between heuristics and process characterization, both of which are usually set up as hierarchical procedures or method toolboxes.

Heuristic methods for process and control design (e.g., Larsson & Skogestad, 2000; Luyben, 2004; Luyben et al., 1999) consist of rules and decision charts that determine how specific design questions should be handled to ensure beneficial control properties. Heuristics thus utilize design experience in its most direct form,

and most ICPD approaches employ at least some degree of heuristics. Notably, heuristics are used in mathematical programming ICPD for complexity reduction (Perkins & Walsh, 1996) and for ensuring solution optimality and feasibility (Lewin, Seider & Seader, 2002). The main downside of heuristics is that they can be challenging to employ for new, complex, and unconventional process applications.

Process characterization uses systematic model and response analysis to form a detailed picture about the factors that influence the control of the process. Multiple criteria are usually analyzed to classify the system and characterize its different properties (e.g., Hernjak, Doyle, Ogunnaike, & Pearson, 2004; Huusom, 2015). The resulting qualitative and quantitative information can then be used for more informed closed-loop synthesis. A process can primarily be characterized on a phenomenological or a system analysis basis, cf. Publication III.

Phenomenon-based analysis evaluates how control performance is affected by the chemical and physical properties of the process through first-principles theory and simulations. Some approaches extend first-principles process design procedures (Smith, 2005) with control considerations, such as the methodology proposed by Alvarado-Morales et al. (2010), and Hamid, Sin, and Gani (2010), where the yield and selectivity of reaction and separation processes were connected to the attainable region and the maximum driving force. System analysis focuses on the dynamics of the multi-loop process, with the aim of identifying correlations between design decisions and control-relevant system properties (cf. section 4.5), such as controllability and resiliency (Jacobsen & Skogestad, 1991; Engell et al., 2004; Weitz & Lewin, 1996). The approach typically relies on low-complexity models and frequency domain methods from classical control theory.

Both phenomenon- and system-oriented process characterization was used in this thesis: chemical and physical analysis for comparing air- and oxy-combustion in Publication I, and relative gain interaction analysis for the OTU-CFB flowsheet in Publication IV. In general, process knowledge ICPD enables the straightforward inclusion of different kinds of control insight into process design, especially qualitative criteria. However, it can be inefficient for managing multiple design objectives, parameter interconnections might be omitted, it is challenging to ensure global optimality, and results may be influenced by designer bias.

3.4   Mathematical programming ICPD

Mathematical programming ICPD formulates the simultaneous process and control design problem as a closed mathematical framework, where solutions are obtained

through optimization. Mathematical programming ICPD was classified according to Fig. 9 in Publication III, where the "ICPD methods" group was listed in Table 2 (third column). Methodologies can contain properties from multiple classes.
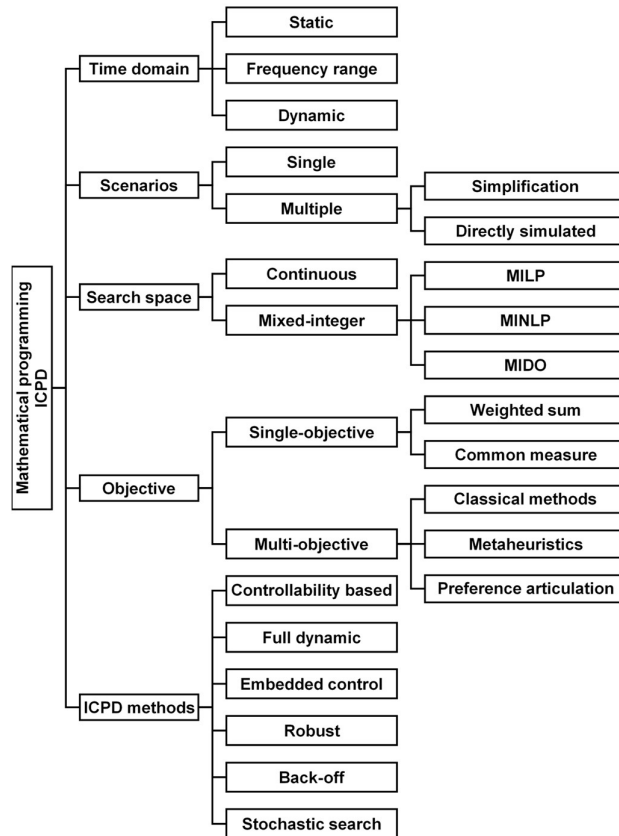
Fig. 9. Classification of mathematical programming oriented ICPD methodologies.

All of the approaches shown in Fig. 9 can be derived from a generalized problem statement for simultaneous process and control optimization, although the specific formulations for objectives, constraints, and the optimization progression depend on the methodology. General problem formulations have been given by Kookos and Perkins (2004), Sakizlis et. al (2004), Swartz and Kawajiri (2019), and Yuan et al. (2012). A basic formulation based on the literature was also presented in Publication III. This definition is generalized further here to generate eqs. (1)–(2).

$$\min_{X,U} J(x, u, y, X, U, t, \omega), \tag{1}$$

$$\begin{cases} f_{\text{proc}}(x', x, u, y, X, U, t) = 0 \\ f_{\text{proc},0}(x, u, y, X, U, t_0) = 0 \\ w_{\text{proc}}(u', x, u, X, t) \leq 0 \\ f_{\text{des}}(x', u', x, u, y, X, U, t, \omega) = 0 \\ w_{\text{des}}(x', u', x, u, y, X, U, t, \omega) \leq 0 \end{cases} , \tag{2}$$

where J is a vector of ICPD objective functions, x are state variables, y are output variables, u are input variables, X are process design variables, U are control design variables, t is time, and ω is frequency. f_{proc} contains all the equations of the physical system model, i.e., the process, controllers, and measurements, with initial conditions $f_{\text{proc},0}$ at time t_0. w_{proc} are the physical system inequality constraints. f_{des} contains all the equations for system performance analysis, including calculated output indicators. w_{des} are performance inequality constraints, including minimum and maximum bounds for X and U, i.e., the ICPD search space.

The remainder of this section discusses the classes illustrated in Fig. 9. First, ICPD optimization can be performed for static calculations, multiple frequencies, or full dynamic responses. This selection influences how constraints are formulated and how the process is simulated during the optimization. Similarly, optimization can be performed either for an open-loop or closed-loop system. Closed-loop optimization adds controller model constraints to the problem. In this thesis, the CFB boiler optimization (Publications III and V) was performed for simulated dynamic closed-loop transients, as well as for open-loop frequency responses.

Dynamic optimization contributes to an increased computational complexity for ICPD. Solution strategies were recently discussed by Biegler (2018), and the ICPD procedure of the thesis employed a simulator-based setup with separate differential equation solver and optimizer layers (Mitsos et al., 2018; Sharifzadeh, 2013). Swartz and Kawajiri (2019) further explored the differences between intentionally dynamic and intrinsically dynamic ICPD problems. The load-following power plant problem can be viewed as intentionally dynamic, although primary regulation already resembles an intrinsically dynamic problem.

Optimization can be performed for one operating point (static) or scenario (dynamic). Alternatively, a range of operating points or scenarios can be evaluated. Many ICPD approaches simplify this multiple scenario setup by considering worst-case disturbances, variability regions, and disturbance rejection capacities. In this thesis, the CFB boiler was optimized for pre-specified scenarios, which were simulated with an internal design model during the optimization iteration.

Depending on the inclusion of structural decisions in the problem (Fig. 7), ICPD optimization is conducted in a continuous framework, or as a mixed-integer linear (MILP) or nonlinear (MINLP) programming setup. This also relates ICPD to flowsheet superstructure optimization (Mencarelli et al., 2020). MINLP is the most comprehensive, but also the most computationally intensive way to synthesize a closed-loop flowsheet. In this thesis, the CFB boiler optimization was continuous, as the flowsheet, control structure, and controller type were determined a priori.

The CFB boiler optimization approach was defined as a weighted sum single-objective problem, where weights were chosen based on objective importance. Alternatively, objectives can be converted into a common measure, e.g., a monetary value. As weighting or normalizing of different types of objectives is often challenging, ICPD can also be performed as proper multi-objective optimization, but in that case additional criteria are necessary for selecting the final solution from the resulting solution plane. Fig. 9 distinguishes between classical multi-objective methods (e.g., ε-constraint, goal programming) and metaheuristics (Alhammadi & Romagnoli, 2004; Liu, Li, Liu, & Guo, 2020), as well as the "preference articulation" between decision and search operations (Chiandussi, Codegone, Ferrero, & Varesio, 2012). Cao et al. (2017) emphasized how the combination of multiple objectives affects the interpretation of process optimization results.

The "ICPD methods" group of Fig. 9 was described in Publication III. The "controllability" approach combines economic optimization with controllability objectives or constraints. "Dynamic optimization" considers the direct optimization of dynamic economic performance, with the most extensive and challenging approach being mixed-integer dynamic optimization (MIDO). "Embedded control optimization" employs iterative process and control design layers. The "back-off" approach minimizes the dynamic back-off region around an economically optimal operating point. "Robust optimization" is based on robust control methods, and "stochastic search" focuses on the effects of uncertain parameters and disturbances on the design outcome. Recent research has largely centered on robust and stochastic ICPD (Grossmann, Apap, Calfa, García-Herreros, & Zhang, 2016; Rafiei & Ricardez-Sandoval, 2020b). Notably, several works have combined aspects of robust optimization (Ricardez-Sandoval et al., 2009) with back-off optimization (Kookos & Perkins, 2004). The normal vector approach that was used recently by Muñoz, Gerhard, and Marquardt (2012) utilizes the distance to feasible operating regions as a back-off type robustness criterion, while another series of works (e.g., Mehta & Ricardez-Sandoval, 2016; Rafiei & Ricardez-Sandoval, 2020a) presented a robust dynamic approach that used a power series expansion for constraints and

variable back-off evaluation through trust-region methods. The need for advanced solution strategies highlights the challenges related to fully simultaneous dynamic optimization, despite the constantly increasing availability of computing power. This applies especially to MIDO, with recent results from e.g., Biegler (2018), Burnak et al. (2019a), and Koller and Ricardez-Sandoval (2017).

The main benefit of mathematical programming ICPD is that it can produce a complete solution to a process/control problem with several interacting objectives, also accounting for unconventional solutions. However, the resulting problem is often computationally intensive, especially for plant-wide models. The entire ICPD problem must be expressed in a feasible mathematical format, which can be a limitation for qualitative and non-continuous criteria. The problem definition has a large impact on the optimization outcome, and calculated optima might not be applicable in practice. These factors served as the motivation for the stepwise ICPD procedure of this thesis, where process knowledge and system analysis pre-design are used to reduce the complexity of the ICPD optimization problem.

3.5 Summary of chosen approach for CFB ICPD

The main components of the ICPD procedure that was derived in the thesis are summarized here, with more detailed descriptions given in Chapter 5. The aim of the procedure is to combine closed-loop load change trajectory design with open-loop system analysis independent of controller type, first-principles modeling, and expert interaction. As such, the procedure consists of dynamic ICPD optimization, systematic control structure selection, and process knowledge pre-design:

– **ICPD optimization:** Continuous process and controller parameters were simultaneously optimized in Publications III and V for simulated closed-loop load change trajectories in a fixed time range. A single weighted optimization objective was used, with the main weight on MW_e setpoint tracking.
– **Control structure selection:** Control connections between MVs and CVs were evaluated in Publications IV and V using different relative gain methods. The analysis provided the preferred control structure and highlighted how process parameters affected controllability and control loop interactions.
– **Process pre-analysis:** The effects of the process and control parameters on dynamic performance were analyzed qualitatively in Publications I and II using the first-principles theory, detailed simulation, and advanced state estimation.

4 Quantifying performance

Publication III emphasized how the performance evaluation framework forms the basis for the ICPD implementation, especially for ICPD optimization. The evaluation methods should accurately quantify the desired system performance, identify the factors that affect it, and provide a suitable ranking of process solutions. The purpose of this chapter is to establish the performance guidelines for the load-following CFB boiler problem, with separate sections 4.1–4.5 for economic performance, environmental performance, thermodynamic analysis, control performance, and system analysis. Section 4.6. summarizes the chosen guidelines.

4.1 Economic performance

Economic performance evaluation aims at minimizing the capital and operating costs of the process or maximizing product revenue compared to production costs (Smith, 2005). Capital costs are principally derived from the process (equipment sizing, nominal throughput, etc.), whereas operating costs are more influenced by process setpoints, control, and scheduling. Some ICPD approaches define more detailed cost decompositions, such as the "communication costs" for the control structure alternatives described by Gutierrez et al. (2014). Process economics can also be assessed in ICPD through on-specification production amounts or standard metrics like the total annual cost, economic potential, return on investment, discounted cash flow, and net present value (Liu, Georgiadis, & Pistikopoulos, 2011; Frumkin & Doherty, 2020; Luyben, 2004; Smith, 2005). Economic performance is usually evaluated for longer timespans, e.g., on an annualized basis.

Contemporary ICPD increasingly aims at optimizing process economics directly, as this is usually the most important design objective for the plant. The main benefit of economic evaluation for ICPD is that it enables a direct comparison of different objectives by assigning economic values to them. This was exemplified for power plants by Kragelund, Wisniewski, Mølbak, Nielsen, and Edlund (2008), who connected process economics to lower-level efficiency, controllability, and availability objectives. Economic evaluation also creates an inherent trade-off between process and control design, as extra disturbance rejection capacity in the process typically leads to capital cost penalties (Huusom, 2015; Luyben, 2004).

Despite these benefits, many authors have highlighted how closed-loop design based on process economics alone is often not sufficient for dynamic performance and sustainability (Liu et al., 2011; Martín & Adams, 2019; Siirola & Edgar, 2012).

Examining operating costs and allocating capital costs can be challenging for short time periods like a load change scenario, and economic penalties for primary regulation MW_e setpoint violations can be unintuitive to estimate or compare with other costs. In addition, assigning representative economic values for objectives like robustness or stability can be difficult. Lastly, fuel and electricity price variations make the design results market scenario dependent, although this limitation can be addressed to some extent through robust and stochastic methods.

Due to these considerations, a separate economic objective was not considered in Publications I–V, although the process parameter search space was based on acceptable capital costs. As stated in Publication V, economic evaluation should be included in future work to avoid designs with significant economic penalties, and Publication III stated that economic performance should be evaluated as the fuel and annualized investment costs, scaled with the generated power. This evaluation could be performed for the final solution candidates from the ICPD procedure, or the ICPD optimization objective could be expanded with an economic penalty term.

4.2   Environmental performance

Environmental performance evaluation aims at minimizing selected emissions or the environmental footprint of the process. Environmental regulations can usually be specified as averages for pollutant mass flows. In addition, relevant performance indices for power plants like the global warming potential are derived from life cycle analysis, LCA (Klöpffer & Grahl, 2014; Smith, 2005). For example, Liu et al. (2011) used a cradle-to-gate greenhouse gas index for the mixed-integer multi-objective process optimization of a poly-generation energy system. In general, the increased capital and operating costs of emission management often call for multi-objective design (Alhammadi & Romagnoli, 2004; Martín & Adams, 2019).

Environmental analysis can be expanded to the general topic of sustainability (Daoutidis et al., 2016; Rafiei & Ricardez-Sandoval, 2020b), which also includes central power plant design objectives like safety. Sustainability and environmental objectives are often evaluated on a steady-state basis, as they can be challenging to align with dynamics and control. Moreover, they can be difficult to translate into actual process modifications (Daoutidis et al., 2016; Siirola & Edgar, 2012).

For solid fuel boilers like the CFB, the main pollutants to be considered are CO_2, NO_X, and SO_X gases, as well as CO for incomplete combustion scenarios. The specific emission factors of these gases were recently analyzed for subcritical and supercritical pulverized coal power plants by Gonzalez-Salazar et al. (2018). The

48

flue gas CO_2 percentage was a central performance target in Publications I and II, as it directly reflects the CCU + CPU operating costs in oxy-combustion. Similarly, either the flue gas CO_2 or the global warming potential should be included as a steady-state objective or constraint for generic CFB boiler problems in the ICPD procedure. The low furnace temperatures and in-bed limestone feed in the CFB (cf. section 2.1) made NO_X and SO_X less relevant concerns for this thesis. Like process economics, environmental goals should be scaled with the generated power.

4.3 First-principles analysis

In first-principles analysis, the chemical and physical properties of the process are direct design objectives, or they are indicative of the desired performance, such as in the approach of Alvarado-Morales et al. (2010) and Hamid et al. (2010). The analysis quantifies how effectively the process transforms raw materials into products by describing the process through first-principles models, which are then linked to the system performance, such as economics in the screening approach of Frumkin and Doherty (2020). First-principles evaluation is prevalent in process knowledge ICPD, such as the analysis outlined in Publication I, where the effects of chemical and physical properties on load change performance were investigated.

Energy and exergy efficiency analysis are notable first-principles performance evaluation fields for power plants (Kaushik, Reddy, & Tyagi, 2011; Joronen et al., 2007). Energy efficiency, eq. (3), has conventionally been a key design objective for base load power plants. Exergy is the maximum useful work performed by a system that brings it into equilibrium with its surroundings. It can be defined for a stream as eq. (4), excluding kinetic, potential, and nuclear exergy (Szargut, 2005). Exergy efficiency, eq. (5), accounts for the thermodynamic irreversibility in the process, and it can be used as a convenient environmental performance measure.

$$\eta_{th} = \frac{W}{Q_{in}} \cdot 100\% = \left(1 - \frac{Q_{out}}{Q_{in}}\right) \cdot 100\% , \tag{3}$$

$$\varepsilon = w \cdot \left(\varepsilon_{ch,w} + (h_w - h_w^*) - T_K^* \cdot (s_w - s_w^*)\right) + Q \cdot \left(1 - \frac{T_K^*}{T_K}\right), \tag{4}$$

$$\eta_{ex} = \frac{\varepsilon_{out}}{\varepsilon_{in}} \cdot 100\% = \left(1 - \frac{B}{\varepsilon_{in}}\right) \cdot 100\% , \tag{5}$$

where η_{th} is energy efficiency, η_{ex} is exergy efficiency, Q is the heat transfer rate, W is work, ε is flow exergy, B is the irreversibility rate, and T_K is the temperature. The stream has a mass flow w, specific enthalpy h_w, specific entropy s_w, and specific chemical exergy $\varepsilon_{ch,w}$, derived from compound Gibbs standard free energies of formation and elemental specific chemical exergies. "*" denotes the reference state.

For CFB boiler ICPD, thermodynamic efficiency is useful as an alternative indicator to economic performance, especially as it is independent of assigned costs and market scenarios. Exergy was accounted for in Publication V by minimizing steam throttling: Turbine valve control action contributes to exergy destruction in eq. (4) due to the increase in specific entropy, but it is also essential for achieving fast load changes. Relevant examples for Publications I and II were provided recently by Jin, Zhao, and Zheng (2016), and Luo, Wang, Guo, Liu, and Zheng (2015), who employed a dynamic exergy analysis framework for comparing control setups and operating modes for the oxy-fired boiler, ASU and CCU + CPU units.

4.4 Dynamics and control performance

Dynamic performance evaluation focuses on optimizing system responses directly, including CV setpoint tracking, CV disturbance rejection and MV trajectories. Performance is evaluated by analyzing closed-loop responses during specified setpoint changes and disturbances or by generating a system with beneficial open-loop dynamics. The approach is thus based on data or dynamic simulation, and the focus is typically on regulative control performance rather than optimizing control.

The closed-loop approach relies on norms and time integrals for CV and MV signals (Skogestad & Postlethwaite, 2005). Setpoint tracking is usually evaluated in ICPD through the integral square error (ISE), the integral absolute error (IAE) or time-weighted IAE and ISE formats (Ogata, 2010; Ogunnaike & Ray, 1994). Notably, Ulbig and Andersson (2015) defined custom dynamic response measures for power system operational flexibility, which were applied by Zhao et al. (2018a, 2018b) to simulated boiler responses. In Publications III and V, electrical power and main steam pressure setpoint tracking were evaluated with the ISE, eq. (6).

$$ISE = \int_0^\Theta |y(t) - z(t)|^2 dt, \tag{6}$$

where y is the output, z is the reference signal, t is time, and Θ is the time range.

Closed-loop disturbance rejection properties include metrics like the MV and CV variances, the MV change rate, the maximum setpoint deviation, the minimum and maximum MV magnitudes, and the idle index (Hovd, Ma, & Braatz, 2003; Jelali, 2006; Lee et al., 1972). In general, control performance can be evaluated based on MV signals by comparing the closed-loop system either to an ideal MV benchmark or an ideally tuned feedback controller. MV benchmarks can be divided further into variance-based methods (e.g., Harris index modifications) and advanced benchmarks, such as those based on linear quadratic Gaussian control.

50

Specifying the investigated disturbance scenarios is an essential part of closed-loop evaluation. An example was provided for load-following boilers by Gonzalez-Salazar et al. (2018), who outlined a set of standard disturbance types for variable-load cyclic operation. In this thesis, the setpoint change magnitudes and rates of load transitions were based on boiler design requirements and in-house data.

When ICPD focuses on open-loop responses, the design assumes that fast and simple MV–CV dynamics contribute to good control performance and enable effective controller tuning. Dynamics can be evaluated from step responses by calculating rise times, settling times, time constants, time delays, overshoots, and inverse response magnitudes (Ogunnaike & Ray, 1994). A more quantitative approach is to compare the response to a suitable low-order linear time-invariant (LTI) model (Hernjak et al., 2004). Another open-loop approach is to evaluate the magnitude of disturbances that can be rejected with available control reserves, back-calculated from simulations or first-principles theory. This approach was used in Publication V by monitoring the saturation time of the turbine valve.

Dynamic analysis is the most direct way of quantifying control performance, which makes it a key tool for load-following CFB boiler ICPD design. However, the design also depends heavily on the chosen simulation scenarios. This includes the examined time range (Fig. 10), which should be short enough to focus on the transition, but long enough to ensure that the new setpoint is maintained. The latter issue can be mitigated by monitoring state derivatives at the end of the time range (Bahri et al., 1996) or through closed-loop stability evaluation (cf. section 4.5).
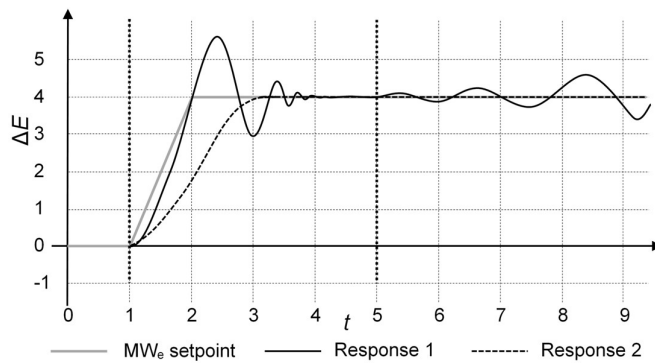
Fig. 10. Conceptual figure of two electrical power (*E*) setpoint ramp responses, where the ISE has been optimized between 1 s and 5 s. The chosen time range results in an unstable system for response 1, and similar ISE values for responses 1 and 2.

Another limitation for measures like the ISE is that they do not explicitly account for the response shape, as any setpoint deviation adds to the error norm value. This can lead to tightly controlled systems with large overshoots, slow integral action, and oscillation. Different responses can produce the same ISE value (Fig. 10), which contributes to the formation of local optima (Schweiger & Floudas, 1998).

4.5 System analysis

System analysis aims at generating processes with inherent properties that are favorable for control, and control systems that contribute to good dynamic performance. Basic approaches rely on concepts from classical control design and are largely based on LTI process descriptions such as transfer function, state-space, frequency response, or impulse response models (Ogunnaike & Ray, 1994; Skogestad & Postlethwaite, 2005). More advanced concepts make use of nonlinear models and dynamic optimization to evaluate performance measures.

   System analysis concepts that are common in ICPD are listed in subsection 4.5.1. The focus is on controllability, which was used as a control structure selection criterion in Publications IV and V, and a design objective in Publications III and V. The relevant system analysis tools for this thesis are discussed in subsection 4.5.2.

   The benefit of system analysis performance evaluation is that it enables the efficient quantification of control-relevant system properties that are difficult to describe through other means. However, methods based on steady-state or linear dynamic analysis may be unsuitable, especially for a wide process operating region, and more advanced nonlinear approaches have elevated computational costs. The connection between performance measure values and the desired system behavior (e.g., economics) is also often not straightforward (Sakizlis et al., 2004; Yuan et al., 2012). Lastly, analysis methods typically only provide a relative ranking of solutions or indicate the existence of control problems (Perkins & Walsh, 1996).

4.5.1 Concepts

Controllability is defined in various ways in the literature (Skogestad & Postlethwaite, 2005). Originally, it was specified as the ability of the process to achieve and maintain a desired equilibrium value (Ziegler & Nichols, 1943). Rosenbrock (1970) later generalized it for all specified control aims, including the evaluation of the degree of controllability. Common controllability definitions are

52

listed below. Integral and input–output controllability were the main forms of controllability considered in this thesis.

– **Input–output controllability:** A system is input–output controllable if it is able to keep outputs $y(t)$ within specified bounds or displacements from their references $z(t)$ despite unknown bounded disturbances and dynamic variations, using available inputs $u(t)$ and measurements (Skogestad, 1994). This has to be verified through multiple criteria (Skogestad & Postlethwaite, 2005).

– **Integral controllability & integrity:** A system is integral controllable if there exists a controller with integral action, $1/s \cdot c(s)$, which will make the system "unconditionally" stable ("internal" stability, detuning of loops is possible). Integrity requires that the closed-loop system remains internally stable when any combination of loops is opened. Together, these concepts form the definitions of ICI and DIC (Campo & Morari, 1994; Chiu & Arkun, 1990). A system is integral controllable with integrity (ICI) if it remains stable when all loops (with integral control action) are detuned by the same factor between 0 and 1. Decentralized integral controllability (DIC) further demands that all loops can be detuned by individual factors.

– **Functional controllability:** A system is functionally controllable if given any suitable output vector $y(t)$, there exists an input vector $u(t)$ ($t > 0$) that generates $y(t)$ from the initial condition $x(0) = 0$ (Rosenbrock, 1970). Controllability can be verified by requiring that the normal rank of the process transfer function matrix (cf. subsection 4.5.2) must equal the amount of outputs $y(t)$.

– **State controllability:** The system $x'(t) = \mathbf{A}x(t) + \mathbf{B}u(t)$, $y(t) = \mathbf{C}x(t) + \mathbf{D}u(t)$ is state controllable if for any initial state $x(0) = x_0$, any time $t_1 > 0$, and any final state x_1, there exists an input $u(t)$ that produces $x(t_1) = x_1$ (Kalman, 1960). While commonly used in control theory, state controllability has limitations in practice (Perkins, 1989; Skogestad & Postlethwaite, 2005). It is verified by evaluating whether the rank of the controllability matrix $[\mathbf{B}, \mathbf{AB}, \dots, \mathbf{A}^{n-1}\mathbf{B}]$ equals the length of the state vector, n. State observability is defined analogously: a system is observable if knowledge of its past inputs $u(t)$ and outputs $y(t)$ between $0 < t < t_1$ fully determines its initial state $x(0) = x_0$. In this case, the rank of the observability matrix $[\mathbf{C}^T, (\mathbf{CA})^T, \dots, (\mathbf{CA}^{n-1})^T]^T$ is n.

– **Structural controllability:** The system $x'(t) = \mathbf{A}x(t) + \mathbf{B}u(t)$ is structurally controllable if there exists a structurally equivalent system (same locations of fixed zero and non-zero matrix entries) to the pair $(\mathbf{A}, \mathbf{B})$ that is controllable (Shields & Pearson, 1976).

Beside controllability, the related concepts of resiliency, flexibility, switchability, and operability have a central role in ICPD performance evaluation (Burnak et al., 2019b; Jørgensen et al., 1999). Dynamic resiliency is defined as the dynamic capability of the process to recover from disturbances quickly and smoothly (Grossmann, Calfa, & Garcia-Herreros, 2014; Weitz & Lewin, 1996). Essentially, it determines the upper bound for the achievable closed-loop performance independent of controller type, originally obtained through internal model control. The main properties that limit plant resiliency are non-minimum phase behavior (time delays, right-half plane zeros), MV constraints, and plant-model mismatch.

Flexibility, switchability, and operability are typically evaluated through optimization. Flexibility is the ability of the process to attain feasible operation at different operating points over a range of uncertainties and disturbances (Grossmann et al., 2014; Mohideen et al., 1996; Koller & Ricardez-Sandoval, 2017), and it has been defined for both steady-state and dynamic operation. The analysis consists of a flexibility test and a flexibility index. The flexibility test maximizes the minimum deviation from the process active constraints, whereas the flexibility index maximizes the largest deviation that can be handled by the system.

Switchability is the ability of the process to move feasibly, effectively, and safely between operating points (Perkins, 1989; Vu, Bahri, & Romagnoli, 1997; White, Perkins, & Espie, 1996). It consists of feasibility and optimality evaluation for the dynamic switch trajectory. Typically, the control signal trajectory is optimized, with CV setpoint tracking error measures as objectives, cf. section 4.3.

Operability is the ability of the closed-loop process to satisfy steady-state and dynamic requirements in the presence of expected disturbances without violating process constraints, using available input MVs (Bahri et al., 1996; Perkins, 1989). It contains aspects of controllability, resiliency, flexibility, and switchability. Operability analysis is usually set up as a dynamic optimization problem. In addition, approaches based on geometric operational input/output regions are notable in ICPD research (Georgakis, Vinson, Subramanian, & Uztürk, 2004).

Like controllability, process stability is defined in various ways (Åström & Murray, 2008; Ogata, 2010; Ogunnaike & Ray, 1994). A common definition is Lyapunov stability for a solution $x(t; x_0)$ to a differential equation system with initial condition x_0. The solution is stable if, for all distances $v > 0$ and times $t > 0$, there exists a distance $\psi > 0$ for which $\|x(t; x_1) - x(t; x_0)\| < v$, when $\|x_1 - x_0\| < \psi$ (Åström & Murray, 2008). Further conditions are defined for asymptotical stability, stability within a domain, and global stability. Stable LTI components do not contain hidden unstable modes, and the injection of bounded external signals at any point in the

54

system results in bounded outputs in the entire system, designated as "internal" stability (Skogestad & Postlethwaite, 2005). Some ICPD approaches are based on the concept of passivity, which guarantees asymptotically stable flowsheets as combinations of passive systems (Jørgensen et al., 1999; Sharifzadeh, 2013).

Process nonlinearity signifies the degree to which the process dynamics deviate from linear responses. Formally, linearity can be verified through three conditions (Åström & Murray, 2008): output linearity in the initial condition response (input is zero), output linearity in the forced response (initial condition is zero), and input superposition. Control nonlinearity can be inherent (e.g., saturation, dead zone, hysteresis), or it can be introduced intentionally for the control design (Ogata, 2010). Nonlinearity analysis is used in ICPD to assess control limitations, control design challenges, problematic process operating modes, and the applicability of linear system analysis methods (Jelali, 2006; Schweickhardt & Allgöwer, 2004).

Robustness is defined as insensitiveness to model uncertainty and plant/model mismatch (Åström & Murray, 2008; Skogestad & Postlethwaite, 2005). Robustness consists of robust stability and robust performance. Robust stability guarantees that the system remains stable for a defined uncertainty set, and robust performance guarantees that all desired performance criteria are satisfied for the uncertainty set.

4.5.2 Methods and tools

Many classical control methods have been used in ICPD for quantifying the concepts described in subsection 4.5.1. These include Nyquist and Bode plots, root locus and pole/zero analysis, H_2 and H_∞ norms, stability criteria (e.g., Routh, Hurwitz), Lyapunov functions, and the v-gap metric. These methods are well-documented in the control literature and are not elaborated on here (e.g., Åström & Murray, 2008; Ogata, 2010; Ogunnaike & Ray, 1994; Skogestad & Postlethwaite, 2005). Process nonlinearity can be quantified by comparing a response to a corresponding linear operator, e.g., through error norms. Various nonlinearity-centric ICPD approaches have been devised (Sharifzadeh, 2013), where control-relevant nonlinearity (Schweickhardt & Allgöwer, 2004) and nonlinear controllability analysis through bifurcations (Jørgensen et al., 1999; Morari, 1992) can be highlighted.

Of the linear approaches, five connected methods are often employed in ICPD: eigenvalues, singular values, the condition number, sensitivity functions, and the relative gain array. These methods are used to examine input–output controllability, resiliency, high- and low-gain parameter/disturbance directions, stability,

robustness, and loop interactions (Engell et al., 2004; Morari, 1992; Perkins, 1989; Skogestad & Postlethwaite, 2005; van de Wal & de Jager, 2001). For their calculation, the MIMO process is described as a matrix of LTI models between system MVs and CVs in the static domain (steady-state gains), eq. (7), or in the dynamic domain for multiple frequencies (transfer functions), eq. (8).

$$\mathbf{G} = \begin{bmatrix} g_{11} & \cdots & g_{1n} \\ \vdots & \ddots & \vdots \\ g_{m1} & \cdots & g_{mn} \end{bmatrix} = \begin{bmatrix} \frac{y_1(0)}{u_1(0)} & \cdots & \frac{y_1(0)}{u_n(0)} \\ \vdots & \ddots & \vdots \\ \frac{y_m(0)}{u_1(0)} & \cdots & \frac{y_m(0)}{u_n(0)} \end{bmatrix}, \tag{7}$$

$$\mathbf{G}(s) = \begin{bmatrix} h_{11}(s) & \cdots & h_{1n}(s) \\ \vdots & \ddots & \vdots \\ h_{m1}(s) & \cdots & h_{mn}(s) \end{bmatrix} = \begin{bmatrix} \frac{y_1(s)}{u_1(s)} & \cdots & \frac{y_1(s)}{u_n(s)} \\ \vdots & \ddots & \vdots \\ \frac{y_m(s)}{u_1(s)} & \cdots & \frac{y_m(s)}{u_n(s)} \end{bmatrix}, \tag{8}$$

where $\mathbf{G}$ is the process gain matrix, $\mathbf{G}(s)$ is the process transfer matrix with Laplace operator s, g_{yu} are the static gains between output y and input u, $h_{yu}(s)$ are the transfer functions between y and u, and m and n are the total amounts of y and u.

State and transfer matrix eigenvalues are used for analyzing dominant process directions, and large eigenvalue variations imply parameter and input sensitivity. The singular value decomposition of $\mathbf{G}(s)$ determines how close the process is to being singular, and it addresses some of the shortcomings of eigenvalue analysis (Skogestad & Postlethwaite, 2005). The process condition number is the ratio between the minimum and maximum singular value. A large condition number can signify that the plant is ill-conditioned, which can manifest itself as correlated CVs or as similar effects of various MVs on the CVs. The sensitivity functions of $\mathbf{G}(s)$ are used for analyzing the changes in input–output sensitivity caused by feedback and interactions. As the relative gain array is a central method in this thesis, it is discussed next in greater detail. While relative gain methods are most commonly used for selecting control structures between MVs and CVs, authors like Jacobsen and Skogestad (1991) also employed them more directly for guiding process design.

Relative gain methods are derived from the static relative gain array, the RGA (Bristol, 1966). The basic RGA is defined as eq. (9) for square systems with an equal number of MVs (columns) and CVs (rows), although it can also be generalized for non-square plants (Skogestad & Postlethwaite, 2005). The RGA is scaling invariant and forms row/column sums of ones. The RGA contains interaction terms λ_{yu} that signify how much MV–CV open-loop gains change due to interactions in the multi-loop system, cf. Publication IV.

56

$$\text{RGA}(\mathbf{G}) = \mathbf{G} \times (\mathbf{G}^{-1})^{\mathrm{T}} = \begin{bmatrix} \lambda_{11} & \cdots & \lambda_{1n} \\ \vdots & \ddots & \vdots \\ \lambda_{m1} & \cdots & \lambda_{mn} \end{bmatrix}, \tag{9}$$

where λ_{yu} are relative gains between outputs y and inputs u (total amounts m and n), and "×" signifies an element-by-element multiplication.

Each control structure with its MV–CV connections is characterized by its λ_{yu} elements, which can also be combined into one measure with the RGA number, eq. (10). λ_{yu} values close to 1 are good and signify minimal loop interaction. Negative λ_{yu} are to be avoided due to gain sign change. Small positive λ_{yu} are poor, as there is a gain increase when other loops are closed. For λ_{yu} larger than 1, the open-loop gain is dampened in the closed-loop system. Large λ_{yu} values (above 10) require large controller gains and may indicate ill-conditioning in the system.

$$nRGA(\mathbf{G}) = \|\text{RGA}(\mathbf{G}) - \mathbf{I}\|_{\mathrm{N}}, \tag{10}$$

where $nRGA$ is the relative gain number, $\mathbf{I}$ is the identity matrix, and "N" indicates a chosen norm. The sum of diagonal elements or the absolute sum were used as "N" in the thesis, cf. Publications IV and V.

Several modifications have been proposed for the static RGA to mitigate some of its shortcomings for practical problems (Sharifzadeh, 2013). The most important is the dynamic RGA (DRGA) for multiple frequencies. Frequency range DRGA examination has also been streamlined by combining static gains with specific frequencies (Xiong, Cai, & He, 2005) or with integrated dynamic response metrics (He, Cai, Ni, & Xie, 2009; Jain & Babu, 2015; Luo, Cao, & Xu, 2016). The block relative gain (BRG) is an RGA generalization for block-decentralized control (Manousiouthakis, Savage, & Arkun, 1986), which is useful in large MV–CV systems. RGA evaluation for uncertain systems has been studied by Kariwala, Skogestad, and Forbes (2006), for example. Exergy-based RGA methods have been proposed as ecoefficiency tools by Montelongo-Luna, Svrcek, and Young (2011), and Munir, Yu, and Young (2013). The available RGA modifications influenced the selection of relative gain methods in Publications III–V. To account for control-relevant high-frequency interactions and partial control in large systems, the DRGA, the performance relative gain array (PRGA), the closed-loop disturbance gain (CLDG), and the partial relative gain (PRG) were chosen for the ICPD procedure (cf. section 5.4). In addition, the Niederlinski index (NI) was used to ensure the stability of selected control structures (Chiu & Arkun, 1990; Häggblom, 1997b).

Lastly, system analysis also contains methods for flowsheet structural analysis, most notably degrees of freedom (DOF) evaluation. DOF signify the amount of

independent MVs available for managing CVs. As a performance measure, they indicate how the flowsheet structure affects the possibilities to control and optimize the process. Further distinctions have been made for design (DDOF), control (CDOF), and steady-state degrees of freedom (Luyben, 1996; Larsson & Skogestad, 2000; Sharifzadeh, 2013). CDOF were considered in Publications I and IV. They account for disturbances by subtracting the number of external variables from the DOF, which corresponds to the available MVs for control (Skogestad, 2004).

4.6   Summary of chosen approach for CFB ICPD

This section summarizes how the approaches from sections 4.1–4.5 are used in the ICPD procedure and how they were implemented in Publications I–V. The ICPD procedure employs a combination of simulation-based dynamic performance, controllability, and first-principles qualitative objectives:

–   **Electrical power setpoint tracking:** The setpoint tracking for the electrical power is the main objective, measured as the ISE error over simulated load change ramps, as described in Publication V.
–   **Main steam quality setpoint tracking:** The secondary objective is to reject main steam quality disturbances that result from MW_e control, evaluated with the ISE for the main steam pressure, as described in Publications III and V.
–   **Disturbance rejection capacity:** Steam path design aims at improving the rejection of unplanned MW_e disturbances during load changes. In Publication V, this objective was specified through MV signal saturation and the CLDG.
–   **Controllability:** The PRG, DRGA, PRGA, and CLDG methods are used in the procedure as measures for interactions and controllability in control structure selection (Publications IV and V) and ICPD process design (Publications III and V).
–   **CDOF analysis:** Control degrees of freedom analysis is used for evaluating the influence of process configurations on control (Publication I) and for plant-wide control design (Publication IV).
–   **Exergy efficiency:** The minimization of destroyed exergy is an objective for steam throttling, implemented indirectly for the turbine valve in Publication V.
–   **Flue gas CO_2:** The maximization of the flue gas CO_2 concentration is a static or low-frequency environmental goal for oxy-combustion, as described in Publications I and II.

58

5 ICPD procedure

This chapter presents the simulation-based ICPD procedure that is proposed for CFB boilers. The design tools from Publications I–V are combined into a hierarchy of steps for obtaining the closed-loop boiler flowsheet from design data. The procedure is listed below, and a more detailed decomposition for step 3 is given in Publication V. As summarized in section 3.5, the hybrid approach employs both process knowledge and mathematical programming ICPD, and each design step focuses on different objectives from section 4.6. The purpose of Chapter 5 is to form guidelines for applying the chosen tools to general CFB boiler problems.

1. Simulator-based pre-design
   1.1. Control-oriented qualitative process analysis (Publication I)
   – CFB process analysis with detailed industrial simulators: How are dynamics and control affected by parameter and flowsheet changes?
   – First-principles parameter analysis & transition scenario simulations.
   1.2. Model-based state estimation (Publication II)
   – Refinement of simulator-based analysis with experimental data.
   – Unscented Kalman filter (UKF) nonlinear state estimation.
   1.3. Control degrees of freedom (CDOF) analysis (Publications I and IV)
   – Selection of MVs and CVs for decentralized control structure.
   – Evaluation of control possibilities based on process structure.
   – Evaluation of throughput manipulator (TPM) dynamics for MW_e control.
2. Control structure & interaction analysis (Publications III–V)
   – Relative gain analysis with different methods and for multiple frequencies.
   – Selection of control connections between MVs and CVs.
   – Variable interaction analysis for ensuring process controllability.
3. ICPD optimization (Publications III and V)
   – Optimization of process and controller parameters together in the defined closed-loop plant structure from steps 1 and 2.
   – Closed-loop dynamic optimization for timeseries, e.g., load ramp tests.
   – Objective: Minimization of MW_e setpoint tracking error together with secondary objectives (weighted single-objective optimization).
4. Design result validation against relevant reference cases (Publication V)

This chapter is structured as follows. Section 5.1 presents the CFB boiler modeling guidelines and industrial case studies that were used throughout the thesis. In section 5.2, the process knowledge oriented design of the CFB hotloop is discussed,

along with the plant-wide CDOF analysis (steps 1.1 and 1.3). Section 5.3 presents the UKF state estimation analysis (step 1.2). Section 5.4 deals with the relative gain analysis (step 2), and section 5.5 presents the ICPD optimization setup (step 3).

5.1 CFB boiler systems and models

The selection of suitable modeling approaches for each design step is a crucial prerequisite for the simulation-based ICPD procedure, as also noted by e.g., Mitsos et al. (2018), and Rafiei and Ricardez-Sandoval (2020b). This section presents the CFB process models from Publications I–V to demonstrate what kind of models are needed when applying the procedure to CFB boiler problems. For this purpose, the industrial case studies of Publications I–V are also summarized here (Table 3), with more specific test matrices in sections 5.2–5.5. Two modeling approaches can be defined: industrial simulators for detailed analysis (subsection 5.1.1), and "design" models that are used directly by the ICPD algorithms (subsection 5.1.2).

Table 3. Summary of all CFB boiler case study simulations in Publications I–V.

Target system and tests	Plant scale	Model	Publications
Air/oxy-fired CFB combustor	Pilot		
Open-loop dynamic simulation	<100 kW$_{th}$	First-principles simulator	I
State estimation		First-principles simulator	II
Closed-loop simulation		First-principles simulator	Hultgren et al. (2015)
Relative gain analysis		Black-box identified static	Hultgren et al. (2015)
OTU-CFB power plant	Industrial		
CDOF analysis	>200 MW$_e$	First-principles simulator	IV
Open-loop step testing		First-principles simulator	IV
Relative gain analysis		Black-box identified dynamic	IV
Drum CFB steam path	Industrial		
ICPD optimization	>100 MW$_e$	Physical design model	III, V
Relative gain analysis		Physical design model	III, V

5.1.1 CFB power plant simulator

First-principles detailed simulators are used in the pre-analysis stage of the ICPD procedure (step 1) for transition simulations and state estimation, as well as for generating design models in step 2. The aim of the thesis was to utilize existing simulators and data from industry to a maximal extent for these steps. The main limitation for the industrial models is set by the state estimation computational load

in step 1.2, as the full simulator is used directly as the UKF internal model in the ICPD procedure. Another requirement is that process parameters of interest must be directly adjustable in the simulator, meaning that even complex black-box models (e.g., MV–CV neural networks) are undesirable.

A dynamic CFB power plant simulator was obtained for the ICPD pre-analysis from the Sumitomo SHI FW company. The simulator had previously been validated for various CFB project deliveries by the company (Kovács et al., 2012), including the plants studied in this thesis. The simulator was implemented in the commercial APROS 5 software, with a separate hotloop block in Matlab/Simulink. The hotloop block was studied in Publications I and II, and the full simulator in Publication IV.

The hotloop block (Ritvanen et al., 2012) was a 1-D model (Fig. 11), where the furnace (furn), separator (sep), and return leg (rleg) were modeled as ideally mixed connected calculation elements (e.g., 20 elements for the furnace), containing mass and energy differential balance equations. A combined energy equation was defined for element temperatures, and the hydrodynamics, density profile, and heat transfer were evaluated using empirical and semi-empirical correlations. The combustion reactions of carbon, hydrogen, and sulfur were considered in the model.
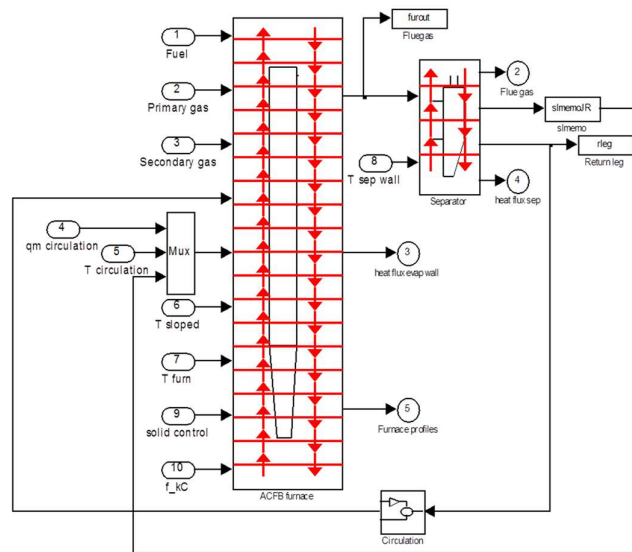
Fig. 11. Hotloop model of the pilot CFB case study. qm and f_kC are the circulation and reactivity parameters (Publication I, adapted with permission from Elsevier).

The main case study for the hotloop model in Publications I and II was an air-/oxy-fired pilot CFB combustor. The fuel power was 20–50 kW$_{th}$ in air mode and 50–100 kW$_{th}$ in oxy mode, with anthracite (1–2 fractions) and petcoke as fuel. The model inputs consisted of the fuel mass flow, oxidant mass flows (mixture of air, pure O$_2$ and RFG), and water-wall temperature parameters for the furnace and the separator. The outputs contained the flue gas flow (mass, composition, temperature), furnace profiles (temperature, density, gas velocity), and the hotloop heat fluxes, which were evaluated iteratively with the wall temperatures in the full simulator.

The main power plant simulator contained sub-models for the water-steam path and the flue gas path in APROS. The full simulator was implemented for a condensing OTU-CFB power plant (Benson steam cycle, one coal fuel fraction) in a range of several hundred megawatts (Fig. 12). Process units beyond the turbine or the flue gas duct were not considered in this work. Unit dimensions and operating conditions for different load levels were obtained from in-house data.
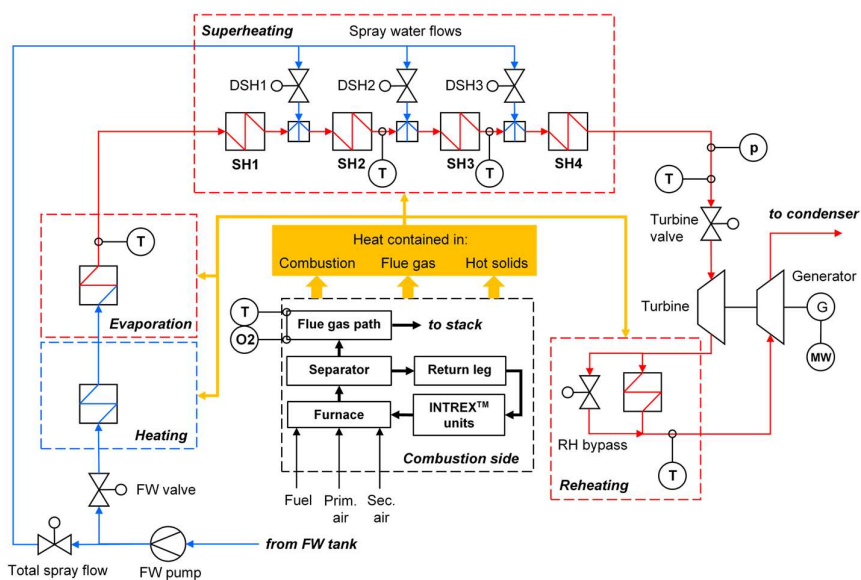
Fig. 12. Schematic figure of the OTU-CFB simulator flowsheet (Publication IV, reprinted with permission. Copyright 2017 American Chemical Society).

In APROS, thermal hydraulics are simulated based on the dynamic conservation equations of mass, momentum, and energy, which are discretized in time and solved

through implicit or semi-implicit integration (Hänninen & Ylijoki, 2008). Process units are divided into control volumes, where mass and energy equations are solved in the middle of the volume, and momentum equations at the border. The OTU-CFB simulator consisted of standard APROS process units (heat exchangers, valves, turbines, etc.), with various correlations for heat transfer and wall friction (cf. Publication IV). Fluid compositions were calculated in a separate elementary layer.

5.1.2 CFB design models

The CFB design model approach proposed in this thesis was illustrated in the case studies of Publications III–V. Simplified internal models are needed in the ICPD procedure especially for the ICPD optimization in step 3, but also for frequency response evaluation in control design step 2. Design models should provide a good computational performance for a large number of simulations, but also have a generic modeling approach that is applicable to different CFB boiler case studies.

Design models are generated in two ways in the ICPD procedure. In the main approach, the process is described as a series of low-order dynamic elements, which are directly derived from first-principles process parameters and describe the relevant dynamics of the ICPD problem. The secondary approach is more conventional, where black-box MV–CV transfer functions are identified from responses that are simulated with the first-principles models described in subsection 5.1.1. Both approaches enable a significant increase in computational performance, at the cost of modeling accuracy and a more restricted validity region.

The main design model approach of connected elements was demonstrated in Publications III and V for the steam path of an industrial drum CFB boiler in the range of >100 MW$_e$. Evaporator and superheater units were modeled as lumped storages of steam, consisting of a storage coefficient equation and a pressure drop equation (Doležal & Varcop, 1970; Smith, 2005). The boiler thermal inertia was modeled as a first order + delay block, and the turbine sections as first-order steam storage blocks. As detailed drum water-steam dynamics were not modeled, this storage model approach can also be applied to OTU boiler case studies.

The overall steam path model, shown in Fig. 13, was formed by combining the low-order unit elements. The model was calibrated for a feasible region around the 80% load level based on design data from Sumitomo SHI FW. Transfer function matrices could then be formed analytically from Fig. 13 for the main unit master control variables, eq. (11), and for DSH mass flow disturbances, eq. (12). The

coefficients α_{mn}, β_{mn}, γ_{mn}, δ_{mn}, ε_{mn}, ζ_{mn}, η_{mn}, θ_{mn}, and κ_{mn} in eqs. (11)–(12), as well as the notation to Fig. 13, are provided in Publication V and are not repeated here.

Fig. 13. CFB steam path design model schematic chart (Publication V, reprinted with permission from Elsevier).

$$\begin{bmatrix} \dfrac{p(s)}{L(s)} & \dfrac{p(s)}{v(s)} \\ \dfrac{E(s)}{L(s)} & \dfrac{E(s)}{v(s)} \end{bmatrix} =$$

$$\begin{bmatrix} e^{-t_I s}\dfrac{\alpha_{11}}{s^4+\beta_{11}s^3+\gamma_{11}s^2+\delta_{11}s+\varepsilon_{11}} & \dfrac{-\alpha_{12}s^2-\beta_{12}s-\gamma_{12}}{s^3+\delta_{12}s^2+\varepsilon_{12}s+\zeta_{12}} \\ e^{-t_I s}\dfrac{\alpha_{21}s+\beta_{21}}{s^6+\gamma_{21}s^5+\delta_{21}s^4+\varepsilon_{21}s^3+\zeta_{21}s^2+\eta_{21}s+\theta_{21}} & \dfrac{\alpha_{22}s^4+\beta_{22}s^3+\gamma_{22}s^2+\delta_{22}s}{s^5+\varepsilon_{22}s^4+\zeta_{22}s^3+\eta_{22}s^2+\theta_{22}s+\kappa_{22}} \end{bmatrix}, \quad (11)$$

$$\begin{bmatrix} \dfrac{p(s)}{d(s)} \\ \dfrac{E(s)}{d(s)} \end{bmatrix} = \begin{bmatrix} \dfrac{\alpha_{d1}s^2+\beta_{d1}s+\gamma_{d1}}{s^3+\delta_{d1}s^2+\varepsilon_{d1}s+\zeta_{d1}} \\ \dfrac{\alpha_{d2}s^3+\beta_{d2}s^2+\gamma_{d2}s+\delta_{d2}}{s^5+\varepsilon_{d2}s^4+\zeta_{d2}s^3+\eta_{d2}s^2+\theta_{d2}s+\kappa_{d2}} \end{bmatrix}, \quad (12)$$

where p is the main steam pressure, E is the electrical power, L is the firing power, v is the turbine valve position, d is the DSH mass flow, and t_I is the thermal inertia time delay.

The black-box modeling approach was used in Publication IV, where a transfer function matrix $\mathbf{G}(s)$, eq. (8), was identified between selected MVs and CVs (cf. subsection 5.2.2) of the full OTU-CFB simulator. The MVs were altered one at a time with ±5–10% steps from the 95% load operating point, while keeping other MVs constant. All responses could be modeled adequately with first- or second-order LTI models: fit percentages were mostly above 90%, and even for moderate fits the general response shape could be replicated well. The process static gain matrix, eq. (7), was obtained from $\mathbf{G}(s)$ at zero frequency, $\mathbf{G}(0)$.

64

5.2 First-principles process analysis and simulation

In the pre-analysis stage of the ICPD procedure (step 1), the CFB boiler is examined through simulations and model analysis on a first-principles basis. The purpose is to integrate the boiler dynamics into the early process design, generate data for the control design and parameter optimization steps 2 and 3, and answer qualitative design questions that would be challenging to address later in the ICPD procedure. The analysis focuses on open-loop dynamics, MV effects, and control connections, and it enables more informed process design decisions for fast load changes.

A pre-analysis was performed in Publications I and IV, where the simulator from subsection 5.1.1 was investigated based on its structure and operating conditions. Structural analysis highlights how the flowsheet design affects process dynamics and control. Operating conditions focus on how specific parameters and states influence control performance in a fixed flowsheet. In this thesis, operating conditions were analyzed qualitatively through dynamic simulation for the oxy-CFB hotloop (subsection 5.2.1). The flowsheet structure was examined for the full OTU-CFB simulator through degrees of freedom analysis (subsection 5.2.2).

5.2.1 Qualitative dynamic analysis

The purpose of the qualitative analysis in ICPD step 1.1 is to discover how a proposed boiler design affects control and load changes in the CFB, with the aim of defining the first-principles reasons for the observed dynamic behavior. Firstly, the chemical/physical properties of the industrial simulator are analyzed based on the theory to connect them to the process dynamics. Secondly, extensive dynamic simulation is carried out to examine how changes in these properties affect specified performance goals. The analysis approach is inherently comparative, where the investigated process is compared to a similar "default" open-loop process.

Publication I focused on comparing air- and oxy-combustion in the CFB hotloop. This case study presented a clear design task for load-following boilers: How should the process and control design of an air-fired CFB be modified to maintain or improve load change performance in oxy mode? Based on the first-principles theory, it was discovered that most of the changes in the oxy-CFB related to operating conditions resulted from the modified combustion atmosphere: CO_2 replaced N_2 as the main gas flow component, and minor components became concentrated due to flue gas recirculation. Another aspect is the possibility to use

varying oxidant O_2 percentages in the gas feed (oxidant O_2 enrichment). Based on these findings, the following questions could be formulated for the pre-analysis:

– Are heat exchanger (static) loads affected by the atmosphere?
– Are hotloop open-loop dynamics affected by the atmosphere?
– Is the fluidization in the furnace bed affected by the atmosphere?
– How does oxidant O_2 enrichment influence hotloop design and control?
– How does the flue gas recirculation modify the open-loop dynamics?

To answer these questions, the open-loop simulation campaign shown in Table 4 was conducted for the pilot combustor model of subsection 5.1.1, with setpoints and operating conditions from the real plant.

Table 4. Test matrix for the air/oxy-fired pilot CFB simulations in Publication I; an elevated oxidant O_2 content was used in oxy mode.

Simulation scenario	Modified flows (others constant)	Modification
Load step tests		
Air mode steps	Fuel, air	Multiple +/– step changes
Oxy mode steps	Fuel, pure O_2, RFG	Multiple +/– step changes
Oxy mode load ramp tests		
Slow ramps	Fuel, pure O_2, RFG	One +/– ramp change from full load
Fast ramps	Fuel, pure O_2, RFG	One +/– ramp change from full load, 3X faster ramp rate
Transitions from air to oxy mode		
"Direct" switch	Fuel, air, pure O_2, RFG	Air –; fuel/pure O_2/RFG + (Fig. 14)
"Sequenced" switch	Fuel, air, pure O_2, RFG	Air –; fuel/pure O_2/RFG + (Fig. 15)
RFG rate tests in oxy mode		
RFG steps	RFG	RFG step changes, approx. +12% – 24% + 12% to total oxidant
Fuel step, constant RFG levels	Fuel, three RFG levels	Fuel –10%; RFG flow at 80%/100%/120% of nominal

The simulations focused on the transitions between air and oxy mode, as they are relevant especially for early generation dual-fired boilers. The "direct" (Fig. 14) and "sequenced" (Fig. 15) switching schemes were compared for the air to oxy mode transitions. Additionally, the control solutions derived in Publication I were tested with the same simulator in the supporting publication by Hultgren et al. (2015), using adequately tuned PID controllers. The reported results included a fuel disturbance (–10%) with flue gas O_2 control, oxidant O_2 percentage setpoint changes with flue gas and oxidant O_2 control, and furnace profile simulations for

different primary/secondary oxidant O_2 percentages. In all scenarios of Table 4, the following output variables were monitored:

- Furnace: temperature in elements 1–20, dense bed density (2 elements), freeboard density (2 elements), grid gas velocity, freeboard gas velocity.
- Flue gas/primary oxidant gas/secondary oxidant gas: O_2 vol%, CO_2 vol%, H_2O vol%, temperature, density.
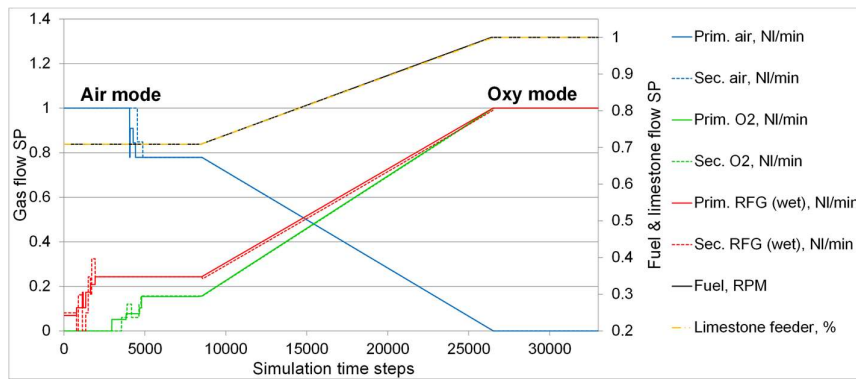
Fig. 14. Direct switching scheme from air to oxy mode (Publication I, reprinted with permission from Elsevier).
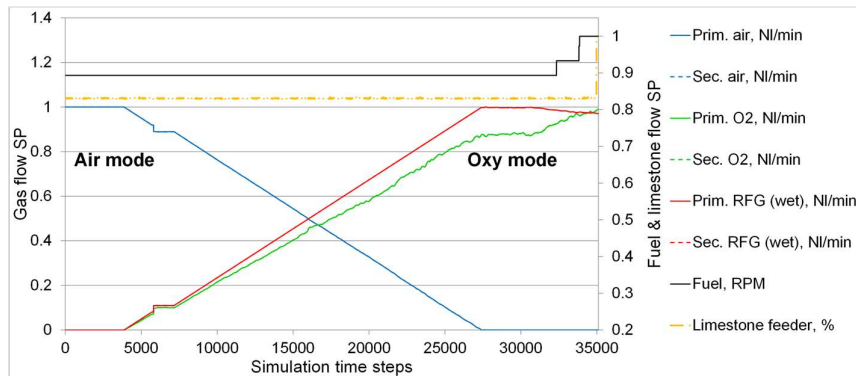
Fig. 15. Sequenced switching scheme from air to oxy mode (Publication I, reprinted with permission from Elsevier).

5.2.2 Degrees of freedom

The degrees of freedom (DOF) analysis (cf. subsection 4.5.2) is performed in step 1.3 of the ICPD procedure for two purposes. The first is to identify how process structural changes affect the control possibilities. This analysis was performed qualitatively for air- and oxy-firing in Publication I. The structural differences were restricted to the oxidant gas streams, as the work only concerned the CFB hotloop:

– Does splitting the oxidant gas inputs into four components (primary/secondary RFG, primary/secondary pure O_2) require an altered oxidant gas control setup?
– Do the separate oxidant flows generate new possibilities for boiler control?

The second purpose of DOF analysis is to generate data for the control structure selection in step 2, mainly for the selection of MVs and CVs. The control degrees of freedom (CDOF) are evaluated for this purpose using the method of Murthy Konda, Rangaiah, and Krishnaswamy (2006), where the CDOF is obtained by comparing the total amount of material/energy streams to the amount of restrained and redundant streams, eq. (13). The restraining number shows how many streams are determined by other streams. Redundancy results from variables that are either self-regulating or sufficiently controlled through the control of other variables.

$$\text{CDOF} = n_{\text{streams}} - \Sigma_{\text{units}}(n_{\text{restrained}} + n_{\text{redundant}}), \qquad (13)$$

where n and its subscripts are the stream amounts: total, restrained, and redundant.

The CDOF were evaluated in Publication IV for the OTU-CFB simulator (Fig. 12). The combustion and flue gas side CDOF are detailed in Table 5, which also adds the bed limestone feed and the Intrex air flow to the results of Publication IV.

Table 5. Combustion and flue gas path CDOF, expanded from Publication IV.

Process section and unit	Process unit type	Streams in + out	Connection streams	Restraining number	Redundant streams
Hotloop		12		2	2
Furnace	Reactor with heat flows	5 + 3	1	0	
Cyclone	Splitter	1 + 2	1	1	
Intrex	HE without inventory	2 + 2	1	1	
Flue gas path		3		3	0
Duct section 1	HE without inventory	1 + 1	1	1	
Duct section 2	HE without inventory	1 + 1	1	1	
Duct section 3	HE without inventory	1 + 1	1	1	
SUM		15		5	2
CDOF	8				

In the analysis shown in Table 5, redundancy resulted from flue gas pressure control and a constant solid material circulation rate. Heat exchangers (HE) were assumed to have a constant inventory, except for the furnace. This analysis is expanded for oxy-combustion in subsection 6.1.2. Similarly to the combustion path, the water-steam path CDOF are expanded from Publication IV and shown in Table 6.

Table 6. Water-steam path CDOF, expanded from Publication IV.

Process section and unit	Process unit type	Streams in + out	Connecting streams	Restraining number	Redundant streams
Feedwater feed		6		4	0
FW pump	Pump	1 + 1	0	1	
EVAP/DSH split	Splitter	1 + 2	1	1	
Main DSH valve	Valve	1 + 1	1	1	
FW valve	Valve	1 + 1	1	1	
Pre-heating		1		1	0
ECO	HE without inventory	1 + 1	1	1	
Evaporation		1		0	0
Evaporator	HE with inventory	1 + 1	1	0	
Superheating		13		7	6
Main DSH split	Splitter	1 + 3	1	1	
DSH1 valve	Valve	1 + 1	1	1	
DSH2 valve	Valve	1 + 1	1	1	
DSH3 valve	Valve	1 + 1	1	1	
Superheater 1	HE with inventory	1 + 1	1	0	
DSH1 spray	Mixer	2 + 1	2	1	
Superheater 2	HE with inventory	1 + 1	1	0	
DSH2 spray	Mixer	2 + 1	2	1	
Superheater 3	HE with inventory	1 + 1	1	0	
DSH3 spray	Mixer	2 + 1	2	1	
Superheater 4	HE with inventory	1 + 1	1	0	
Turbine		3		3	0
Turbine valve	Valve	1 + 1	1	1	
HP turbine	Compressor	1 + 1	1	1	
LP turbine	Compressor	1 + 1	1	1	
Reheating		5		3	2
RH bypass split	Splitter	1 + 2	1	1	
RH bypass valve	Valve	1 + 1	1	1	
Reheater	HE with inventory	1 + 1	1	0	
RH bypass mix	Mixer	2 + 1	2	1	
SUM		29		18	8
CDOF	3				

In Table 6, all of the heat exchangers except for the ECO (liquid phase preheater) were defined as units with pressure changes, with redundancy from main steam and condenser pressure control. The streams and restraining numbers of the combustion side HE units (Table 5) are not repeated in Table 6. The feedwater pump and HP/LP turbine were evaluated without separate input/output energy streams.

The analysis resulted in 11 CDOF, and 9 CDOF remained without the Intrex air and limestone input flows in Table 5. MVs were chosen based on these CDOF in Publication IV: the FW flow, turbine valve position (T.valve), DSH flows 1–3, the reheater bypass valve position (RHvalve), fuel flow, and prim./sec. oxidant flows. Three combined MVs were also formed: "firing power" (fuel + airs), "boiler load" (fuel + airs + FW), and "total DSH flow" (DSH1 + DSH2 + DSH3). Potential CVs were chosen based on section 2.3: the electrical power, main steam pressure, main steam temperature, EVAP steam temperature, SH2 and SH3 steam temperatures, RH steam temperature, flue gas temperature, and flue gas O_2 content.

The third design task in ICPD step 1.3 is to analyze the candidates for throughput manipulator (TPM) variables in the system. The TPM can be defined as the control degree of freedom that is used to regulate the throughput in the primary process path (Price, Lyman, & Georgakis, 1994). In the load-following boiler, throughput is determined by the generated electrical power. Three MVs were identified in Publication IV as TPM candidates for the OTU-CFB power plant: the turbine valve, the firing power (fuel + air), and the feedwater flow. The open-loop dynamics of these variables were evaluated in the supplementary material of Publication IV based on step responses, cf. subsection 5.1.2. The responses were quantified for the main steam pressure and temperature, the evaporator temperature, and the electrical power CVs based on properties from section 4.4:

– **Rise time:** Time between 10% and 90% of the response magnitude.
– **Settling time:** Time to reach ±2% region around the new steady-state.
– **Time delay:** Time after MV step change before the CV changes.

5.3 Simulator-based state estimation

Unscented Kalman filter (UKF) state estimation is used in step 1.2 of the ICPD procedure to refine the analysis results from step 1.1. The main purpose is to adapt the parameters and nominal input signals of the industrial dynamic simulator with experimental data. Bayesian filters, such as the UKF, enable the effective use of uncertain process data for this task, which supports the overall goal of improving

the utilization of existing data and models for ICPD. The secondary purpose is to examine discrepancies between measured and simulated data that cannot be linked to reported process states or inputs, i.e., to test hypotheses for observed process behavior. On the whole, both purposes contribute to improved simulator predictions and thus to more informed process design decisions in the ICPD pre-analysis.

The UKF was applied to the oxy-CFB hotloop in Publication II to extend the process analysis from Publication I. A UKF tool was implemented for the hotloop model shown in subsection 5.1.1, and the tool was used for two case studies to illustrate how the UKF can be utilized in the ICPD procedure. The UKF algorithm is summarized in subsection 5.3.1 and the case study test matrix in subsection 5.3.2.

Publication II constitutes the first proper application of the UKF filter for CFB boiler analysis. Previously, Ikonen et al. (2012) and Ikonen, Kovács, and Ritvanen (2013) employed nonlinear particle filter state estimation for the CFB hotloop, including brief considerations about the applicability of the UKF. The linearized extended Kalman filter has been used more frequently for fluidized bed boilers (e.g., Bardelli et al., 1994; Bittanti et al., 1996). For other power plants, the UKF was applied to the commonly used Åström-Bell drum boiler model by Arasu, Prakash, and Prasad (2013), for example. In contrast to this low-dimensional state-space model, a detailed simulator with 855 and 660 states was used in Publication II for the case studies. Only a subset of these states was considered uncertain, however.

5.3.1 Unscented Kalman filter

Bayesian filters form estimates and predictions of evolving states and parameters, given the process dynamics and uncertain data (Särkkä, 2013). The estimation constructs a representation of an unknown vector of random states through its posterior probability density function (pdf) based on measured data. Bayesian filtering consists of prediction, eq. (14), and update, eqs. (15)–(16), operations.

$$p(x_k|\mathbf{Y}_{k-1}) = \int p(x_k|x_{k-1})\, p(x_{k-1}|\mathbf{Y}_{k-1}) dx_{k-1}, \qquad (14)$$
$$p(x_k|\mathbf{Y}_k) = p(y_k|x_k) p(x_k|\mathbf{Y}_{k-1})/p(y_k|\mathbf{Y}_{k-1}), \qquad (15)$$
$$p(y_k|\mathbf{Y}_{k-1}) = \int p(y_k|x_k)\, p(x_k|\mathbf{Y}_{k-1}) dx_k, \qquad (16)$$

where k is the sampling instance, x is the state vector, y is the output vector, $\mathbf{Y}_k$ contains all output measurements up to k, and $p(i|j)$ is the pdf of event i, given j.

The utilized Bayesian algorithm depends on the assumptions made about the system and defines how eqs. (14)–(16) can be solved (Daum, 2005). The most common approaches are the linear Kalman filter and the extended Kalman filter.

Nonlinear algorithms (Patwardhan, Narasimhan, Jagadeesan, Gopaluni, & Shah, 2012) like the unscented Kalman filter (UKF) and particle filter methods enable the direct use of a nonlinear system model without linearization. With the UKF, the full hotloop simulator could thus be directly implemented in Publication II as the state equation f_{ss} in eq. (17), while maintaining an acceptable computational load.

$$\begin{cases} x(k+1) = f_{ss}(x(k), u(k), c_{ss}(k)) \\ y(k) = w_{ss}(x(k), u(k)) + d_{ss}(k) \end{cases},$$
(17)

where f_{ss} is the state equation, w_{ss} is the measurement equation, u is the process input vector, c_{ss} is the state noise vector and d_{ss} is the measurement noise vector.

The UKF algorithm (Julier & Uhlmann, 1997) was described in Publication II, where the scaled UKF formulation was used (van der Merwe, Doucet, de Freitas, & Wan, 2000). In short, the unscented transform, eq. (18), is used to approximate the state distribution with "sigma" points $\mathcal{X}$, driven through eq. (17) to obtain $\mathcal{X}_{k+1|k}$ and the transformed measurements Υ_{k+1}. The predicted mean and covariance of the states ($\bar{x}_{k+1|k}$ and $C_{k+1|k}$) and the measurements ($\bar{y}_{k+1}$ and C_{yy}) are estimated from $\mathcal{X}_{k+1|k}$ and $\Upsilon_{k+1|k}$. The posterior state mean and covariance are obtained from new measurements y_{k+1} in the measurement update through eq. (19).

$$\begin{cases} \mathcal{X}_0 = \bar{x} \\ \mathcal{X}_i = \bar{x} + \left(\sqrt{(n_x + \lambda)C_x}\right)_i, i = 1, \dots, n_x \\ \mathcal{X}_i = \bar{x} - \left(\sqrt{(n_x + \lambda)C_x}\right)_i, i = n_x + 1, \dots, 2n_x \\ \lambda = \alpha^2(n_x + \kappa) - n_x \end{cases},$$
(18)

$$\begin{cases} \bar{x}_{k+1} = \bar{x}_{k+1|k} + K_{k+1}(y_{k+1} - \bar{y}_{k+1}) \\ C_{k+1} = C_{k+1|k} - K_{k+1}C_{yy}K_{k+1}^T \end{cases},$$
(19)

where $\mathcal{X}_i$ is the sigma point i, $\bar{x}$ is the state vector mean, $\bar{y}$ is the measurement vector mean, C is the covariance of states (x) and measurements (yy), n_x is the state vector dimension, α and κ are parameters in the scaled unscented transform, and K is the UKF Kalman gain, calculated from C_{yy} and the x–y cross-correlation matrix.

5.3.2 Target system and test matrix

The UKF tool was used in Publication II to explore potential disturbances and parameter variations related to observed outputs in the oxy-CFB pilot combustor. For scale-up purposes, the tool was also implemented for a medium-scale air-fired CFB power plant, with a similar validated hotloop model from Sumitomo SHI FW.

72

Dynamic measurement data was supplied for both plants by the company, and the data was compared to simulations with similar input flows and operating conditions.

The data for the pilot CFB case study consisted of three oxy-fired load ramp sets (fuel + oxidant flows, ramped at the same speed): slow 15% ramps, fast 15% ramps, and slow 30% ramps. The state estimation was used to investigate whether variations in the reported fuel flows (three fractions) and the hotloop air leakage could have caused the differences observed between the measured and simulated flue gas CO_2 and O_2 percentages, which were used as measurements in eq. (17).

The industrial CFB case study contained primary air tests (±6% steps) and load change tests (±8% steps). One of the furnace heat transfer coefficients and the fuel moisture content were estimated using the UKF to explain the differences observed between the measured and simulated flue gas O_2 content and furnace temperature values. These process states were used as measurements for the state estimation.

5.4   Control structure selection and interaction analysis

The main purpose of the relative gain analysis in the ICPD procedure is to select the control structure between the MVs and CVs from the DOF analysis in step 1.3. This forms the closed-loop process structure for the subsequent ICPD optimization stage. The secondary purpose is to support the qualitative process design in step 1 by evaluating the effect of open-loop parameters on variable interactions and controllability. In this approach, the design ensures that control connections and design parameter changes do not contribute to performance-limiting interactions.

The relative gain analysis approach of the thesis was defined in Publication IV (Fig. 16) and is summarized in subsection 5.4.1 to facilitate its application to boiler ICPD problems. The approach expands on the standard literature by considering multiple relative gain methods and control tasks as a stepwise procedure. Control structures are first analyzed at zero frequency through a full partial relative gain (PRG) analysis in order to establish integral controllability with integrity (ICI, cf. subsection 4.5.1). Next, ICI structures and non-ICI structures with fast electrical power control (from the TPM analysis, cf. subsection 5.2.2) are studied at higher frequencies to determine how the observed interactions are altered in the dynamic domain. The dynamic analysis was carried out using the dynamic relative gain array (DRGA) in Publications III and IV, while the performance relative gain array (PRGA) and closed-loop disturbance gain (CLDG) were used in Publication V, as they are more relevant for control performance limiting interactions. In the stepwise analysis, MV–CV sets of increasing size are examined separately with the chosen

relative gain methods. The purpose is to highlight interactions associated with specific control tasks.
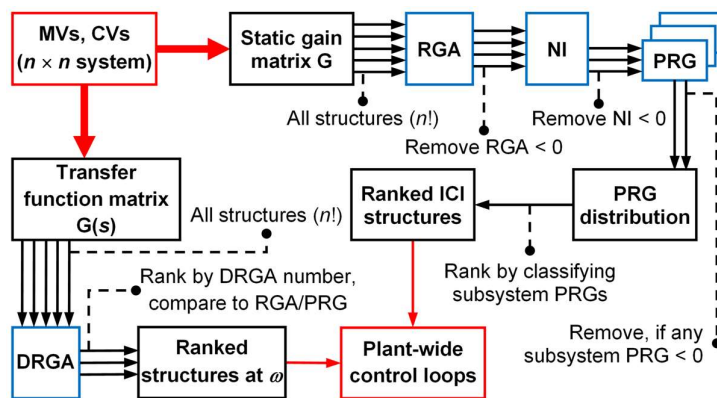
Fig. 16. Relative gain control structure selection and analysis procedure (Publication IV, reprinted with permission. Copyright 2017 American Chemical Society).

The control structure selection procedure was implemented for the OTU-CFB simulator (Fig. 12) in Publication IV, and dynamic relative gain tools were used for ICPD process design in Publications III and V. These results have been extended for oxy-combustion by Hultgren et al. (2015) and Niva et al. (2017), who performed static ICI PRG analysis on the oxy-CFB hotloop shown in Fig. 11. Detailed relative gain analysis for multiple frequencies and MV–CV systems had not been applied to a plant-wide steam power plant flowsheet prior to Publication IV, where past references on the topic were listed. Additional references include DRGA and NI analysis of a small drum model (Balko & Rosinová, 2015), DRGA analysis of pulverized fuel boiler unit master control (Sun et al., 2017), DRGA analysis of fluidized bed boiler combustion control (Wu et al., 2020), control structure design for individual heat exchanger sections of a steam path based on a non-square RGA formulation (Chandrasekharan, Panda, Swaminathan, & Panda, 2018), and flue gas recirculation setup selection based on the static RGA and the NI (Luo et al., 2015).

5.4.1 Relative gain methods

A full PRG analysis is based on the PRG matrix (Häggblom, 1997a, 1997b). The PRG extends the RGA for partially controlled systems, where specific loops are

74

closed under integral control. The PRG, eq. (20), is evaluated at zero frequency by applying eq. (9) to the partial subsystem $\bar{\mathbf{G}}_{mn}$. $\bar{\mathbf{G}}_{mn}$ can be obtained from $\mathbf{G}$ in eq. (7) by applying eq. (21) to all closed MV–CV control connections.

$$\text{PRG}_{mn}(\mathbf{G}) = \text{RGA}(\bar{\mathbf{G}}_{mn}) = \bar{\mathbf{G}}_{mn} \times (\bar{\mathbf{G}}_{mn}^{-1})^{\text{T}}, \tag{20}$$

$$\bar{\mathbf{G}}_{mn} = \mathbf{G}(y_{\text{o}}, u_{\text{o}}) - \mathbf{G}(y_{\text{o}}, u_{\text{c}}) \cdot \mathbf{G}(y_{\text{c}}, u_{\text{c}})^{-1} \cdot \mathbf{G}(y_{\text{c}}, u_{\text{o}}), \tag{21}$$

where $\mathbf{G}$ is the process gain matrix, $\bar{\mathbf{G}}_{mn}$ is the partial subsystem gain matrix with loops y_{c}–u_{c} closed (CV and MV indices "m" and "n"), and "o" denotes open loops.

In the full PRG analysis of the thesis, the PRG is calculated for all possible partial subsystems of a control structure. The analysis reveals whether any of these PRG matrices contain infeasible elements or whether large relative gain changes occur under partial control. In Publication IV, control structures were ranked based on the amount of beneficial and unwanted PRG elements in all subsystems.

As outlined in Publication IV, conditions for ICI controllability can be formed based on the PRG (Häggblom, 1997a, 1997b). $\mathbf{G}$ is ICI controllable if all control connection RGA elements and all control connection PRG elements in all partially controlled subsystems $\bar{\mathbf{G}}_{mn}$ are positive. If the Niederlinski index (cf. subsection 4.5.2) in eq. (22) is positive, checking 2×2 subsystems is redundant.

$$\text{NI} = \det(\mathbf{G})/\det(\hat{\mathbf{G}}), \tag{22}$$

where $\hat{\mathbf{G}}$ is obtained by setting to zero all elements of $\mathbf{G}$ that do not correspond to an input–output pairing in a block-decentralized control structure.

The DRGA (Skogestad & Postlethwaite, 2005) is obtained by applying the RGA definition in eq. (9) to the process transfer matrix $\mathbf{G}(s)$, eq. (8), at multiple frequencies. The DRGA was calculated using eq. (23) from the system frequency responses in Publications III and IV.

$$\text{DRGA}(\mathbf{G}(s)) = \mathbf{H}(j\omega) \times (\mathbf{H}(j\omega)^{-1})^{\text{T}} = \begin{bmatrix} a_{11} + b_{11}j & \cdots & a_{1n} + b_{1n}j \\ \vdots & \ddots & \vdots \\ a_{m1} + b_{m1}j & \cdots & a_{mn} + b_{mn}j \end{bmatrix}, \tag{23}$$

where $\mathbf{G}(s)$ is the process transfer matrix, $\mathbf{H}(j\omega)$ is the frequency response matrix, and a_{yu} and b_{yu} are the real and complex terms of the DRGA elements between output y and input u, total amounts m and n.

The PRGA, eq. (24), extends the DRGA for one-way interactions and control performance (Skogestad & Postlethwaite, 2005). It is evaluated separately for each control structure, where control connections are on the diagonal, and off-diagonal elements signify performance-limiting interactions, which should be minimized.

$$\boldsymbol{\Gamma}(s) = \hat{\mathbf{G}}(s) \cdot \overline{\mathbf{G}}(s)^{-1} = \begin{bmatrix} \frac{\tilde{y}_1(s)}{\tilde{u}_{c1}(s)} & \cdots & 0 \\ \vdots & \ddots & \vdots \\ 0 & \cdots & \frac{\tilde{y}_m(s)}{\tilde{u}_{cm}(s)} \end{bmatrix} \cdot \begin{bmatrix} \frac{\tilde{y}_1(s)}{\tilde{u}_1(s)} & \cdots & \frac{\tilde{y}_1(s)}{\tilde{u}_n(s)} \\ \vdots & \ddots & \vdots \\ \frac{\tilde{y}_m(s)}{\tilde{u}_1(s)} & \cdots & \frac{\tilde{y}_m(s)}{\tilde{u}_n(s)} \end{bmatrix}^{-1},$$

(24)

where $\boldsymbol{\Gamma}(s)$ is the PRGA, $\overline{\mathbf{G}}(s)$ is the scaled process transfer matrix with scaled inputs $\tilde{u}$ and outputs $\tilde{y}$ (total amounts n and m), and $\hat{\mathbf{G}}(s)$ is the scaled diagonal transfer matrix of the control connections ($\tilde{u}_{ci}$ is the input for controlling output "i").

DRGA and PRGA elements were presented for multiple frequencies as absolute magnitudes in Publications IV and V. Control structure ranking was simplified by using the RGA number, eq. (10), which is shown for the DRGA in eq. (25).

$$nDRGA(\mathbf{H}(j\omega)) = ||DRGA(\mathbf{H}(j\omega)) - \mathbf{I}||_N,$$

(25)

where $nDRGA$ is the dynamic relative gain number and $\mathbf{I}$ is the identity matrix.

The CLDG, eq. (26), represents the apparent gains from disturbances to CVs when control loops are closed (Skogestad & Postlethwaite, 2005). It is evaluated separately for each control structure. In order to minimize the effect of disturbances on CVs, the control structure CLDG elements should be small, preferably smaller than the frequency response magnitudes of the corresponding MV–CV connections.

$$\hat{\mathbf{G}}_{\mathrm{d}}(s) = \boldsymbol{\Gamma}(s) \cdot \overline{\mathbf{G}}_{\mathrm{d}}(s),$$

(26)

where $\hat{\mathbf{G}}_{\mathrm{d}}(s)$ is the CLDG and $\overline{\mathbf{G}}_{\mathrm{d}}(s)$ is the scaled disturbance–CV transfer matrix.

PRG, DRGA, and PRGA elements can be classified based on the principles listed in subsection 4.5.2: values close to 1 are ideal, negative values are infeasible, and small and large values should be avoided. More detailed classes were devised in Publication IV: <0, 0–0.1, 0.1–0.5, 0.5–0.85, 0.85–1.2, 1.2–5, 5–10, and >10. These classes are used in the ICPD procedure.

5.4.2 Target system and test matrix

The control structure was selected for the OTU-CFB in Publication IV based on the procedure illustrated in Fig. 16. The PRG and DRGA were calculated for the MVs and CVs listed in subsection 5.2.2, using the process static gain and transfer function matrices that were generated in subsection 5.1.2. Frequency responses were obtained from Matlab for the DRGA evaluation, and the 0–0.5 rad/s range was chosen based on typical load disturbance ramps. Four MV–CV systems were

considered in the stepwise analysis, focusing on the main CVs (case 1), steam temperature control (case 2), combustion and steam generation (case 3), and the plant-wide system (case 4).

The MV–CV sets of the OTU-CFB are listed in Table 7. In the scope of this thesis, replacing the DRGA analysis in Publication IV with the PRGA and CLDG represents the final template for step 2 in the ICPD procedure. Therefore, the unit master control setup was selected in Publication V for the CFB steam path model (Fig. 13) based on the PRGA and the CLDG, as PRG analysis was not necessary for the 2×2 system. The PRGA and CLDG were evaluated at 0–0.5 rad/s for eqs. (11)–(12), and appropriate scaling was applied to the MVs (turbine valve, firing power), CVs (electrical power, steam pressure), and disturbances (DSH flow).

Table 7. MVs and CVs of Publication IV control structure analysis cases 1–4.

Variable	Unit	Case 1	Case 2	Case 3	Case 4
Manipulated input (MV)					
Turbine valve	%	X	X	X	X
Feedwater flow	kg/h			X	X
Fuel flow	kg/h			X	
Firing power	% of nominal				X
Boiler load	% of nominal	X	X		
Primary air flow	kg/h			X	
Secondary air flow	kg/h			X	X
DSH1 flow	kg/h		X		X
DSH2 flow	kg/h		X		X
DSH3 flow	kg/h		X		X
Total DSH flow	kg/h	X		X	
RH bypass valve	%				X
Controlled output (CV)					
Output electrical power	MW	X	X	X	X
Main steam pressure	bar	X	X	X	X
Main steam temperature	°C	X	X	X	X
Temperature after SH2	°C		X		X
Temperature after SH3	°C		X		X
Temperature after EVAP	°C			X	X
Temperature after RH	°C				X
Flue gas temperature	°C			X	
Flue gas O_2 content	vol%			X	X

The steam path model was also studied with the DRGA in publication III. The aim was to discover how the evaporator and superheater steam storage parameters

influenced control loop interactions during load changes. Boiler-following PI control was defined for the 2×2 MV–CV system, and the DRGA was evaluated at a frequency of 0–0.2 rad/s. Three storage values were tested (nominal, +100% evaporator/+200% superheater, –70% evaporator/–80% superheater), and the resulting changes in the DRGA magnitudes were recorded. These parameter values were then tested for a controlled triangular ±5% electrical power setpoint ramp, and the setpoint tracking performance was compared to the DRGA values.

5.5 Simultaneous ICPD optimization

Dynamic optimization of the closed-loop process is performed in step 3 of the ICPD procedure. The purpose is to find values for the open-loop CFB boiler parameters that were identified in step 1, together with optimal tunings for the controllers in the control structure from step 2. The parameter values are chosen to optimize electrical power tracking for specified load change requirements, while maintaining additional secondary design goals for the process and the control signal.

The ICPD optimization approach was specified in Publication V based on the literature review in Publication III. The approach is briefly described in this section to facilitate the implementation of the ICPD procedure. Subsection 5.5.1 introduces the problem setup, and subsections 5.5.2 and 5.5.3 elaborate on the optimization objective and algorithm. The optimization was applied to the industrial CFB steam path in Publication V, and this case study is summarized in subsection 5.5.4.

5.5.1 Problem formulation

The ICPD problem was formulated in Publication V as the fully simultaneous dynamic optimization of continuous process and controller parameters for simulated closed-loop electrical power setpoint ramps. The load ramp speeds and magnitudes were based on the boiler design criteria, and the simulation time window length was chosen so that the settling of all CV responses was guaranteed. Controllability evaluation was also included in the optimization for the expected MW_e disturbance frequencies to ensure that optimal solutions did not result in uncontrollable systems.

In total, the ICPD problem was defined as eqs. (27)–(28). This setup forms the guideline for step 3 of the ICPD procedure. During the optimization, load changes are simulated for the calculation of objective J with the internal model of the algorithm, generated through the connected element approach of subsection 5.1.2.

78

$$\min_{X,U} J(y(t), u(t), X, U),\qquad(27)$$

$$\begin{cases} \xi(x'(t), x(t), u(t), X) = 0 \\ \quad \xi_0(x(0), u(0), X) = 0 \\ \quad \mu(y(t), x(t), u(t)) = 0 \\ \delta(u'(t), u(t), X, U) \leq 0 \\ \quad \varphi(y(t), u(t), U) = 0 \\ \quad \sigma(y(j\omega), u(j\omega), X) = 0 \\ \qquad t\epsilon[0, \Theta] \\ \qquad \omega\epsilon[0, \Omega] \end{cases},\qquad(28)$$

where J is the optimization objective, t is time, $[0,\Theta]$ is the simulated time range, ω is frequency, $[0,\Omega]$ is the analyzed frequency range, x are state variables, u are input variables, X are process design parameters, U are controller design parameters, ξ are open-loop process equations with initial conditions ξ_0, δ are process inequality constraints, φ are controller equations, y are output variables, μ are measurement equations for obtaining y, and σ are controllability equations.

5.5.2 Objective function

The optimization objective was constructed in Publication V as a weighted single-objective function based on section 4.6. This forms the default setup for load-following CFB boiler ICPD problems in this thesis. Function J is set up around the electrical power control performance during the simulated load change, augmented with additional objectives according to eqs. (29)–(30).

$$J = \frac{1}{j_{n1}}j_1 + \frac{1}{j_{n2}}j_2 + \frac{1}{j_{n3}}j_3 + \frac{1}{j_{n4}}j_4 + \frac{1}{j_{n5}}j_5 + \frac{1}{j_{n6}}j_6,\qquad(29)$$

$$\begin{cases} j_1 = \int_0^\Theta \left(p(t) - z_p(t)\right)^2 dt \\ j_2 = 10 \cdot \int_0^\Theta \left(E(t) - z_E(t)\right)^2 dt \\ j_3 = -2 \cdot v(0) \cdot \int_0^\Theta v(t)\, dt \\ j_4 = \int_0^\Theta |v(t) - \max(v(t), v_{\min})|\, dt + \int_0^\Theta |v(t) - \min(v(t), v_{\max})|\, dt \\ j_5 = \int_0^\Omega ||\Gamma(\mathbf{H}(j\omega)) - \mathbf{I}||_N\, d\omega \\ j_6 = 2 \cdot \int_0^\Omega \Sigma |\widehat{\mathbf{G}}_d(j\omega)|\, d\omega \end{cases},$$

(30)

where J is the ICPD objective, j_i is an individual objective i with nominal value j_{ni}, p is pressure, E is electrical power, z_i is the setpoint of output i, $v_{\min}$ and $v_{\max}$ are the

minimum and maximum bounds of turbine valve signal v, $\boldsymbol{\Gamma}$ is the PRGA, $\mathbf{H}$ is the frequency response matrix, $\mathbf{I}$ is the identity matrix and $\hat{\mathbf{G}}_d$ is the CLDG.

Objectives j_1 and j_2 are the ISE error terms (cf. section 4.4) for the main steam pressure and electrical power. The electrical power term j_2 has the largest weight as it is the main objective. The weighting of steam pressure objective j_1 depends on the operating mode of the boiler (constant or sliding pressure, cf. section 2.2).

Objectives j_3 and j_4 are specified for fast turbine valve control action. Since the electrical power output can be altered quickly with the steam control reserve, the capacity to reject unplanned additional MW_e disturbances during load changes can be maximized by minimizing turbine valve saturation, j_4. However, as constraining the steam flow also contributes to exergy destruction (cf. section 4.3), turbine valve action should be limited, especially during steady-state operation, resulting in j_3.

Objectives j_5 and j_6 are the objectives for input–output and disturbance controllability, respectively. j_5 is measured as the "PRGA number" by applying eq. (25) to eq. (24). j_6 consists of the integral sum of all terms in the CLDG matrix, eq. (26). Both terms are integrated over the investigated frequency range.

A single objective was chosen over a multi-objective approach for the ICPD optimization in Publication V to enable a ranking of solutions without additional decision criteria. For this approach, objectives j_1–j_6 were scaled by dividing them by their nominal values j_{n1}–j_{n6}, which were calculated by simulating the target load changes with nominal process parameters and feasible controller tunings. This approach enables a percentage-wise comparison of objectives, where the effect of improved load change performance on other objectives can conveniently be observed. This general approach is proposed for the ICPD procedure in this thesis.

5.5.3 Optimization algorithm

The ICPD optimization was carried out using a hybrid two-level algorithm in Publication V to locate a global optimum for multiple parameters with good computational performance. On the upper level, feasible solution regions were mapped through a global random search with a wide search space and limited iterations. On the lower level, the located regions were refined using a faster local algorithm. Both levels used the same problem formulation, eqs. (27)–(30).

The upper level algorithm was the genetic algorithm (Goldberg, 1989) of Matlab 2017. In the algorithm, a population of solutions evolves towards a global optimum, where solutions are either passed on as elites or modified through

crossover and mutation operations. In Publication V, the genetic algorithm search consisted of a maximum of 50 rounds and a population of 500 units.

The lower level was a modified version of the Nelder-Mead simplex search (Lagarias, Reeds, Wright, & Wright, 1998) of Matlab 2017. In this approach, a simplex of solution points is modified through reflection, expansion, contraction, or shrink operations during the optimization. The modified algorithm enabled the use of minimum and maximum bounds, as well as periodic simplex reinitialization to avoid local optima.

5.5.4 Target system and test matrix

The ICPD optimization was performed in Publication V for the CFB boiler steam path (Fig. 13). The aim was to optimize the evaporator/superheater mass storage distribution and steam throttling (process targets) together with the boiler unit master controller parameters (control targets) for electrical power setpoint ramps from partial load to full load, where PID controllers had been applied to the control structure from ICPD step 2. The optimized parameters are listed in Table 8. While the combustion side was not included in Publication V, the case study represents a template for simultaneous load-following CFB design. Preliminary tests were also performed in Publication III, where only the steam pressure tracking was optimized by adjusting the superheater storage and the PID parameters.

Table 8. Process and controller parameters for ICPD design (Publication V, adapted with permission from Elsevier).

Parameter	Name	Min	Max
Total steam storages	τ_{TOT}	0.42	1.69
Evaporator storage percentage of τ_{TOT}	q_E	0.97	1.25
Storage percentage before DSH of SH storage	q_{S1}	0.20	1.80
Turbine valve nominal position	$\bar{v}$	0.73	1.22
Steam p gain, P	P_p	0.00	5.20
Steam p integrator, I	I_p	0.01	36944.30
Steam p derivator, D	D_p	0.00	12.17
Steam p derivative filter, N	N_p	0.00	1991.49
Output E gain, P	P_E	0.02	114.04
Output E integrator, I	I_E	0.00	3873.03

The optimization was conducted separately for four load change scenarios, with the same ramping speed for the electrical power and the steam pressure in sliding-

pressure mode (Table 9). The scenarios corresponded to planned load transitions (slow 15% ramps) and unexpected electrical power disturbances (fast 5% ramps). The starting point for the ramps was the 80% load level of the power plant.

Table 9. Load change scenarios optimized through ICPD (Publication V, adapted with permission from Elsevier).

Load change scenario	E setpoint %	Ramp time steps	Ramp speed %MW/step	p setpoint %
I: Fast constant-pressure	+5	13	0.385	0
II: Slow constant-pressure	+15	210	0.07	0
III: Fast sliding-pressure	+5	13	0.385	+5
IV: Slow sliding-pressure	+15	210	0.07	+15

The time window of one simulation was 3750 time steps after the load ramp, and objectives j_1–j_4 were integrated over this range. Objectives j_5 and j_6 were evaluated for the 0–0.5 rad/s range, using Matlab frequency responses. Suggested solutions were verified through closed-loop simulations with the steam path model and benchmarked against cases where only the PID parameters were optimized.

6 CFB boiler ICPD design results

This chapter summarizes the main results of Publications I–V and their significance for the CFB boiler ICPD procedure. The results validated the chosen design and analysis methods as being suitable for ICPD. The results also established the methods for the CFB boiler process, as many of them had not been applied to fluidized bed power plants in the existing research literature. As a whole, the results also provided new guidelines for CFB boiler process and control design research.

Section 6.1 discusses the simulation-based design results for the oxy-CFB (Publication I). Section 6.2 shows the hotloop state estimation results (Publication II). Section 6.3 gives an overview of the relative gain results for the OTU-CFB control structure selection (Publication IV) and the CFB steam path process design (Publication III). Section 6.4 discusses the simultaneous steam path optimization (Publications III and V). Finally, section 6.5 presents considerations based on the results for applying the ICPD procedure to generic CFB power plant problems.

6.1 Simulation-based process analysis

The simulations and first-principles analysis in Publication I revealed that oxy-combustion affects dynamics and control in the CFB in three main ways: by altering the combustion atmosphere, through flue gas recirculation dynamics, and by modifying the control degrees of freedom (CDOF). Publication I also listed several additional effects that are not discussed here. Subsection 6.1.1 deals with the first two categories, while subsection 6.1.2 examines the CDOF effects. Some of the control structures of subsection 6.1.2 were also studied by Hultgren et al. (2015) through closed-loop simulations. Subsection 6.1.3 discusses the air to oxy switch simulations, with the aim of evaluating how transitions between air and oxy mode should be made. In addition, the open-loop response analysis of the OTU-CFB throughput manipulator variables (TPM) from Publication IV is discussed in subsection 6.1.4.

6.1.1 Combustion atmosphere & recirculation dynamics

In Publication I, it was established how the elevated CO_2 and H_2O content of the oxidant and the flue gas in oxy mode led to elevated gas heat capacities (CO_2, H_2O) and densities (CO_2) compared to air-firing. The specific heat capacity elevation resulted in slower heat flux and temperature responses in oxy mode compared to

air mode. This could clearly be seen from the load step simulations in Fig. 17 and can also be derived through first-principles dynamics. The slower response in the heat transfer needs to be considered for process unit sizing and controller tuning in load-following power plants. For static operating points, the heat capacity contributes to lowered furnace temperatures and shifts in heat exchanger loads.
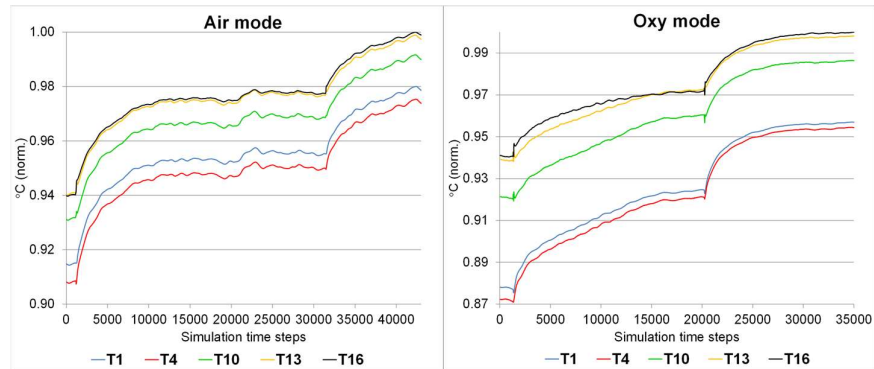

Fig. 17. Normalized furnace temperature responses to two consecutive air and oxy load steps (Publication I, reprinted with permission from Elsevier).

Publication I explained how the lower temperature levels can be compensated in oxy mode through oxidant O_2 enrichment, i.e., an oxidant O_2 content higher than that of air. In retrofit and dual-fired boilers, the combustion conditions should be similar to air-firing, which would require an increased oxidant O_2 content and fuel firing power to match the gas specific heat capacity elevation. In oxy greenfield plants, the oxidant O_2 content can be elevated even further, leading to significantly different hotloop and flue gas path designs with higher temperatures and smaller gas flows for added efficiency.

The oxidant and flue gas densities influence the fluidization in the oxy-CFB furnace compared to air-firing. At constant oxidant mass flow, the density increase leads to a reduced volumetric flowrate and thus a decreased fluidization velocity. This was verified from simulations and theory. In Publication I, it was suggested that the density change should be compensated with a constant oxidant volumetric flowrate during air to oxy transitions to maintain the fluidization velocity.

Using RFG as the main oxidant gas component in the oxy-CFB (instead of air) introduces recirculation dynamics for oxidant and flue gas composition responses, unlike air-firing. The effect of the flue gas recirculation rate on the gas composition

84

responses could be seen from the simulations illustrated in Fig. 18. This outcome mainly needs to be considered for the open-loop dynamics and controller design, as the steady-state flue gas composition is largely unaffected by the recycle.
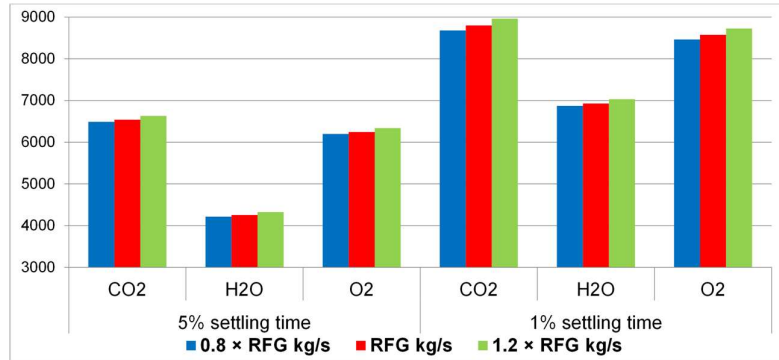
Fig. 18. Flue gas CO_2, H_2O, and O_2 concentration settling times (time steps) for a −10% fuel mass flow disturbance with different RFG rates (Publication I, reprinted with permission from Elsevier).

6.1.2 Oxy-CFB combustion control

The separate RFG and pure O_2 streams in oxy mode lead to two additional CDOF compared to air-firing, see Table 10, which is obtained by expanding Table 5 to include oxy-firing. How the extra CDOF affected combustion control in the CFB was explored in Publication I. Unlike air-firing, the oxygen supply, furnace cooling and fluidization become partially decoupled in oxy mode. The oxygen supply to the system is determined by the pure O_2 flow. The RFG flow, in turn, has the largest effect on temperatures (cooling) and fluidization in the furnace. The pure O_2 flow elevates furnace temperatures through combustion while fuel remains; further oxygen can contribute to cooling.

The decoupling of the oxidant properties was clearly visible in the simulations, shown in Fig. 19, where the RFG steps had a significant effect only on the furnace temperature and fluidization. This decoupling can produce unexpected outcomes during fast load changes. For example, the oxy load ramp simulations described in Publication I revealed that fast ramps for the fuel and oxidant flows did not necessarily produce fast temperature responses, most probably due to an imbalance between heat generation and furnace cooling during the fast MV changes.

Table 10. Modified CDOF analysis for the oxy-fired CFB boiler combustion side.

Process section and unit	Process unit type	Streams in + out	Connection streams	Restraining number	Redundant streams
Oxidant gas feed		6		4	
Prim RFG fan	Compressor	1 + 1	1	1	
Sec RFG fan	Compressor	1 + 1	1	1	
Prim O_2/RFG mix	Mixer	2 + 1	1	1	
Sec O_2/RFG mix	Mixer	2 + 1	1	1	
Hotloop		10		2	2
Furnace	CSTR with heat flows	5 + 3	3	0	
Cyclone	Splitter	1 + 2	1	1	
Intrex	HE without inventory	2 + 2	1	1	
Flue gas path		7		5	
Duct section 1	HE without inventory	1 + 1	1	1	
Duct section 2	HE without inventory	1 + 1	1	1	
Duct section 3	HE without inventory	1 + 1	1	1	
FG recycle point	Splitter	1 + 2	1	1	
Prim/sec RFG split	Splitter	1 + 2	1	1	
SUM		23		11	2
CDOF	10				
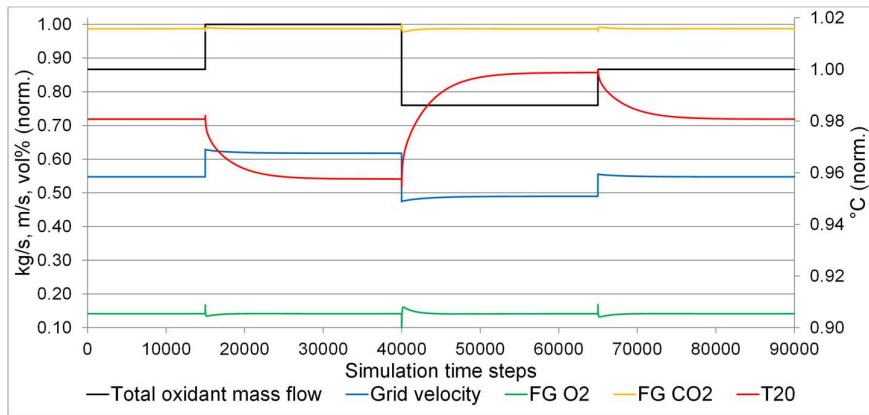
Fig. 19. Normalized gas velocity, furnace temperature, and flue gas O_2 and CO_2 percentage responses to simulated RFG steps in oxy mode with constant firing power (Publication I, adapted with permission from Elsevier).

The control structure in Fig. 20 was proposed for the oxy-CFB in Publication I, based on the decoupling of the oxidant properties. The decoupling calls for oxygen management, and Publication I outlined how the secondary pure O_2 flow or the total secondary oxidant flow could be used for flue gas O_2 control. While the previous option results in smaller fluidization disturbances and a larger flue gas O_2 gain, the oxidant O_2 percentage varies with time. The latter option offers a similar arrangement to air-firing. These findings were confirmed through simulations by Hultgren et al. (2015). The oxidant O_2 content can be controlled with the pure O_2 flow or the RFG flow. Pure O_2 was deemed to be preferable for the primary oxidant, while no preference was found for the secondary oxidant by Hultgren et al. (2015).
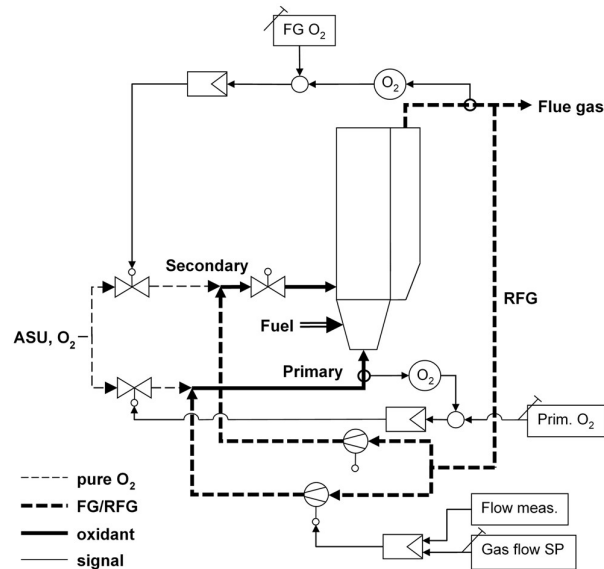

Fig. 20. Proposed oxidant gas control setup in the oxy-CFB (Publication I, reprinted with permission from Elsevier).

Publication I includes an explanation of how the oxy-CFB benefits from oxidant flowrate control, especially for the primary oxidant, to avoid fluidization disturbances. As shown in Fig. 20, the primary RFG is used for this purpose, and the total gas flow setpoint is determined by the boiler firing power. A more extensive option would be to control the bed density or fluidization velocity directly, for example by utilizing a UKF filter as a soft sensor.

87

The conclusion was drawn in Publication I that the additional CDOF in oxy-firing introduce new control possibilities, but some of these CDOF are consumed by CFB operating constraints. Notably, existing air-fired combustion control structures should not be applied directly to oxy-fired boilers. The decoupled properties of the pure O_2 and RFG flows highlighted that CDOF evaluation should be combined with an analysis of MV–CV dynamics, as was done for the OTU-CFB in subsection 6.1.4.

6.1.3 Air to oxy mode switching

The switch simulations (Fig. 21) showed that feasible air to oxy switches could be made with both the "direct" and the "sequenced" schemes (Figs. 14–15). Air-like conditions were maintained throughout the switches (with O_2 enrichment in oxy mode), with no major combustion disturbances based on the flue gas O_2 content.
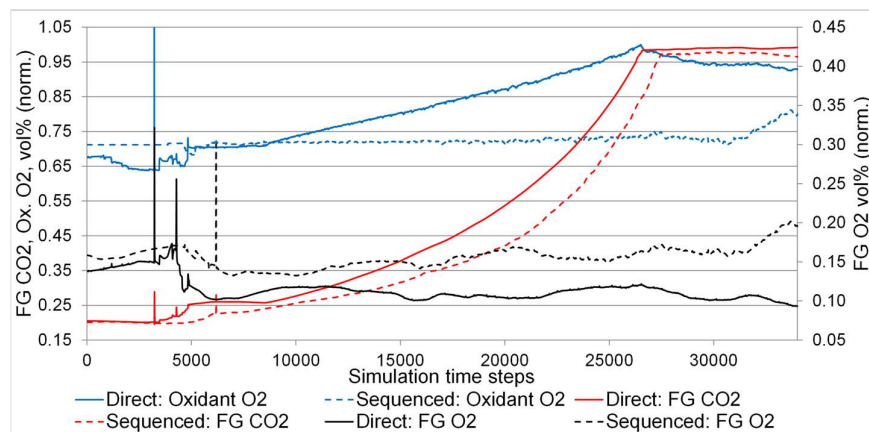
Fig. 21. Normalized primary oxidant (Ox.) O_2, flue gas CO_2, and flue gas O_2 content for the "direct" and "sequenced" switches (Publication I, adapted with permission from Elsevier).

The main differences between the switching methods were observed in the furnace temperatures (Fig. 22). The "direct" method resulted in a faster and smoother transition than the "sequenced" method, which displayed a decrease both in temperatures and fluidization during the RFG and pure O_2 ramps before the firing power increase at 30000 time steps. This showed how this method was affected more by the oxy-fired gas specific heat capacity elevation than the "direct" method.
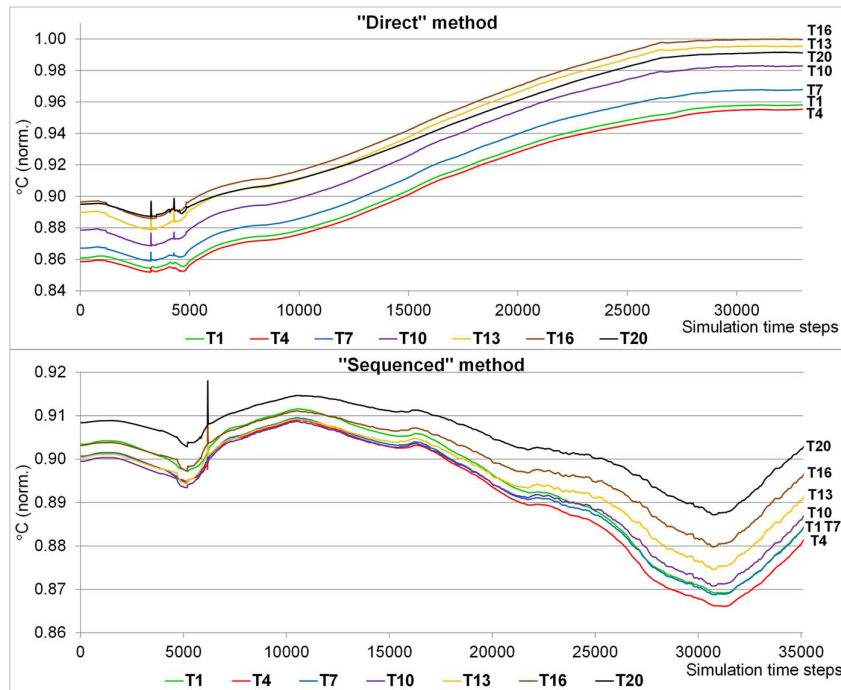
Fig. 22. Normalized temperature responses in furnace elements 1–20 for the "direct" and "sequenced" switches (Publication I, reprinted with permission from Elsevier).

Based on the results, it was suggested in Publication I that the "direct" method was preferable for the oxy-CFB hotloop, although modifying all MVs at the same time might be restrictive in practice. For "sequenced" transitions, particular attention should be paid to the final portions of the gas flow ramps. The switch simulations also verified several of the observations made in subsections 6.1.1–6.1.2.

6.1.4 Load change TPM variable dynamics

The open-loop dynamics of the TPM variables were analyzed from the OTU-CFB simulator responses according to the principles described in subsection 5.2.2 (Table 11). The turbine valve had the fastest overall response for electrical power and steam pressure, which justifies its use as a TPM for fast load changes. The steam temperature responses were slower due to transient steam flow dynamics. The small static gain between the turbine valve and the electrical power should be noted.

Table 11. Dynamics of load change TPM variables. Results are percentages of the largest value for each CV (Publication IV supporting material, adapted with permission. Copyright 2017 American Chemical Society).

| TPM property (% of max)	Electrical power	Main steam p	Main steam T	Evaporator T
Turbine valve				
Rise time	0.01	5	100	17
Settling time	33	26	100	60
Time delay	0	0	0	0
Static gain	0.2	−68	−3	−20
Firing power				
Rise time	100	100	74	100
Settling time	100	100	82	100
Time delay	0	67	60	100
Static gain	100	100	100	100
Feedwater flow				
Rise time	0.1	0.4	83	96
Settling time	90	89	94	95
Time delay	0	100	100	50
Static gain	10	18	−98	−72

The firing power predictably had much slower electrical power and steam pressure responses than the turbine valve. However, MV changes also resulted in the largest static gains. Additional testing also revealed that modifying the feedwater and firing power together enabled faster CV responses ("boiler load" MV in subsection 5.2.2).

Feedwater step changes resulted in fast initial responses for steam pressure and electrical power. This was caused by the response shapes, which contained transient overshoots. These observations are potentially useful for obtaining fast load changes in the OTU path, as the output MW_e could in theory be modified using the feedwater flow in turbine-following transitions, and the fast pressure dynamics could be useful in sliding-pressure mode. As a result, the control structure analysis described in Publication IV put special emphasis on the feedwater flow as an MV.

6.2   CFB hotloop analysis with UKF state estimation

The UKF state estimation tool was implemented successfully for the oxy-CFB pilot combustor and the industrial air-fired boiler, as described in Publication II. The UKF was proven to be applicable to a complex simulator like the hotloop model, and could thus be incorporated into the ICPD procedure. The results showed the benefits of the UKF for the model analysis: good performance, direct use of

industrial simulators, and reduced computational load compared to other nonlinear Bayesian algorithms. The estimated fuel mass flow variations and air leakage mass flow for the load ramps in the pilot oxy-CFB case study are illustrated in Fig. 23. The corresponding estimated flue gas concentrations are shown in Fig. 24.
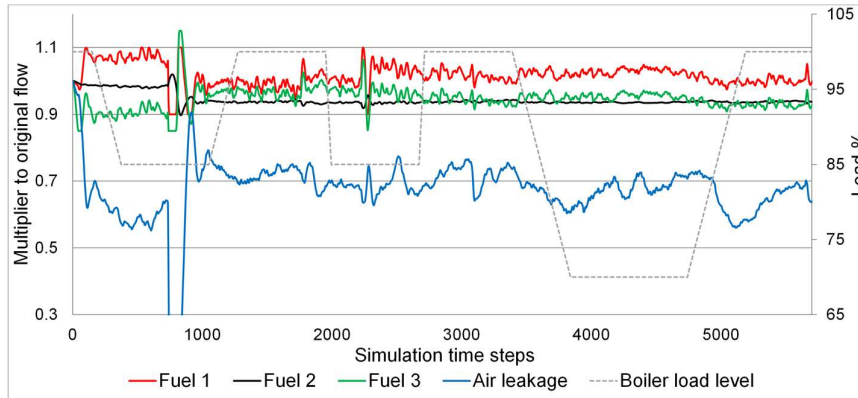
Fig. 23. Estimated fuel flow and air leakage mass flow multipliers during the load ramps in the pilot oxy-CFB (Publication II, adapted with permission. © 2014 IEEE).
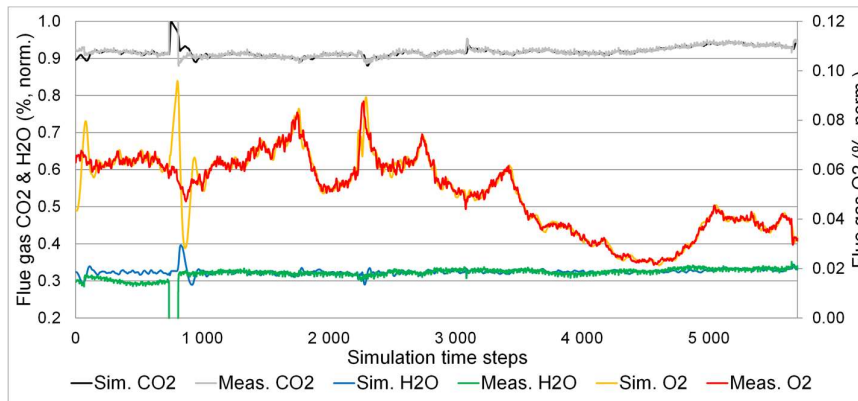
Fig. 24. Measured (Meas.) and estimated (Sim.) flue gas component percentages (normalized) in the pilot oxy-CFB (Publication II, reprinted with permission. © 2014 IEEE).

The estimates provided a feasible explanation for the observed process behavior and an excellent agreement between the measured and simulated flue gas

compositions. The results suggested that a mostly constant level of air leakage had been present during the pilot measurements. This information can be used in oxy-CFB process design, for example for optimizing CO_2 processing costs. The estimated fuel flows contained mostly small oscillations, and these estimates were essential for obtaining accurate input data for the simulator-based ICPD analysis.

The industrial air-fired case study results are provided in Publication II. As in Figs. 23 and 24, the fuel moisture and heat transfer coefficient parameters were adjusted successfully based on the temperature and flue gas O_2 data for all tests described in subsection 5.3.2, especially for the primary air tests. The estimated fuel moisture variations can be used in ICPD for equipment sizing to reject typical moisture content disturbances, while parameters like the heat transfer coefficient are crucial when adapting the ICPD simulator with noisy dynamic data.

6.3   CFB relative gain analysis

The defined relative gain approach was established as feasible for the CFB control design based on the results in Publications III–V. Plant-wide control structures were successfully defined according to the procedure shown in Fig. 16, and the results illustrated the need for stepwise interaction analysis both at zero frequency and for higher frequencies. The results also demonstrated how the methods could be used for indicating electrical power control limiting interactions; in Publication III it was shown how this information could be employed in ICPD decision-making. These two aspects are discussed separately in subsections 6.3.1 and 6.3.2.

6.3.1 Control structure selection

Based on the PRG and DRGA analyses in Publication IV, the suggested control structure of the OTU-CFB was a combination of turbine-following control (I or III) for low-frequency planned disturbances and basic boiler-following control (VI) for high-frequency unplanned disturbances. This setup provided ICI controllability with a good PRG distribution at low frequencies, and a low degree of loop interactions at high frequencies, albeit without ICI controllability. The more unconventional structure III employed the feedwater flow to control the electrical power, similar to what was suggested in the TPM analysis of subsection 6.1.4. Structures I, III, and VI are illustrated in Fig. 25. In the figure, the blue signals correspond to the steam pressure CV, the red signals to the electrical power CV, and the yellow signals to the evaporator temperature CV.

92
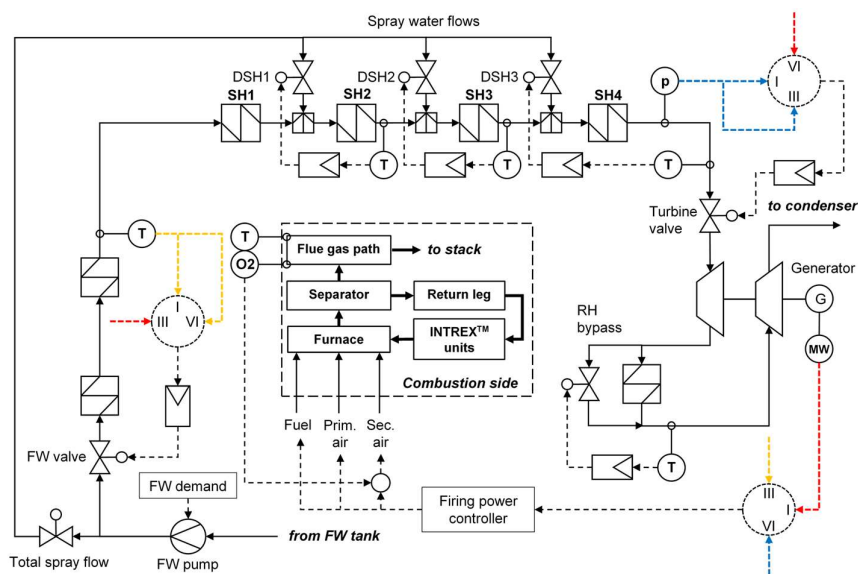
Fig. 25. Control structures I, III, and VI from the stepwise relative gain analysis (Publication IV, adapted with permission. Copyright 2017 American Chemical Society).

The corresponding PRG and DRGA analyses of the plant-wide case 4 (cf. Table 7) are illustrated in Table 12 and Fig. 26. Three structures were deemed as ICI controllable based on the full PRG analysis shown in Table 12. Structure II had limited practical significance, although it and other PRG results of case 4 revealed an interaction between the feedwater flow and the reheater. The basic turbine-following structure I was ranked the highest in terms of its PRG distribution. This outcome was observed for all cases in Table 7, especially case 1. The dominance of turbine-following control was caused by the small static gain between the turbine valve and the electrical power, cf. subsection 6.1.4.

Table 12. PRG distributions and NI values of the ICI control structures of case 4. The control connection notation is given in Fig. 26 (Publication IV, reprinted with permission. Copyright 2017 American Chemical Society).

Structure	Control connections	NI	Number of PRG elements in range						
			0–0.1	0.1–0.5	0.5–0.85	0.85–1.2	1.2–5	5–10	>10
I	[1 6 2 3 4 5 7 8]	0.321	0	4	7	919	76	2	0
II	[1 6 7 3 4 5 2 8]	0.358	117	47	116	643	85	0	0
III	[1 6 8 3 4 5 7 2]	2.320	122	60	99	632	95	0	0
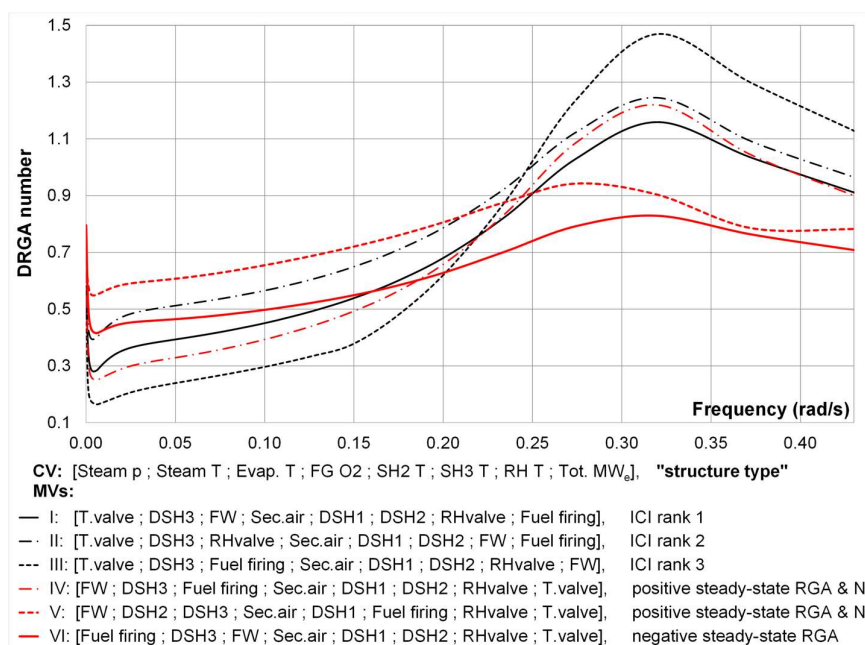
Fig. 26. DRGA numbers for the control structures I–VI in case 4 (Publication IV, adapted with permission. Copyright 2017 American Chemical Society).
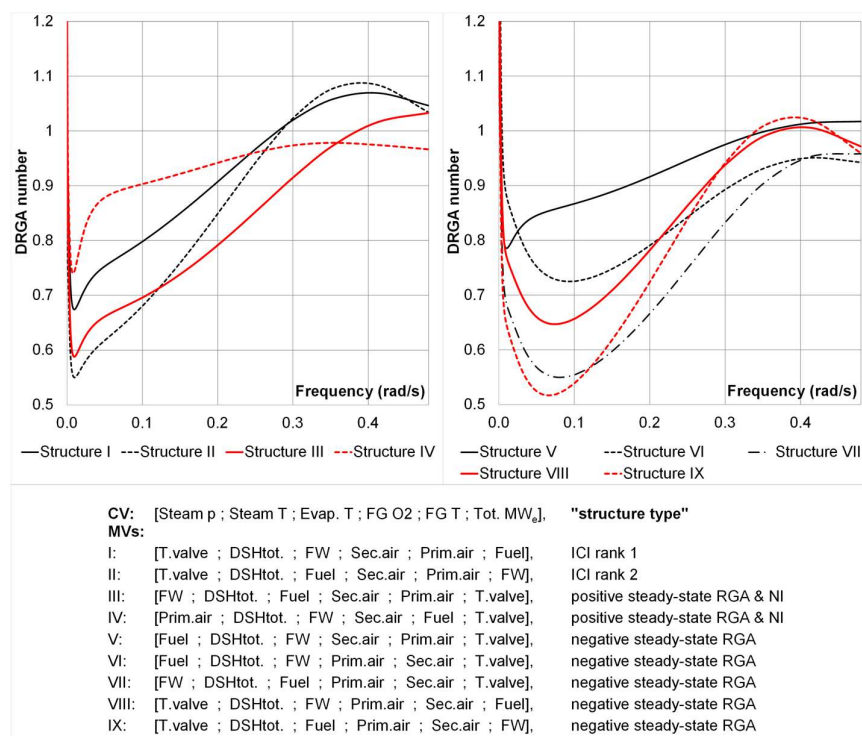
No conventional boiler-following structures (electrical power–turbine valve, main steam pressure–firing power) were validated as ICI controllable (e.g., structure VI) due to the small negative static RGA element between the firing power and the steam pressure. This result was repeated for the "boiler load" MV in cases 1 and 2. However, positive RGA and NI values were obtained for structures IV and V, which utilized the turbine valve for fast electrical power control. The steam pressure was controlled with the feedwater, which supported the observations of subsection 6.1.4.

The DRGA ranking in Fig. 26 shows the contrast between preferred control structures at zero and higher frequencies. Structure I was surpassed by structure III even at low frequencies, and structure VI was preferred above 0.2 rad/s. This outcome was even clearer in Publication V: Turbine-following control was only preferable at zero frequency based on the PRGA, and the CLDG indicated that turbine-following electrical power control suffered from DSH spray interactions. Turbine-following control became more feasible at high frequencies in Publication IV when the "boiler load" MV was used in cases 1 and 2.

94

Combustion control connections were studied in case 3, thus expanding on the results of section 6.1 by considering the interactions of variables on the combustion side. The PRG analysis is shown in Table 13 and the corresponding DRGA plots in Fig. 27.

Table 13. PRG distributions and NI values of the ICI control structures in case 3. The control connection notation is given in Fig. 27 (Publication IV, reprinted with permission. Copyright 2017 American Chemical Society).

Structure	Control connections	NI	Number of PRG elements in range						
			0–0.1	0.1–0.5	0.5–0.85	0.85–1.2	1.2–5	5–10	>10
I	[1 6 2 5 4 3]	0.231	0	0	1	117	62	0	0
II	[1 6 3 5 4 2]	1.600	30	26	21	65	38	0	0

CV: [Steam p ; Steam T ; Evap. T ; FG O2 ; FG T ; Tot. MW$_e$],   "structure type"
MVs:
I: [T.valve ; DSHtot. ; FW ; Sec.air ; Prim.air ; Fuel],   ICI rank 1
II: [T.valve ; DSHtot. ; Fuel ; Sec.air ; Prim.air ; FW],   ICI rank 2
III: [FW ; DSHtot. ; Fuel ; Sec.air ; Prim.air ; T.valve],   positive steady-state RGA & NI
IV: [Prim.air ; DSHtot. ; FW ; Sec.air ; Fuel ; T.valve],   positive steady-state RGA & NI
V: [Fuel ; DSHtot. ; FW ; Sec.air ; Prim.air ; T.valve],   negative steady-state RGA
VI: [Fuel ; DSHtot. ; FW ; Prim.air ; Sec.air ; T.valve],   negative steady-state RGA
VII: [FW ; DSHtot. ; Fuel ; Prim.air ; Sec.air ; T.valve],   negative steady-state RGA
VIII: [T.valve ; DSHtot. ; FW ; Prim.air ; Sec.air ; Fuel],   negative steady-state RGA
IX: [T.valve ; DSHtot. ; Fuel ; Prim.air ; Sec.air ; FW],   negative steady-state RGA

Fig. 27. DRGA numbers for the control structures I–IX in case 3 (Publication IV, adapted with permission. Copyright 2017 American Chemical Society).

The PRG analysis in Table 13 resulted in two ICI structures, where only the fuel and feedwater control connections were switched. This emphasizes how these MVs together determine the amount of generated steam, but how the feedwater–electrical power connection leads to reduced ICI controllability. Similar interchangeable MV pairs were observed for the oxy-CFB hotloop in the ICI PRG analysis of Hultgren et al. (2015), for example the primary RFG and pure O_2 flows.

At higher frequencies, nine alternative control structures could be considered for case 3 based on the DRGA (Fig. 27). Similarly to case 4, turbine-following structures were favored below 0.12 rad/s, and boiler-following structures above that. However, the preferred structure varied more at different frequencies than in case 4, with structures I, II, IX, VII, and VI all being preferable in specific ranges. In general, the DRGA favored control setups for high-frequency disturbances that increased the decoupling between the evaporator, the steam flow, and the turbine.

In general, the chosen relative gain approach was shown to be effective in generating and ranking control structures for the CFB system. The suggested control structures corresponded to industrial practices and thus validated their feasibility. The analysis was also able to highlight unorthodox control connections, as well as disturbance frequencies that caused controllability issues for specific control setups.

6.3.2 Loop interaction analysis

Several loop interactions were discussed for the OTU-CFB in Publication IV, and the DRGA elements of individual MVs were analyzed in detail, especially for the plant-wide case 4. It could be seen that the interactions caused little change in the preferred control connections for the DSH1, DSH3, and reheater bypass valve MVs in the whole frequency range. The preferred connection was less clear for the other MVs, most importantly the main load change TPM variables: the turbine valve, firing power, and feedwater flow.

The DRGA elements of all MVs in case 4 are shown in Fig. 28. The interaction between electrical power and main steam pressure control was clearly visible from the overall results described in Publication IV, especially for the turbine valve and feedwater flow. Likewise, the PRGA in Publication V showcased a major off-diagonal interaction in the electrical power for both turbine-following and boiler-following control. For the feedwater, the interaction with the firing power in the steam formation was highlighted especially in case 3, and many of the suggested control connections for these variables were interchangeable.

96
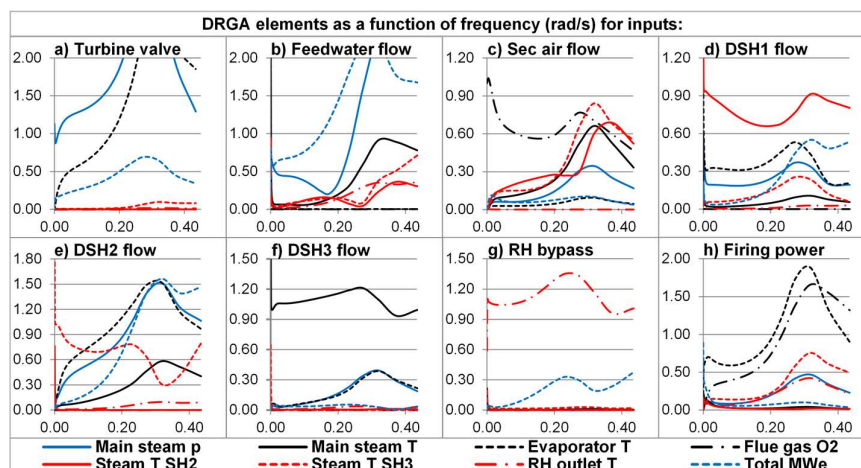
Fig. 28. DRGA element magnitudes for all MV–CV connections in case 4 (Publication IV, reprinted with permission. Copyright 2017 American Chemical Society).

The ill-conditioning related to steam temperature control was identified as another source of variable interaction. Similar effects of the feedwater and DSH flows on steam temperatures were observed as large PRG elements in cases 2 and 4. The DRGA indicated controllability issues for the middle spray DSH2 (Fig. 28), as well as steam temperature interactions for the feedwater at high frequencies.

On the combustion side, ill-conditioning was observed in case 3 for the primary and secondary oxidant gas flows, as they affect flue gas and furnace properties in a similar way. These findings could be compared to the PRG results of Hultgren et al. (2015) for the oxy-CFB hotloop, where large PRG values and similar effects of gas flow MVs were reported, especially for furnace temperature CVs.

In addition to Publication IV, the DRGA was used for process design in Publication III, by examining how evaporator and superheater steam storage parameters affected loop interactions in the CFB steam path (cf. subsection 5.4.2). The DRGA plots for the different process parameter levels are shown in Fig. 29. The results illustrated that increasing the superheating mass storage improved controllability by increasing the decoupling between steam generation and the turbine. Increasing the evaporator storage improved controllability in the low-frequency region, but above 0.04 rad/s a small storage was preferable. These findings were directly connected to electrical power setpoint tracking performance through closed-loop simulations, cf. Publication III. The results demonstrated how

the DRGA could be used for guiding design decisions in ICPD and thus enabled the use of the PRGA and CLDG as optimization objectives in Publication V.
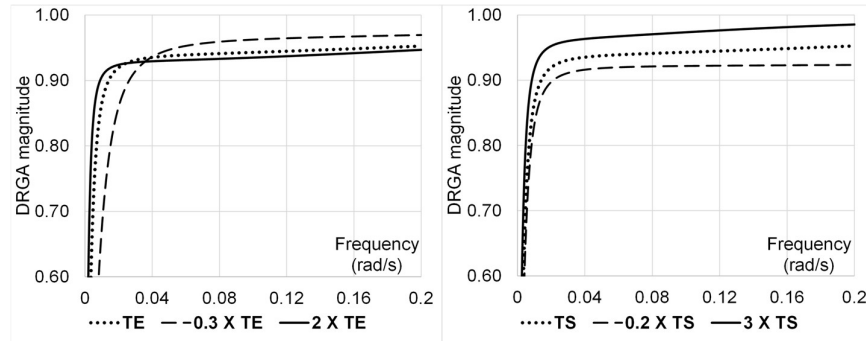
Fig. 29. Effect of lumped evaporator storage (TE) and superheater storage (TS) parameters (change from nominal value) on DRGA element magnitudes (Publication III, reprinted with permission from IFAC).

6.4   CFB steam path ICPD optimization

The ICPD optimization was carried out successfully for the storage distribution, nominal turbine valve position, and unit master PID parameters of the CFB steam path model, as described in Publication V. The optimized load ramp scenario I is shown in Fig. 30. The results for scenarios II–IV are provided in Publication V.
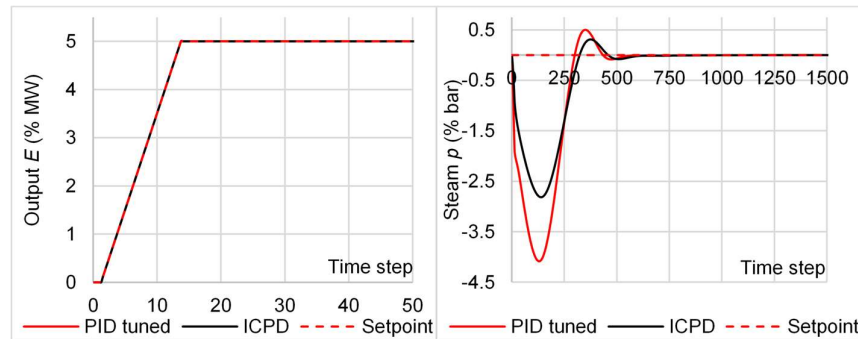
Fig. 30. Scenario I with ICPD optimized and PID optimized parameters (Publication V, reprinted with permission from Elsevier).

98

The optimized process and controller parameters are shown in Table 14. The ICPD optimization maximized the steam storage in the whole steam path for both the constant-pressure and sliding-pressure ramps. The evaporator storage was minimized, the superheater storage was maximized, and the superheater storage was distributed close to the turbine. The turbine valve opening at 80% load was decreased for the large slow ramps and increased for the small fast ramps.

Table 14. The ICPD optimized process and controller parameters (Table 8) for the scenarios in Table 9. Reported values are multipliers to the nominal starting parameters (Publication V, reprinted with permission from Elsevier).

Ramp scenario	τ_{TOT}	q_E	q_{S1}	$\bar{v}$	P_p	I_p	D_p	N_p	P_E	I_E
I: Fast constant p	1.69	0.97	0.20	1.08	2.91	2.23	5.09	727.26	2.71	118.88
II: Slow constant p	1.69	0.97	0.20	0.97	1.44	2.48	3.70	55.06	2.31	35.58
III: Fast sliding p	1.69	0.97	0.20	1.08	1.99	0.56	3.78	11.94	2.87	133.01
IV: Slow sliding p	1.69	0.97	0.20	0.97	1.64	0.41	3.33	782.93	1.99	0.08

The ICPD optimization clearly provided better results than the benchmark cases, where only the PID controller parameters were optimized. Table 15 shows that the design resulted in a good trade-off between the objectives in subsection 5.5.2 for all load changes. Accurate electrical power tracking was obtained, steam throttling was minimized, a sufficient steam control reserve was maintained, and no reduction in controllability was observed in terms of the PRGA and CLDG.

Table 15. Objectives j_1–j_6 and total objective J for the ICPD optimized and PID optimized load ramps I–IV. Values are % of nominal objective values (Publication V, reprinted with permission from Elsevier).

Objective	Ramp I		Ramp II		Ramp III		Ramp IV	
(%)	ICPD	PID	ICPD	PID	ICPD	PID	ICPD	PID
j_1	0.3995	0.7866	0.4686	0.5271	0.8080	0.9536	0.9986	0.8480
j_2	0.0013	0.0000	0.0001	0.3912	0.0012	0.0000	0.0007	0.3865
j_3	1.1563	0.9992	0.9441	0.9956	1.1596	1.0015	0.9602	1.0050
j_4	1.0001	1.0000	0.0005	0.0003	1.0001	1.0000	0.0006	0.0041
j_5	0.9978	1	0.9054	1	0.9980	1	0.9082	1
j_6	0.5662	1	0.5730	1	0.5662	1	0.5728	1
J	0.095	0.215	0.049	0.419	0.125	0.227	0.088	0.439

The results contributed towards setting guidelines for CFB steam path design. For example, it was pointed out in Publication V how the steam storage was maximized even for sliding-pressure mode, although a small storage capacity essentially

contributes to fast steam pressure transitions. The outcome could be explained by the chosen optimization objective, as a large steam storage capacity reduces the electrical power disturbances caused by boiler-following turbine valve action. Indeed, the steam path optimization described in Publication III resulted in a small superheater storage capacity in sliding-pressure mode, as only the main steam pressure tracking was optimized in this case.

The results showed how dynamic ICPD optimization inherently contributes to the formation of local optima even for simple process systems. This was mainly attributed to the simultaneous optimization of the process and its controllers, but also to the single-objective formulation and the chosen performance criteria. The challenging nature of the ICPD problem validated the chosen hybrid optimization algorithm, as well as the simplified internal model approach.

6.5   Future directions

In Publications I–V the application of the chosen ICPD design methods was demonstrated for individual CFB boiler design problems, all supporting the overall goal of faster load changes. In addition, several observations were made from these case studies for refining the ICPD procedure for generic load-following CFB power plant design problems. These development suggestions are briefly discussed here.

As a whole, a toolbox of design steps can be assembled from Publications I, II, and IV for qualitative dynamic simulation and control-oriented process design in the CFB. These steps include mapping the effects of altered operating conditions on the open-loop dynamics, mapping the effects of structural changes on the process operation, analyzing the control degrees of freedom (CDOF), evaluating the MV–CV dynamics of TPM variables based on the CDOF, and extending the simulations with measured data through nonlinear state estimation. While the MV–CV analysis and degrees of freedom evaluation were already carried out for the full OTU-CFB flowsheet in Publication IV, the simulator-based analysis from Publications I and II also needs to be expanded to the CFB water-steam cycle. For the state estimation, the main task is to evaluate the feasibility of using the full OTU-CFB simulator in Fig. 12 as the internal model of the UKF tool.

With the PRGA/CLDG modification introduced in Publication V, the relative gain control structure selection procedure of Publication IV is directly applicable to generic CFB problems. Notably, the stepwise relative gain procedure for large MV–CV systems, using multiple methods, is a novel contribution of the thesis.

Moreover, the use of relative gain methods as ICPD performance measures should be expanded on, especially for the pre-analysis stage, similarly to Publication III.

The ICPD optimization procedure was validated for the simple CFB steam path model in Publication V. Based on these findings, the next step in CFB boiler ICPD research would be to optimize the plant-wide power plant flowsheet based on the procedure. The main research questions arise from the internal design model structure, the controller type, and the objective function formulation.

For the internal model, the main task is to expand the mass storage model described in Publication V with heat exchanger specific mass storages, instead of using lumped storage parameters. Secondly, steam energy content variations should be included by adding heat transfer state equations for the water-steam and combustion/flue gas sides. The water-steam temperature dynamics can be modeled by describing the heat exchanger as an ideal plug flow in a set of pipes, with heat transfer from the pipe wall. The combustion/flue gas side heat storages can be assumed to be ideally mixed tanks, as they are significantly larger than the water-steam side heat storages.

The closed-loop design model can be obtained for the OTU-CFB flowsheet in Fig. 12 by applying PID controllers to the control structures in subsection 6.3.1. As stated in Publication V, MPC control should also be investigated for the proposed ICPD procedure in future research efforts. If MIMO controllers are considered, the relative gain control structure selection procedure described in Publications IV and V could readily be modified with the block relative gain (cf. subsection 4.5.2).

A default ICPD objective function was presented for load-following boilers in subsection 5.5.2. For a generic CFB problem, objective j_1 should be expanded with an ISE setpoint tracking measure for the main steam temperature, especially if steam temperature controllers or superheater parameters are optimized. Similarly, the exergy penalty associated with evaporative DSH cooling could be considered for efficiency objective j_3. The objective could be employed similarly to the turbine valve, where optimal solutions minimize the use of DSH water during load disturbances, while also minimizing control signal saturation. The sliding-pressure optimization did not consider a separate setpoint trajectory for the steam pressure, the inclusion of which would call for minor integration of process design, control design, and scheduling (cf. section 3.1). Lastly, an economic constraint should be included in the ICPD optimization, or a separate economic evaluation stage should be added to the results of the ICPD procedure, as suggested in section 4.1.

7 Conclusions

The increased use of renewable energy in the power grid requires steam power plants to perform fast and frequent load changes, and emission mitigation requires designers to implement process modifications such as carbon capture and storage (CCS) in solid fuel boilers. This thesis presents a systematic study and analysis on how integrated control and process design (ICPD) can contribute to improved load change performance and flexibility regarding process modifications in circulating fluidized bed boiler (CFB) power plants. CFB boilers with increased dynamic performance can be obtained through the ICPD tools and design guidelines that were utilized in this thesis. Therefore, the work enables CFB design to better adjust to the changing demands of modern sustainable power generation, compared to a conventional approach with sequential process and control design steps.

Systematic ICPD was applied to CFB boilers for the first time in this thesis. It was discovered that little ICPD design experience is available for steam power plants in the literature, despite the well-documented benefits of integrating process and control design for various chemical processes. Extreme load change requirements present a major design challenge for solid fuel boilers with slow and interacting dynamics. This challenge has been addressed in the literature through improved control methods (e.g., MPC control) and operating modes (e.g., condensate throttling), but the process and its control system are still largely treated as separate design problems. The thesis concludes that significant potential for increased CFB generation flexibility lies in making control design an intrinsic part of the boiler process design, as the open-loop dynamics determine the upper limit for the load change performance. Another conclusion is that greater effort is needed from the research community to identify industrial case studies, where improved performance could be reached through design integration. ICPD is often considered to be a mature science at this point, even though it has practically never been applied to large-scale load-following combustion power plants prior to this thesis.

A systematic view of the application of ICPD was taken in this thesis. The work provided a novel ICPD characterization focusing on commonly occurring features in ICPD methodologies. The work indicates that this approach helps in the selection of design and analysis methods for a novel application area like the CFB boiler, especially since the scope of current ICPD research is wide and somewhat ill-defined. The characterization places great significance on systematic performance evaluation, which is not commonly emphasized in current ICPD literature. The author would argue that the proper definition and quantification of desirable closed-

loop performance forms the basis for the whole design–control interaction. The suggested performance evaluation approach for the load-following CFB boiler can be labeled as "trajectory design": the electrical power setpoint tracking error is minimized during simulated load ramps together with main steam state variable errors, similar to switchability analysis. This main objective is augmented with additional goals for first-principles efficiency, disturbance rejection capacity, and controllability. The thesis work concludes that this approach is more suitable for load-following problems than, for example, an economic objective, which is commonly used especially in mathematical programming ICPD and has been a defining guideline for boiler process design in the past.

The work carried out during this thesis resulted in a hierarchical ICPD procedure that was shown to be suitable for generating CFB flowsheets with good load-following performance and design flexibility for the oxy-combustion CCS technology. The thesis work concludes that load change performance can be improved most effectively by combining a closed-loop process optimization problem with first-principles knowledge and system analysis. In Publications I–V, it was shown that ICPD methods based on dynamic trajectory optimization, relative gain array tools (partial relative gain, performance relative gain array, closed-loop disturbance gain, Niederlinski index), and first-principles simulation augmented with unscented Kalman filter (UKF) state estimation provided a means for improved control and process design in the CFB boiler. The overall approach can be summarized as simulation-oriented ICPD, as the methods ultimately rely on high-accuracy industrial process simulators. The proposed procedure and its application to the CFB boiler are the novel contributions of the thesis: The chosen design and analysis methods are mostly established in the literature, but many of them were applied here to the CFB boiler for the first time.

In Publication I, it was demonstrated how the chemical, physical and structural properties of the CFB boiler can be connected to its control performance and how monitoring these properties enables more informed process design decisions for control. The thesis thus emphasizes the importance of first-principles process knowledge and simulation for effective closed-loop design, which somewhat contrasts with the current trend of black-box neural network modeling in process digitalization. The simulation-oriented focus of the thesis is supported by the increasing availability of computing power, which enables the rapid evaluation of complex models in ICPD algorithms. This outlook was reflected in the chosen UKF approach in Publication II: A fully detailed industrial CFB simulator could be used directly for data post-processing, while maintaining acceptable computational

performance. The work also employed Bayesian state estimation unconventionally in ICPD as a model analysis tool rather than for process monitoring and control.

Based on the control structure selection and analysis in Publications III–V, it can be concluded that a comprehensive picture of control interactions in the CFB can only be obtained by investigating different control variable subsystems using multiple relative gain methods. For the same reason, relative gains were examined for the entire load disturbance frequency range instead of analyzing steady-state data or individual frequencies. Furthermore, the thesis demonstrates how relative gain methods can be used as performance measures for interactions and controllability, not just as heuristic pairing rules for manipulated and controlled variables. These findings expand on the typical relative gain analysis literature.

In Publication V, it was outlined that the fully simultaneous optimization of the CFB process and its unit master PID controllers is a feasible, yet challenging task. Most importantly, process parameters and their preferred controller tunings form multiple local optima that call for global optimization approaches. While this aspect will be influenced by the available computing power in the future, the thesis indicates that dynamic response optimization will still require advanced algorithms and simplification in the near future to make the problem practically feasible.

Aside from its contributions to ICPD, the thesis also contributes to increasing CFB boiler design knowledge by providing guidelines for specific process and control design problems. Of these, the most important were how the air-fired CFB should be modified for oxy-firing, how transitions between air and oxy mode should be conducted, how plant-wide OTU-CFB control connections should be selected, which variable interactions have the potential to cause issues for OTU-CFB control performance, and how steam storage capacity should be allocated in the steam path to improve load change performance, ultimately translating into superheater sizing and placement. Notably, these outcomes were specifically enabled by the chosen methods and the overall ICPD approach of the thesis.

This thesis constitutes the first systematic research effort in improving CFB power plant design practices through ICPD. This development should be expanded through additional research. While the present work only concerns the CFB power plant, the outcomes of the thesis are essentially also applicable to other solid fuel power plants to improve their operation for sustainable power generation. The suggested ICPD procedure serves as an improvement over existing CFB design practices. The methods of the procedure were shown to be readily applicable to different industrial CFB boiler problems. In conclusion, the integration of control aspects into process design is both a feasible and a necessary development.

104

List of references

Alhammadi, H. Y., & Romagnoli, J. A. (2004). Process design and operation: Incorporating environmental, profitability, heat integration and controllability considerations. In P. Seferlis, & M. C. Georgiadis (Eds.), *Computer aided chemical engineering: Vol. 17. The integration of process design and control* (pp. 264–305). Amsterdam: Elsevier. https://doi.org/10.1016/S1570-7946(04)80063-4

Alvarado-Morales, M., Hamid, M. K. A., Sin, G., Gernaey, K. V., Woodley, J. M., & Gani, R. (2010). A model-based methodology for simultaneous design and control of a bioethanol production process. *Computers & Chemical Engineering, 34*(12), 2043–2061. https://doi.org/10.1016/j.compchemeng.2010.07.003

Anthony, E. J., & Hack, H. (2013). Oxy-fired fluidized bed combustion: Technology, prospects and new developments. In F. Scala (Ed.), *Woodhead publishing series in energy: Vol. 59. Fluidized bed technologies for near-zero emission combustion and gasification* (pp. 867–894). Cambridge: Woodhead Publishing. https://doi.org/10.1533/9780857098801.4.867

Arasu, S. K., Prakash, J., & Prasad, V. (2013). Derivative-free estimator based non-linear model predictive control of a boiler-turbine unit. In M. A. Henson, G. Pannocchia, R. Gudi, & S. Patwardhan (Eds.), *10th IFAC International Symposium on Dynamics and Control of Process Systems (DYCOPS 2013), IFAC Proceedings Volumes 46*(32) (pp. 660–665). https://doi.org/10.3182/20131218-3-IN-2045.00090

Åström, K. J., & Murray, R. M. (2008). *Feedback systems: An introduction for scientists and engineers*. Princeton, NJ: Princeton University Press.

Bahri, P. A., Bandoni, A., & Romagnoli, J. (1996). Operability assessment in chemical plants. *Computers & Chemical Engineering, 20*(Supplement 2), S787–S792. https://doi.org/10.1016/0098-1354(96)00139-1

Balko, P., & Rosinová, D. (2015). Robust decentralized control of nonlinear drum boiler. In M. Fikar (Ed.), *8th IFAC Symposium on Robust Control Design ROCOND 2015, IFAC-PapersOnLine 48*(14) (pp. 432–437). https://doi.org/10.1016/j.ifacol.2015.09.495

Bardelli, R., Bittanti, S., Bolzern, P., Campi, M., Carugati, E., De Marco, A., … Prandoni, W. (1994). Application of the extended Kalman filter to the estimation of the char mass in a fluidized bed combustor. In M. Blanke, & T. Söderström (Eds.), *10th IFAC Symposium on System Identification (SYSID '94), IFAC Proceedings Volumes 27*(8) (pp. 221–226). https://doi.org/10.1016/S1474-6670(17)47719-6

Basu, P. (2006). *Combustion and gasification in fluidized beds*. Boca Raton, FL: Taylor & Francis.

Biegler, L. T. (2018). Advanced optimization strategies for integrated dynamic process operations. *Computers & Chemical Engineering, 114*, 3–13. https://doi.org/10.1016/j.compchemeng.2017.10.016

Bittanti, S., Bolzern, P., Campi, M., De Marco, A., Panseri, R., Poncia, G., & Prandoni, W. (1996). A model of a bubbling fluidized bed combustor for the estimation of the char mass via extended Kalman filter. In J. J. Gertler, J. B. Cruz Jr., & M. Peshkin (Eds.), *Proceedings of the 13th World Congress of IFAC, IFAC Proceedings Volumes 29*(1) (pp. 6909–6914). https://doi.org/10.1016/S1474-6670(17)58793-5

Bolea, I., Romeo, L. M., & Pallarés, D. (2012). The role of external heat exchangers in oxy-fuel circulating fluidized bed. *Applied Energy, 94*, 215–223. https://doi.org/10.1016/j.apenergy.2012.01.050

Bristol, E. H. (1966). On a new measure of interaction for multivariable process control. *IEEE Transactions on Automatic Control, 11*(1), 133–134. https://doi.org/10.1109/TAC.1966.1098266

Buckley, P. S. (1964). *Techniques of process control*. New York, NY: Wiley.

Burnak, B., Diangelakis, N. A., Katz, J., & Pistikopoulos, E. N. (2019a). Integrated process design, scheduling, and control using multiparametric programming. *Computers & Chemical Engineering, 125*, 164–184. https://doi.org/10.1016/j.compchemeng.2019.03.004

Burnak, B., Diangelakis, N. A., & Pistikopoulos, E. N. (2019b). Towards the grand unification of process design, scheduling, and control—Utopia or reality? *Processes, 7*(7), 461. https://doi.org/10.3390/pr7070461

Campo, P. J., & Morari, M. (1994). Achievable closed-loop properties of systems under decentralized control: Conditions involving the steady-state gain. *IEEE Transactions on Automatic Control, 39*(5), 932–943. https://doi.org/10.1109/9.284869

Cao, Y., Fuentes-Cortes, L. F., Chen, S., & Zavala, V. M. (2017). Scalable modeling and solution of stochastic multiobjective optimization problems. *Computers & Chemical Engineering, 99*, 185–197. https://doi.org/10.1016/j.compchemeng.2017.01.021

Capra, F., & Martelli, E. (2015). Numerical optimization of combined heat and power Organic Rankine Cycles – Part B: Simultaneous design & part-load optimization. *Energy, 90*(1), 329–343. https://doi.org/10.1016/j.energy.2015.06.113

Chandrasekharan, S., Panda, R. C., Swaminathan, B. N., & Panda, A. (2018). Operational control of an integrated drum boiler of a coal fired thermal power plant. *Energy, 159*, 977–987. https://doi.org/10.1016/j.energy.2018.06.157

Chen, C., & Bollas, G. M. (2017, January). *Semi-batch chemical-looping reactors integrated with combined cycle power plants operating at transient electricity demand.* Paper presented at the FOCAPO / CPC 2017, Foundations of Computer Aided Process Operations / Chemical Process Control Conference, Tucson, AZ, United States.

Chiandussi, G., Codegone, M., Ferrero, S., & Varesio, F. E. (2012). Comparison of multi-objective optimization methodologies for engineering applications. *Computers & Mathematics with Applications, 63*(5), 912–942. https://doi.org/10.1016/j.camwa.2011.11.057

Chiu, M.-S., & Arkun, Y. (1990). Decentralized control structure selection based on integrity considerations. *Industrial & Engineering Chemistry Research, 29*(3), 369–373. https://doi.org/10.1021/ie00099a012

106

Daoutidis, P., Zachar, M., & Jogwar, S. S. (2016). Sustainability and process control: A survey and perspective. *Journal of Process Control, 44*, 184–206. https://doi.org/10.1016/j.jprocont.2016.06.002

Daum, F. (2005). Nonlinear filters: Beyond the Kalman filter. *IEEE Aerospace and Electronic Systems Magazine, 20*(8), 57–69. https://doi.org/10.1109/MAES.2005.1499276

Diangelakis, N. A., Burnak, B., & Pistikopoulos, E. N. (2017, January). *A multi-parametric programming approach for the simultaneous process scheduling and control – Application to a domestic cogeneration unit.* Paper presented at the FOCAPO / CPC 2017, Foundations of Computer Aided Process Operations / Chemical Process Control Conference, Tucson, AZ, United States.

Diangelakis, N. A., & Pistikopoulos, E. N. (2017a). Modelling, design and control optimization of a residential scale CHP system. In G. M. Kopanos, P. Liu, & M. C. Georgiadis (Eds.), *Advances in energy systems engineering* (pp. 475–506). Cham: Springer. https://doi.org/10.1007/978-3-319-42803-1_16

Diangelakis, N. A., & Pistikopoulos, E. N. (2017b). A multi-scale energy systems engineering approach to residential combined heat and power systems. *Computers & Chemical Engineering, 102*, 128–138. https://doi.org/10.1016/j.compchemeng.2016.10.015

Doležal, R., & Varcop, L. (1970). *Process dynamics: Automatic control of steam generation plant.* Amsterdam: Elsevier.

Engell, S., Trierweiler, J. O., Völker, M., & Pegel, S. (2004). Tools and indices for dynamic I/O-controllability assessment and control structure selection. In P. Seferlis, & M. C. Georgiadis (Eds.), *Computer aided chemical engineering: Vol. 17. The integration of process design and control* (pp. 430–463). Amsterdam: Elsevier. https://doi.org/10.1016/S1570-7946(04)80069-5

Frumkin, J. A., & Doherty, M. F. (2020). A rapid screening methodology for chemical processes. *Computers & Chemical Engineering, 142*, 107039. https://doi.org/10.1016/j.compchemeng.2020.107039

Georgakis, C., Vinson, D. R., Subramanian, S., & Uztürk, D. (2004). A geometric approach for process operability analysis. In P. Seferlis, & M. C. Georgiadis (Eds.), *Computer aided chemical engineering: Vol. 17. The integration of process design and control* (pp. 96–125). Amsterdam: Elsevier. https://doi.org/10.1016/S1570-7946(04)80056-7

Goldberg, D. E. (1989). *Genetic algorithms in search, optimization & machine learning.* Reading, MA: Addison-Wesley.

Gonzalez-Salazar, M. A., Kirsten, T., & Prchlik, L. (2018). Review of the operational flexibility and emissions of gas- and coal-fired power plants in a future with growing renewables. *Renewable and Sustainable Energy Reviews, 82*(1), 1497–1513. https://doi.org/10.1016/j.rser.2017.05.278

Grossmann, I. E., Apap, R. M., Calfa, B. A., García-Herreros, P., & Zhang, Q. (2016). Recent advances in mathematical programming techniques for the optimization of process systems under uncertainty. *Computers & Chemical Engineering, 91*, 3–14. https://doi.org/10.1016/j.compchemeng.2016.03.002

Grossmann, I. E., Calfa, B. A., & Garcia-Herreros, P. (2014). Evolution of concepts and models for quantifying resiliency and flexibility of chemical processes. *Computers & Chemical Engineering, 70*, 22–34. https://doi.org/10.1016/j.compchemeng.2013.12.013

Grossmann, I. E., & Harjunkoski, I. (2019). Process Systems Engineering: Academic and industrial perspectives. *Computers & Chemical Engineering, 126*, 474–484. https://doi.org/10.1016/j.compchemeng.2019.04.028

Gutierrez, G., Ricardez-Sandoval, L. A., Budman, H., & Prada, C. (2014). An MPC-based control structure selection approach for simultaneous process and control design. *Computers & Chemical Engineering, 70,* 11–21. https://doi.org/10.1016/j.compchemeng.2013.08.014

Häggblom, K. E. (1997a). Control structure selection via relative gain analysis of partially controlled systems. In *1997 European Control Conference (ECC)* (pp. 3019–3024). Brussels: Institute of Electrical and Electronics Engineers (IEEE). https://doi.org/10.23919/ECC.1997.7082571

Häggblom, K. E. (1997b, November). *Partial relative gain: A new tool for control structure selection*. Paper presented at the 1997 AIChE Annual Meeting, Los Angeles, CA, United States. Retrieved from http://users.abo.fi/khaggblo/RS/aic971.pdf

Hamid, M. K. A., Sin, G., & Gani, R. (2010). Integration of process design and controller design for chemical processes using model-based methodology. *Computers & Chemical Engineering, 34*(5), 683–699. https://doi.org/10.1016/j.compchemeng.2010.01.016

Hänninen, M., & Ylijoki, J. (2008). *VTT tiedotteita – Research notes: Vol. 2443. The one-dimensional separate two-phase flow model of APROS*. Espoo: VTT Technical Research Centre of Finland. Retrieved from https://www.vttresearch.com/sites/default/files/pdf/tiedotteet/2008/T2443.pdf

He, M.-J., Cai, W.-J., Ni, W., & Xie, L.-H. (2009). RNGA based control system configuration for multivariable processes. *Journal of Process Control, 19*(6), 1036–1042. https://doi.org/10.1016/j.jprocont.2009.01.004

Hernjak, N., Doyle, F. J., III., Ogunnaike, B. A., & Pearson, R. K. (2004). Chemical process characterization for control design. In P. Seferlis, & M. C. Georgiadis (Eds.), *Computer aided chemical engineering: Vol. 17. The integration of process design and control* (pp. 42–75). Amsterdam: Elsevier. https://doi.org/10.1016/S1570-7946(04)80054-3

Hovd, M., Ma, D. L., & Braatz, R. D. (2003). On the computation of disturbance rejection measures. *Industrial & Engineering Chemistry Research, 42*(10), 2183–2188. https://doi.org/10.1021/ie010533w

Hultgren, M., Kovács, J., & Ikonen, E. (2015). Combustion control in oxy-fired circulating fluidized bed combustion. In D. Bankiewicz, M. Mäkinen, & P. Yrjas (Eds.), *Proceedings of the 22nd International Conference on Fluidized Bed Conversion: Vol. 2* (pp. 1195–1205). Turku: Åbo Akademi.

Huusom, J. K. (2015). Challenges and opportunities in integration of design and control. *Computers & Chemical Engineering, 81*, 138–146. https://doi.org/10.1016/j.compchemeng.2015.03.019

Ikonen, E., Kovacs, J., Aaltonen, H., Ritvanen, J., Selek, I., & Kettunen, A. (2012). Analysis and tuning of a CFB model using particle filtering. In M. Fadel, & S. Caux (Eds.), *8th Power Plant and Power System Control Symposium - PPPSC 2012, IFAC Proceedings Volumes 45*(21) (pp. 711–716). https://doi.org/10.3182/20120902-4-FR-2032.00124

Ikonen, E., Kovács, J., & Ritvanen, J. (2013). Circulating fluidized bed hot-loop analysis, tuning, and state-estimation using particle filtering. *International Journal of Innovative Computing, Information and Control, 9*(8), 3357–3376. Retrieved from http://www.ijicic.org/ijicic-12-06061.pdf

International Energy Agency. (2011). *Harnessing variable renewables: A guide to the balancing challenge*. Paris: OECD Publishing. https://doi.org/10.1787/9789264111394-en

Jacobsen, E. W., & Skogestad, S. (1991). Design modifications for improved controllability of distillation columns. In L. Puigjaner, & A. Espuña (Eds.), *Computer-Oriented Process Engineering: Proceedings of COPE-91* (pp. 123–128). Amsterdam: Elsevier. Retrieved from https://folk.ntnu.no/skoge/publications/1991/cope91_Design/cope91_Design.pdf

Jain, A., & Babu, B. V. (2015). Relative response array: A new tool for control configuration selection. *International Journal of Chemical Engineering and Applications, 6*(5), 356–362. https://doi.org/10.7763/IJCEA.2015.V6.509

Jelali, M. (2006). An overview of control performance assessment technology and industrial applications. *Control Engineering Practice, 14*(5), 441–466. https://doi.org/10.1016/j.conengprac.2005.11.005

Jin, B., Zhao, H., & Zheng, C. (2016). Dynamic exergy method and its application for CO_2 compression and purification unit in oxy-combustion power plants. *Chemical Engineering Science, 144*, 336–345. https://doi.org/10.1016/j.ces.2016.01.044

Jørgensen, S. B., Gani, R., & Andersen, T. R. (1999, June). *Towards integration of controllability into plant design*. Paper presented at the 7th IEEE Mediterranean Conference on Control and Automation (MED '99), Haifa, Israel. Retrieved from http://www.med-control.org/main/conferences

Joronen, T., Kovács, J., & Majanne, Y. (Eds.). (2007). *SAS julkaisusarja: Vol. 33. Voimalaitosautomaatio*. Helsinki: Suomen Automaatioseura ry (SAS).

Julier, S. J., & Uhlmann, J. K. (1997). New extension of the Kalman filter to nonlinear systems. In I. Kadar (Ed.), *AeroSense '97, Proceedings of SPIE: Vol. 3068. Signal Processing, Sensor Fusion, and Target Recognition VI* (pp. 182–193). Orlando, FL: The International Society for Optical Engineering (SPIE). https://doi.org/10.1117/12.280797

Kalman, R. E. (1960). On the general theory of control systems. In J. F. Coales (Ed.), *1st International IFAC Congress on Automatic and Remote Control, IFAC Proceedings Volumes 1*(1) (pp. 491–502). https://doi.org/10.1016/S1474-6670(17)70094-8

Kariwala, V., Skogestad, S., & Forbes, J. F. (2006). Relative gain array for norm-bounded uncertain systems. *Industrial & Engineering Chemistry Research, 45*(5), 1751–1757. https://doi.org/10.1021/ie050790r

Kaushik, S. C., Reddy, V. S., & Tyagi, S. K. (2011). Energy and exergy analyses of thermal power plants: A review. *Renewable and Sustainable Energy Reviews, 15*(4), 1857–1872. https://doi.org/10.1016/j.rser.2010.12.007

Klefenz, G. (1986). *Automatic control of steam power plants* (3rd rev. ed.). Mannheim: B.I.-Wissenschaftsverlag.

Klöpffer, W., & Grahl, B. (2014). *Life cycle assessment (LCA): A guide to best practic*e. Weinheim: Wiley.

Koller, R. W., & Ricardez-Sandoval, L. A. (2017). A dynamic optimization framework for integration of design, control and scheduling of multi-product chemical processes under disturbance and uncertainty. *Computers & Chemical Engineering, 106*, 147–159. https://doi.org/10.1016/j.compchemeng.2017.05.007

Kookos, I. K., & Perkins, J. D. (2004). The back-off approach to simultaneous design and control. In P. Seferlis, & M. C. Georgiadis (Eds.), *Computer aided chemical engineering: Vol. 17. The integration of process design and control* (pp. 216–238). Amsterdam: Elsevier. https://doi.org/10.1016/S1570-7946(04)80061-0

Kovács, J., Kettunen, A., Ikonen, E., Hultgren, M., & Niva, L. (2015). Addressing the challenge of fast load change requirements. In D. Bankiewicz, M. Mäkinen, & P. Yrjas (Eds.), *Proceedings of the 22nd International Conference on Fluidized Bed Conversion: Vol. 1* (pp. 253– 262). Turku: Åbo Akademi.

Kovács, J., Kettunen, A., & Ojala, J. (2012). Modelling and control design of once-through boilers. In M. Fadel, & S. Caux (Eds.), *8th Power Plant and Power System Control Symposium - PPPSC 2012, IFAC Proceedings Volumes 45*(21) (pp. 196–200). https://doi.org/10.3182/20120902-4-FR-2032.00036

Kragelund, M., Wisniewski, R., Mølbak, T., Nielsen, R. J., & Edlund, K. (2008). On propagating requirements and selecting fuels for a Benson boiler. In M. J. Chung, & P. Misra (Eds.), *17th IFAC World Congress, IFAC Proceedings Volumes 41*(2) (pp. 347–352). https://doi.org/10.3182/20080706-5-KR-1001.00059

Lagarias, J. C., Reeds, J. A., Wright, M. H., & Wright, P. E. (1998). Convergence properties of the Nelder-Mead simplex method in low dimensions. *SIAM Journal on Optimization, 9*(1), 112–147. https://doi.org/10.1137/S1052623496303470

Lappalainen, J., Tourunen, A., Mikkonen, H., Hänninen, M., & Kovács, J. (2014). Modelling and dynamic simulation of a supercritical, oxy combustion circulating fluidized bed power plant concept—Firing mode switching case. *International Journal of Greenhouse Gas Control, 28*, 11–24. https://doi.org/10.1016/j.ijggc.2014.06.015

Larsson, T., & Skogestad, S. (2000). Plantwide control—A review and a new design procedure. *Modeling, Identification and Control, 21*(4), 209–240. https://doi.org/10.4173/mic.2000.4.2

Leckner, B., & Gómez-Barea, A. (2014). Oxy-fuel combustion in circulating fluidized bed boilers. *Applied Energy, 125*, 308–318. https://doi.org/10.1016/j.apenergy.2014.03.050

Lee, H. H., Koppel, L. B., & Lim, H. C. (1972). Integrated approach to design and control of a class of countercurrent processes. *Industrial & Engineering Chemistry Process Design and Development, 11*(3), 376–382. https://doi.org/10.1021/i260043a009

Lewin, D. R., Seider, W. D., & Seader, J. D. (2002). Integrated process design instruction. *Computers & Chemical Engineering, 26*(2), 295–306. https://doi.org/10.1016/S0098-1354(01)00747-5

Liu, P., Georgiadis, M. C., & Pistikopoulos, E. N. (2011). Advances in energy systems engineering. *Industrial & Engineering Chemistry Research, 50*(9), 4915–4926. https://doi.org/10.1021/ie101383h

Liu, Q., Li, X., Liu, H., & Guo, Z. (2020). Multi-objective metaheuristics for discrete optimization problems: A review of the state-of-the-art. *Applied Soft Computing, 93*, 106382. https://doi.org/10.1016/j.asoc.2020.106382

Liu, Q., Shi, Y., Zhong, W., & Yu, A. (2019). Co-firing of coal and biomass in oxy-fuel fluidized bed for CO_2 capture: A review of recent advances. *Chinese Journal of Chemical Engineering, 27*(10), 2261–2272. https://doi.org/10.1016/j.cjche.2019.07.013

Luo, X., Cao, P., & Xu, F. (2016). Dynamic interaction analysis and pairing evaluation in control configuration design. *Chinese Journal of Chemical Engineering, 24*(7), 861–868. https://doi.org/10.1016/j.cjche.2016.04.016

Luo, W., Wang, Q., Guo, J., Liu, Z., & Zheng, C. (2015). Exergy-based control strategy selection for flue gas recycle in oxy-fuel combustion plant. *Fuel, 161*, 87–96. https://doi.org/10.1016/j.fuel.2015.08.036

Luyben, W. L. (1996). Design and control degrees of freedom. *Industrial & Engineering Chemistry Research, 35*(7), 2204−2214. https://doi.org/10.1021/ie960038d

Luyben, W. L. (2004). The need for simultaneous design education. In P. Seferlis, & M. C. Georgiadis (Eds.), *Computer aided chemical engineering: Vol. 17. The integration of process design and control* (pp. 10–41). Amsterdam: Elsevier. https://doi.org/10.1016/S1570-7946(04)80053-1

Luyben, W. L., Tyréus, B. D., & Luyben, M. L. (1999). *Plantwide process control*. New York, NY: McGraw-Hill.

Lyman, P. R., & Luyben, W. L. (1994). A method for assessing the effects of design parameters on controllability. In E. Zafiriou (Ed.), *IFAC Workshop on Integration of Process Design and Control (IPDC'94), IFAC Proceedings Volumes 27*(7) (pp. 85–91). https://doi.org/10.1016/S1474-6670(17)47969-9

Majanne, Y., & Maasalo, M. (2009). Dynamic simulation assisted design of industrial power plant process and control. In Y. Majanne (Ed.), *6th IFAC Symposium on Power Plants and Power Systems Control, IFAC Proceedings Volumes 42*(9) (pp. 326–331). https://doi.org/10.3182/20090705-4-SF-2005.00058

Manousiouthakis, V., Savage, R., & Arkun, Y. (1986). Synthesis of decentralized process control structures using the concept of block relative gain. *AIChE Journal, 32*(6), 991–1003. https://doi.org/10.1002/aic.690320609

Martín, M., & Adams, T. A., II. (2019). Challenges and future directions for process and product synthesis and design. *Computers & Chemical Engineering, 128*, 421–436. https://doi.org/10.1016/j.compchemeng.2019.06.022

Mehta, S., & Ricardez-Sandoval, L. A. (2016). Integration of design and control of dynamic systems under uncertainty: A new back-off approach. *Industrial & Engineering Chemistry Research, 55*(2), 485–498. https://doi.org/10.1021/acs.iecr.5b03522

Mencarelli, L., Chen, Q., Pagot, A., & Grossmann, I. E. (2020). A review on superstructure optimization approaches in process system engineering. *Computers & Chemical Engineering, 136*, 106808. https://doi.org/10.1016/j.compchemeng.2020.106808

Mertens, N., Alobaid, F., Starkloff, R., Epple, B., & Kim, H.-G. (2015). Comparative investigation of drum-type and once-through heat recovery steam generator during start-up. *Applied Energy, 144*, 250–260. https://doi.org/10.1016/j.apenergy.2015.01.065

Mitsos, A., Asprion, N., Floudas, C. A., Bortz, M., Baldea, M., Bonvin, D., … Schäfer, P. (2018). Challenges in process optimization for new feedstocks and energy sources. *Computers & Chemical Engineering, 113*, 209–221. https://doi.org/10.1016/j.compchemeng.2018.03.013

Mohideen, M. J., Perkins, J. D., & Pistikopoulos, E. N. (1996). Optimal synthesis and design of dynamic systems under uncertainty. *Computers & Chemical Engineering, 20*(Supplement 2), S895–S900. https://doi.org/10.1016/0098-1354(96)00157-3

Montelongo-Luna, J. M., Svrcek, W. Y., & Young, B. R. (2011). The relative exergy array—A new measure for interactions in process design and control. *The Canadian Journal of Chemical Engineering, 89*(3), 545–549. https://doi.org/10.1002/cjce.20422

Morari, M. (1992). Effect of design on the controllability of chemical plants. In J. Perkins (Ed.), *IFAC Workshop on Interactions between Process Design and Process Control, IFAC Proceedings Volumes 25*(24) (pp. 3–16). https://doi.org/10.1016/S1474-6670(17)54006-9

Munir, M. T., Yu, W., & Young, B. R. (2013). The relative exergy-destroyed array: A new tool for control structure design. *The Canadian Journal of Chemical Engineering, 91*(10), 1686–1694. https://doi.org/10.1002/cjce.21797

Muñoz, D. A., Gerhard, J., & Marquardt, W. (2012). A normal vector approach for integrated process and control design with uncertain model parameters and disturbances. *Computers & Chemical Engineering, 40*, 202–212. https://doi.org/10.1016/j.compchemeng.2012.01.016

Murthy Konda, N. V. S. N., Rangaiah, G. P., & Krishnaswamy, P. R. (2006). A simple and effective procedure for control degrees of freedom. *Chemical Engineering Science, 61*(4), 1184–1194. https://doi.org/10.1016/j.ces.2005.08.026

Narraway, L. T., Perkins, J. D., & Barton, G. W. (1991). Interaction between process design and process control: Economic analysis of process dynamics. *Journal of Process Control, 1*(5), 243–250. https://doi.org/10.1016/0959-1524(91)85015-B

Nikačević, N. M., Huesman, A. E. M., Van den Hof, P. M. J., & Stankiewicz, A. I. (2012). Opportunities and challenges for process control in process intensification. *Chemical Engineering and Processing: Process Intensification, 52*, 1–15. https://doi.org/10.1016/j.cep.2011.11.006

Niva, L., Hultgren, M., Ikonen, E., & Kovács, J. (2017). Control structure design for oxy-fired circulating fluidized bed boilers using self-optimizing control and partial relative gain analyses. In D. Dochain, D. Henrion, & D. Peaucelle (Eds.), *20th IFAC World Congress, IFAC-PapersOnLine 50*(1) (pp. 2023–2030). https://doi.org/10.1016/j.ifacol.2017.08.199

Ogata, K. (2010). *Modern control engineering* (5th ed.). New Jersey, NJ: Prentice Hall.

Ogunnaike, B. A., & Ray, W. H. (1994). *Process dynamics, modeling, and control*. New York, NY: Oxford University Press.

Oyama, H., & Durand, H. (2020). Interactions between control and process design under economic model predictive control. *Journal of Process Control, 92*, 1–18. https://doi.org/10.1016/j.jprocont.2020.05.009

Patwardhan, S. C., Narasimhan, S., Jagadeesan, P., Gopaluni, B., & Shah, S. L. (2012). Nonlinear Bayesian state estimation: A review of recent developments. *Control Engineering Practice, 20*(10), 933–953. https://doi.org/10.1016/j.conengprac.2012.04.003

Perkins, J. D. (1989). Interactions between process design and process control. In J. E. Rijnsdorp, J. F. MacGregor, B. D. Tyreus, & T. Takamatsu (Eds.), *IFAC Symposium on Dynamics and Control of Chemical Reactors, Distillation Columns and Batch Processes (DYCORD+'89), IFAC Proceedings Volumes 22*(8) (pp. 195–203). https://doi.org/10.1016/S1474-6670(17)53357-1

Perkins, J. D., & Walsh, S. P. K. (1996). Optimization as a tool for design/control integration. *Computers & Chemical Engineering, 20*(4), 315–323. https://doi.org/10.1016/0098-1354(95)00022-4

Pistikopoulos, E. N., & Diangelakis, N. A. (2016). Towards the integration of process design, control and scheduling: Are we getting closer?. *Computers & Chemical Engineering, 91*, 85–92. https://doi.org/10.1016/j.compchemeng.2015.11.002

Pistikopoulos, E. N., Diangelakis, N. A., Oberdieck, R., Papathanasiou, M. M., Nascu, I., & Sun, M. (2015). PAROC—An integrated framework and software platform for the optimisation and advanced model-based control of process systems. *Chemical Engineering Science, 136*, 115–138. https://doi.org/10.1016/j.ces.2015.02.030

Powell, K. M., Hedengren, J. D., & Edgar, T. F. (2014). Dynamic optimization of a hybrid solar thermal and fossil fuel system. *Solar Energy, 108*, 210–218. https://doi.org/10.1016/j.solener.2014.07.004

Price, R. M., Lyman, P. R., & Georgakis, C. (1994). Throughput manipulation in plantwide control structures. *Industrial & Engineering Chemistry Research, 33*(5), 1197–1207. https://doi.org/10.1021/ie00029a016

Rafiei, M., & Ricardez-Sandoval, L. A. (2020a). Integration of design and control for industrial-scale applications under uncertainty: A trust region approach. *Computers & Chemical Engineering 141*, 107006. https://doi.org/10.1016/j.compchemeng.2020.107006

Rafiei, M., & Ricardez-Sandoval, L. A. (2020b). New frontiers, challenges, and opportunities in integration of design and control for enterprise-wide sustainability. *Computers & Chemical Engineering, 132*, 106610. https://doi.org/10.1016/j.compchemeng.2019.106610

Ricardez-Sandoval, L. A., Budman, H. M., & Douglas, P. L. (2009). Integration of design and control for chemical processes: A review of the literature and some recent results. *Annual Reviews in Control, 33*(2), 158–171. https://doi.org/10.1016/j.arcontrol.2009.06.001

Ritvanen, J., Kovacs, J., Salo, M., Hultgren, M., Tourunen, A., & Hyppänen, T. (2012). 1-D dynamic simulation study of oxygen fired coal combustion in pilot and large scale CFB boilers. In *Proceedings of the 21st International Conference on Fluidized Bed Combustion: Vol. 1* (pp. 72–79). Naples: EnzoAlbanoEditore.

Rosenbrock, H. H. (1970). *State-space and multivariable theory*. London: Nelson.

Sakizlis, V., Perkins, J. D., & Pistikopoulos, E. N. (2004). Recent advances in optimization-based simultaneous process and control design. *Computers & Chemical Engineering, 28*(10), 2069–2086. https://doi.org/10.1016/j.compchemeng.2004.03.018

Sargent, R. W. H. (1967). Integrated design and optimization of processes. *Chemical Engineering Progress, 63*(9), 71–78.

Sarkar, D. K. (2015). *Thermal power plant: Design and operation*. Amsterdam: Elsevier. https://doi.org/10.1016/C2014-0-00536-9

Särkkä, S. (2013). *Institute of Mathematical Statistics textbooks: Vol. 3. Bayesian filtering and smoothing*. Cambridge: Cambridge University Press. https://doi.org/10.1017/CBO9781139344203

Schweickhardt, T., & Allgöwer, F. (2004). Quantitative nonlinearity assessment – An introduction to nonlinearity measures. In P. Seferlis, & M. C. Georgiadis (Eds.), *Computer aided chemical engineering: Vol. 17. The integration of process design and control* (pp. 76–95). Amsterdam: Elsevier. https://doi.org/10.1016/S1570-7946(04)80055-5

Schweiger, C. A., & Floudas, C. A. (1998). Interaction of design and control: Optimization with dynamic models. In W. H. Hager, & P. M. Pardalos (Eds.), *Applied Optimization: Vol. 15. Optimal control: Theory, algorithms, and applications* (pp. 388–435). Dordrecht: Springer. https://doi.org/10.1007/978-1-4757-6095-8_19

Seddighi, S. (2017). Design of large scale oxy-fuel fluidized bed boilers: Constant thermal power and constant furnace size scenarios. *Energy, 118*, 1286–1294. https://doi.org/10.1016/j.energy.2016.11.004

Seddighi, S., Clough, P. T., Anthony, E. J., Hughes, R. W., & Lu, P. (2018). Scale-up challenges and opportunities for carbon capture by oxy-fuel circulating fluidized beds. *Applied Energy, 232*, 527–542. https://doi.org/10.1016/j.apenergy.2018.09.167

Seddighi, S., Pallarès, D., Normann, F., & Johnsson, F. (2015). Heat extraction from a utility-scale oxy-fuel-fired CFB boiler. *Chemical Engineering Science, 130*, 144–150. https://doi.org/10.1016/j.ces.2015.03.015

Sharifzadeh, M. (2013). Integration of process design and control: A review. *Chemical Engineering Research and Design, 91*(12), 2515–2549. https://doi.org/10.1016/j.cherd.2013.05.007

Sharifzadeh, M., Bumb, P., & Shah, N. (2016). Carbon capture from pulverized coal power plant (PCPP): Solvent performance comparison at an industrial scale. *Applied Energy, 163*, 423–435. https://doi.org/10.1016/j.apenergy.2015.11.017

Sharifzadeh, M., & Shah, N. (2019). MEA-based CO_2 capture integrated with natural gas combined cycle or pulverized coal power plants: Operability and controllability through integrated design and control. *Journal of Cleaner Production, 207*, 271–283. https://doi.org/10.1016/j.jclepro.2018.09.115

Shields, R. W., & Pearson, J. B. (1976). Structural controllability of multiinput linear systems. *IEEE Transactions on Automatic Control, 21*(2), 203–212. https://doi.org/10.1109/TAC.1976.1101198

Siirola, J. J., & Edgar, T. F. (2012). Process energy systems: Control, economic, and sustainability objectives. *Computers & Chemical Engineering, 47*, 134–144. https://doi.org/10.1016/j.compchemeng.2012.06.019

Singh, R. I., & Kumar, R. (2016). Current status and experimental investigation of oxy-fired fluidized bed. *Renewable and Sustainable Energy Reviews, 61*, 398–420. https://doi.org/10.1016/j.rser.2016.04.021

Skogestad, S. (1994). A procedure for SISO controllability analysis - With application to design of pH processes. In E. Zafiriou (Ed.), *IFAC Workshop on Integration of Process Design and Control (IPDC'94), IFAC Proceedings Volumes 27*(7) (pp. 25–30). https://doi.org/10.1016/S1474-6670(17)47959-6

Skogestad, S. (2004). Control structure design for complete chemical plants. *Computers & Chemical Engineering, 28*(1–2), 219–234. https://doi.org/10.1016/j.compchemeng.2003.08.002

Skogestad, S., & Postlethwaite, I. (2005). *Multivariable feedback control: Analysis and design* (2nd ed.). Chichester: Wiley.

Smith, R. (2005). *Chemical process design and integration* (2nd ed.). Chichester: Wiley.

Stanger, R., Wall, T., Spörl, R., Paneru, M., Grathwohl, S., Weidmann, M., … Santos, S. (2015). Oxyfuel combustion for CO_2 capture in power plants. *International Journal of Greenhouse Gas Control, 40*, 55–125. https://doi.org/10.1016/j.ijggc.2015.06.010

Stephanopoulos, G., & Ng, C. (2000). Perspectives on the synthesis of plant-wide control structures. *Journal of Process Control, 10*(2–3), 97–111. https://doi.org/10.1016/S0959-1524(99)00023-2

Sun, L., Hua, Q., Li, D., Pan, L., Xue, Y., & Lee, K. Y. (2017). Direct energy balance based active disturbance rejection control for coal-fired power plant. *ISA Transactions, 70*, 486–493. https://doi.org/10.1016/j.isatra.2017.06.003

Swartz, C. L. E., & Kawajiri, Y. (2019) Design for dynamic operation - A review and new perspectives for an increasingly dynamic plant operating environment. *Computers & Chemical Engineering, 128*, 329–339. https://doi.org/10.1016/j.compchemeng.2019.06.002

Szargut, J. (2005). *Developments in heat transfer: Vol. 18. Exergy method: Technical and ecological applications*. Southampton: WIT Press.

Teichgraeber, H., Brodrick, P. G., & Brandt, A. R. (2017). Optimal design and operations of a flexible oxyfuel natural gas plant. *Energy, 141*, 506–518. https://doi.org/10.1016/j.energy.2017.09.087

Ulbig, A., & Andersson, G. (2015). Analyzing operational flexibility of electric power systems. *International Journal of Electrical Power & Energy Systems, 72*, 155–164. https://doi.org/10.1016/j.ijepes.2015.02.028

van der Merwe, R., Doucet, A., de Freitas, N., & Wan, E. (2000). *The unscented particle filter, Technical report CUED/F-INFENG/TR 380*. Cambridge: Cambridge University Engineering Department.

van de Wal, M., & de Jager, B. (2001). A review of methods for input/output selection. *Automatica, 37*(4), 487–510. https://doi.org/10.1016/S0005-1098(00)00181-3

Vasbinder, E. M., Hoo, K. A., & Mann, U. (2004). Synthesis of plantwide control structures using a decision-based methodology. In P. Seferlis, & M. C. Georgiadis (Eds.), *Computer aided chemical engineering: Vol. 17. The integration of process design and control* (pp. 375–400). Amsterdam: Elsevier. https://doi.org/10.1016/S1570-7946(04)80067-1

Vega, P., Lamanna de Rocco, R., Revollar, S., & Francisco, M. (2014). Integrated design and control of chemical processes – Part I: Revision and classification. *Computers & Chemical Engineering, 71*, 602–617. https://doi.org/10.1016/j.compchemeng.2014.05.010

Vu, T. T. L., Bahri, P. A., & Romagnoli, J. A. (1997). Operability considerations in chemical processes: A switchability analysis. *Computers & Chemical Engineering, 21*(Supplement), S143–S148. https://doi.org/10.1016/S0098-1354(97)87493-5

Weitz, O., & Lewin, D. R. (1996). Dynamic controllability and resiliency diagnosis using steady state process flowsheet data. *Computers & Chemical Engineering, 20*(4), 325–335. https://doi.org/10.1016/0098-1354(95)00023-2

White, V., Perkins, J. D., & Espie, D. M. (1996). Switchability analysis. *Computers & Chemical Engineering, 20*(4), 469–474. https://doi.org/10.1016/0098-1354(95)00037-2

Wu, Z., Li, D., Xue, Y., Sun, L., He, T., & Zheng, S. (2020). Modified active disturbance rejection control for fluidized bed combustor. *ISA Transactions, 102*, 135–153. https://doi.org/10.1016/j.isatra.2020.03.003

Xiong, Q., Cai, W.-J., & He, M.-J. (2005). A practical loop pairing criterion for multivariable processes. *Journal of Process Control, 15*(7), 741–747. https://doi.org/10.1016/j.jprocont.2005.03.008

Yuan, Z., Chen, B., Sin, G., & Gani, R. (2012). State-of-the-art and progress in the optimization-based simultaneous design and control for chemical processes. *AIChE Journal, 58*(6), 1640–1659. https://doi.org/10.1002/aic.13786

Zhang, H., Gao, M., Hong, F., Liu, J., & Wang, X. (2019). Control-oriented modelling and investigation on quick load change control of subcritical circulating fluidized bed unit. *Applied Thermal Engineering, 163*, 114420. https://doi.org/10.1016/j.applthermaleng.2019.114420

Zhao, Y., Liu, M., Wang, C., Li, X., Chong, D., & Yan, J. (2018a). Increasing operational flexibility of supercritical coal-fired power plants by regulating thermal system configuration during transient processes. *Applied Energy, 228*, 2375–2386. https://doi.org/10.1016/j.apenergy.2018.07.070

Zhao, Y., Wang, C., Liu, M., Chong, D., & Yan, J. (2018b). Improving operational flexibility by regulating extraction steam of high-pressure heaters on a 660 MW supercritical coal-fired power plant: A dynamic simulation. *Applied Energy, 212*, 1295–1309. https://doi.org/10.1016/j.apenergy.2018.01.017

Ziegler, J. G., & Nichols, N. B. (1943). Process lags in automatic-control circuits. *Transactions of the A.S.M.E., 65*, 433–444.

Zimmerman, N., Kyprianidis, K., & Lindberg, C.-F. (2018). Waste fuel combustion: Dynamic modeling and control. *Processes, 6*(11), 222. https://doi.org/10.3390/pr6110222

Zotică, C., Nord, L. O., Kovács, J., & Skogestad, S. (2020). Optimal operation and control of heat to power cycles: A new perspective from a systematic plantwide control approach. *Computers & Chemical Engineering, 141*, 106995. https://doi.org/10.1016/j.compchemeng.2020.106995

Original publications

I   Hultgren, M., Ikonen, E., & Kovács, J. (2014). Oxidant control and air-oxy switching concepts for CFB furnace operation. *Computers & Chemical Engineering, 61*, 203–219. https://doi.org/10.1016/j.compchemeng.2013.10.018

II   Hultgren, M., Ikonen, E., & Kovács, J. (2014). Circulating fluidized bed boiler state estimation with an unscented Kalman filter tool. In *2014 IEEE Conference on Control Applications (CCA)* (pp. 310–315). Antibes: Institute of Electrical and Electronics Engineers (IEEE). https://doi.org/10.1109/CCA.2014.6981364

III Hultgren, M., Ikonen, E., & Kovács, J. (2017). Integrated control and process design in CFB boiler design and control – Application possibilities. In D. Dochain, D. Henrion, & D. Peaucelle (Eds.), *20th IFAC World Congress, IFAC-PapersOnLine 50*(1) (pp. 1997–2004). https://doi.org/10.1016/j.ifacol.2017.08.180

IV Hultgren, M., Ikonen, E., & Kovács, J. (2017). Once-through circulating fluidized bed boiler control design with the dynamic relative gain array and partial relative gain. *Industrial & Engineering Chemistry Research, 56*(48), 14290–14303. https://doi.org/10.1021/acs.iecr.7b03259

V   Hultgren, M., Ikonen, E., & Kovács, J. (2019). Integrated control and process design for improved load changes in fluidized bed boiler steam path. *Chemical Engineering Science, 199*, 164–178. https://doi.org/10.1016/j.ces.2019.01.025

Reprinted with permission from Elsevier (I, V), IEEE (II), IFAC (III), American Chemical Society (IV).

Original publications are not included in the electronic version of the dissertation.

120

Computers and Chemical Engineering

Oxidant control and air-oxy switching concepts for CFB furnace operation

Matias Hultgren [a,*], Enso Ikonen [a], Jenö Kovács [b]

[a] *Systems Engineering Laboratory, University of Oulu, Linnanmaa, POB 4300, FI-90014 Oulun yliopisto, Finland*
[b] *Foster Wheeler Energia Oy, Relanderinkatu 2, POB 201, FI-78201 Varkaus, Finland*

ABSTRACT

Oxy combustion in circulating fluidized bed (CFB) boilers was investigated in this paper. Oxy combustion is a carbon capture and storage technology, which uses oxygen and recirculated flue gas (RFG) instead of air as an oxidant. Air and oxy combustion were compared through physical considerations and simulations, focusing on process dynamics, transients and control. The oxidant specific heat capacity and density are elevated in oxy combustion, which leads to slower temperature dynamics. Flue gas recirculation introduces internal feedback dynamics to the process. The possibility to adjust the RFG and oxygen flows separately gives an additional degree of freedom for control. In the simulations, "direct" and "sequenced" switches between air- and oxy-firing were compared. Fast "direct" switches with simultaneous ramping of all inputs should be preferred due to the resulting smooth temperature responses. If these process input changes are unfeasible, the fuel should be altered after the gaseous flows ("sequenced" method).

© 2013 Elsevier Ltd. All rights reserved.

1. Introduction

This paper investigates the differences between oxy combustion ("oxyfuel" process) and air combustion in circulating fluidized bed (CFB) power plants, with a particular focus on the process dynamics and transient behaviour in the oxy-CFB. Oxy combustion is one of the major industrial carbon capture and storage (CCS) technologies, which also include pre- and post-combustion capture, as well as chemical looping combustion (CLC). Carbon dioxide emissions have received an increasing attention because of the concern for climate change, especially for industrial branches consuming fossil fuels. One solution for reducing CO_2 emissions in power plants is to capture the CO_2 from flue gases with CCS. The captured and processed CO_2 is transported to underground or underwater high-pressure storage sites or, alternatively, used in industrial applications.

In oxy combustion, solid fuel is combusted with a mixture of pure oxygen and recirculated flue gas (RFG) from the process instead of air as an oxidant, resulting in a flue gas CO_2 concentration of 70–98 vol.% (dry) and thus an easier recovery of the carbon dioxide from the flue gas. Oxy combustion has been deemed as one of the most promising options for CO_2 capture, when considering the energy, cost efficiency and extremely small atmospheric CO_2 release of the process. The main structural and operational

differences between air and oxy combustion plants are presented in this paper, concentrating on the dynamic aspects leading to control considerations. Even though the ultimate goal of the overall research is to develop controls for oxy-CFB, this paper deals with the general aspects and concepts of combustion control suitable for both air- and oxy-fired CFB boilers.

In fluidized bed (FB) combustion of solid fuels, fuel particles are fluidized and combusted in a bed of incombustible material of e.g. sand or ash in the furnace riser. The fluidizing medium is the primary input gas flow, which commonly contains the oxidizing agent needed for combustion. In circulating fluidized beds (CFBs), a sufficiently high gas velocity and small particle size enable the solids to become entrained with the bed and to leave the furnace riser tube. The solids are separated from the flue gas in a gas–solid separator, from which the flue gas continues to the backpass and the solids are recycled back to the bed through the solids circulation system. Together, these process components form the hotloop (Fig. 1), which is the studied CFB boiler subsystem of this paper. CFB combustion is used for solid fuels and also for liquid fuels to some extent.

When designing control solutions for CFB combustion, the main issues affecting both the steady-state and dynamic behaviour of the process can be summarized with the key points below:

- Fluidization

As the furnace input gas (oxidant) flows are responsible for the fluidization in the CFB, any effects the oxy-firing process

* Corresponding author. Tel.: +358 503502923; fax: +358 85532304.
E-mail addresses: matias.hultgren@oulu.fi (M. Hultgren), enso.ikonen@oulu.fi (E. Ikonen), jeno.kovacs@fwfin.fwc.com (J. Kovács).
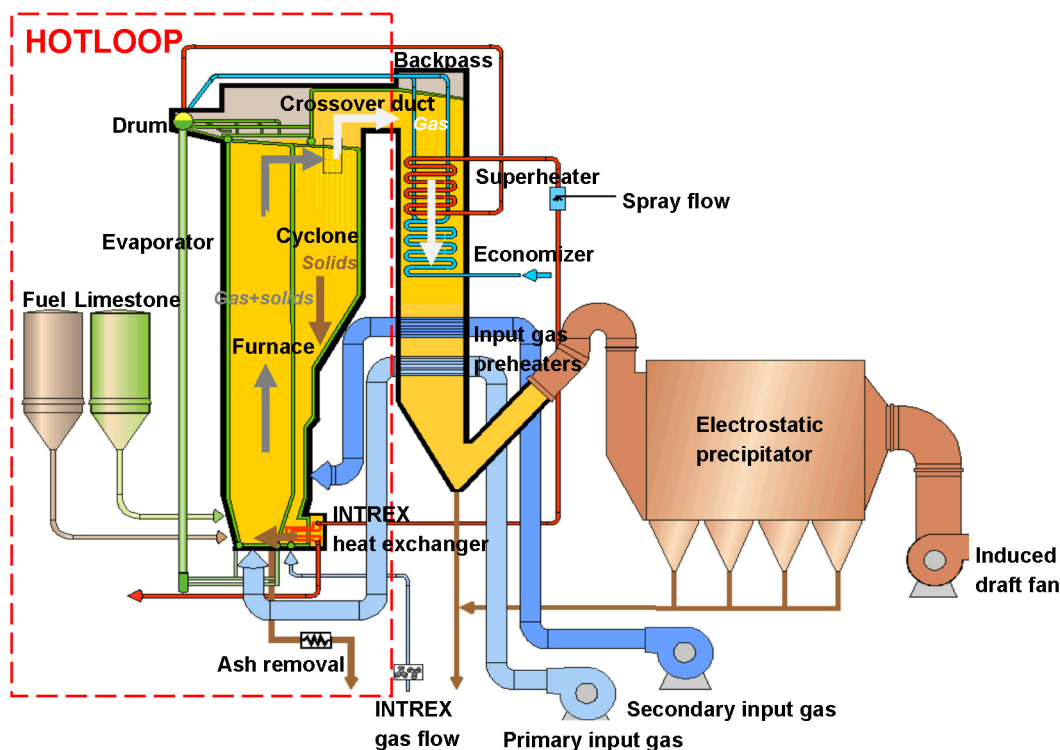
Fig. 1. Operation schematic of the CFB boiler, with the hotloop highlighted with the dashed line. Modified from Foster Wheeler Energia Oy (2012).

configuration has on the gas flows have the potential to alter the fluidization and thus the mixing and heat transfer in the bed. Proper fluidization has to be maintained in the bed.

• Input oxidant flows, i.e. input gas flows

The oxidant flow is air for air-fired FB processes and oxygen + recirculated flue gas for oxy combustion. This is the main cause for the differences between air and oxy combustion. The heat capacity, density and chemical component concentrations of the oxidant are directly related to the differences between the combustion atmospheres. For the combustion dynamics, especially the oxygen input and thus the oxidant O_2 percentage are of importance.

• Heat transfer & boiler MW output

The heat transfer in the dense bed, the upper furnace, the flue gas path and the return leg affects the selection of heat exchanger sizes and the power plant performance optimization. The differences in heat transfer between air and oxy combustion are thus significant factors for combustion control. Maintaining a correct heat transfer distribution is especially important for once-through (OTU) boilers, as these units don't contain a water-steam drum as a buffer for steam generation.

• Combustion & firing power

The combustion in the CFB furnace riser determines the generated amount of heat in the boiler. When comparing air and oxy combustion, the effect of the atmosphere change on the combustion reactions and the heat generation has to be considered. Important process variables are furnace temperatures at different points in the riser and the flue gas O_2 content.

• Combustion-related reactions

Because of the flue gas recirculation and absence of air in oxy combustion, the concentrations of emission components such as SO_x, NO_x and CO will be affected by the combustion mode. This has the potential to cause changes in the gaseous emissions of power generation, as well as in the mechanisms and balances of emission formation reactions.

• Fuel

The fuel input determines the combustion progression and the emission formation. Knowledge of fuel flow properties such as heating values, carbon and moisture contents, solids/volatiles distributions, as well as mass flow accuracies can be used in feed-forward and model-based control solutions. As the fuel flow is set separately from the input gas flows, no notable differences between air and oxy combustion should occur because of the fuel alone.

• Integration of the boiler and supporting units

In oxy combustion, the boiler island depends on the oxygen production and CO_2 post-processing units. As a result, coordinated or plant-wide boiler island control might be of importance. The O_2 is produced with an air separation unit (ASU), while the CO_2 is captured using carbon compression (CCU) and purification (CPU) units. Dynamic properties such as production rates, startup times and load following capabilities of these units need to be considered in the overall control design.

• Water-steam cycle

The water-steam cycle contains the main power plant control loops, such as live steam temperature control, boiler-turbine unit control, feedwater control and drum level control. As the heat used on the water-steam side comes from the combustion and as the

main focus of this work was on hotloop dynamics, the water-steam control issues in oxy-firing boilers were not discussed in this paper.

- Boiler island in grid control

Special requirements arise, when the boiler participates in grid frequency or district heating network control. As the focus of this paper was on the CFB hotloop, these matters were not discussed here.

Currently oxy combustion is in its pilot testing and early commercialization stage. Both theoretical and experimental research is being conducted on the CCS process chain by universities and companies in the field. For example, six demonstration projects are supported by the European Energy Programme for Recovery (EEPR 2010–2013), with the aim of making CCS zero emission power generation commercially feasible by the year 2020. One of these projects is the planned CCS supercritical CFB Compostilla project in Spain. The necessary technology for this process is currently being tested at the same location with the CIUDEN 30MW oxy combustion and CCS test facility. From large-scale general CCS investigations, the "Special Report on Carbon Dioxide Capture and Storage" report by the IPCC (IPCC, 2005) is one of the most extensive and it includes a section on oxy combustion. Aside from solid fuel combustion, oxy combustion is being researched for other power generation systems like natural gas burners and gas turbine cycles (e.g. Hasegawa, 2013; Thorbergsson, 2012; Yin, Rosendahl, & Kaer, 2011).

So far, oxyfuel research has mostly considered steady-state process conditions and the pulverized coal (PC) oxy-coal process. Although this paper focuses on the fluidized bed combustion technology, oxy-PC research results offer valuable insights into the general differences between air- and oxy-firing. Toftegaard, Brix, Jensen, Glarborg, and Jensen (2010) combined a wide array of oxyfuel PC references into an extensive review article focusing on the differences between air and oxy combustion. Davidson and Santos (2010) also reported on pulverized fuel oxy combustion and the overall development of the oxy-firing technology. Wall et al. (2009) focused on fuel reactivity, combustion characteristics, heat transfer and emission formation in oxy-PC.

Despite the usefulness of the oxy-PC research results, the CFB has its own requirements and thus calls for specific CFB references. In general, the fluidized bed technology has been widely documented in the literature; see e.g. Basu (2006). For oxy-CFB, Czakiert et al. concentrated on combustion kinetics and conversion rates of different fuel components (Czakiert & Nowak, 2010; Czakiert, Bis, Muskala, & Nowak, 2006; Czakiert, Sztekler, Karski, Markiewicz, & Nowak, 2010). Duan, Zhao, Zhou, Chengrui, and Chen (2011) presented results from 50 kW$_{th}$ pilot oxy-CFB measurements. The particular focus of these authors was on the input oxidant O$_2$ percentage and its effects on the differences between air and oxy combustion. Practical design issues were considered by Romeo et al. (2011). Oxy-CFB research from Foster Wheeler was presented e.g. by Eriksson et al. (2007) and Hack et al. (2008), who described the air/oxy Flexi-Burn^{TM} technology, oxy modelling studies, pilot and bench scale experiments and conceptual oxyfuel retrofit designs. E.g. Suraniti, ya Nsakala, and Darling (2009) and ya Nsakala et al. (2004) discussed the oxy-CFB research work and experimental testing of Alstom Power.

Few papers related to oxyfuel control design have been published up to date, for oxy-CFB in particular. Oxy combustion results in several changes in the operation of the process which require attention during boiler control design. Due to a different composition of the combustion atmosphere, the furnace temperature and heat transfer dynamics will become slower. In addition, the flue gas recirculation in oxy mode introduces internal feedback dynamics to the system, a feature not found in basic air combustion (without flue gas recirculation). As modern fossil fuel power plants

Table 1
The properties of the fuels that were used in the simulation tests.

Components	Spanish anthracite	Petcoke
Ultimate analysis (wt%, dry)		
C	55.2	86.4
H	2.2	3.9
N	0.8	1.7
O	4.4	1.8
S	1.8	5.7
Proximate analysis (wt%)		
Moisture	12.1	3.1
Ash (dry basis)	35.6	0.4
Volatiles (dry basis)	10.2	12.8
Heat value (MJ/kg)		
LHV (as received)	20.3	34.5

(including oxyfuel plants) have to be able to provide fast responses to load changes, careful control design is needed. For oxy combustion, switches between air and oxy mode are also an essential part of e.g. the startup and shutdown sequences of the plant. Some references about air-oxy-air switches can be found in the literature (e.g. McDonald & Zadiraka, 2007; Weigl, 2009). The separate oxygen and RFG gas flow inputs in oxy combustion give more degrees of freedom for performing combustion control. The investigation of the specific features of oxy-CFB dynamics and the combustion control challenges related to the technology form the motivation for this paper.

After this introduction, the process model used in this paper and its background experimental research are presented in Section 2. Section 3 deals with oxyfuel static aspects and the steady-state differences between air and oxy combustion in order to form a background for understanding oxy-firing process dynamics. Section 4 discusses the main differences in the process dynamics of oxy and air combustion and presents the challenges and possibilities in the oxy-CFB hotloop control structure. The dynamic simulations of this work are discussed in Section 5 through switching tests between air and oxy combustion. Section 6 summarizes the conclusions of this work.

2. Experimental setup

A dynamic 1-D Matlab/Simulink hotloop model was used to investigate the dynamics of the oxy-CFB process. This model has been developed in cooperation between Foster Wheeler Energia Oy, the Lappeenranta University of Technology (LUT) and the University of Oulu. A description of the model can be found in Ritvanen et al. (2012). The hotloop model structure had been previously validated and used extensively for various air-fired circulating fluidized bed boilers of different sizes. In the preparation work for this paper, a successful initial model validation in oxy mode was performed using measurement data from an air/oxy-fired pilot combustor (Tourunen, 2010) with a fuel power of 50–100 kW$_{th}$ in oxy mode and 20–50 kW$_{th}$ in air mode. The pilot contained a furnace tube (height 8 m, inner diameter 167 mm), a solid material circulation tube, cyclones for solids and fly ash separation, flue gas processing equipment, a flue gas recirculation system, as well as fuel, limestone and oxidant feeding lines. In the testing campaign, a fuel blend with an approximate 70/30 mass percentage ratio of anthracite (primary fuel) and petcoke (secondary fuel) was burned (Table 1). To form the oxyfuel oxidant, RFG from the flue gas line was mixed with room temperature high purity bottled O$_2$, resulting in a realistic oxy-firing process configuration. The primary oxidant was introduced through the grid with primary air preheating for air mode, while the secondary oxidant was fed from three different levels in the riser.

The model validation was conducted through air/oxy load steps and oxy load ramps, using filtered actual input data from the pilot.
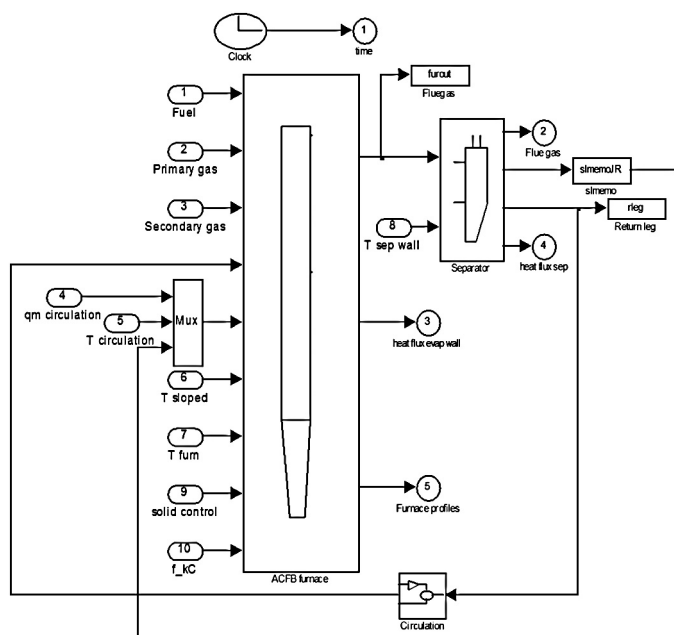
Fig. 2. The hotloop module of the air/oxy dynamic model used in this study.

For the measurement campaign, the pilot was equipped with extensive temperature, heat transfer, pressure, solid material sampling and flue gas composition measurements. The input data included RFG, pure O_2 and air mass flows, fuel silo weight measurements and fuel feeding screw RPM values, as well as primary and secondary oxidant temperatures. The calculation of fuel mass flows was based on least squares fits from fuel silo weight decreases with minor modifications based on alternations in the process outputs. Output measurements used in the validation mainly contained flue gas composition data and furnace temperatures.

For this paper, separate air-oxy-air switch test simulations were conducted with the hotloop model. Like the validation cases, the model was configured according to the pilot plant and thus only contained the furnace, the gas–solid separator and the solids circulation system. These subsystems were included in the hotloop Simulink model (Fig. 2), while the calculation codes of the furnace and the separator had been implemented as C-coded s-functions. For oxy-firing simulations, a separate input gas mixing module for mixing the RFG, pure O_2 and air flows to form the primary and secondary oxidants was also included into the simulator. A pure O_2 flow purity of 96.6 wt% was used for all simulations in this study, with the rest of the pure O_2 consisting of nitrogen.

The CFB process was modelled using both physical and empirical approaches. The furnace riser tube consisted of 20 ideally mixed calculation elements, for which element specific mass and energy balances were solved against time with an ODE solver. A combined energy equation for the gaseous and solid phases was defined to solve the element temperatures, while the hydrodynamics, combustion characteristics, vertical density profile and heat transfer inside the modules were calculated using empirical and semi-empirical correlations. The heterogeneous reactions of carbon, hydrogen and sulphur were considered for the solid fuel combustion. Hotloop cooling could be applied through element-specific surface temperature parameters to simulate the effects of the water-steam cycle. Although the model contained no water-steam side calculations, it is usually used as the hotloop component in a complete power plant simulation software application.

The number of hotloop model system states depended on the process configuration and the inputs. For this paper, 855 states in total were used. Because of the large amount of states, the model is

Fig. 3. Simplified input–output structure of the hotloop model.

mainly a simulator for investigating process dynamics and testing control solutions, and should not be applied directly in e.g. model-based control. Nevertheless, a state estimation approach for model-based analysis of an experiment campaign has also been developed (Ikonen, Kovács, & Ritvanen, 2013). An input–output "black box" structure of the model is illustrated in Fig. 3.

3. Oxy-CFB combustion, static aspects

The static aspects of oxy combustion need to be considered before investigating, how oxy process dynamics will differ from air-firing. This chapter presents the oxyfuel-related changes in the CFB operation that lead to steady-state differences in heat transfer, fluidization, combustion and emission formation. Furthermore, the additional process units needed for oxy combustion are discussed.

3.1. Recirculated flue gas

Replacing the input air with oxygen and recirculated flue gas (RFG) is the source for the various differences between air and oxy combustion, although the basic operational principle of solid fuel combustion remains the same in both combustion modes. In the oxy-CFB, pure oxygen is required for the combustion, while RFG serves as the main fluidizing medium. The RFG is essential for the fluidization, as the pure O_2 volumetric flow rate is much smaller than the corresponding amount of input air. The other main functions of the RFG are to act as a heat transporting medium and to bring furnace temperatures to the optimal operating regions (typically 850–900 °C in CFB) of combustion, heat transfer and bed sulphur capture. It is important to acknowledge that the cooling and fluidizing effects of the RFG are opposite: an RFG-based increase in fluidization simultaneously contributes to lowering the furnace temperatures. This is different from air-firing, as an increase in the air input automatically leads to an increased O_2 input, as well. As the RFG is extracted from the flue gas, the exhaust gas heat loss will be smaller in oxy mode than in air mode.

A flue gas recirculation system with mixers for mixing oxygen, RFG and also air during combustion mode switches is mandatory for the oxy-firing operation. Even though flue gas recirculation can also be used in air-fired boilers for e.g. temperature control, the RFG is the main component of the input oxidant in oxy combustion. The flue gas recirculation system can be designed in various ways, mainly involving the choice of the RFG withdrawal point from the flue gas line and the operations performed to the recycled flue gas. The chosen recirculation point affects the RFG composition and thus the properties of the process input oxidant, as well as the size, energy and material requirements of flue gas and RFG processing units. Choosing between a wet and a dry flue gas recycle is especially important (Toftegaard et al., 2010; Eriksson et al., 2007). Air leakage into the boiler also needs to be dealt with in the process chain, as the CO_2 product quickly becomes diluted by nitrogen and the CO_2 separation difficulty is increased, if air leakage into the oxyfuel boiler is extensive.

Due to the oxy-firing process configuration, the concentrations of gaseous components in the oxidant and the flue gas become markedly different from air combustion (Table 2). Especially the remarkable increases in CO_2 and H_2O and the reduction in N_2 should be noted here. As the specific heat capacities of both CO_2
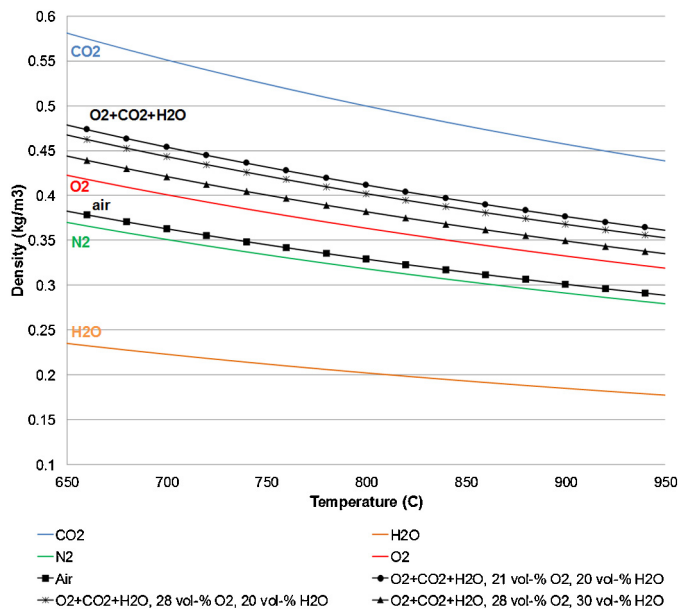
Table 2
Typical concentrations of gaseous components in the oxidant and the flue gas before water condensing in air and oxy combustion.

		Percentage vol.% in gas (wet basis)	
		Air combustion	Oxy combustion
Input oxidant gas	O_2	21	21–30
	N_2	79	0–10
	CO_2	0	40–50
	H_2O	Small	10–20
	NO_x, SO_x	No	Yes
Flue gas	O_2	3–4	3–4
	N_2	70–75	0–10
	CO_2	12–14	60–70
	H_2O	10–15	20–25
	NO_x, SO_x	Yes	Yes

Data from Davidson and Santos (2010).

Fig. 4. Density values for various gaseous components and mixtures at 1 atm and different temperatures, when the ideal gas assumption is used for non-water species.

and H_2O are higher than that of N_2 (Table 3) in the boiler temperature range, the heat capacities of the gaseous flows in the CFB will increase in oxy combustion. CO_2 also has a larger molecular weight and density than nitrogen (Fig. 4), resulting in a higher oxyfuel oxidant gas density than the density of air. Therefore, if the nitrogen of air is simply replaced with RFG and the total input gas mass flow is kept constant, the oxidant gas volume flow will be smaller in oxy mode than in air mode, which causes a change in the fluidization conditions. Like in air combustion, the steady-state composition and thus the physical/chemical properties of the oxy-fuel flue gas flow will depend on the input fuel feed properties.

However, the flue gas recirculation in oxy mode will also link the oxidant composition to the fuel flow in the oxy-CFB.

3.2. Heat transfer distribution

The oxyfuel oxidant heat capacity and density elevations mean that furnace temperatures will be lowered, if the heating power or furnace cooling in oxy mode remains unchanged from air mode. As the oxidant O_2 contents of Table 2 and research literature indicate, the lower temperature levels can be prevented by oxidant O_2 enrichment, i.e. by controlling the mixing ratio of pure oxygen and RFG to increase the oxidant O_2 content above the 21 vol.% value of air. The O_2 percentage required for air-like furnace temperatures depends on several factors, most notably the fuel type and the flue gas recirculation system. The oxidant O_2 enrichment issue is elaborated on in Section 3.4.

Since the gas flow through the boiler would not give up heat as willingly in oxy combustion as in air combustion due to its elevated heat capacity, combustion heat is transported further downstream in oxy mode and the heat distribution between heat exchangers might be affected. In general, the conduction of heat further downstream in the process chain contributes towards an improved convective heat transfer, while the radiative heat transfer close to the furnace decreases. Indeed, improved heat transfer efficiencies at least in the convective section of the boiler have been reported by e.g. Hack et al. (2008) and IPCC (2005).

Despite the heat capacity elevation, it is difficult to make conclusions about the overall heat transfer differences between air- and oxy-firing, as heat transfer is influenced by multiple factors. For convective heat transfer, these include the fluid dynamics of the system and thus the fluidization (e.g. Reynolds and Prandtl numbers), the heat conductivity of the gas and the gas temperatures of the superheaters (Toftegaard et al., 2010). Moreover, the main gaseous components of oxy combustion (CO_2 and H_2O) are radiative species, unlike N_2 in air combustion. This, along with possible furnace temperature or particle size distribution effects, has the potential to boost oxy mode radiative heat transfer. Radiative heat transfer is also not as crucial for the CFB as convective heat transfer (Romeo et al., 2011). Although the oxy heat transfer is thus going to be case specific, a potential shift in heat exchanger duties should not be overlooked, as it might affect the operational points of process subsystems and bring models used in control outside their validity regions.

3.3. Combustion and emissions

A basic point of comparison between air and oxy mode is how the gaseous atmosphere affects the combustion reactions. The combustion progression is determined by the combustion reaction rate and the oxygen diffusion rate to the particle surface. Basically, the diffusivity of both oxygen and small hydrocarbons is lower in a CO_2-based medium than in an N_2 atmosphere (Toftegaard et al., 2010; Wall et al., 2009). As a result, oxygen will be less available for combustion and the volatile consumption rate will be hindered. If

Table 3
Experimental values of gaseous species at 1123 °C.

Quantity	Unit	Species				CO_2/N_2 property ratio
		H_2O	O_2	N_2	CO_2	
Density (ρ)	kg/m^3	0.157	0.278	0.244	0.383	1.6
Specific heat capacity (c_p)	kJ/kmol K	45.67	36.08	34.18	57.83	1.7
Specific heat capacity (c_p)	kJ/kg K	2.53	1.00	1.22	1.31	1.1
Heat sink (ρc_p)	kJ/m^3 K	0.397	0.278	0.298	0.502	1.7
Mass diffusivity of O_2 (D_{O_2}/species)	m^2/s	–	–	1,70E−04	1.30E−04	0.8

Data from Toftegaard et al. (2010).

the oxidant O_2 content is thus kept at 21 vol.% in oxy mode, the combustion reactions will slow down, the particle heat generation rate decrease and the amount of unburned carbon potentially increase because of the diffusivity change and the lowered oxy-firing furnace temperatures. However, with oxidant O_2 enrichment, the oxygen partial pressure in the furnace will be larger than in air-firing and the temperatures will increase, resulting in raised combustion efficiency, reaction rate and char burnout levels (Duan et al., 2011; Czakiert et al., 2006), although the burnout depends heavily on the fuel type, as well. Furthermore, carbon gasification increases in oxy-firing due to the high CO_2 and H_2O contents in the gas.

The formation of emission components will be affected by the flue gas recirculation and the changes in reaction mechanisms. Due to the accelerated fuel gasification, the formation of CO will be larger in oxy-firing than in air-firing, although the formed extra CO will probably be consumed before leaving the furnace (Duan et al., 2011). Due to the lack of elemental nitrogen from air and through several specific reaction mechanisms, NO_x formation can be minimized in oxy combustion (Toftegaard et al., 2010). The absolute amount of char and ash will stay approximately similar for both combustion modes, while the size distribution of the solids might be altered e.g. by changes in furnace temperatures. So far, bed agglomeration, slagging and fouling have not presented any significant problems for oxy combustion in FB boilers.

In fluidized bed limestone sulphur capture, the CO_2 partial pressure and furnace temperature changes in oxy combustion have the potential to alter the predominant sulphation reaction mechanism from indirect (first calcinated, then sulphated) to direct sulphation (Toftegaard et al., 2010). The overall differences between the air and oxy combustion sulphur capture efficiencies are debated upon. Additional oxyfuel process requirements come from the possibility of limestone recarbonation into $CaCO_3$ and from locally elevated concentrations of acidic SO_x gaseous species.

3.4. Oxyfuel boiler configuration

Because of the different air and oxy combustion oxidant and flue gas compositions, existing air-fired boiler designs would not necessarily be optimal for oxy-firing from a heat transfer, fluidization or combustion perspective. Therefore, it should be defined whether the goal of the design is an oxyfuel retrofit of an existing boiler or an oxyfuel greenfield plant optimized mainly for oxy combustion. The target of oxy retrofits is to obtain air-like combustion conditions in the furnace, as the structure of the oxyfuel power plant will then differ from air-fired plants with slight modifications only.

In order to produce similar furnace temperatures and temperature profiles to air-firing in oxy combustion, oxidant O_2 enrichment is needed. In principle, the O_2 content of the oxidant and the

furnace temperatures can be increased either by primarily reducing the cooling RFG flow or by raising the firing power by increasing the pure oxygen input. Consequently, the latter option results in a simultaneous increase in the fuel flow and thus a greater heat generation through combustion. Both of these methods have their own disadvantages: a smaller RFG flow leads to a smaller input gas volume flow (RFG is the main gas component) and might thus hamper the fluidization in the bed, while increasing the pure O_2 input flow results in higher oxygen production costs. However, as proper fluidization has to be ensured at all times in the CFB, the temperature target will most likely mainly be achieved by increasing the pure O_2 flow and firing more fuel (Hack et al., 2008).

In oxy greenfield plants with no restrictions from air combustion compatibility, the oxidant O_2 percentage can be raised well beyond the values required for air-like combustion conditions, leading to higher temperatures, smaller entropy losses and potentially a more efficient combustion with better char burnout and a smaller oxygen excess. If the RFG flow can be reduced to achieve this, the gas flows and total gas volume in the system will be reduced compared to air-fired boilers, resulting in smaller oxy power plants with an unaltered firing power. This will lead to reduced construction costs, thermal radiation heat losses and flue gas recirculation power requirements. Because of the risks associated with new technologies like oxy combustion with high oxidant O_2 levels, the first generation of oxyfuel boilers is likely to consist of modifications of existing air-fired units.

The notions presented for retrofits can, to some extent, be applied to dual-firing and oxy-ready boilers, which strive for the process to function well in both air and oxy mode. Beside new technology risk mitigation, these solutions offer operational flexibility regarding the power demand and the prices of emission rights. The Foster Wheeler Flexi-Burn[TM] boiler (Fig. 5) is one example of a flexible air/oxy boiler technology. As both air- and oxy-firing are used, switches between air and oxy combustion and also between different oxy-firing oxidant O_2 percentages are an integral part of the operation. Air-firing is also used in retrofits during startups and shutdowns of the boiler.

3.5. ASU, CCU and CPU

On a plant-wide scale, the major differences between air and oxy combustion come from the oxy-firing pre- and post-processing units, namely the ASU, CCU and CPU. The necessary processing steps and product quality requirements in the carbon compression and purification units (CCU + CPU) are largely determined by the uses and storage methods of the CO_2. The CCS flue gas processing will at least require a stage-wise compression of the gas to high or even supercritical pressures, dehydration, cooling and non-condensable species removal. The input oxygen is usually produced with one or
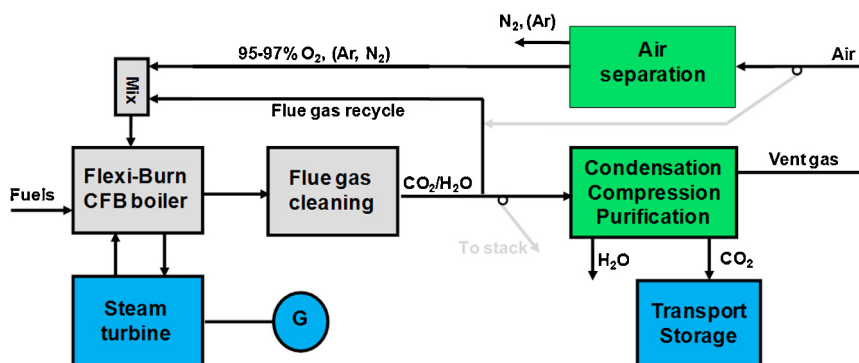

Fig. 5. Schematic of a Flexi-Burn[TM] CFB power plant (Foster Wheeler Energia Oy, 2012).
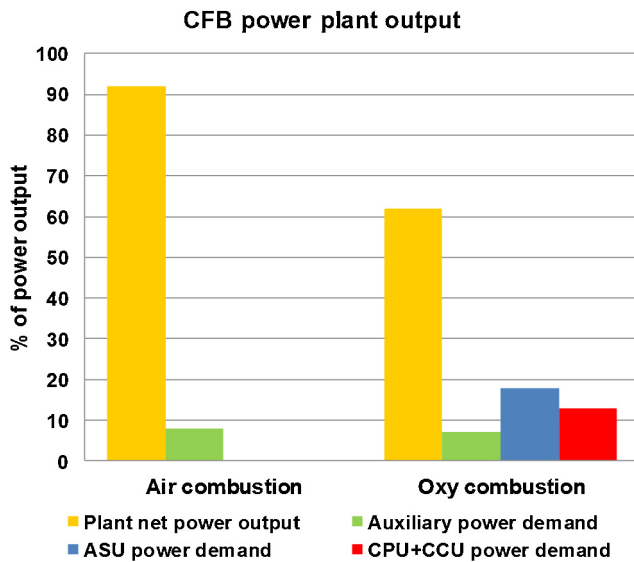
Fig. 6. Air/oxy-CFB output power distribution example. Data from ya Nsakala et al. (2004).
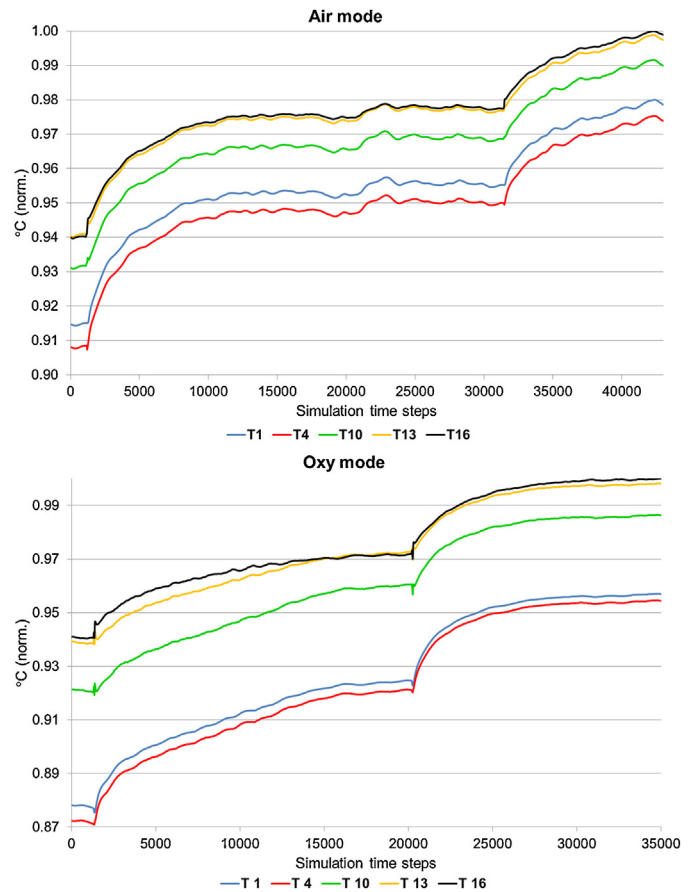

Fig. 7. Normalized furnace temperature responses at different riser heights (T) of air combustion (upper) and oxy combustion (lower) load step simulations, hotloop model validation simulations.

several parallel air separation units (ASU), which will typically be based on cryogenic distillation of air, when considering the current industrial scale O_2 production options.

The ASU, CCU and CPU are perhaps the most important challenge of the oxyfuel development, as the high pressures and low temperatures in oxygen production and CO_2 compression require a lot of energy and thus have a negative effect on the power plant net efficiency (Fig. 6). This applies especially to the ASU, which might cause the power plant efficiency to drop 7–9% and be responsible for 60% of the additional energy requirement of CCS (Toftegaard et al., 2010). The operating costs of the ASU, CCU and CPU are influenced by the purity of the produced oxygen and the RFG withdrawal point in the flue gas line, forming an optimization problem between air separation and post-processing costs. The oxygen production limitations in the ASU might also restrict the performance of the boiler, as current air separation solutions are only able to reach a load range of 60–100% and a maximum ramp rate of 3%/min (Toftegaard et al., 2010). The startup time of the ASU also needs to be considered.

4. Dynamic aspects and control: differences between air and oxy combustion

The main differences in the process dynamics and control of air and oxy combustion can be examined from three different angles. Firstly, the altered gaseous atmosphere composition affects the heat transfer, combustion reactions and emission formation in the bed. Secondly, the flue gas recirculation introduces dynamic aspects to the process, which need to be considered in oxy combustion control. Thirdly, the possibility to adjust the input oxygen and RFG flows separately gives an additional degree of freedom for process control. These differences present challenges and possibilities for the oxy-CFB control and will be discussed in detail in this section.

4.1. Oxidant and combustion atmosphere

The most important effect of the oxidant and flue gas compositions on the oxy-CFB dynamics are derived from the increases in gas specific heat capacity and density in oxy mode. The elevated heat capacity will cause the gas flow inside the oxyfuel boiler to heat up and cool down more slowly than in air combustion, resulting in slower temperature transients and thus slower process responses

to load changes. The slower oxy-firing transients are demonstrated in the load step simulations of Fig. 7. As the furnace temperatures are directly connected to the heat transfer and water-steam cycle of the power plant, the indicated changes will most likely be visible in the time constants and settling times of the process MW responses, as well. The slower temperature dynamics can be considered as a disadvantage for the load following capabilities of oxy control and special attention should be paid to the selection of the combustion control structure, as the slower dynamics might have to be compensated with adjustments to the furnace cooling or fuel firing power.

The effect of the oxidant gas density on fluidization is a point of concern in the oxy-CFB switching control. The oxidant density increase in oxy mode presents an optimization problem between the particle residence time and the fluidization efficiency. As indicated in Fig. 4, the gas densities in air and oxy mode will also respond differently to temperature changes. The oxidant density effects can be summarized with the following points:

- If the oxidant mass flow is kept constant during a switch from air to oxy combustion, the gas volume flow will decrease due to its elevated oxy mode density. This means that without sufficient control measures the velocity of the fluidizing gas will decrease, which will hamper the fluidization in the bed by decreasing the turbulence and the mixing efficiency of solids. However, the smaller gas velocity will also contribute to a longer residence time of solids and thus potentially even to a better burnout.
- If the gas volume flow is kept constant during the air to oxy switch by adjusting the RFG and pure O_2 feeds to compensate for the gas

density increase, a denser oxyfuel oxidant with a similar velocity to a corresponding air flow will be able to carry solids better in the riser and improve fluidization. Similarly, this mode of operation could lead to smaller residence times and larger solids circulation amounts, as well as larger pressure difference requirements and thus an increased energy demand of the input gas feeding equipment.

In practice, the best way to run the switches will most likely be to maintain a constant gas volume flow at least for the primary oxidant in order to ensure a proper fluidization throughout the switch. Furthermore, the residence time of the fuel will have a small importance in the CFB because of the solids circulation in the hotloop. The overall effect of the oxidant on the residence time also does not seem to be straightforward and contradictory results have been presented in the literature.

The changes in the oxidant properties affect the oxy-CFB process dynamics and should be considered in its control design, as measurement and control components might need to compensate for the property differences. The task is especially problematic during load and combustion mode transitions due to the alternating gaseous component concentrations. This could lead to an adaptive control system, a lookup-table based feedforward solution or even online calculations. The effects of oxy-firing on heat transfer and fluidization depend on the fuel feed properties (see Section 3.1). However, as the dominating effect is caused by the elevated CO_2 and H_2O contents in the gaseous flows, the fuel type considerations can be omitted in this context from a process dynamics point of view. Compared to air-firing, the gas property changes also call for additional strategies for selecting the level of oxidant O_2 enrichment, handling possible heat transfer distribution changes in the steam generation and ensuring proper fluidization at all times. The special requirements of oxy-firing become especially apparent for retrofits, which are based on air-like combustion conditions.

4.2. Flue gas recirculation

The dynamics of the flue gas recirculation mainly concern oxidant and flue gas component concentrations, although gas compositions are also related to other furnace properties, as described in the previous chapters. The RFG is a combustion reaction product of the process and because it is also the main component of the oxyfuel oxidant, the fluidization and heat transfer are more linked to the combustion in an oxy-CFB than in air-firing. However, at the same time the degree of fluidization greatly affects the combustion and heat transfer in the boiler. This kind of a cause-effect relation introduces new dynamic aspects to the oxy-CFB process. As the recirculation links the oxidant to the fuel feed properties, variations in the fuel quality will cause different responses in the furnace outputs compared to air combustion. Apart from the recirculation itself, additional features to the total process dynamics might be presented by O_2/RFG/air mixers.

For control engineering, the most crucial flue gas component is oxygen, as the flue gas O_2 contains information about the combustion in the furnace. Because of the flue gas recirculation in oxy combustion, the total oxygen input is a combination of pure O_2 from the ASU and RFG O_2 from the flue gas. However, at low frequencies the actual oxygen demand of the process is unaffected by the recycled oxygen, as the required O_2 amount is determined by the corresponding fuel flow and the set O_2 excess. The hotloop and the RFG system can be viewed as a combined process, in which the flue gas recirculation is an internal circulation of gaseous components in the CFB furnace. Consequently, the required O_2 amount is determined by the mass balance of this system.

Like the flue gas O_2, the steady-state values of other flue gas components are not affected by flue gas recirculation, as indicated by the RFG step simulations of Fig. 8. This is dictated by the input–output mass balances of the system. However, the recirculation amount and the changes in the RFG have an effect on the flue gas composition dynamics, for example on the settling times of flue gas composition responses (Fig. 9). From these viewpoints, the flue gas recirculation system once more has analogies with an inner circulation, although the gases in the RFG line are not in active contact with the solid bed. It should be noted that the steady-state compositions remain constant with different RFG amounts only when no flue gas components are removed outside the mass balance boundary as a result of RFG processing. In Fig. 8, this was observed to a minor degree due to SO_2 removal from the RFG. The RFG amount might thus become significant for oxy-firing steady-states, if e.g. H_2O is removed from the RFG line in a dry flue gas recirculation.

The feedback nature of flue gas recirculation will cause both additional flue gas composition dynamics and larger time constants during load or process operation changes. Furthermore, the delay of the firing system will increase, as a change in the combustion reactions will not immediately be visible in the input oxidant composition. The distance of the flue gas recirculation point from the furnace thus not only influences the flue gas processing requirements, but also the process time delay for combustion-related changes. In general, controlling oxidant properties is difficult in oxy-firing, because changes in the combustion or fuel quality will also have an indirect effect on the oxidant quality. This has the potential to cause accumulation or even stability issues for the combustion, if controlled poorly.

The delay and dynamics of flue gas recirculation become visible during air-oxy-air switches, in particular. Based on the results of Weigl (2009), the most important changes in flue gas component concentrations during a switch seem to occur only after the actual switch or during the last stages of the transition ramps of air, pure O_2 and RFG, forming an s-shaped figure in the concentrations. This would suggest that special attention should be paid to the last stages of the transitions and that quick gas flow ramps would be useful in order to obtain the full oxy combustion steady-states as quickly as possible.

Unlike the switch dynamics, hotloop model load test validation simulations showed no major effects related to flue gas recirculation for flue gas composition responses. The flue gas O_2 in oxy mode behaved in a similar way to air combustion and no large changes in the CO_2 and H_2O were seen as a result of load steps and ramps. The results indicated that the crucial control parameter of the flue gas composition dynamics is the RFG/pure O_2 ratio rather than simply the O_2 input. These findings were also supported by literature. When the goal is to alter the fluidization and the firing power in the same way to reach different load levels, the oxidant composition and thus the RFG/pure O_2 ratio should remain similar on all operational levels. As a result, the dynamics of the flue gas recirculation should not disturb the process in these cases.

4.3. Separate control of oxidant components

In oxyfuel boilers, the oxygen supply is independent from the RFG flow, meaning that both the pure O_2 from the ASU and the RFG from the process can be adjusted with their own control structures. This gives an additional degree of freedom to the oxy-CFB control design compared to air-firing, which uses a single oxidant component with an unaltered gas composition. As a result, it is possible to use oxidant O_2 contents differing from air and to alter the oxidant O_2 percentage during the operation in oxy mode. In a way, the oxygen supply, temperature and fluidization become decoupled to some degree: the pure O_2 flow is connected to the combustion, while the RFG is mainly responsible for adjusting temperatures
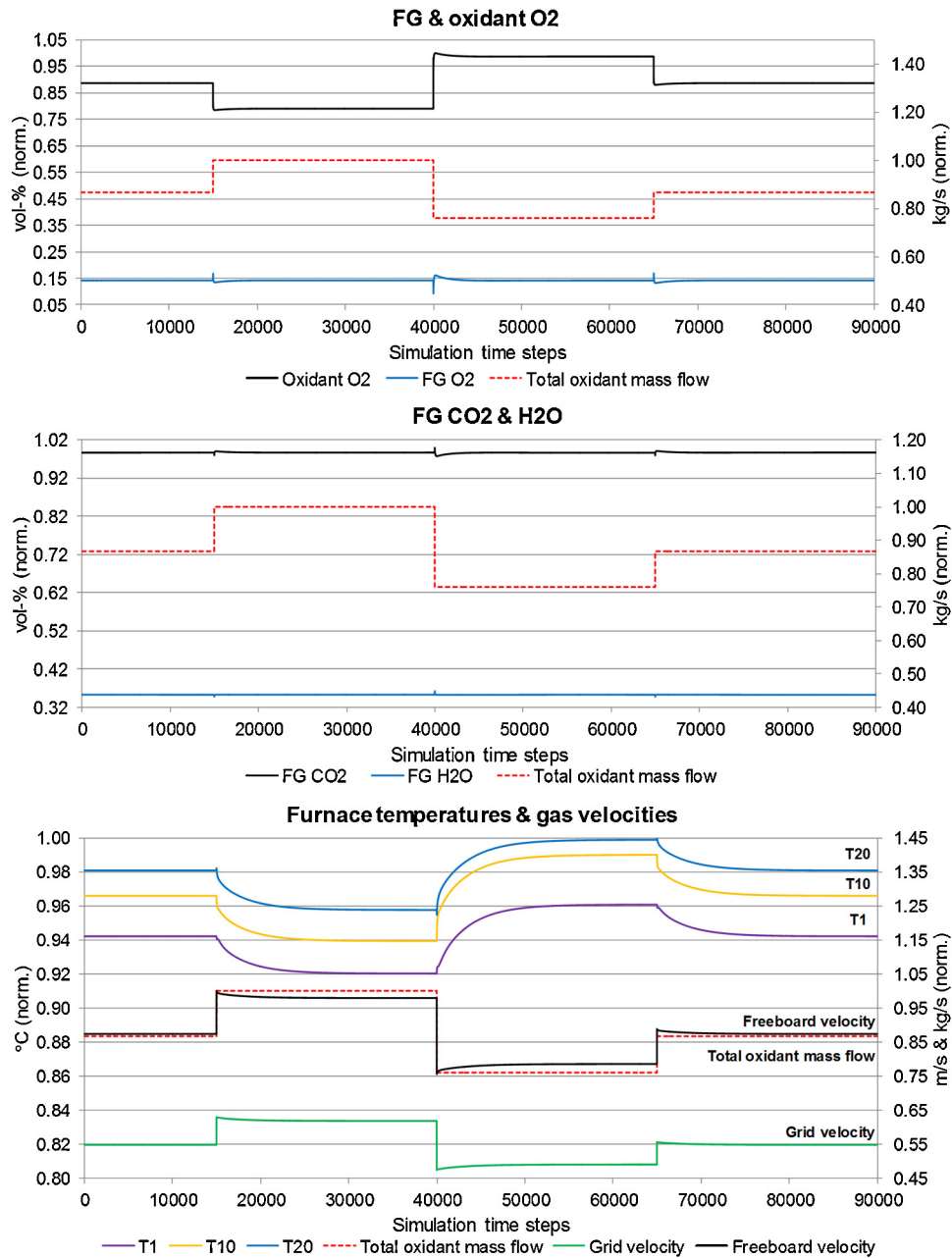
Fig. 8. Normalized simulated flue gas O_2, CO_2 and H_2O responses, furnace temperatures and bed/freeboard velocities for RFG step changes in oxy combustion with a constant firing power (constant fuel and pure O_2 flows).

and fluidization. For example, zone-wise fluidizing RFG flows could be used during load changes to speed up furnace temperature dynamics and to obtain a more uniform temperature profile without directly affecting the combustion. These kinds of considerations introduce entirely new control tasks for solid fuel combustion.

In oxy combustion, the freedom to control the pure O_2 separately from the RFG can be used in flue gas O_2 or oxidant O_2 control. In flue gas O_2 feedback control, one or several pure O_2 or oxidant flows are adjusted according to the measured flue gas O_2 percentage. A flue gas O_2 trim is often compulsory for combustion processes. Like air combustion, the most reasonable flow to be used for flue gas O_2 control is most likely the secondary pure O_2 or oxidant flow, so as not to disrupt the fluidization or the combustion. These control ideas have been illustrated on a conceptual level in Fig. 10, which shows the flue gas O_2 control concepts separately from other hotloop control loops.

Since the pure O_2 can be controlled independently from the RFG, flue gas O_2 control alone will result in a time-variant input oxidant O_2 percentage in oxy combustion, which might be undesirable for the process operation. Oxidant O_2 control concepts (Fig. 11) can be used in oxy combustion to maintain the input oxidant O_2 percentage. The oxidant O_2 is often regarded as a significant process parameter, as it is connected to the pure O_2/RFG ratio and thus the relation between furnace cooling and heat generation. Moreover, the input oxidant O_2 concentration contains information about the flue gas O_2 content because of flue gas recirculation. Oxidant O_2 control is especially important from a safety point of view, as handling gaseous flows with high oxygen contents together with small fuel particles or oxidant preheating might pose risks for the solid fuel power plant. Oxidant O_2 control is essentially a feedforward control solution, as its aim is to supply an oxidant stream with a certain O_2 percentage, regardless of its effect on the combustion.
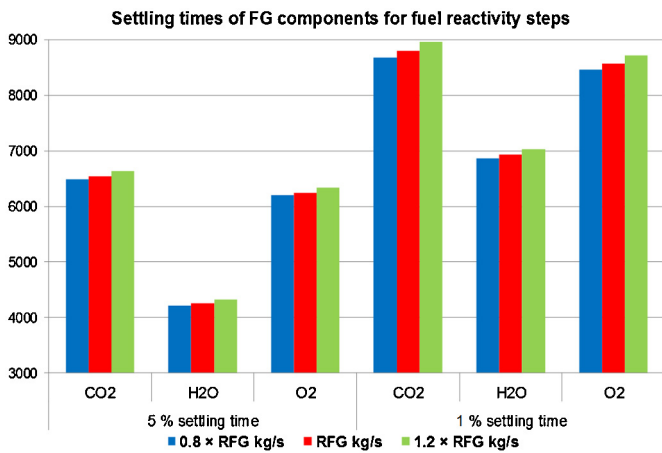
Fig. 9. ±1% and ±5% settling times (time steps) of flue gas CO_2, H_2O and O_2 contents with different flue gas recirculation rates, when the fuel mass flow was decreased with a 10% step. "RFG kg/s" is the nominal RFG mass flow value for the respective load level.

Fig. 11. Example of an oxidant O_2 control concept in oxy-CFB. The primary and secondary pure O_2 flows are used to control the respective O_2 contents. The control is shown on a conceptual level and the figure only displays the oxidant O_2 control, excluding other hotloop control loops.

The oxidant O_2 content can be maintained by adjusting either the pure O_2 flow or the RFG flow. As stated in Section 3 (also illustrated in Fig. 11), the oxidant O_2 percentage should preferably be adjusted with the pure O_2 flows and by modifying the fuel input accordingly. However, controlling the oxidant O_2 without considering the changes in the fluidization might not be enough for the CFB operation. As a result, it might be necessary to control the input gas flow rate beside its O_2 content in oxidant O_2 control. A combined flue gas O_2, oxidant O_2 and total oxidant flow control structure (Fig. 12) would offer a convenient way to control the oxygen input, the combustion and the fluidization in the boiler, even though attention must be paid to conflicting control actions in this solution. Oxidant O_2 control could also be applied only to certain input gas flows.

In oxy combustion, the oxygen excess is easier to maintain at a desired level than in air combustion, as the pure O_2 flow can be determined based on the fuel requirement of the load level, while

the RFG flow can be set according to the desired CFB gas velocity. It is also important to note that the excess air supply of air-firing differs from the excess in oxy-firing, as the λ parameter has to be selected in a different way for a pure O_2 flow with no N_2 and as flue gas recirculation reduces the flue gas flow in the boiler. O_2 excess considerations are important in oxy combustion, because too high λ values carry an ASU oxygen production energy penalty.

One particular advantage and challenge for oxyfuel control is presented by the possibility of using different oxygen concentrations for different oxidant inlets (primary air, secondary air, etc.). This is called oxidant O_2 staging and it can be used in oxy combustion to provide improved furnace profile control for e.g.

Fig. 10. Flue gas O_2 control concepts in oxy-CFB. The secondary pure O_2 (a) and the secondary oxidant (b) are used to control the flue gas O_2 content. The control is displayed on a conceptual level and the figure only shows the flue gas O_2 control, excluding other hotloop control loops.

Fig. 12. Concept for input oxidant control: combined flue gas O_2, primary oxidant O_2 and total input oxidant flow control. The gas volume/mass flow measurement can be designed in various ways. The control is illustrated on a conceptual level and the actual implementation is not considered here.

Fig. 13. Oxidant O_2 staging concept for adjusting riser temperature profiles. The primary oxidant O_2 content is used to modify the dense bed temperature, while the secondary oxidant O_2 content controls the freeboard temperature. The solution is shown on a conceptual level: no other control loops are included and the implementation of control loops or measurements is not considered.

Fig. 14. Air to oxy switch schematic with matching ramp speeds and starting times for all inputs.
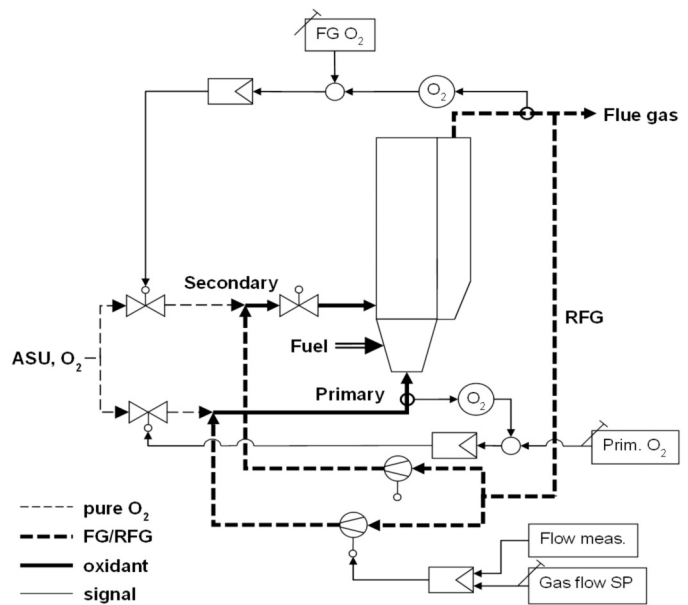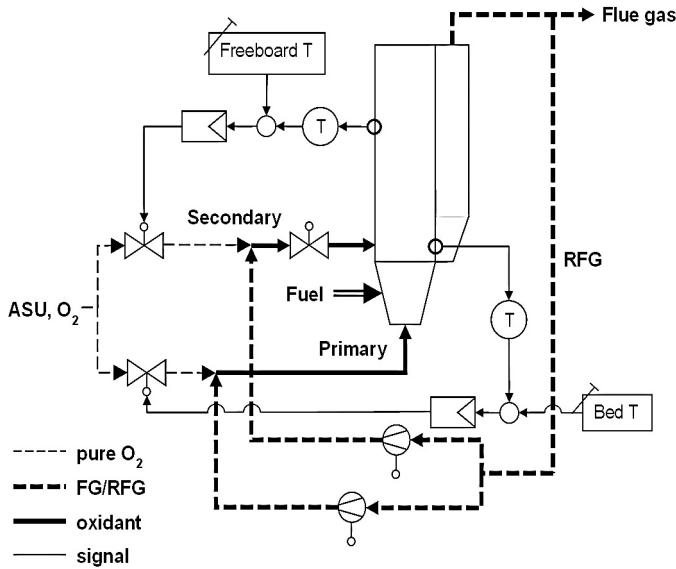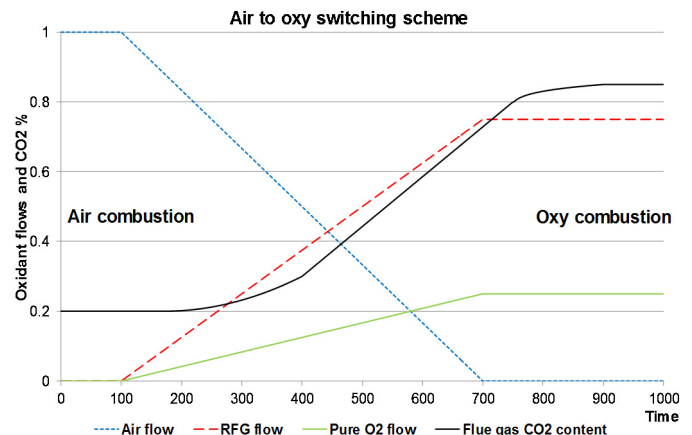
temperatures and heat transfer (Fig. 13). Through oxygen staging, the main combustion zone can be shifted along the bed, which affects the principal burning zones of volatiles and char, as well as the oxidative and reductive potentials of the bed. When a low oxidant O_2 level is used in the dense bed, char ascends higher up in the riser, leading to a more uniform riser temperature profile, but possibly also to increases in unburned fuel, the flue gas O_2 content and exhaust gas heat losses. An elevated O_2 content of the primary oxidant, on the other hand, prolongs the contact between the fuel and the oxygen, improving the combustion efficiency, but also increasing the temperature differences along the furnace (Duan et al., 2011). If oxygen staging is used in the hot-loop control, it has to be taken into account in the boiler O_2 control designs and it should not clash with systems such as flue gas O_2 control.

Oxidant O_2 staging could be used to selectively assist load transitions in certain parts of the riser. This might be important for load changes with slow and large responses in the furnace temperatures and the heat transfer, as was hinted by the oxy-ramp hotloop model validation simulations. Interestingly, oxygen can also be fed directly into the oxy-firing furnace bed to perform more extreme operations related to combustion and temperature control (McDonald & Zadiraka, 2007). This oxygen boost might help to increase the speed of transitions between combustion modes or load levels and provide a significant advantage in oxy combustion compared to air-firing.

The oxyfuel oxidant temperature presents additional variation to the furnace temperatures compared to air-firing, as the oxidant is a mixture of low-temperature oxygen and RFG from the process flue gas line, much unlike an air flow. If extensive air flow preheating or RFG cooling is not used to make the gas temperatures similar in both combustion modes, oxidant temperature differences will almost certainly occur. Preheating is often not an option in oxy mode due to safety aspects of handling pure oxygen flows or oxidants with elevated O_2 percentages. The oxidant temperature issue might be especially problematic during air-oxy-air switches, as the RFG is a reaction product of the process, leading to potential oxidant temperature changes during the switch. The oxidant temperatures will further be reflected in the furnace temperatures.

It is evident that the number of control possibilities for the oxy-CFB plant will increase compared to air-firing. The flue gas O_2, oxidant O_2 and total gas flow controls can be combined in various ways and the oxyfuel oxidant components can be used to adjust different furnace properties. This will complicate the overall control structure of the power plant and make control design more challenging. In a sense, the SISO control problem of air-firing becomes more of a MISO problem in oxy mode. One approach to facilitate the design could be to put more emphasis on controlling input oxygen mass flows instead of the total oxidant flows and their O_2 percentages, as the oxidant O_2 percentage alone offers no definite information about the actual oxygen input to the process. This was pointed out by Fig. 8, as the flue gas O_2 base level remained constant throughout the testing despite the significant changes in the oxidant O_2 percentage. The oxygen mass flow control concept would potentially lead to a more straightforward control solution.

4.4. Switch dynamics

One specific point of concern in the control of the oxyfuel oxidant components lies in the air-oxy-air switches and in the transitions between oxy modes with different oxidant O_2 contents. These tasks are especially challenging, as up to three different gaseous inputs (oxygen, RFG and air) and the solid process flows
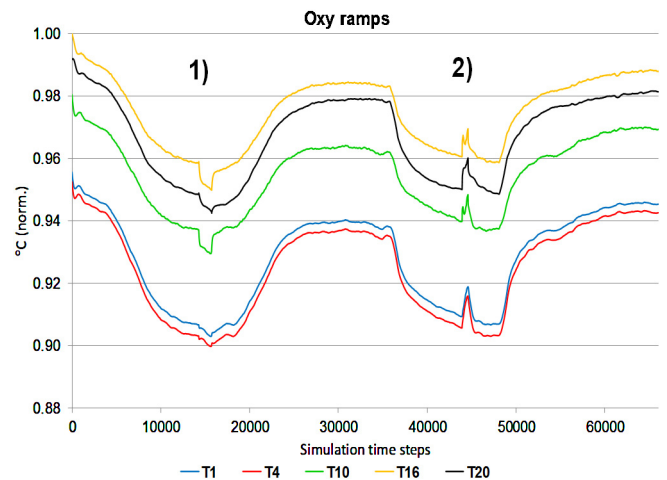
Fig. 15. Normalized furnace temperature responses at different riser heights (T) for two oxy load ramp sets (ramp to a lower load level and back, similar load change), hotloop model validation simulations. The input flow ramping speeds of set (2) were three times larger than those of set (1).

(at least one fuel flow and limestone) need to be adjusted simultaneously. Furthermore, the sequence of the input adjustments has to be determined, which is more complicated in oxy-firing than with an air input flow. The relation between the solid and gaseous inputs is especially important. As a result, input flows need to be coordinated in order to keep process variables at their desired values and achieve stable combustion mode transitions.

Switching between air and oxy mode requires great care, as fast switches have a tendency to cause rapid changes in furnace temperatures and FB velocities (Romeo et al., 2011), which may disturb the process operation. At the same time, switches should also be performed with a required speed, especially when they are based on load demands or cost factors. Fast transitions between combustion modes are also attractive, as the major changes in the flue gas composition take place at the end of the switch ramping (see Section 4.2). The control problem is further complicated by the possible interactions between the switching schemes and the control loops of the process. This might produce unexpected responses and limitations to the switch, which might require decoupling or feedforward control actions.

Testing different switching methods is an integral part in the characterization of oxy-CFB process dynamics. Switches between air and oxy mode can be conducted in different ways by varying the slopes and starting times of gaseous and solid input transition ramps between combustion mode steady-states. The switching scheme often contains one main gaseous flow ramp, during which the major changes in the air, pure O_2 and RFG take place. Ramping sequences with similar ramping speeds for all gaseous flows seem to be common in the literature (Fig. 14). In these sequences, the fuel/oxidant O_2 ratio remains constant throughout the switch.

Beside combustion mode switches, the sequencing of process inputs needs to be configured for oxy load changes, as well. For example, it was discovered during oxy load ramp simulations that a fast ramping of process inputs did not necessarily produce a faster temperature response compared to slower ramps. Fig. 15 shows that even though the temperature time constant for the faster ramp set (2) was smaller than for the slower ramp set (1), the response settling time was actually longer for the faster ramps than for the slower ones. It was suspected that the low reactivity of anthracite-based fuels and the simultaneous change of fuel, RFG and O_2 flows made the furnace cooling change faster than the combustion heat generation during the ramps, creating a momentary imbalance between these two factors. This would have the potential to slow down the response, and the effect would be more visible for fast ramps with rapid RFG transitions than for slower ones.

5. Simulations of switches between air and oxy combustion

Air-oxy-air switches present challenges for CFB process control due to their influences on the combustion dynamics. The switches should ensure good fluidization, combustion and heat transfer conditions, and be sufficiently fast for flexible dual-firing operation. In this section, switching schemes between air and oxy combustion are examined with the dynamic 1-D hotloop model.

5.1. Test setup

The simulated switching schemes from air-firing to oxy-firing were derived from pilot tests. In all simulations, the starting state was air combustion and the target state full oxy mode with oxidant O_2 enrichment. The pure O_2 input was mainly used for oxidant O_2 enrichment and the elevated pure O_2 flow was accompanied by an increase in fuel power. Different oxidant O_2 percentages above 21 vol.% (typically 28 vol.%) were examined in oxy mode to obtain air-like combustion temperatures. In the tested switches, the normal volumetric flow rate (in STP conditions) of the total input gas flow was kept constant. Apart from the final oxy-firing states, a switching scheme could include possible intermediate states for the fuel flow and the oxidant O_2 content.

In the switching schemes reported here, a "direct" ramp was compared to a "sequenced" approach to investigate the relation between gaseous (pure O_2, RFG, air) and solid inputs (fuel and limestone). In the "direct" method (Fig. 16), the solid feeds were ramped together with the pure O_2, RFG and air flows. All ramps were started and ended at the same time, making the method fast. In the "sequenced" method (Fig. 17), the RFG, pure O_2 and air flows were first ramped from air (21 vol.% O_2) to oxy mode without oxidant O_2 enrichment. After the main gas flow ramps, the oxidant O_2 content and the solid feeds were raised to their full oxy mode setting.

The minor anomalies in the sequences of Figs. 16 and 17 were due to the pilot testing practical implementation and they were also reflected in the simulation test runs. Similarly, the fuel power level increase in the "sequenced" method was simulated with a few small steps in the fuel mass flow. Note that analysis of the pilot test outcomes is outside the scope of this paper.

5.2. Simulation results

The two switching schemes resulted in significantly different process responses. The "sequenced" scheme was more affected by
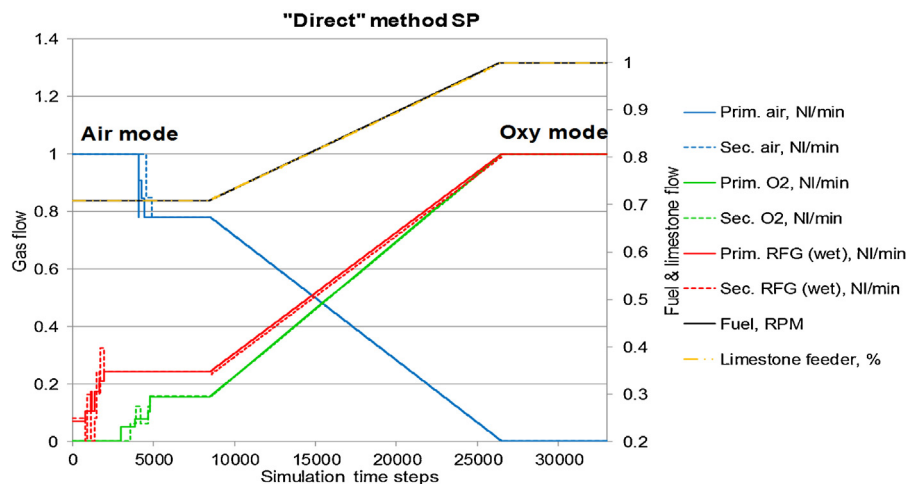
Fig. 16. Input flow setpoints of the "direct" air to oxy switch method. The fuel flow was increased simultaneously with the main gas flow ramps. The normalized inputs correspond to percentages.
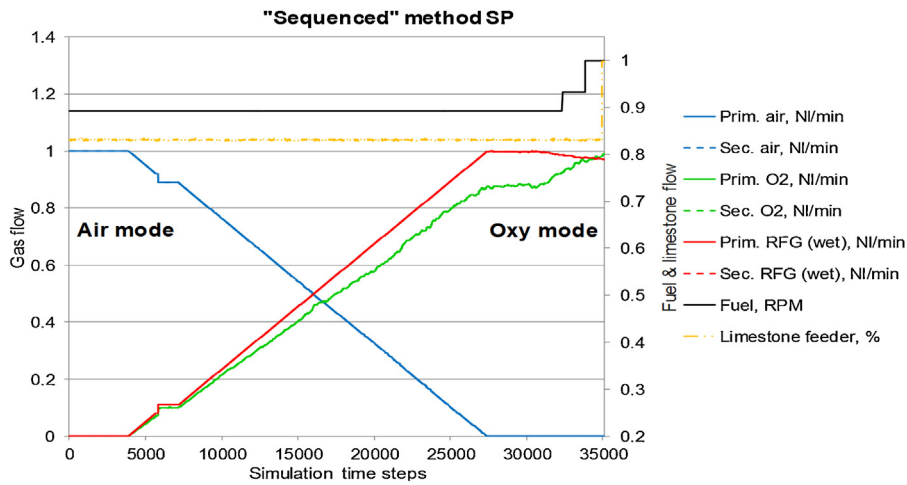
Fig. 17. Input flow setpoints of the "sequenced" air to oxy switch method. The fuel was increased gradually after the main gas flow ramping. The normalized inputs correspond to percentages.

the oxyfuel gaseous medium specific heat capacity elevation than the "direct" method (Fig. 18). As the CO_2 and H_2O concentrations in the oxidant increased, the furnace temperatures slowly decreased for the "sequenced" switch. The lowest temperatures were observed during the final stages of the main gas flow ramps before the oxidant O_2 content elevation and the temperatures regained

their original levels, when the fuel steps were performed. This illustrated the phenomena discussed in Sections 3 and 4. In the "direct" scheme, the change in the fuel firing rate was conducted simultaneously with the shift in the atmospheric conditions. Therefore, the temperature drop associated with the heat capacity increase was compensated. The transition in the furnace temperatures from
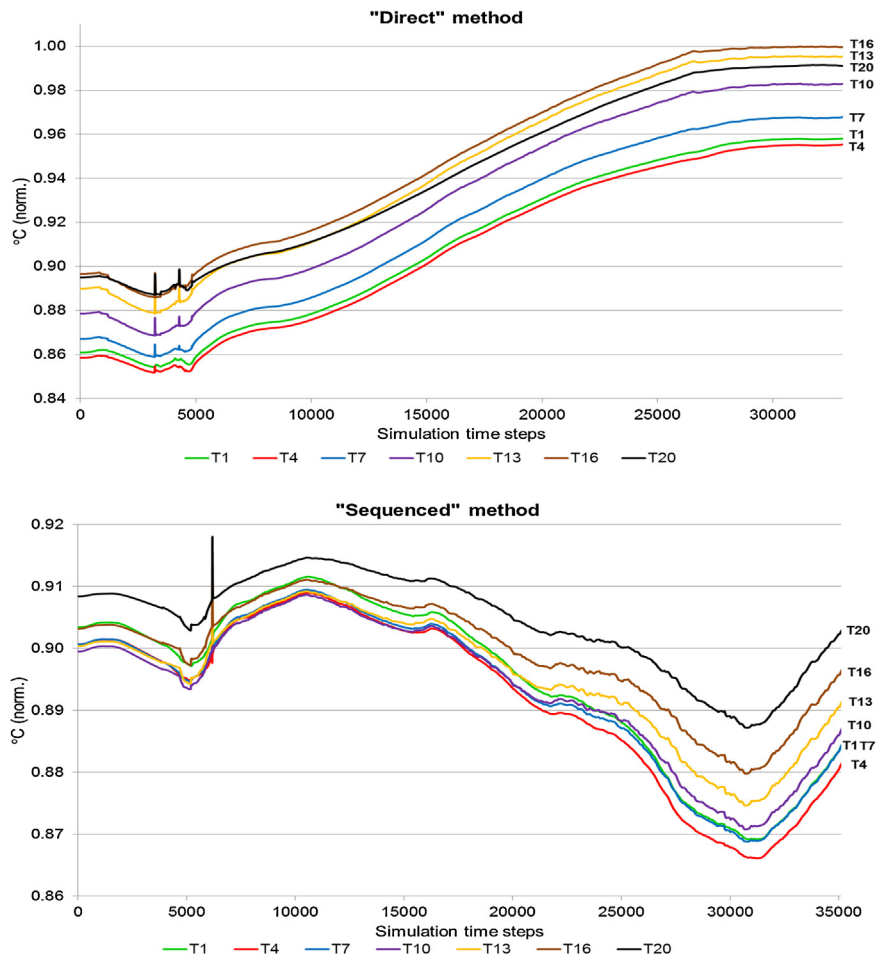
Fig. 18. Simulated furnace temperatures of different riser calculation elements (T) for the "direct" and "sequenced" switch simulations, normalized by the global furnace temperature maximum.
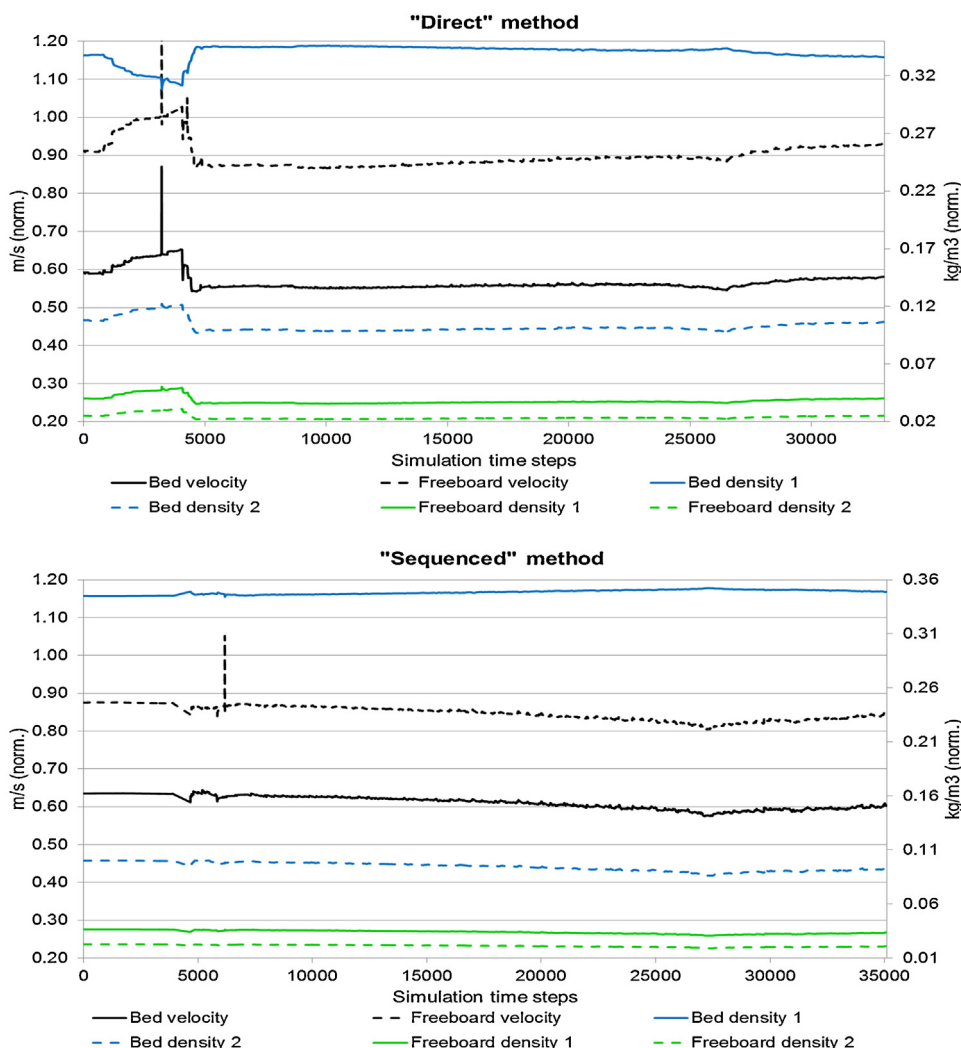
Fig. 19. Simulated bed/freeboard velocities and solids densities of different riser elements (points 1 and 2, point 1 located lower than point 2) for the "direct" and "sequenced" switch simulations, normalized by velocity and global density maxima in the furnace.

air to full oxy mode was smooth and the full oxy-firing steady-state temperatures were reached faster than in the "sequenced" method.

In both switching schemes, the deviations between different temperatures in the CFB riser increased in oxy combustion compared to air combustion. This was most likely caused by the different input oxidant temperatures in air- and oxy-firing. In oxy combustion, the primary and secondary oxidants had the same temperatures, while primary air preheating was used in air mode. The lower secondary air temperature thus led to a more even temperature profile in air mode than in oxy mode. E.g. oxidant O_2 staging could be used as a solution for this issue in oxy mode.

The simulations indicated that it was possible to achieve oxy mode combustion temperatures comparable to those of air mode, if oxidant O_2 enrichment was used. With the selected fuel type, the oxidant O_2 concentrations of the "sequenced" method were close to the ones required by air-like furnace temperatures. The final temperatures of the "direct" scheme were higher than this due to its slightly higher oxidant O_2 enrichment level. The heat transfer power values for the various riser elements followed the trends in the furnace temperatures.

Fluidization during switches was analyzed by examining the gas velocities in the bed and the freeboard, as well as the respective solid material densities (Fig. 19). In general, the gas velocities

remained relatively constant throughout the switches, ensuring proper fluidization conditions. The solids densities were in close agreement with the velocities: whenever the gas velocity increased, the dense bed solids content decreased and the densities higher up in the riser increased.

On closer inspection, the "direct" method seemed to produce better fluidization conditions than the "sequenced" switch. The small density and velocity variations during the switch were also less monotonous in the "direct" method than for the "sequenced" switch. The "sequenced" scheme showed a reduction in fluidization at the end of the main gas flow ramps, although the input gas normal volumetric flow rate remained constant. The changes in the fluidization could be addressed to the observed drop in furnace temperatures before the oxidant O_2 enrichment, as the actual input gas volume flow entering the process was altered due to thermal expansion. This highlights the importance of keeping furnace temperature levels constant during the switch. The changes in the fluidization were mostly dictated by the furnace temperatures rather than the oxidant temperatures.

A flue gas and oxidant density increase in oxy mode was clearly observed for both switching methods (Fig. 20). The differences between the methods were quite small, as the main density changes took place during the main gas flow ramps and the densities
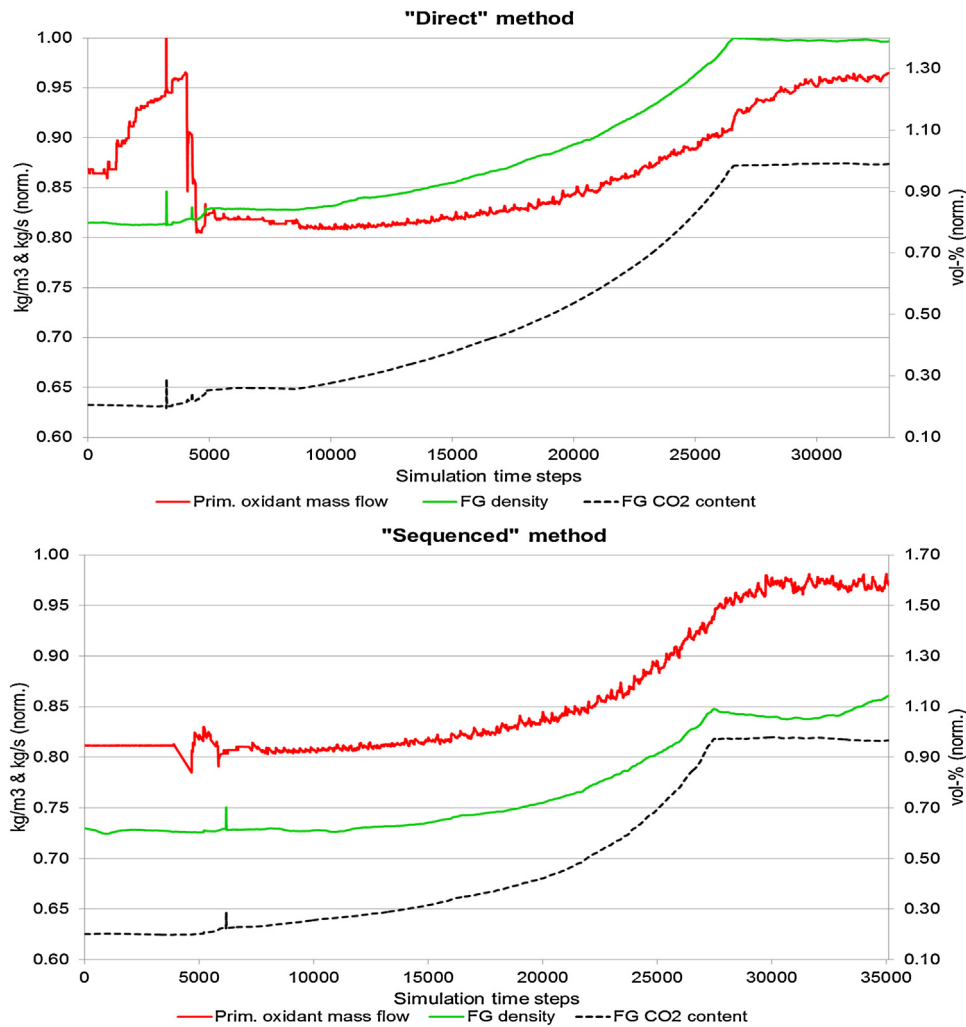
Fig. 20. Flue gas densities (calculated with the ideal gas law and water-steam tables), input primary oxidant mass flows and flue gas CO_2 contents for the "direct" and "sequenced" switch simulations, normalized by the respective maxima.

showed a non-linear response to the switches. The results also displayed that maintaining a constant oxidant volumetric flow caused an increase in the gas mass flow. However, any effects the density changes had on the fluidization were not directly visible in Fig. 19. The flue gas CO_2 and H_2O responses were very similar for the two methods and the component concentrations especially increased towards the end of the gas flow ramping. The flue gas SO_2 marked no preference between the switching methods.

The flue gas O_2 contents (Fig. 21) remained largely constant during both switches and the differences between the methods were small. Since the combustion of fuel was not radically affected by the shift in the atmosphere, air-like combustion conditions could be obtained in oxy mode. The small variability in the flue gas O_2 was particularly surprising for the "direct" scheme, which included rapid and large changes in the process inputs. Some flue gas O_2 drops could be observed during the oxidant adjustments prior to the main gas flow ramps, when air was replaced by RFG with a significantly lower O_2 content. This illustrated the fact that air, pure O_2 and RFG need to be considered as a combined gaseous input during the switch rather than as individual flows.

On a whole, the switch simulations indicated that feasible transitions between air and oxy mode can be performed in CFB boilers. The main differences between the methods were observed in the furnace temperatures, as the fluidization properties were linked to

the temperatures. The flue gas O_2 content behaved similarly for both switching schemes and indicated similar oxy-firing combustion conditions to air-firing. The other flue gas emission responses were very similar for both schemes.

The "sequenced" method resulted in a rather slow combustion mode switch with an intermediate drop in furnace temperatures, which was connected to the elevation in the gas specific heat capacity. The "direct" method resulted in smoother and faster temperature responses than those of the "sequenced" method and the drop in furnace temperatures could be compensated with the firing power. "Direct" switching can turn out to be especially useful for rapid transitions, when requirements for combustion and heat transfer are high (e.g. cost/demand-based switches). However, the extensive adjustments to the manipulated variables of the "direct" method might be restrictive in real-world applications. This was already hinted during pilot experiments, with partial clogging of the boiler grid and setpoint tracking problems for the RFG. The simultaneous ramping of all inputs may be more sensitive to process disturbances and more challenging to conduct than a gradual switch. The "sequenced" method thus has potential for startups and shutdowns, when the speed requirements are less strict and when simultaneous input changes are not necessarily feasible. In the separate fuel and gas flow ramping, particular attention has to be paid on the last stages of the oxidant ramps because of the changes in the gas specific heat capacity and the furnace temperatures.
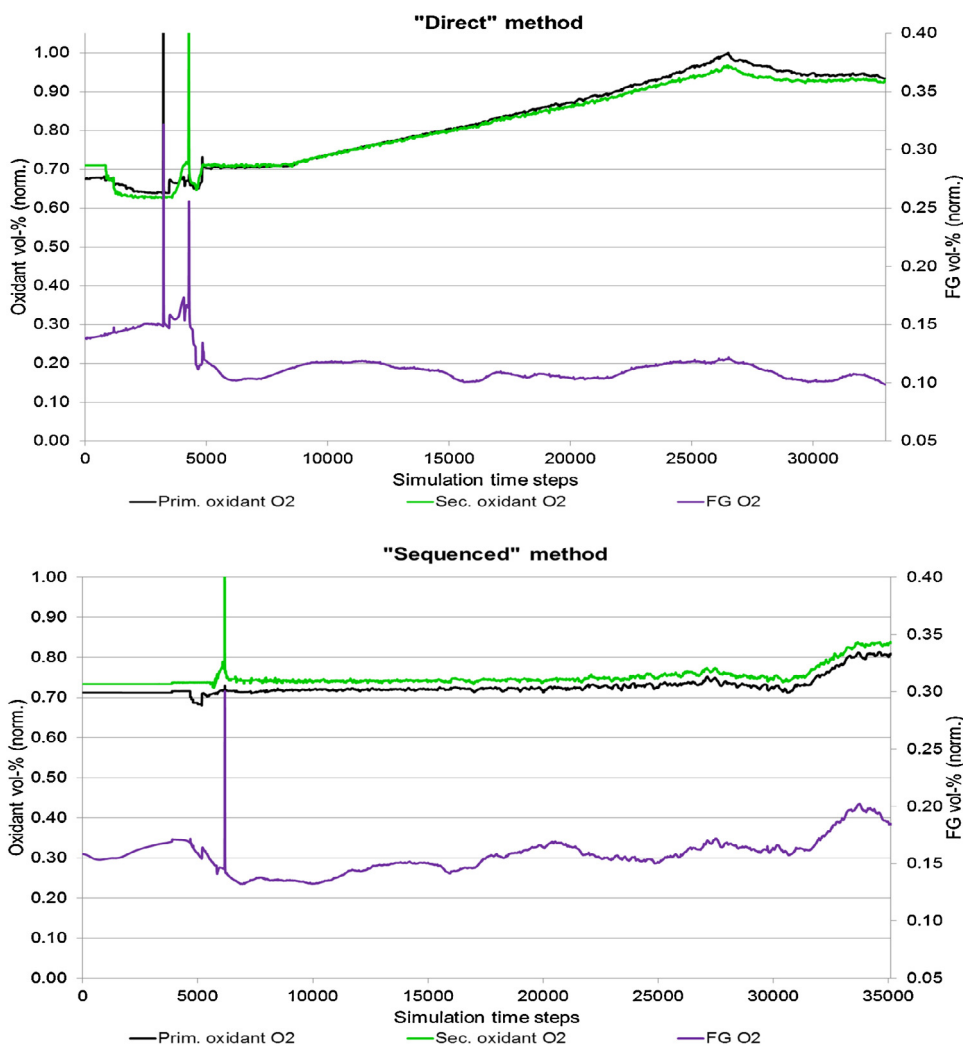
Fig. 21. Flue gas and oxidant O_2 concentrations for the "direct" and "sequenced" switch simulations, normalized by the oxidant O_2 percentage maximum.

6. Conclusions

This paper investigated the differences between oxy- and air-firing in circulating fluidized bed (CFB) boilers. Specific oxy-firing CFB combustion control features and process dynamics were highlighted. Both static and dynamic aspects of the process were investigated through physical considerations and dynamic hotloop simulations. In particular, oxy-CFB control structures were discussed. Two switching methods between air- and oxy-firing were examined through simulations, with the focus on determining how combustion mode transitions should be carried out in the CFB.

The oxidant and flue gas specific heat capacities and densities will be elevated in the oxyfuel boiler compared to air-firing due to the higher gas CO_2 and H_2O contents. The increase in the heat capacity leads to lowered furnace temperatures, slower temperature responses and possible shifts in heat exchanger duties. The temperature level changes can be compensated by increasing the pure O_2 and fuel inputs in oxy mode, i.e. through oxidant O_2 enrichment. To maintain a similar fluidization in air and oxy mode, the input gas volume flow should be kept constant during combustion mode transitions. The oxyfuel atmosphere also influences the combustion and emission formation, e.g. by reducing the diffusivity of oxygen and small hydrocarbons and by increasing fuel gasification.

Flue gas recirculation introduces specific process dynamics to oxyfuel boilers, as the RFG is both a reaction product and the main component of the oxidant flow. The recirculation will add to the time delay of the system and introduce an internal feedback to the process. Although steady-state concentration levels are not affected by the flue gas recirculation amount, the RFG flow determines the concentration dynamics. This is particularly important for air-oxy-air switches, and the RFG/pure O_2 ratio is also an important control parameter for load changes in oxy combustion.

The possibility to adjust the RFG and pure O_2 inputs separately from each other introduces an additional degree of freedom for oxy-CFB control. The RFG is mainly responsible for fluidization and furnace cooling, while the pure O_2 input is regulated by the fuel firing power. Separate pure O_2 and RFG flows enable a more accurate and zone-wise control of furnace properties, profiles and dynamics, including the possibilities to use varying oxidant O_2 percentages, different oxidant O_2 contents for different inlets (O_2 staging), as well as oxygen boosts or extra RFG flows during load or combustion mode transitions. On the other hand, the separate oxidant components call for more advanced combustion control solutions, increasing the complexity of the overall power plant control structure. One comprehensive way to design the combustion control in the oxy-CFB would be to combine a flue gas O_2 trim with oxidant O_2 control and total oxidant volume flow control.

For air-oxy-air combustion mode switches, the most important thing to consider is how the fuel, limestone, pure O_2, RFG and air flows should be altered to obtain optimal combustion, fluidization

and heat transfer conditions throughout the switch. Particular attention has to be paid to the relation between solid and gaseous flows. Based on the simulation results, fast "direct" transitions between air- and oxy-firing with simultaneous ramping of all input flows should be used whenever possible. This switching method produced smooth temperature transitions with no decreases in furnace temperatures or deterioration of combustion and fluidization conditions. However, these switches may be challenging to perform correctly. If "direct" switching results in changes that are too extreme for the process, the fuel flow should be altered only after the main gas flow ramping. With this "sequenced" method, a drop in the furnace temperatures due to the elevated oxyfuel oxidant heat capacity should be expected at the end of the main gas flow ramping. This decrease will also be reflected in the fluidizing gas velocities due to temperature effects on the oxidant volume flow.

Air-fired combustion control cannot be applied directly to the oxy-CFB, as the specific features and dynamics of oxy combustion need to be considered in the control design and tuning. Indeed, oxy combustion presents both challenges and advantages for boiler control. Future oxy-CFB control research will involve implementing control solutions for the process and investigating new control possibilities e.g. by ramping oxidant components in different ways during load and combustion mode transitions. Oxy-CFB control should also be analyzed on a plant-wide scale, as the greatest challenges for the technology are derived from the operating costs, efficiency penalties and performance restrictions of oxygen production (ASU) and CO_2 processing units (CCU + CPU). Furthermore, as the oxyfuel gaseous atmosphere influences heat transfer in the boiler, water-steam side modelling should be included in the oxy-firing power plant simulations.

References

Basu, P. (2006). *Combustion and gasification in fluidized beds*. Boca Raton: CRC Press, Taylor & Francis Group.

Czakiert, T., & Nowak, W. (2010). Kinetics of coal char combustion in oxygen-enriched environment. In G. Yue, H. Zhang, C. Zhao, & Z. Luo (Eds.), *Proceedings of the 20th international conference on fluidized bed combustion; 2009 May 18–21* (pp. 618–623). Xi'an, China/Beijing: Springer/Tsinghua University Press.

Czakiert, T., Sztekler, K., Karski, S., Markiewicz, D., & Nowak, W. (2010). Oxy-fuel circulating fluidized bed combustion in a small pilot-scale test rig. *Fuel Processing Technology*, *91*(November (11)), 1617–1623.

Czakiert, T., Bis, Z., Muskala, W., & Nowak, W. (2006). Fuel conversion from oxy-fuel combustion in a circulating fluidized bed. *Fuel Processing Technology*, *87*(June (6)), 531–538.

Davidson, R. M., & Santos, S. O. (2010, June). *Oxyfuel combustion of pulverized coal*. London (UK): IEA Clean Coal Centre. Report No.: CCC/168, ISBN: 978-92-9029-488-7.

Duan, L., Zhao, C., Zhou, W., Chengrui, Q., & Chen, X. (2011). O_2/CO_2 coal combustion characteristics in a 50 kW$_{th}$ circulating fluidized bed. *International Journal of Greenhouse Gas Control*, *5*(July (4)), 770–776.

Eriksson, T., Sippu, O., Hotta, A., Fan, Z., Myöhänen, K., Hyppänen, T., et al. (2007). Oxyfuel CFB boiler as a route to near zero CO_2 emission coal firing [Internet]. In Power-Gen Europe (Ed.), *15th POWER-GEN Europe conference, conference proceedings – power-gen europe [CD-ROM]*; 2007 June 26–28; Madrid, Spain. Madrid (ES): PennWell Corporation [cited 2011 Nov 28]. Available from http://www.fwc.com/publications/tech_papers/files/TP_CCS_07_02.pdf

Foster Wheeler Energia Oy. Foster Wheeler figure material [database]. Varkaus: Foster Wheeler Energia Oy; [Date unknown] [updated 2012; cited 2013 June 05]. Available from internal company database.

Hack, H., Fan, Z., Seltzer, A., Eriksson, T., Sippu, O., & Hotta, A. (2008). Development of integrated flexi-burn dual oxidant CFB power plant [Internet]. In American Society of Mechanical Engineers: Power Division, United States: Department of Energy, National Energy Technology Laboratory (US), Coal Technology Association, American Public Power Association (Eds.), The Proceedings of the 33rd International Technical Conference on Coal Utilization & Fuel Systems; June 01–05. Clearwater (FL), USA. Clearwater (FL, US): Coal Technology Association 2008 [cited 2011 Nov 28]. Available from http://www.fwc.com/publications/tech_papers/files/TP_CCS_08_02.pdf

Hasegawa, T. (2013). Development of semiclosed cycle gas turbine for oxy-fuel IGCC power generation with CO_2 capture. In E. Benini (Ed.), *Progress in gas turbine performance* (pp. 25–50). Rijeka: InTech.

Ikonen, E., Kovács, J., & Ritvanen, J. (2013). Circulating fluidized bed hot-loop analysis, tuning, and state-estimation using particle filtering. *International Journal of Innovative Computing, Information and Control*, *9*(August (8)), 3357–3376.

IPCC. (2005). 3 capture of CO_2. In B. Metz, O. Davidson, H. C. de Coninck, M. Loos, & L. A. Meyer (Eds.), *Working group III of the intergovernmental panel on climate change. IPCC special report on carbon dioxide capture and storage* (pp. 105–178). Cambridge (UK) and New York (NY, US): Cambridge University Press.

McDonald, D. & Zadiraka, A. (2007). Control of pulverized coal oxy-combustion systems [Internet]. In The International Society of Automation (ISA) (Ed.), *Power – 17th annual ISA power industry division and EPRI controls and instrumentation conference [CD-ROM]* 2007 June 10–15, Pittsburgh (PA), USA. Pittsburgh (PA, US): ISA; [cited 2011 Nov 28]. Available from http://www.babcock.com/library/pdf/BR-1798.pdf

ya Nsakala, N., Liljedahl, G. N., Marion, J., Levasseur, A. A., Turek, D., Chamberland, R., et al. (2004). Oxygen-fired circulating fluidized bed boilers for greenhouse gas emissions control and other applications [Internet]. In The National Energy Technology Laboratory (NETL) (Ed.), *3rd annual conference on carbon capture & sequestration, conference proceedings [Internet]*; 2004 May 03–06; Alexandria (VA), USA. Alexandria (VA, US): NETL, U.S. Department of Energy (DOE) [cited 2011 Nov 28]. Available from http://www.netl.doe.gov/publications/proceedings/04/carbon-seq/031.pdf

Ritvanen, J., Kovács, J., Salo, M., Hultgren, M., Tourunen, A., & Hyppänen, T. (2012). 1-D dynamic simulation study of oxygen fired coal combustion in pilot and large scale CFB boilers. In International Conference on Fluidized Bed Combustion (Ed.), *21st international conference on fluidized bed combustion proceedings* (Vol. 1, pp. 72–79). 2012 June 03–06; Naples, Italy. Naples (IT): EnzoAlbanoEditore.

Romeo, L. M., Díez, L. I., Guedea, I., Bolea, I., Lupiáñez, C., González, A., et al. (2011). Design and operation assessment of an oxyfuel fluidized bed combustor. *Experimental Thermal and Fluid Science*, *35*(April (3)), 477–484.

Suraniti, S. L., ya Nsakala, N., & Darling, S. L. (2009). Alstom oxyfuel CFB boilers: A promising option for CO_2 capture. *Energy Procedia*, *1*(February (1)), 543–548.

Thorbergsson, E. M. (2012). *Conceptual gas turbine modelling for oxy-fuel power cycles*. Gothenburg (SE): Chalmers University of Technology (Dissertation).

Toftegaard, M. B., Brix, J., Jensen, P. A., Glarborg, P., & Jensen, A. D. (2010). Oxy-fuel combustion of solid fuels. *Progress in Energy and Combustion Science*, *36*(October (5)), 581–625.

Tourunen, A. (2010). *A study of combustion phenomena in circulating fluidized beds by developing and applying experimental and modelling methods for laboratory-scale reactors, Acta Universitatis Lappeenrantaensis 419*. Lappeenranta: Lappeenranta University of Technology (Dissertation).

Wall, T., Liu, Y., Spero, C., Elliott, L., Khare, S., Rathnam, R., et al. (2009). An overview on oxyfuel coal combustion – State of the art research and technology development. *Chemical Engineering Research and Design*, *87*(August (8)), 1003–1016.

Weigl, S. (2009). Modellierung und experimentelle Untersuchungen zum Oxyfuel-Prozess an einer 50 kW Staubfeuerungs-Versuchsanlage ['Dissertation, Internet]. Dresden (DE): Technische Universität Dresden 2009 [cited 2011 Nov 28]. German. Available from http://www.qucosa.de/fileadmin/data/qucosa/documents/2612/100110%20Promotion%20Sebastian%20Weigl.pdf

Yin, C., Rosendahl, L. A., & Kaer, S. K. (2011). Chemistry and radiation in oxy-fuel combustion: A computational fluid dynamics modeling study. *Fuel*, *90*(July (7)), 2519–2529.

Circulating Fluidized Bed Boiler State Estimation with an Unscented Kalman Filter Tool

M. Hultgren, E. Ikonen and J. Kovács

Abstract— The paper discusses the development of a state estimation tool for circulating fluidized bed (CFB) boiler dynamic hotloop models. Bayesian state estimation was used to determine inputs, states and time-variant parameters based on output observations. The goal was to apply advanced state estimation to the original nonlinear model and utilize it for real-life CFB applications. The main algorithm of the tool was the unscented Kalman filter (UKF), with an SIR particle filter as a backup solution. The implementation of the tool and the UKF algorithm were described. The tool was tested with two simulation cases. In the first case, fuel flows and an air leakage parameter were identified based on flue gas compositions for pilot oxy combustion measurements. In the second case, heat transfer coefficient and fuel moisture content values were estimated in an industrial boiler based on the dense bed furnace temperature and the flue gas O_2 content. The results showed a good agreement between measurements and simulations, as well as a good computational performance for the UKF.

I. INTRODUCTION

The use of modern state estimation methods in circulating fluidized bed (CFB) power plants is discussed in this paper. Models used for process control typically have relatively simple structures [1], such as transfer function or input response models. More complex models are used in process design. As these models are often at least partially based on process knowledge, they are larger and heavier to run, with many states and equations to be solved. There is an increasing interest towards utilizing these models also for control purposes. This development is driven by the continuous increase in available computing power.

Deviations between simulated and measured outputs can be attributed to an insufficient model, measurement or input inaccuracies and unmeasured disturbances during test periods. As power plant experiments are typically expensive and time-consuming to conduct, measurements with inaccuracies, noise and disturbances often have to be used for model validation and design. Bayesian state estimation enables an effective utilization of this data in a stochastic framework. By estimating unmeasured states and time-varying parameters (e.g. fuel quality, gas flows, fouling), observed outputs can be explained through changes in the process or its inputs. Information about e.g. heat transfer coefficients is also required during process modeling. In control, state estimation is mainly utilized for filtering (e.g. Kalman filters), state observers and monitoring.

This paper describes the development of a Bayesian state estimation tool for a dynamic CFB simulator. The main goal was to apply advanced state estimation techniques to the existing nonlinear model. The unscented Kalman filter (UKF) was selected as the main algorithm for the tool due to its reported performance [2,3]. An additional goal was to show, how state estimation can be used in CFB engineering. To this end, two simulation cases were studied. In the first case, fuel flows and an air leakage parameter were adjusted to reach a better agreement between measured and simulated flue gas compositions for pilot oxy combustion load ramp tests. In the second case, a furnace heat transfer coefficient and the time-varying fuel moisture content were estimated in an industrial boiler to reach the measured dense bed temperature and flue gas O_2 content.

While the unscented Kalman filter is starting to become relatively well-known, the main contribution of this work is its implementation to a complex industrial CFB model. To the authors' knowledge, the UKF has not been applied in CFB boilers before, and its potential for solving estimation problems in this environment should be properly assessed before developing the algorithm further. State estimation work is scarce in the CFB field. Kalman, extended Kalman and H_∞ estimators were examined in [4,5] for a cold flow CFB, with the intention of determining the void fraction and bed height in the standpipe by measuring the pressure drop. A strong tracking filter was proposed in [6] to implement a furnace water-wall tube erosion monitoring system and to overcome the related robustness limitations of the extended Kalman filter. The particular state estimation problems of the current paper have not been addressed before (cf. preceding work [7]). The variations in the fuel moisture content and the heat transfer coefficients, the accuracy of reported fuel flows and the possibility of air leakage during oxy combustion are all important topics for CFB operation.

The CFB process and the used hotloop model are described in chapter II. The functionality of the hotloop state estimation tool and the principles of unscented Kalman filtering are explained in chapter III. Chapter IV gives an account of the state estimation tool simulations and their results. Chapter V sums up the conclusions of the work.

II. PROCESS & PROCESS MODEL

The circulating fluidized bed (CFB) boiler belongs to fluidized bed boilers, based on the combustion of solid fuels in a bed of incombustible material, e.g. sand or ash. The material is fluidized with the input gas flows, which contain the oxidizing agent needed for combustion. In the CFB configuration, solids become entrained with the gas flow and leave the furnace from the top, where they are separated

M. Hultgren and E. Ikonen are with the Systems Engineering Laboratory, University of Oulu, Oulu, CO 90014 Finland (phone: +358 50 350 2923; fax: +358 8 553 2304; e-mail: firstname.lastname@oulu.fi).

J. Kovács is with Foster Wheeler Energy Ltd, Varkaus, CO 78201 Finland (e-mail: jeno.kovacs@fwfin.fwc.com).

from the flue gas in gas-solid separators. The solids are then recycled back to the bed. Together, these process components form the CFB hotloop (Fig. 1).

The boiler heat exchangers for steam generation are located in the hotloop and the flue gas backpass, and they form the contact surface between the combustion side and the water-steam cycle of the boiler. The input oxidant in the CFB is typically air, but other oxidants can also be used. For example, in the oxy combustion carbon capture and storage (CCS) technology fuels are combusted with a mixture of pure oxygen and recirculated flue gas (RFG) instead of an air oxidant gas flow. This causes the CO_2 content to be elevated to 70–98 vol-% (dry) in the flue gas, enabling an easier separation and recovery of CO_2 emissions for storage [8].

The hotloop dynamics were modeled with a 1-D Matlab/Simulink model, which has been developed in cooperation between Foster Wheeler Energy Ltd, the Lappeenranta University of Technology and the University of Oulu. The model structure has been extensively validated and tested with various CFB boilers, and the model contains different process components depending on the boiler configuration (Fig. 2).
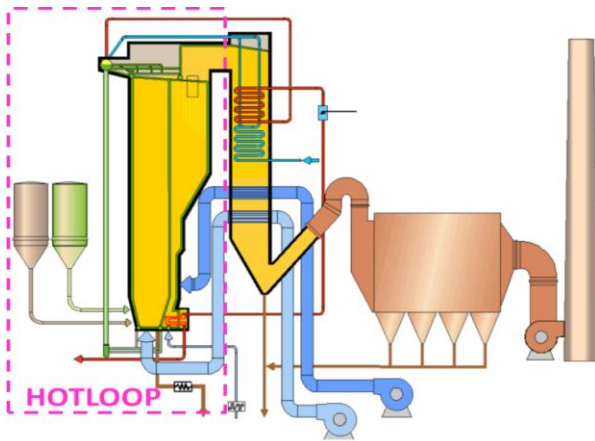
Figure 1.   The circulating fluidized bed boiler hotloop.
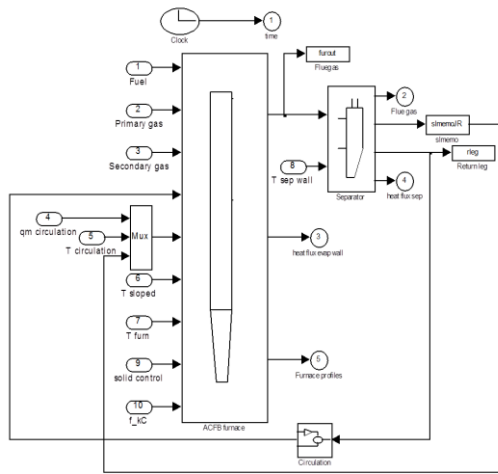
Figure 2.   The hotloop model structure of the pilot plant case of this paper, containing the furnace, the separator and the return leg.

The model is nonlinear and quite large with a significant number of states, 855 for the pilot case and 660 for the industrial scale example of this paper. As a result, the model is mainly a simulator for investigating process dynamics and testing control solutions. The modeling is based on both physical and empirical approaches. A mathematical description of the model is provided in [9].

The furnace riser tube consists of 20 ideally mixed calculation elements, for which element specific mass and energy balances are solved against time with an ODE solver. A combined energy equation for gaseous and solid phase temperatures is defined, while the hydrodynamics, combustion characteristics and heat transfer inside the modules are calculated using empirical and semi-empirical correlations. The effects of the water-steam cycle are simulated through element-specific heat exchanger surface temperature parameters. The model contains no water-steam side calculations, and it is primarily used as the hotloop component in complete power plant simulators.

III.   STATE ESTIMATION TOOL

This chapter presents the developed CFB state estimation tool and introduces the used algorithms.

A. Implementation

The CFB state estimation tool is an add-on package for the existing family of Foster Wheeler hotloop models and can readily be used for various power plant setups. The tool is utilized for estimating values for states, time-varying process parameters or "active" process inputs (e.g. fuel and gas flows). The estimates are applied as gain coefficients for model input vector elements with an initial value of 1. Several elements can also be modified with the same gain.

The aim of the tool was to utilize the original process model directly for state estimation without additional remodeling. To this end, the general model structure was implemented into the state-space representation (1).

$$\begin{cases} x(k+1) = f\big(x(k),u(k),v(k)\big) \\ y(k) = h\big(x(k),u(k)\big) + w(k) \end{cases} \qquad (1)$$

The process state vector $x(k)$ is propagated into the next step $x(k+1)$ by simulating the hotloop model for the state-space timestep, starting from the initial states and applying the inputs $u(k)$. The function "f" thus consists of the original hotloop model nonlinear equations [9]. The probability density functions (pdf) of the measurement noise $w(k)$ and the process noise $v(k)$ are assumed to be known. The measurement equation "h" defines, how observations $y(k)$ are derived from $x(k)$, $u(k)$ and $w(k)$. Here, "h" is simply an index function that picks those elements from the hotloop model output vector that are compared to the measurements.

The aim of Bayesian state estimation is to construct a representation of the unknown state vector x through its posterior pdf $p(x_k|\widetilde{Y}_k)$. $\widetilde{Y}_k$ denotes all measurements y_k up to and including timestep k. The Bayesian filter provides a recursive mechanism for updating the probability of a phenomenon with evidence, i.e. updating the posterior pdf

with new output measurement data. The filter consists of prediction and update operations. In the prediction phase (2), the state posterior pdf at timestep *k-1* is propagated into a prior pdf with the model of the process dynamics.

$$\underbrace{p(x_k \mid \widetilde{Y}_{k-1})}_{prior,k} = \int \underbrace{p(x_k \mid x_{k-1})}_{process\,dynamics} \underbrace{p(x_{k-1} \mid \widetilde{Y}_{k-1})}_{posterior,k-1} dx_{k-1} \quad (2)$$

In the update phase (3)–(4), this result is updated with new observations to reach the posterior pdf at timestep *k*.

$$\underbrace{p(x_k \mid \widetilde{Y}_k)}_{posterior,k} = \underbrace{p(y_k \mid x_k)}_{likelihood} \underbrace{p(x_k \mid \widetilde{Y}_{k-1})}_{prior,k} \Big/ \underbrace{p(y_k \mid \widetilde{Y}_{k-1})}_{normalization} \quad (3)$$

$$p(y_k \mid \widetilde{Y}_{k-1}) = \int p(y_k \mid x_k) p(x_k \mid \widetilde{Y}_{k-1}) dx_k \quad (4)$$

The state estimation algorithm determines, how (2)–(4) is solved to gain p($x_k|\widetilde{Y}_k$). A closed form solution can be found for linear-Gaussian models with the Kalman filter, while mildly nonlinear problems can be handled by the extended Kalman filter (EKF) through linearization [7]. The hotloop tool contains two algorithms for nonlinear model state estimation. The unscented Kalman filter (UKF) is the main algorithm, while a more powerful, but also computationally demanding sampling-importance-resampling (SIR) particle filter (PF) can be used for challenging cases. Particle filters employ sequential Monte Carlo methods to describe state posterior probabilities as a set of random samples (particles), which is propagated through the system model. The approximation accuracy depends on the used amount of particles. The SIR-PF is described in [7].

B. Unscented Kalman Filter

The basic idea of the UKF is that a state variable distribution can be approximated through its mean and covariance [2,3]. The calculations rely on the unscented transform, in which a minimal set of sample points **X** ("sigma points", indicated in bold) with a mean $\bar{x}$ and a covariance P_x is used to represent an n_x-dimensional random state variable *x*. Unlike PF particles, the *2n+1* sigma points are selected according to a deterministic algorithm, which depends on the unscented transform formulation. The tool utilizes the scaled unscented transform (5)–(8) [3], while the original transform representation can be found e.g. in [2].

$$\mathbf{X}_0 = \bar{x} \quad (5)$$

$$\mathbf{X}_i = \bar{x} + \left(\sqrt{(n_x + \lambda)P_x} \right)_i, \ i=1,...,n_x \quad (6)$$

$$\mathbf{X}_i = \bar{x} - \left(\sqrt{(n_x + \lambda)P_x} \right)_i, \ i=n_x+1,...,2n_x \quad (7)$$

$$\lambda = \alpha^2(n_x + \kappa) - n_x \quad (8)$$

In the unscented transform, the sigma points are driven through *"f"* and *"h"* in (1) to gain a cloud of transformed points **Y** (indicated in bold). The mean $\bar{y}$ is calculated as a weighted sum (9)–(12) of the transformed points, while the

covariance P_y is obtained through (13). The scaled unscented transform formulation utilizes the three scaling parameters α ($0 \le \alpha \le 1$), β ($\beta \ge 0$) and κ ($\kappa \ge 0$) [3].

$$\bar{y} = \sum_{i=0}^{2n_x} W_i^{(m)} \mathbf{Y}_i \quad (9)$$

$$W_0^{(m)} = \lambda / (n_x + \lambda) \quad (10)$$

$$W_0^{(c)} = \lambda / (n_x + \lambda) + 1 - \alpha^2 + \beta \quad (11)$$

$$W_i^{(m)} = W_i^{(c)} = 1 / (2n_x + 2\lambda), \ i=1,...,2n_x \quad (12)$$

$$P_y = \sum_{i=0}^{2n_x} W_i^{(c)} \{\mathbf{Y}_i - \bar{y}\}\{\mathbf{Y}_i - \bar{y}\}^T \quad (13)$$

Equations (5)–(13) form the basis for the UKF recursive filter. In the scaled UKF [3], *x* is redefined into x^a, which contains both *x* and the system noise variables (state noise *v* and measurement noise *n*). As a result, n_x will be replaced by $n_a = n_x + n_v + n_n$ in (5)–(13). x^a is then applied to (5)–(8) to generate the sigma points $\mathbf{X}^a$ at *k*. The algorithm is initialized with (14)–(15), where $\bar{x}_0$ is the state vector initial expected value, P_0 is the initial covariance, *Q* is the process noise covariance and *R* is the measurement noise covariance.

$$\bar{x}_0^a = E[x_0^a] = \begin{bmatrix} \bar{x}_0^T & \underline{0}^T & \underline{0}^T \end{bmatrix}^T \quad (14)$$

$$P_0^a = E\left[\left(x_0^a - \bar{x}_0^a\right)\left(x_0^a - \bar{x}_0^a\right)^T \right] = \begin{bmatrix} P_0 & \underline{0} & \underline{0} \\ \underline{0} & Q & \underline{0} \\ \underline{0} & \underline{0} & R \end{bmatrix} \quad (15)$$

Together with the process inputs *u(k)*, the sigma points are propagated through *"f"* to yield $\mathbf{X}^a_{k+1|k}$. The predicted state variable mean $\bar{x}_{k+1|k}$ is determined by applying (9) to the prior sigma points $\mathbf{X}^a_{k+1|k}$ and the weights $W^{(m)}$. Similarly, the predicted covariance $P_{k+1|k}$ is calculated with (13) by replacing $\mathbf{Y}_i$ and $\bar{y}$ with $\mathbf{X}^a_{k+1|k}$ and $\bar{x}_{k+1|k}$. Next, the transformed output points $\mathbf{Y}_{k+1}$ are gained through the measurement model *"h"*. From $\mathbf{Y}_{k+1}$, (9) will give the predicted observation and (13) the respective covariance P_{yy}.

The UKF Kalman gain is determined with (16) from the cross correlation matrix P_{xy} (17) and the covariance P_{yy}.

$$K_{k+1} = P_{xy} P_{yy}^{-1} \quad (16)$$

$$P_{xy} = \sum_{i=0}^{2n_a} W_i^{(c)} \{\mathbf{X}_{k+1|k} - \bar{x}_{k+1|k}\}\{\mathbf{Y}_{k+1} - \bar{y}_{k+1}\}^T \quad (17)$$

Finally, $\bar{x}_{k+1}$ and P_{k+1} are calculated through (18).

$$\begin{cases} \bar{x}_{k+1} = \bar{x}_{k+1|k} + K_{k+1}\left(y_{k+1} - \bar{y}_{k+1}\right) \\ P_{k+1} = P_{k+1|k} - K_{k+1}P_{yy}K_{k+1}^T \end{cases} \quad (18)$$

The steps of the UKF algorithm are summarized below:

1. Define and initialize state mean vector and covariance matrix, set UKF scaling parameters.

2. Calculate sigma points **X** and corresponding weights W at timestep k.

3. Propagate each sigma point $\mathbf{X}_{k|k}$ through f (hotloop model in state-space format) to get points $\mathbf{X}_{k+1|k}$.

4. Calculate prior mean and covariance values of states: $\bar{x}_{k+1|k}$ and $P_{k+1|k}$.

5. Pass $\mathbf{X}_{k+1|k}$ through h (selection of relevant hotloop model outputs) to get $\mathbf{Y}_{k+1}$.

6. Calculate predicted observation mean/covariance.

7. Calculate cross-correlation matrix P_{xy}.

8. Calculate Kalman gain.

9. Calculate posterior mean and covariance of states, given measurements y_{k+1}.

10. Next calculation round.

The main benefits of the UKF are its estimation accuracy and ease of implementation for nonlinear systems. The estimation quality is improved compared to EKF, especially for the covariance [3]. The UKF contains only standard matrix operations and the original process model can be used directly, just like particle filters. The unscented transform makes it possible to capture high order information with a much smaller sample size than in particle filtering (amount of particles) [2]. These aspects make the UKF suitable for hotloop state estimation. One limitation of the UKF is that it doesn't apply to general non-Gaussian distributions [3].

IV. SIMULATIONS

The hotloop state estimation tool was tested through two CFB simulation cases. The aim was to illustrate the different engineering uses of the tool and to validate its functionality.

A. Pilot Case Study: Flue Gas Compositions

A measurement and dynamic simulation campaign was carried out in a pilot combustor using oxy combustion. The aim was to compare air- and oxy-firing in the CFB and to perform an initial validation of the hotloop model in oxy mode. The pilot contained the furnace, a gas-solid separator cyclone, a solids return leg, as well as flue gas recirculation and processing equipment. The oxidant was formed out of high-purity bottled O_2 and recirculated flue gas.

The state estimation case concerned a set of oxy load ramps (Fig. 3), which was conducted using a fuel blend with an approximate 70/30 mass percentage ratio of anthracite (two fractions) and petcoke. The tests showed a deviation between measured and simulated flue gas concentrations. The measured volume percentages showed variations which weren't present in the simulations and which couldn't be directly attributed to any changes in reported inputs. Moreover, the general levels of the largest concentration

components CO_2 and H_2O were a bit higher in the simulations than in the measurements.
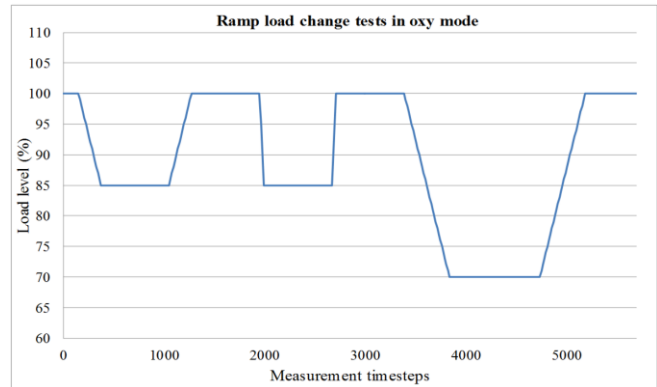
Figure 3.   The boiler load levels of the oxy-firing load ramp test program.

The state estimation tool was used to investigate, whether the accuracy of the reported fuel flows and potential air leakage into the system could have caused the observed differences. The original fuel mass flows were calculated as least squares fits from fuel silo weights, effectively removing any possible higher frequency variations in the feed. Air leakage is a widely recognized problem in oxy combustion [10], as air dilutes the flue gas, and boiler overpressure can't be used. Because of the unavailability of flue gas mass flow values, a direct calculation of the air leakage amount into the boiler could not be made here. The state estimation targets were set to be the three fuel mass flows and an air leakage mass flow, which was defined as an additional input air flow to the combustion side. The air leakage was given a nominal value significantly below the primary and secondary input gas flows. The flue gas CO_2 and O_2 volume percentages were used as the measurements for the state estimation.

The estimation results in Figs. 4−5 displayed a good agreement between measurements and simulations, when the small flue gas concentration changes and the general levels of the larger components were considered. Notably, the flue gas moisture content was also on target, although it hadn't been used for state estimation. This was especially apparent after the FTIR moisture sensor cleaning at timestep 900.
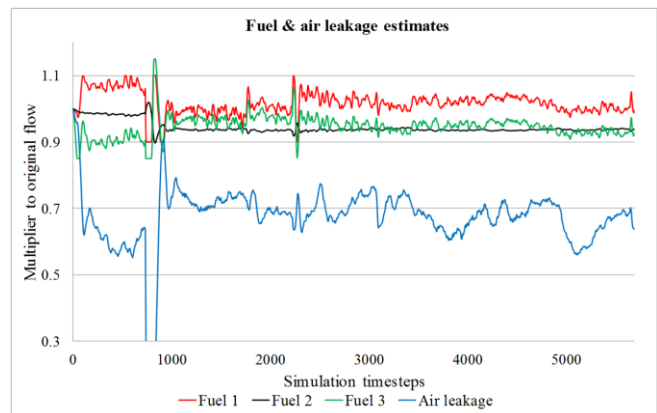
Figure 4.   Estimated fuel mass flow (3 parameters) and air leakage gain coefficients of the pilot oxy load ramp test program.

313
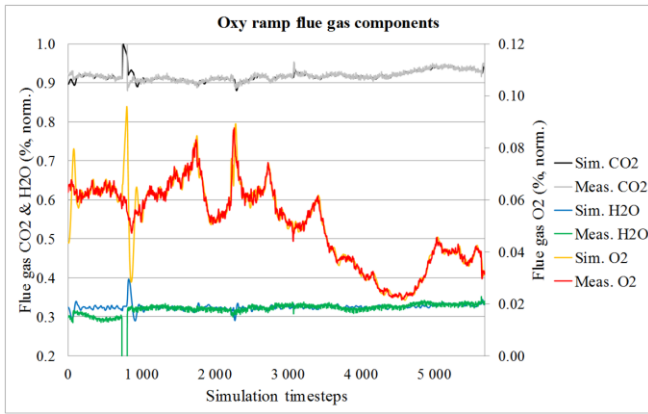
Figure 5. Normalized flue gas vol-% outputs (CO_2, H_2O and O_2) of the oxy load ramp state estimation simulations and the pilot scale measurements. The values were normalized with the concentration maxima.

The estimates offered a plausible explanation for the differences between the simulations and the measurements. It was also apparent that adjusting only the fuel flows was not enough to achieve the measured O_2 and CO_2 values. The estimated parameter values were deemed to be realistic, as both the fuel flow corrections and the air leakage remained reasonably constant, and the fuel corrections were small enough. The air ingress into the boiler was also significantly smaller than the actual primary and secondary gas inputs.

B. Industrial Case Study: Heat Transfer & Fuel Moisture

Here, tests with a full scale air-fired industrial boiler with one input fuel fraction (coal-firing) were examined. The measurement campaign consisted of the three test sets below. From these, the reactivity test data was previously utilized in [7] for SIR-PF and initial UKF state estimation testing.

1. Reactivity tests – stepwise changes in the fuel flow.

2. Primary tests – stepwise changes in the primary air:
   + 6 % to primary input air flow at timestep 230.
   − 6 % to primary input air flow at timestep 650.

3. Load tests: stepwise changes in fuel and air flows:
   − 8 % to input fuel and air flows at timestep 310.
   + 8 % to input fuel and air flows at timestep 540.

The dynamic tests showed differences between measured and modeled dense bed furnace temperatures and flue gas O_2 contents. Temperature differences could be seen both for the general temperature level and for smaller variations, while the measured O_2 general level matched the simulations better. Based on process knowledge and sensitivity analyses, state estimation was implemented to determine one furnace heat transfer coefficient and the fuel moisture content, using the furnace temperature and the flue gas O_2 as outputs. Tuning of heat transfer coefficients is a common operation in hotloop model synthesis and it's often done iteratively. The variation in the fuel H_2O content is an acknowledged control challenge in solid fuel combustion, mainly due to the difficulties related to online moisture measurements [11], fuel quality variations and co-firing of different fuels.

Figs. 6−7 display the estimated parameters and outputs of the load steps, while the primary test results can be seen in Figs. 8−9. There was mostly a good agreement between measurements and simulations and the results corresponded to the reactivity tests in [7]. The simulated temperature settled on the average level of the measurements, and the smaller variations in the temperature and the flue gas O_2 could be captured in most cases. For both tests here and the reactivity tests, the heat transfer coefficient settled between 1.4−1.6. As a result, the dense bed heat transfer coefficient should be multiplied by 1.5 to improve modeling accuracy.

The state estimation produced better results for the primary tests than for the load tests. This applied especially to load change temperatures, and at 540, the temperature was even corrected in the opposite direction than the measured output. The reduced performance of the estimation can be related to the instantaneous changes in all inputs, which cause more significant alternations in the heat generation than just primary air steps. This is supported by the good load ramp simulation results in Figs. 4−5. However, there might also be a need to investigate other parameters and outputs, as there may have been unobserved changes in the process that aren't covered by the selected variables of this work. Indeed, load level changes might not be visible enough in temperatures close to the furnace grate or the flue gas O_2.
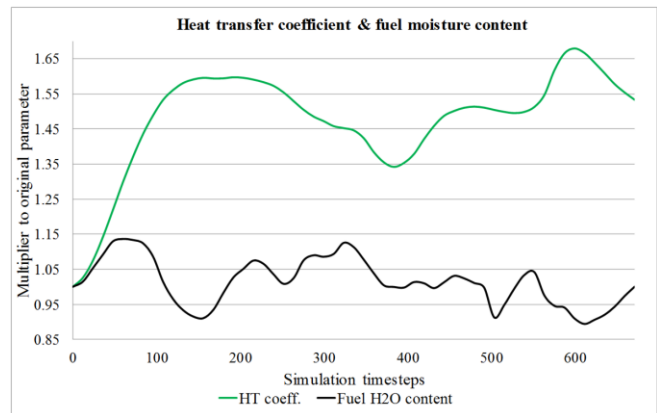
Figure 6. Estimated furnace heat transfer (HT) coefficient and fuel moisture content gain coefficient for the industrial load step tests.
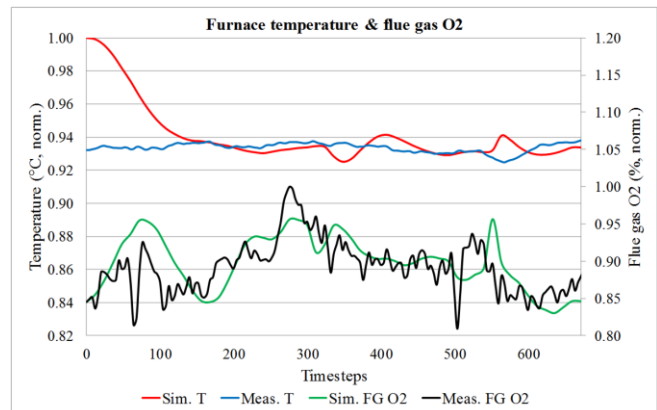
Figure 7. Normalized dense bed furnace temperatures (T) and flue gas O_2 w-% outputs of the load step state estimation simulations and industrial measurements. The outputs were normalized with the respective maxima.
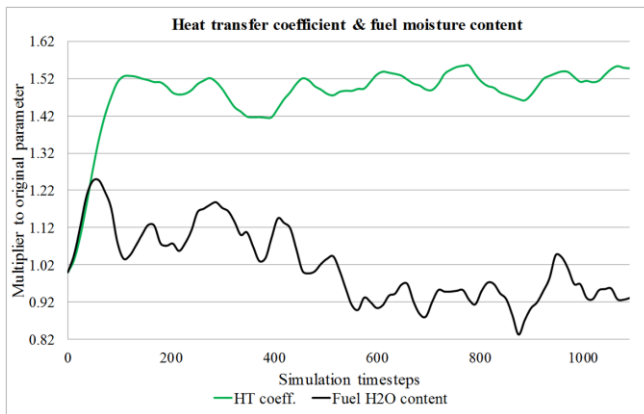
Figure 8. Estimated furnace heat transfer (HT) coefficient and fuel moisture content gain coefficient for the industrial primary air tests.
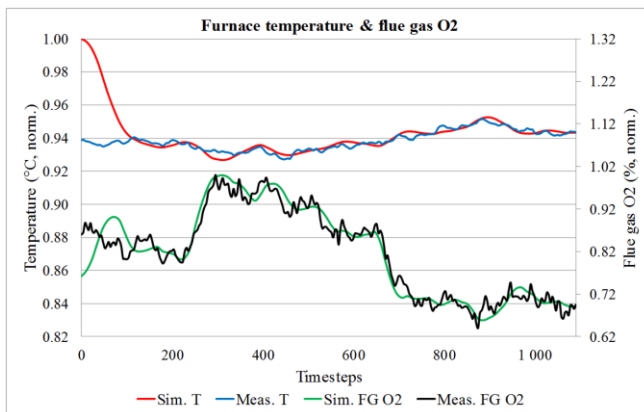
Figure 9. Normalized dense bed furnace temperatures (T) and flue gas O_2 w-% outputs of the primary air state estimation simulations and industrial measurements. The outputs were normalized with the respective maxima.

The fuel moisture content changes were quite realistic and the parameter window was approximately the same for all tests. The primary tests showed slightly higher moisture values at the start, suggesting a gradual change in fuel quality. It could be stated that a constant fuel moisture content assumption was not enough for accurate hotloop modeling. On a whole, the estimated heat transfer coefficient and fuel moisture content values could successfully be used to explain the differences between measurements and simulations. Moreover, the UKF proved to have a significant computational advantage over the current implementation of the SIR-PF in the tool, as comparable results to the PF were obtained in a much shorter calculation time with the UKF.

V. Conclusion

A Bayesian state estimation tool for circulating fluidized bed hotloop models was constructed and tested in this paper, with the scaled unscented Kalman filter as the main algorithm. The tool proved to be readily useable for various CFB model versions and design problems, as was showcased by two case study setups. The examples illustrated the applicability of state estimation to different tasks: The pilot oxy combustion case concentrated on model validation, while the industrial case investigated fuel quality variations

and heat transfer changes during the boiler operation. Both examples yielded good results concerning the outputs and the estimates. Furthermore, Bayesian state estimation hasn't previously been applied to solve the modeling and analysis problems presented in this work. The computational performance of the UKF was good, and the results were comparable to a heavier particle filtering approach. The algorithm was also directly applicable to the original hotloop model without additional modeling, e.g. linearization.

Future work with the state estimation tool concerns applying it to various boiler models and tasks in order to assess its performance. The UKF framework of the tool can be developed further to increase its performance and accuracy. One particular topic of interest would be the possibility to gain rough estimates of time-varying heat transfer coefficients and heat exchanger surface temperatures during model tuning based on hotloop MW targets.

References

[1] E. Ikonen and K. Najim, *Advanced Process Identification and Control*. New York (NY): Marcel Dekker Inc., 2002, 328 p.

[2] S. J. Julier and J. K. Uhlmann, "A New Extension of the Kalman Filter to Nonlinear Systems," in *Proc. AeroSense: 11th Int. Symp. Aerosp./Def. Sens., Simul. Controls, Vol. Multi Sens. Fusion, Track. Resour. Manag. II*, Orlando (FL), 1997, pp. 182–193.

[3] R. van der Merwe, A. Doucet, N. de Freitas and E. Wan, "The Unscented Particle Filter," Technical report CUED/F-INFENG/TR 380, Cambridge Univ. Eng. Dept., Cambridge, UK, 2000, 46 p.

[4] J. Park., "System Identification and Control of the Standpipe in a Cold Flow Circulating Fluidized Bed," Ph.D. dissertation, Lane Dept. Comp. Sci. Elect. Eng., West Virginia Univ., Morgantown, WV, 2004.

[5] A. A. Jalali, J. Park, P. Famouri, R. Turton and E. J. Boyle, "H_∞ based state estimation on standpipe of a cold flow circulating fluidized bed," in *Proc. IEEE Int. Conf. Syst. Man Cybern., Vol. 3*, Washington D.C., 2003, pp. 2320–2325.

[6] L. Sun, J. Dong, D. Li and Y. Zhang "Model-Based Water Wall Fault Detection and Diagnosis of FBC Boiler Using Strong Tracking Filter," *Math. Probl. Eng.*, vol. 2014, ID 504086, 8 p., Apr. 2014.

[7] E. Ikonen, J. Kovács and J. Ritvanen, "Circulating Fluidized Bed Hot-Loop Analysis, Tuning, and State-Estimation Using Particle Filtering," *Int. J. Innov. Comput. Inf. Control*, vol. 9, no. 8, pp. 3357–3376, Aug. 2013.

[8] M. Hultgren, E. Ikonen and J. Kovács, "Oxidant control and air-oxy switching concepts for CFB furnace operation," *Comput. Chem. Eng.*, vol. 61, pp. 203–219, Feb. 2014.

[9] J. Ritvanen, J. Kovács, M. Salo, M. Hultgren, A. Tourunen and T. Hyppänen, "1-D Dynamic Simulation Study of Oxygen Fired Coal Combustion in Pilot and Large Scale CFB Boilers," in *Proc. 21st Int. Conf. Fluid. Bed Combust., Vol. 1*, Naples, 2012, pp. 72–79.

[10] M. B. Toftegaard, J. Brix, P. A. Jensen, P. Glarborg and A. D. Jensen, "Oxy-fuel combustion of solid fuels," *Prog. Energy Combust. Sci.*, vol. 36, no. 5, pp. 581–625, Oct. 2010.

[11] J. Kortela and S.-L. Jämsä-Jounela, "Fuel-quality soft sensor using the dynamic superheater model for control strategy improvement of the BioPower 5 CHP plant," *Int. J. Electr. Power Energy Syst.*, vol. 42, no. 1, pp. 38–48, Nov. 2012.

Integrated control and process design in CFB boiler design and control – application possibilities

Matias Hultgren*,
Enso Ikonen*, Jenö Kovács**

*University of Oulu, Systems Engineering
P.O. Box 4300, FI-90014 University of Oulu, Finland (e-mail: firstname.lastname@oulu.fi).
**Amec Foster Wheeler R&D
Relanderinkatu 2, P.O. Box 201, FI-78201 Varkaus, Finland (email: jeno.kovacs@amecfw.com)

Abstract: Integrated control and process design (ICPD) practices focus on an interaction between process and control design. The paper investigates ICPD design in circulating fluidized bed (CFB) power plants, which face increasing load change, efficiency and emission requirements. The state of ICPD research is examined and a classification of its methodologies is provided. The applicability of ICPD to large-scale CFB boilers is discussed for the first time based on this classification. Two ICPD case studies with a simple steam path mass storage model are presented for an industrial CFB boiler, with the aim of illustrating possibilities and challenges related to boiler ICPD. The steam mass storage amounts of the boiler superheating and evaporation sections are modified based on the dynamic relative gain array and closed-loop process optimization to generate processes with improved constant pressure mode output power setpoint tracking performance.

Keywords: Power plant control system design, Interaction between design and control, Circulating fluidized bed boiler, Power plant simulation, Control of large-scale systems, Process optimization.

1. INTRODUCTION

The paper investigates integrated control and process design (ICPD) in the circulating fluidized bed boiler (CFB). In ICPD, the process and its control system are designed at the same time, so that control requirements affect the process, and process dynamics become better incorporated into the control (Fig. 1). This gives improved closed-loop responses, and design decisions with negative dynamic effects can be avoided. The approach differs from conventional sequential design, where the process is designed based on steady-state goals, and control is designed after this to satisfy stability and dynamic performance criteria. This limits achievable control performance by the open-loop dynamics from process design.
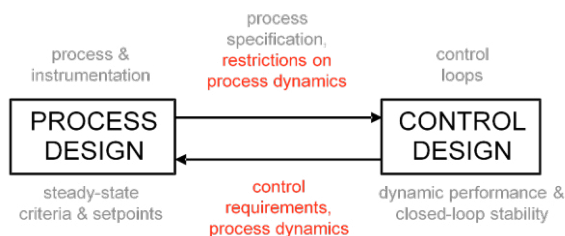
Fig. 1. Process and control design interaction in ICPD.

A deeper interaction between process and control design is needed for steam boilers, which currently face many control design challenges. While combustion power plants were previously mainly operated at constant load, nowadays they are facing fast and frequent load transitions with accurate MW_e setpoint tracking demands, as well as extended partial load operation periods. Power generation efficiency needs to be maximized, which is reflected as complicated flowsheets and extreme operating conditions. In CFB plants, increasing boiler sizes and technologies like carbon capture and storage (CCS) have introduced new requirements. The ICPD problem gains another dimension in utility power plants that supply power to a process, but also operate in a power grid (Chen & Bollas 2017, Dowling & Zavala 2017).

This paper examines how ICPD can be applied to CFB boiler design. General features of ICPD are outlined and its main approaches are classified. ICPD design is also demonstrated with an industrial CFB boiler steam path model. Available ICPD approaches need to be outlined for boiler design, since the topic spans a wide range of design practices. The review of Huusom (2015) should be noted, as it similarly focuses on the challenges and opportunities of ICPD in industry.

Few ICPD studies have been carried out for combustion power plants. Diangelakis & Pistikopoulos (2016) performed ICPD for a small scale cogeneration plant, considering the combustor size and PID controller parameters. The work has also been extended to scheduling and model-based control (Diangelakis et al. 2017). Chen & Bollas (2017) determined air preheating and main steam temperature setpoints together with supervisory control for a chemical looping–combined cycle plant. ICPD presents major possibilities for large-scale boilers, which forms the motivation for the present work. Previous ICPD work for heat exchanger networks and power grids offers a starting point for the design (e.g. Adeodu & Chmielewski 2017, Alhammadi & Romagnoli 2004), but these findings can't be applied directly to boiler control.

The paper is structured as follows. Chapter 2 introduces the CFB boiler and its control tasks. Chapter 3 presents a basic classification of ICPD approaches, which is elaborated on for process knowledge and mathematical programming ICPD in chapters 4 and 5, together with the design examples for the CFB steam path. Chapter 6 presents the conclusions.

2. CFB PROCESS & CONTROL

In fluidized bed boilers (Fig. 2), fuel particles are fluidized and combusted in a bed of incombustible material by the input primary and secondary gas flows (Basu 2006). In the circulating fluidized bed setup (CFB), particles leave the furnace with the gas flows. The solids are separated and returned to the furnace, while the flue gas goes to the flue gas duct. The input gas is usually air, but in the oxy combustion CCS setup a mix of recirculated flue gas and pure O_2 is used.
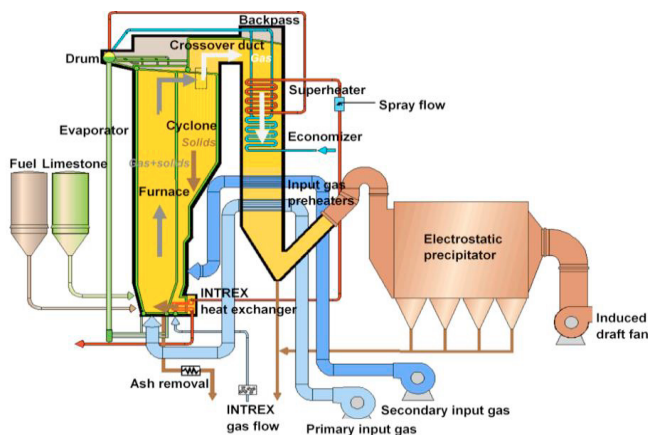
Fig. 2. Operational schematic figure of a drum CFB boiler (modified from Hultgren et al. 2014).

Combustion heat is used to generate steam in the steam path. Feedwater is evaporated in the furnace evaporator. The steam is superheated to form main steam in a block of superheaters (SH), with cooling desuperheater (DSH) spray flows between the stages. The steam expands in the turbine to generate power. In drum boilers, water is separated from steam after the evaporator. Once-through (OTU) boilers generate steam in a "once-through" pass with no separation stage. The setup

enables supercritical and sliding-pressure operation, but it also leads to control challenges, as there is a connection between the feedwater and the main steam, and as the steam storage capacity is small. (Joronen et al. 2007, Klefenz 1986)

The control objectives of a power plant are to maintain the generated power at its setpoint and to maximize boiler efficiency. The main individual control tasks are feedwater flow control, main steam temperature and pressure control, combustion control, turbine-generator unit control (output MW_e, frequency and voltage) and furnace pressure control (Joronen et al. 2007, Klefenz 1986). The unit master control strategy determines how the main steam pressure and MW_e output controls are coordinated. In turbine-following control, the MW_e is adjusted with the boiler firing power, and the steam pressure is controlled with the turbine valve. In boiler-following control, the opposite control pairings are used.

3. INTEGRATED CONTROL & PROCESS DESIGN

3.1 ICPD features

On a broad scale, ICPD involves all processing sequence, flowsheet, equipment sizing, control topology and controller design decisions of the process. An ICPD methodology can be characterized based on how these decisions are formulated and how they interact with each other. Important questions are what the goals for the increased design stage interaction are, how extensive it should be and how it is implemented.

A classification of the features of ICPD is given in Table 1, which is a novel contribution of this work. In sections 3.2–3.4, some aspects of Table 1 are discussed for CFB design. The main grouping is made between process knowledge and mathematical programming (chapters 4–5). Alternative ICPD reviews have been presented e.g. by Perkins & Walsh (1996), Ricardez-Sandoval et al. (2009), Sakizlis et al. (2004), Sharifzadeh (2013), Vega et al. (2014a) and Yuan et al. (2012). An emerging ICPD-related field is integrated scheduling and control (Baldea & Harjunkoski 2014, Dowling & Zavala 2017). Although the topic has even been studied for thermal power plants (Bindlish 2017, Diangelakis et al. 2017), scheduling is out of scope for this paper. ICPD is similarly often connected to process integration in literature.

Table 1. General features and characteristics of integrated control and process design (ICPD) methodologies.

Integrated control and process design		
Problem definition	*Design structure*	*Methodology basis*
Performance evaluation o Economic & environmental o Thermodynamic analysis o Disturbance rejection & setpoint tracking o Relevant process properties for control	**Degree of interaction** o "Anticipating" sequential (Meeuse & Grievink 2004) o Partially integrated o Fully integrated	**Process knowledge ICPD** o Heuristics o Phenomenon based o System analysis based
Purpose o Find best achievable performance o Improve dynamics through design o Generate best process+control system	**Decomposition** o Hierarchy of connected design steps o Decomposition method o "Closed" input−output design framework	**Mathematical programming ICPD** o Controllability based optimization o Full dynamic optimization, MIDO o Embedded control optimization o Robust optimization
Scope o Continuous or discrete decisions o Dynamic or steady-state operation o Process or control design basis	**Control design** o Adapt control template to process o Plantwide control design o Model-based control ICPD	o Back-off optimization o Multi-objective optimization o Stochastic/probabilistic optimization

3.2 Scope and structure

The scope of CFB boiler ICPD should be on the entire plant, as the process is a cyclic network of connected units with overlapping control tasks and process interactions. This is emphasized in the OTU steam path with its steam pressure, steam temperature and feedwater control interactions. Thus, design results for control tasks like superheater temperature control are ultimately relevant only on a plantwide scale.

In ICPD, operational decisions concern continuous variables (e.g. unit sizing, controller tuning), while structural decisions are discrete (flowsheet, control loops). The controller type and process structure are often predefined (Sharifzadeh 2013), and ICPD focuses on continuous process parameters and control connections between manipulated (MV) and controlled (CV) variables. This applies to boilers: flowsheets are mostly based on convention and PID control is prevalent.

The starting point for ICPD is often an existing process and/or control structure that is modified by the design. CFB examples include the application of drum-CFB control to the OTU-CFB, and oxy-CFB control design based on air-fired control (Hultgren et al. 2014). Standard CFB setups can be obtained from literature (Basu 2006, Joronen et al. 2007, Klefenz 1986). The main source of design variability is the amount and placement of SH units and DSH sprays, as the evaporator and many preheaters have "fixed" positions in the boiler. The three-superheater system is a common example.

ICPD principally aims at optimal steady-state or dynamic operation. If optimal dynamic performance with feasible economics is desired (e.g. load-following boilers), accurate dynamic modelling is needed during early design stages. Similarly, ICPD is usually based on tools and practices from either control or process design. Due to its transient-oriented design requirements, CFB ICPD should focus on control.

3.3 Design goals and performance evaluation

The most crucial property of an ICPD methodology is how desirable closed-loop performance is defined.

- **Economics:** Balance between capital (process) and operating costs (process and control), revenue vs. costs.
- **Thermodynamics:** Energy and exergy efficiency, "first-principles" chemical/physical approach.
- **Control:** Dynamic simulation with chosen disturbances, stability and minimal reference trajectory error.
- **System analysis:** Process properties relevant for control, indicates good performance or need for advanced control.

CFB boiler economics should consist of annualized fuel and investment costs, scaled with the generated MW_e. Quality related ICPD (e.g. Elliott & Luyben 1995) can't necessarily be used directly for the output power/frequency, but a penalty for setpoint deviations should be included. Environmental performance mainly depends on steady-states. Efficiency, exergy and heat rate analysis can also be used in boiler ICPD design (Bindlish 2017, Chen & Bollas 2017, Ray et al. 2010).

Load setpoint tracking is emphasized in boiler design, except when the plant is predominantly used for base load operation.

Setpoint tracking is studied in ICPD with dynamic error based measures like the integral square (ISE) or absolute (IAE) error (e.g. Ekawati 2003). Nonlinearity also needs to be analyzed due to the complex boiler dynamics, using e.g. linear error norms, bifurcation analysis or optimal control law (Kiss et al. 2007, Schweickhardt & Allgöwer 2004).

Control design properties that are utilized in ICPD include controllability and its various definitions, switchability, flexibility, operability, resiliency, and robustness (Bahri et al. 1997, Bogle et al. 2004, Ekawati 2003, Engell et al. 2004, Sharifzadeh 2013, Weitz & Lewin 1996). Switchability, i.e. the ability to move feasibly between operating points, should especially be considered in load-following boilers. Common analysis methods are the eigenvalue and singular value decomposition, the condition number, and different relative gain array (RGA) modifications like the dynamic RGA (DRGA), the partial relative gain (PRG, Häggblom 1997), the performance-RGA (Skogestad & Postlethwaite 2005) and the block relative gain (BRG, Manousiouthakis et al. 1986). These metrics can be used for studying interactions, stability, disturbance sensitivity and robustness in the CFB boiler.

3.4 Control design framework

Because of its procedural nature, control-oriented design and plantwide focus, ICPD is related to plantwide control, which aims at defining an overall control strategy for an entire plant of connected units (Skogestad 2004). The focus is on the selection of MVs, CVs and measurements, as well as on their control connections. In the CFB, plantwide control should be utilized for upper level solutions like unit master control, or for complex tasks like combustion control (Niva et al. 2015).

Model-based control has recently gained significant interest in ICPD research (Huusom 2015). As the control algorithm is based on the open-loop system, the controller can be linked to process changes in a closed framework, and discrete MV–CV connection variables are not needed. MPC ICPD has been studied e.g. by Bahakim & Ricardez-Sandoval (2014), Brengel & Seider (1992), Chawankul et al. (2007), Francisco et al. (2011) and Gutierrez et al. (2014). Especially economic model-based control could enable a joint process-controller optimization with one economic objective, like in the EMPC/ELOC based approach of Adeodu & Chmielewski (2017) for power grid energy storage. The applicability of MPC in CFB boiler ICPD is affected by how well suitable controller models can be constructed for the plantwide boiler flowsheet.

4. PROCESS KNOWLEDGE BASED ICPD

4.1 General principles

Process knowledge oriented ICPD uses modelling and operational knowledge from the process to guide the design decision-making. The simplest way to do this is to use a process model during the design to verify that decisions do not lead to reduced control performance (for steam boilers e.g. Majanne & Maasalo 2009). However, this approach requires many simulations, and results are easily obscured by overlapping effects and modelling assumptions. Systematic process knowledge oriented ICPD is thus often preferable.

Process knowledge ICPD has three modes: identification of design choices that cause control bottlenecks, design of open-loop systems that are inherently "easy" to control, and system classification based on selected criteria. Process knowledge ICPD is able to address design issues that would be difficult to define in formal algorithms, and there is an active interaction with the designer. The approach is particularly useful for screening candidate solutions for further analysis.

The downsides of process knowledge ICPD are that the design is often unable to manage multiple tasks effectively, optimality is hard to ensure, and solution templates easily lead to conservative designs. Connecting design parameters to process performance might also be limited for black-box systems, and first-principles models often have high computational costs for large flowsheets like steam boilers.

4.2 Methods

Process knowledge ICPD can be separated into heuristic design rules and systematic process characterization. While heuristics are easy to implement, they are strictly rule-based and inflexible. Moreover, while process and control design heuristics for individual boiler units like heat exchangers are readily available, plantwide design aspects are often ignored.

A process can be characterized through its chemical/physical phenomena or through control oriented analysis (Vega et al. 2014a). In phenomenon based analysis, thermodynamic properties are linked to control performance, considering energy, mass and momentum balances, generation terms, and driving forces (e.g. Alhammadi & Romagnoli 2004, Bogle et al. 2004, Hamid 2011, Meeuse & Grievink 2004). This approach has significant potential for power plant ICPD. The physical reasons for the non-minimum phase "shrink" and "swell" behaviour in drum boilers (Åström & Bell 2000) is a good example of phenomenon oriented control design. Similarly, Hultgren et al. (2015, 2014) defined how air-fired CFB control should be modified for oxy-firing based on the flowsheet and the properties of the combustion atmosphere.

In system analysis based characterization, system behaviour is evaluated through lower-complexity (linear) models, using common or custom performance indices for the properties in section 3.3 (e.g. Alhammadi & Romagnoli 2004, Bogle et al. 2004, Ekawati 2003, Engell et al. 2004, Weitz & Lewin 1996). For example, Skogestad & Postlethwaite (2005) outlined an approach for input-output controllability, using sensitivity, pole-zero, minimum singular value, RGA and condition number analysis. Indeed, ICPD design approaches are often combinations of different methods, such as the process characterization cube of Hernjak et al. (2004).

Controllability and interactions are central topics in the CFB, especially for the OTU boiler. Steam temperature control with multiple DSH sprays can result in ill-conditioning, and similar issues can be encountered for the primary and secondary oxidant flows (Hultgren et al. 2015). Relative gain analysis is well-suited for this design purpose. The analysis should be performed in the dynamic domain (DRGA), and the large dimensionality of the CFB flowsheet might require RGA modifications like the PRG or BRG. The BRG was used for boiler temperature control by Manousiouthakis et al.

(1986). Hultgren et al. (2015) employed the PRG for oxy-CFB plantwide control structure design and process interaction analysis. Maffezzoni et al. (1985) used control tools like Nyquist plots for solar power plant ICPD.

4.3 Case study: steam path DRGA design

System analysis in CFB boiler ICPD can be demonstrated with the DRGA and a simple steam path model that describes the relation between steam pressure, steam flow and the turbine MW_e output. It consists of first-order blocks for the evaporation, superheating and turbine sections derived from (1)–(2), where section sizes are represented by time constants ("mass storage coefficients") (Doležal & Varcop 1970). The resulting 2×2 transfer function model has the boiler load and turbine valve as MVs, and the main steam pressure and output MW_e as CVs. The evaporation and superheating mass storages TE and TS are modified, and the resulting DRGAs are calculated as a function of frequency (Fig. 3).
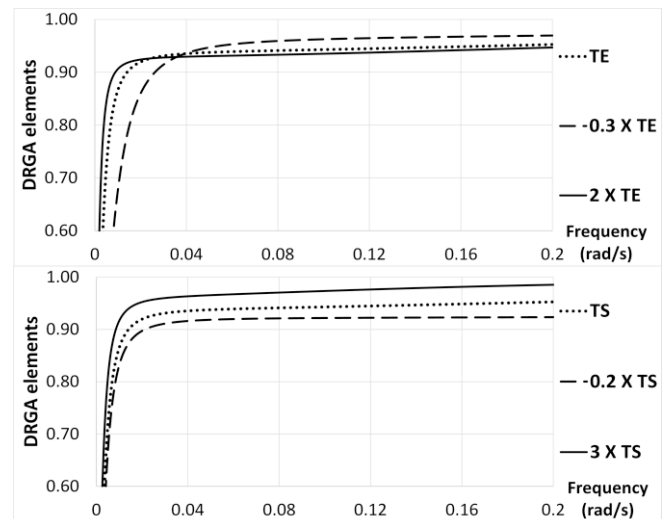
Fig. 3.   DRGA elements of boiler-following control connections for evaporator (TE) and superheater (TS) sizes.

$$\frac{dp}{dt} = \frac{1}{C}\left(m_{S,in} - m_{S,out}\right), \tag{1}$$

$$\Delta p = f\frac{m_{S,out}}{\rho_S}, \tag{2}$$

where C is mass storage (TE/TS), p is pressure, m_S is steam mass flow, ρ_S is steam density and f is a pipe friction factor.

Based on the DRGA, a large superheating mass storage TS leads to improved controllability, as stored steam between the turbine and the evaporator increases the decoupling between MW_e and pressure control. Increasing the evaporating section size (TE) also improves controllability at low frequencies, but above 0.04 rad/s the situation is reversed, which could be explained by the evaporator and superheater size differences. The findings are visible as MW_e control performance during output power setpoint changes (Table 2), using tightly tuned boiler-following PI control (turbine valve–output MW_e, main steam pressure–boiler load loops) at constant steam pressure.

Table 2. MW$_e$ setpoint error during a triangular ±5 % MW$_e$ setpoint disturbance, normalized by largest error.

Ramp speed (s)		500	200	100	80	60	40	20	15	10
TS, MW$_e$ error	TS	1.00	0.98	0.97	0.97	0.98	0.99	0.99	0.99	0.98
	0.2×TS	1.00	1.00	1.00	1.00	1.00	1.00	1.00	1.00	1.00
	3×TS	0.98	0.92	0.90	0.92	0.94	0.96	0.97	0.97	0.96
TE, MW$_e$ error	TE	0.86	0.72	0.78	0.86	0.93	0.99	0.99	0.99	1.00
	0.3×TE	1.00	1.00	1.00	1.00	1.00	1.00	0.97	0.97	0.98
	2×TE	0.83	0.62	0.73	0.83	0.92	0.99	1.00	1.00	1.00

5. MATHEMATICAL PROGRAMMING BASED ICPD

5.1 General principles

Mathematical programming ICPD defines the problem in a formal mathematical framework and searches for solutions systematically within it using an optimization algorithm. All approaches can essentially be derived from the basic problem statement "F" (3)–(4) (Hamid 2011, Sakizlis et al. 2004).

$$\min_{x,y,u} F(x',x,y,u) = \begin{bmatrix} F_1(x,y,u) \\ F_2(x,y,u) \end{bmatrix}, \qquad (3)$$

$$\begin{cases} f(x,y,u,t) = 0 \\ h(x,y,u) = 0 \\ g(x,y,u) \geq 0 \\ x^L \leq x \leq x^U \\ x(t_0) = x_0 \\ u(t_0) = u_0 \end{cases} \qquad (4)$$

where x are states, y and u are process and design variables, t is time, F_1 is economic objective, F_2 is control objective, f are process equality constraints, h are performance equality constraints, g are performance inequality constraints, "L"/"U" are lower/upper bounds, and "0" denotes initial conditions.

The setup of a mathematical programming ICPD approach largely depends on which design decisions are included in the problem, most importantly the need for dynamic optimization and discrete decisions. Structural decisions are formulated as mixed-integer (MILP or MINLP) problems, where the design progression is characterized by the chosen mixed-integer solver (Grossmann 2002). Likewise, ICPD can be performed either in the open-loop or the closed-loop. Methodologies are usually restricted to set controller types (Yuan et al. 2012), although research has aimed at including different controllers into the same formulation through perfect control, inverse optimality or controller parameterization (Alvarez et al. 2004, Lear et al. 1995, Perkins & Walsh 1996, Sharifzadeh & Thornhill 2013, Swartz 2004). Closed-loop design should include the controller parameters into the optimization to make different process setups comparable. As CFB boiler ICPD aims at improving load transitions, dynamic closed-loop optimization will be necessary at least to some extent.

The design goal is formed as a single economic objective or a set of goals, including dedicated control performance and controllability measures. The tradeoff between economic and control objectives can be formulated as a weighted sum, but

as making objectives comparable is challenging, ICPD often relies on multi-objective optimization (Alhammadi & Romagnoli 2004, Ekawati 2003, Egea et al. 2007, Schweiger & Floudas 1998, Sharifzadeh & Thornhill 2013, Vega et al. 2014b). Stochastic and probabilistic approaches are used for global optimization of difficult nonconvex IPCD problems (Bahakim & Ricardez-Sandoval 2014, Sendin et al. 2004). Defined disturbance scenarios and uncertainties also greatly affect the results of ICPD optimization. CFB design should center on fuel, air and feedwater disturbances for base load operation and load demand ramps for load-following boilers.

Mathematical programming ICPD is effective at locating optimal and unconventional solutions, but it also results in difficult calculation problems and poor convergence for large flowsheets. This is a limitation for thermal power plants, where a plantwide perspective is preferable. "Optimal" results might also not be applicable in real life (Alvarez et al. 2004). In fully simultaneous design, separating the effects of control and process design decisions can also be difficult.

5.2 Methods

The simplest way to implement mathematical programming based ICPD is to incorporate control performance measures to process optimization as constraints or cost function terms (e.g. Francisco et al. 2011, Vega et al. 2014b, Yuan et al. 2012), forming a tradeoff between economics and control. Control indices easily result in local optima, non-convexities and multiplicities in the cost function (Egea et al. 2007, Schweiger & Floudas 1998). This has to be considered for design goal definitions in transient-driven CFB design.

In dynamic optimization, ICPD is carried out with a dynamic model and a single economic objective, considering process and control design together from the start. Especially the comprehensive mixed-integer dynamic optimization (MIDO) approach has attracted interest (Bahri et al. 1997, Bansal et al. 2000, Flores-Tlacuahuac & Biegler 2008, Miranda et al. 2008, Mohideen et al. 1997, Sakizlis et al. 2004, Terrazas-Moreno et al. 2008). A MIDO is solved by converting it into a MINLP through simultaneous, sequential or hybrid discretization (Sharifzadeh 2013). MIDO design is limited by its high computational requirements for large industrial CFB flowsheets. MIDO was used for combustion power plants by Diangelakis et al. (2017) and Diangelakis & Pistikopoulos (2016). Dynamic optimization was also employed in the efficiency oriented boiler ICPD of Chen & Bollas (2017).

Embedded control optimization casts the dynamic ICPD task as an iterative bi-level framework (Moon et al. 2011, Yuan et al. 2012). The outer level looks for design parameters that govern the dynamics with a first-principles model. The inner level tests the dynamic performance with state-space models based on outer level design decisions. Deshmukh & Allison (2013) utilized a similar approach for wind turbine ICPD.

In robust optimization ICPD, robust control tools are used for evaluating stability and flexibility by describing the system with low-order models with uncertainty (Chawankul et al. 2007, Grosch et al. 2008, Mönnigmann & Marquardt 2002, Ricardez-Sandoval et al. 2009). Robust ICPD is divided into Lyapunov linear matrix inequality and structured singular

value methods (Ricardez Sandoval 2008). The focus on worst-case disturbances easily leads to conservative designs.

In back-off optimization, the starting point of the design is a steady-state process optimum with control. The system dynamics are examined together with disturbances to find the process variability region, and the operating point is "backed off" from system constraints accordingly. The minimization of the back-off penalty leads to the optimal dynamic operating point (Kookos & Perkins 2004, Yuan et al. 2012). The approach is quite limited for load-following CFB design, as load change disturbances would require a large back-off, but it could be considered e.g. for steam temperature control.

5.3 Case study: closed-loop steam path optimization

ICPD optimization can be demonstrated with the chapter 4.3 steam path model. Boiler-following PID control is applied for the main steam pressure and output power, with tight tuning for the MW_e controller. The pressure controller parameters are then optimized together with the superheater storage TS to minimize the pressure control error in constant pressure operation. The process is excited with two fast output MW_e setpoint ramps. The cost function is the steam pressure IAE error, and the optimization is performed with the Nelder-Mead algorithm. The results are compared to optimal PID parameters for the original TS mass storage (Fig. 4).
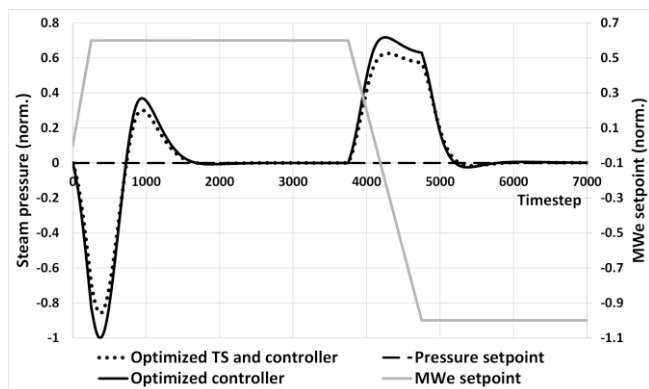
Fig. 4. Boiler-following steam pressure control for MW_e setpoint ramps. Optimized PID parameter base case (minimal pressure tracking error) vs. ICPD case with optimized superheating mass storage TS and PID controller parameters.

The optimization successfully determined the TS storage and modified the pressure controller parameters accordingly. At constant pressure, a large superheater enables accurate steam pressure control and also slightly improved MW_e control (Table 3), as was also indicated by the DRGA in section 4.3. However, when the optimization is run in sliding-pressure mode (MW_e and pressure setpoints change according to load level), a small superheating section gives the most effective pressure control. The loop decoupling suggested by the DRGA is thus overshadowed by the fast dynamics of a small steam storage. Moreover, including the MW_e controller and a MW_e setpoint tracking objective into the optimization resulted in local optima, since TS mainly affects the steam pressure response. Indeed, fast MW_e control with the turbine valve can basically be achieved for any superheater size.

Table 3. Optimal ICPD results for constant and sliding pressure MW_e ramps, normalized by optimized PID controller base case. DN = derivative PID filter.

	P	I	D	DN	TS	p IAE	MW_e IAE
Constant pressure	1.12	1.12	1.12	0.43	2.00	0.87	0.97
Sliding pressure	1.20	1.01	2.12	4.53	0.50	0.97	0.99

6. CONCLUSIONS

Steam boiler control is a specific field with requirements that differ from many other chemical processes: strong loop interactions, a wide range of operating points, and a focus on load transition performance. Based on literature, integrated control and process design (ICPD) is useful for improving load change speed in circulating fluidized bed (CFB) power plants. Almost no ICPD studies exist for large-scale boilers, and as ICPD is a wide research field, a review of its approaches was provided here, focusing on CFB design.

Both process knowledge and mathematical programming ICPD is basically applicable to the CFB. Phenomenon based process characterization is a good starting point, as it can use existing design knowledge, and as dynamic optimization, in particular, is computationally heavy for the CFB flowsheet. Phenomenon based boiler analysis constitutes the steam thermodynamics, combustion reactions and heat transfer.

ICPD design was demonstrated on an industrial CFB steam path model. Evaporation and superheating mass storages were modified through DRGA analysis and closed-loop optimization to generate improved load changes. However, the cases also highlighted challenges related to the chosen optimization objective formulation and analysis methods.

REFERENCES

Adeodu, O. and Chmielewski, D.J. (2017). Optimal Sizing and Placement of Grid-level Energy Storage. In *FOCAPO/CPC 2017 conference*, Tucson, USA, Jan 8–12.

Alhammadi, H.Y. and Romagnoli, J.A. (2004). Process design and operation: Incorporating environmental, profitability, heat integration and controllability considerations. In Seferlis, P. and Georgiadis, M.C. (ed.), *The Integration of Process Design and Control*, 264–305. Elsevier, Amsterdam.

Alvarez, J., Zaldo, F. and Oaxaca, G. (2004). Towards a joint process and control design for batch processes: application to semibatch polymer reactors. In Seferlis, P. and Georgiadis, M.C. (ed.), *The Integration of Process Design and Control*, 604–634. Elsevier, Amsterdam.

Bahakim, S.S. and Ricardez-Sandoval, L.A. (2014). Simultaneous design and MPC-based control for dynamic systems under uncertainty: A stochastic approach. *Comput. Chem. Eng.*, 63, 66–81.

Bahri, P.A., Bandoni, J.A. and Romagnoli, J.A. (1997). Integrated flexibility and controllability analysis in design of chemical processes. *AIChE J.*, 43(4), 997–1015.

Baldea, M. and Harjunkoski, I. (2014). Integrated production scheduling and process control: A systematic review. *Comput. Chem. Eng.*, 71, 377–390.

Bansal, V., Perkins, J.D., Pistikopoulos, E.N., Ross, R. and van Schijndel, J.M.G. (2000). Simultaneous design and control optimisation under uncertainty. *Comput. Chem. Eng.*, 24(2–7), 261–266.

Basu, P. (2006). *Combustion and Gasification in Fluidized Beds*. CRC Press, Taylor & Francis Group, Boca Raton.

Bindlish, R. (2017). Scheduling, Optimization and Control of Power for Industrial Cogeneration plants. In *FOCAPO/ CPC 2017 conference*, Tucson, USA, Jan 8–12.

Bogle, I.D.L., Ma, K., Hagemann, J. and Fraga, E.S. (2004). Analysing the controllability of nonlinear process systems. In Seferlis, P. and Georgiadis, M.C. (ed.), *The Integration of Process Design and Control*, 168–186. Elsevier, Amsterdam.

Brengel, D.D. and Seider, W.D. (1992). Coordinated design and control optimization of nonlinear processes. *Comput. Chem. Eng.*, 16(9), 861–886.

Chawankul, N., Ricardez Sandoval, L.A., Budman, H. and Douglas, P.L. (2007). Integration of Design and Control: A Robust Control Approach Using MPC. *Can. J. Chem. Eng.*, 85(4), 433–446.

Chen, C. and Bollas, G.M. (2017). Semi-batch Chemical-looping Reactors Integrated with Combined Cycle Power Plants Operating at Transient Electricity Demand. In *FOCAPO/CPC 2017 conference*, Tucson, USA, Jan 8–12.

Deshmukh, A.P. and Allison, J.T. (2013). Simultaneous Structural and Control System Design for Horizontal Axis Wind Turbines. In *54th AIAA/ASME/ASCE/AHS/ ASC Structures, Structural Dynamics, and Materials Conference*, Boston, USA, Apr 8–11.

Diangelakis, N.A., Burnak, B. and Pistikopoulos, E.N. (2017). A multi-parametric programming approach for the simultaneous process scheduling and control – Application to a domestic cogeneration unit. In *FOCAPO/CPC 2017 conference*, Tucson, USA, Jan 8–12.

Diangelakis, N.A. and Pistikopoulos, E.N. (2016). Modelling, Design and Control Optimization of a Residential Scale CHP System. In Kopanos, G.M., Liu, P. and Georgiadis, M.C. (ed.), *Advances in Energy Systems Engineering*, 475–506. Springer, Cham.

Doležal, R. and Varcop, L. (1970). *Process Dynamics, Automatic Control of Steam Generation Plant*. Elsevier, Amsterdam.

Dowling, A.W. and Zavala, V.M. (2017). Redesigning Decision-making Architectures to Exploit Multi-scale Electricity Markets. In *FOCAPO/CPC 2017 conference*, Tucson, USA, Jan 8–12.

Egea, J.A., Vries, D., Alonso, A.A. and Banga, J.R. (2007). Global Optimization for Integrated Design and Control of Computationally Expensive Process Models. *Ind. Eng. Chem. Res.*, 46(26), 9148–9157.

Ekawati, E. (2003). *The Development of Systematic Controllability Assessment for Process Control Designs*. Murdoch University, Perth.

Elliott, T.R. and Luyben, W.L. (1995). Capacity-Based Economic Approach for the Quantitative Assessment of Process Controllability during the Conceptual Design Stage. *Ind. Eng. Chem. Res.*, 34(11), 3907–3915.

Engell, S., Trierweiler, J.O., Völker, M. and Pegel, S. (2004). Tools and indices for dynamic I/O-controllability assessment and control structure selection. In Seferlis, P. and Georgiadis, M.C. (ed.), *The Integration of Process Design and Control*, 430–463. Elsevier, Amsterdam.

Flores-Tlacuahuac, A. and Biegler, L.T. (2008). Integrated control and process design during optimal polymer grade transition operations. *Comput. Chem. Eng.*, 32(11), 2823–2837.

Francisco, M., Vega, P. and Álvarez, H. (2011). Robust Integrated Design of processes with terminal penalty model predictive controllers. *Chem. Eng. Res. Des.*, 89(7), 1011–1024.

Grosch, R., Mönnigmann, M. and Marquardt, W. (2008). Integrated design and control for robust performance: Application to an MSMPR crystallizer. *J. Proc. Control*, 18(2), 173–188.

Grossmann, I.E. (2002). Review of Nonlinear Mixed-Integer and Disjunctive Programming Techniques. *Optim. Eng.*, 3(3), 227–252.

Gutierrez, G., Ricardez-Sandoval, L.A., Budman, H. and Prada, C. (2014). An MPC-based control structure selection approach for simultaneous process and control design. *Comput. Chem. Eng.*, 70, 11–21.

Hamid, M.K.A. (2011). *Model-Based Integrated Process Design and Controller Design of Chemical Processes*. Technical University of Denmark, Copenhagen.

Hernjak, N., Doyle III, F.J., Ogunnaike, B.A. and Pearson, R.K. (2004). Chemical process characterization for control design. In Seferlis, P. and Georgiadis, M.C. (ed.), *The Integration of Process Design and Control*, 42–75. Elsevier, Amsterdam.

Hultgren, M., Ikonen, E. and Kovács, J. (2015). Combustion Control in Oxy-fired Circulating Fluidized Bed Combustion. In *22nd International Conference on Fluidized Bed Conversion*, Turku, Finland, Jun 14–17.

Hultgren, M., Ikonen, E. and Kovács, J. (2014). Oxidant control and air-oxy switching concepts for CFB furnace operation. *Comput. Chem. Eng.*, 61, 203–219.

Huusom, J.K. (2015). Challenges and opportunities in integration of design and control. *Comput. Chem. Eng.*, 81, 138–146.

Häggblom, K.E. (1997). Partial Relative Gain: A New Tool for Control Structure Selection. In *1997 AIChE Annual Meeting*, Los Angeles, USA, Nov 16–21.

Joronen, T., Kovács, J. and Majanne, Y. (2007). *Voimalaitosautomaatio*. Suomen Automaatioseura, Helsinki.

Kiss, A.A., Bildea, C.S. and Dimian, A.C. (2007). Design and control of recycle systems by non-linear analysis. *Comput. Chem. Eng.*, 31(5–6), 601–611.

Kookos, I.K. and Perkins, J.D. (2004). The back-off approach to simultaneous design and control. In Seferlis, P. and Georgiadis, M.C. (ed.), *The Integration of Process Design and Control*, 216–238. Elsevier, Amsterdam.

Klefenz, G. (1986). *Automatic Control of Steam Power Plants*. B.I.-Wissenschaftsverlag, Mannheim.

Lear, J.B., Barton, G.W. and Perkins, J.D. (1995). Interaction between process design and process control: the impact of disturbances and uncertainty on estimates of

achievable economic performance. *J. Proc. Control*, 5(1), 49–62.

Majanne, Y. and Maasalo, M. (2009). Dynamic Simulation Assisted Design of Industrial Power Plant Process and Control. In Majanne, Y. (ed.), *6th IFAC Symposium on Power Plants and Power Systems Control,* Tampere, Finland, Jul 5–8.

Maffezzoni, C., Magnani, G.A. and Quatela, S. (1985). Process and Control Design of High-Temperature Solar Receivers: An Integrated Approach. *IEEE Trans. Autom. Control*, 30(3), 194–209.

Manousiouthakis, V., Savage, R. and Arkun, Y. (1986). Synthesis of Decentralized Process Control Structures Using the Concept of Block Relative Gain. *AIChE J.*, 32(6), 991–1003.

Meeuse, F.M. and Grievink, J. (2004). Thermodynamic controllability assessment in process synthesis. In Seferlis, P. and Georgiadis, M.C. (ed.), *The Integration of Process Design and Control*, 146–167. Elsevier, Amsterdam.

Miranda, M., Reneaume, J.M., Meyer, X., Meyer, M. and Szigeti, F. (2008). Integrating process design and control: An application of optimal control to chemical processes. *Chem. Eng. Proc. Proc. Intensif.*, 47(11), 2004–2018.

Mohideen, M.J., Perkins, J.D. and Pistikopoulos, E.N. (1997). Towards an efficient numerical procedure for mixed integer optimal control. *Comput. Chem. Eng.*, 21(Suppl.), S457–S462.

Mönnigmann, M. and Marquardt, W. (2002). Normal Vectors on Manifolds of Critical Points for Parametric Robustness of Equilibrium Solutions of ODE Systems. *J. Nonlinear Sci.*, 12(2), 85–112.

Moon, J., Kim, S. and Linninger, A.A. (2011). Integrated design and control under uncertainty: Embedded control optimization for plantwide processes. *Comput. Chem. Eng.*, 35(9), 1718–1724.

Niva, L., Ikonen, E. and Kovács, J. (2015). Self-optimizing control structure design in oxy-fuel circulating fluidized bed combustion. *Int. J. Greenh. Gas Control*, 43, 93–107.

Perkins, J.D. and Walsh, S.P.K. (1996). Optimization as a Tool for Design/Control Integration. *Comput. Chem. Eng.*, 20(4), 315–323.

Ray, T.K., Datta, A., Gupta, A. and Ganguly, R. (2010). Exergy-based performance analysis for proper O&M decisions in a steam power plant. *Energy Convers. Manag.*, 51(6), 1333–1344.

Ricardez-Sandoval, L.A., Budman, H.M. and Douglas, P.L. (2009). Integration of design and control for chemical processes: A review of the literature and some recent results. *Annu. Rev. Control*, 33(2), 158–171.

Ricardez Sandoval, L.A. (2008). *Simultaneous Design and Control of Chemical Plants: A Robust Modelling Approach*. University of Waterloo, Waterloo.

Sakizlis, V., Perkins, J.D. and Pistikopoulos, E.N. (2004). Recent advances in optimization-based simultaneous process and control design. *Comput. Chem. Eng.*, 28(10), 2069–2086.

Schweickhardt, T. and Allgöwer, F. (2004). Quantitative nonlinearity assessment – An introduction to nonlinearity measures. In Seferlis, P. and Georgiadis, M.C. (ed.), *The Integration of Process Design and Control*, 76–95. Elsevier, Amsterdam.

Schweiger, C.A. and Floudas, C.A. (1998). Interaction of Design and Control: Optimization with Dynamic Models. In Hager, W.W. and Pardalos, P.M. (ed.), *Optimal Control: Theory, Algorithms, and Applications*, 388–435. Springer, Dordrecht.

Sendin, O.H., Moles, C.G., Alonso, A.A. and Banga, J.R. (2004). Multi-objective integrated design and control using stochastic global optimization methods. In Seferlis, P. and Georgiadis, M.C. (ed.), *The Integration of Process Design and Control*, 555–581. Elsevier, Amsterdam.

Sharifzadeh, M. (2013). Integration of process design and control: A review. *Chem. Eng. Res. Des.*, 91(12), 2515–2549.

Sharifzadeh, M. and Thornhill, N.F. (2013). Integrated design and control using a dynamic inversely controlled process model. *Comput. Chem. Eng.*, 48, 121–134.

Skogestad, S. and Postlethwaite, I. (2005). *Multivariable Feedback Control, Analysis and Design*. Wiley, Chichester.

Skogestad, S. (2004) Control structure design for complete chemical plants. *Comput. Chem. Eng.*, 28(1–2), 219–234.

Swartz, C.L.E. (2004). The use of controller parametrization in the integration of design and control. In Seferlis, P. and Georgiadis, M.C. (ed.), *The Integration of Process Design and Control*, 239–263. Elsevier, Amsterdam.

Terrazas-Moreno, S., Flores-Tlacuahuac, A. and Grossmann, I.E. (2008). Simultaneous Design, Scheduling, and Optimal Control of a Methyl-Methacrylate Continuous Polymerization Reactor. *AIChE J.*, 54(12), 3160–3170.

Vega, P., Lamanna de Rocco, R., Revollar, S. and Francisco, M. (2014a). Integrated design and control of chemical processes – Part I: Revision and classification. *Comput. Chem. Eng.*, 71, 602–617.

Vega, P., Lamanna, R., Revollar, S. and Francisco, M. (2014b). Integrated design and control of chemical processes – Part II: An illustrative example. *Comput. Chem. Eng.*, 71, 618–635.

Weitz, O. and Lewin, D.R. (1996). Dynamic Controllability and Resiliency Diagnosis Using Steady State Process Flowsheet Data. *Comput. Chem. Eng.*, 20(4), 325–335.

Yuan, Z., Chen, B., Sin, G. and Gani, R. (2012). State-of-the-Art and Progress in the Optimization-based Simultaneous Design and Control for Chemical Processes. *AIChE J.*, 58(6), 1640–1659.

Åström, K.J. and Bell, R.D. (2000). Drum-boiler dynamics. *Automatica*, 36(3), 363–378.

Once-through Circulating Fluidized Bed Boiler Control Design with the Dynamic Relative Gain Array and Partial Relative Gain

Matias Hultgren,*,‡ Enso Ikonen, and Jenő Kovács

Systems Engineering, University of Oulu, POB 4300, Oulun yliopisto, FI-90014, Finland

S *Supporting Information*

ABSTRACT: Combustion power plants currently face major performance challenges, which require robust control design methods. Extensive relative gain analysis was conducted in this paper to generate plantwide control structures for a full-scale once-through circulating fluidized bed boiler. No such study has been reported before for steam boilers. The partial relative gain was employed to generate decentralized control structures based on integral controllability with integrity. The approach provided feasible control structures and verified that basic turbine-following boiler control is preferable in terms of controllability. The steady-state results were extended with the dynamic relative gain array for higher frequencies, which revealed that boiler-following control becomes feasible for faster disturban-

ces. The results highlight the complex interactions between steam pressure and output electrical power control, as well as the loop interactions caused by the feedwater flow in the once-through steam path.
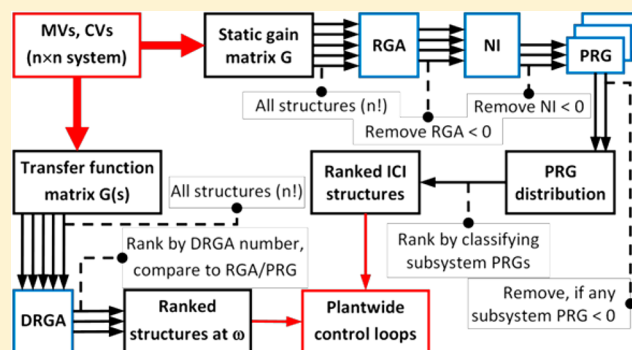
1. INTRODUCTION

This work applies relative gain analysis to once-through circulating fluidized bed (OTU-CFB) boiler plantwide control design. The steam power plant is a complex process with inter-acting control tasks.[1−3] The steam and combustion sides have different time constant magnitudes, and heat exchangers are located at different positions in the boiler. Dynamics and control are important because of increasing demands for operational flexibility and efficiency. Large boilers are increasingly used for variable loads and fast load transitions with accurate set point tracking demands instead of base load operation. Flowsheets are heavily interconnected, and plants are run close to their operational boundaries. Increased boiler sizes and technologies such as carbon capture and storage (CCS) have also introduced new design requirements for fluidized beds.[4−6]

The new requirements call for advanced design approaches to obtain improved output power responses (Figure 1). First, a deeper interaction between process and control design is needed. In integrated control and process design (ICPD), the two design stages take place simultaneously so that their specific requirements can influence each other.[7] Second, con-trol design should be conducted on a plantwide scale to ensure an effective operation of the whole process.[8] While multi-variable dynamic (model predictive) control is rarely feasible on a plantwide level, a more practiced approach is the pairing/decoupling of inputs and outputs into control loops using dedi-cated selection procedures. Moreover, methods for analyzing system behavior are needed in both plantwide control and ICPD. Relative gain analysis is used in this paper for these purposes.
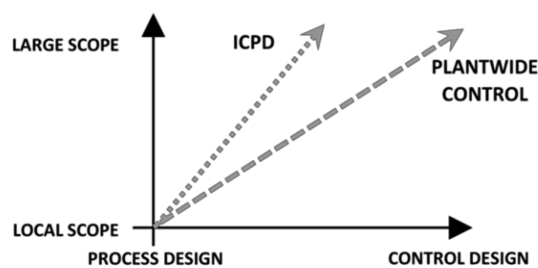
Figure 1. Process and control design directions that aim at improved overall performance of large process systems: plantwide control and integrated control and process design (ICPD).

Relative gain based design is well suited for evaluating control-lability and interactions for processes with multiple inputs and outputs,[9,10] such as the OTU-CFB. Another advantage is that closed-loop properties can be determined on the basis of open-loop data, which is useful especially in ICPD.[11] Relative gain analysis is based on the relative gain array, RGA.[12] Modifications of the RGA include the dynamic RGA (DRGA) and the partial relative gain (PRG). The DRGA investigates interactions at higher frequencies,[10,13] while the PRG considers partially controlled sys-tems[14] and can be used as a condition for integral controllability with integrity (ICI).[15,16] While the RGA and the DRGA are established methods, the PRG is featured in few publications.

The purpose of this work is to study the PRG and DRGA as tools for controllability analysis and plantwide control design in the OTU-CFB, with potential application to ICPD at a later stage. By evaluating interactions related to specific control connections, this approach can lead to improved electrical power (MW_e) responses. The contribution of this paper is 2-fold. First, systematic plantwide control structure selection is performed for a full industrial OTU-CFB boiler. Only a few studies on plantwide power plant control have been reported in the literature. Niva et al.[17] applied the self-optimizing approach of Skogestad[18] to an oxy-fired CFB pilot. Prasad et al.[19] used centralized model predictive control for a drum boiler, while Garduno-Ramirez and Lee[20] combined loop decoupling methods in drum boiler plantwide operation. Notably, existing studies focus on drum boilers, which have a different control setup compared to the OTU.

The second contribution is that extensive controllability and interaction analysis is performed for the entire CFB boiler using the DRGA and the PRG, which has not been done before. The steady-state RGA has been used to some extent,[21−23] commonly for the 3 × 3 input−output Åström−Bell drum boiler model.[20,24] For example, the block relative gain was also used for a 4 × 4 furnace temperature control problem by Manousiouthakis et al.[25] Unlike the existing papers, the present work not only addresses the control structure selection in a large 8 × 8 system, but also aims at analyzing the OTU-CFB to provide reasons for reduced controllability. The focus is on current OTU-CFB layouts, but the paper also serves as an evaluation of the chosen methods for future flowsheets, which may differ from current designs (e.g., combined heat and solar power). Similarly, relative gain analysis can also be used to uncover unconventional control connections.

The paper is structured as follows. Chapter 2 introduces the OTU-CFB and its main control tasks. Chapter 3 discusses plantwide control design and controllability analysis with the DRGA and PRG methods. Chapter 4 presents the industrial OTU-CFB design case. Chapter 5 shows the results of the PRG and DRGA analysis, and chapter 6 gives the conclusions of the work.

2. THE OTU-CFB PROCESS AND CONTROL

The circulating fluidized bed (CFB) combustion technology[3,26,27] and the once-through (OTU) steam cycle[1,2] are well-known on their own, but the first industrial scale supercritical OTU-CFB was only constructed in 2009.[28,29] CFB boilers enable flexible cocombustion of different fuels and reduced solid fuel emissions. The OTU water-steam setup is the most viable steam cycle for constructing large boilers with fast output power responses, but it is also challenging to control.

2.1. OTU-CFB Process. In a fluidized bed boiler, fuel particles are combusted in a bed of incombustible material. The bed is fluidized by the input oxidant gas flows (primary and secondary). In the CFB setup (Figure 2), particles are entrained with the gas and leave the furnace from the top. Solids are separated from the flue gas in a cyclone and circulated back to the furnace, while the flue gas goes to the backpass duct. Heat exchangers are located in the CFB hotloop and the backpass. The oxidant gas is typically air, but can also be formed in other ways (e.g., oxy combustion).[4−6,30−33]

The steam cycle consists of preheating, evaporation, superheating, expansion, and condensing stages. Feedwater is evaporated in the furnace evaporator and the steam temperature is elevated in the superheating section. This "main steam"
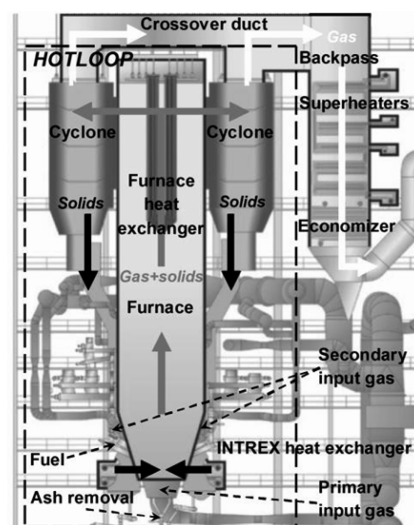
Figure 2. Operational schematic figure of an OTU-CFB, modified from Sumitomo SHI FW.

expands in the turbine, often in several stages with reheating between them. Boilers are classified into drum and once-through units. In drum boilers, water is separated from steam after the evaporator in a drum and circulated back to the evaporator. In OTU boilers, water transforms directly into main steam in a "once-through" pass, and as there is no steam separation stage, the boundaries between preheating, evaporation, and superheating may shift. This setup enables the use of supercritical and sliding-pressure operation, which facilitates the construction of large and efficient boilers with short startup times.

2.2. Main Control Tasks. The control objectives of a power plant can be divided into those related to the steam at the turbine, and those related to efficiency and safety state variables.[1,2,4] The main objectives are to maximize boiler efficiency and to maintain the generated power at its set point, that is, electrical megawatts (MW_e) for condensing plants and heat/electrical power for cogeneration plants. Set point tracking is emphasized in order to follow load demand changes accurately, but disturbance rejection becomes more important for boilers that are primarily run on base load.

2.2.1. Unit Master Control. Unit master control is an upper-level strategy for coordinating steam pressure and output MW_e control. The main setups are boiler-following and turbine-following control (Figure 3).
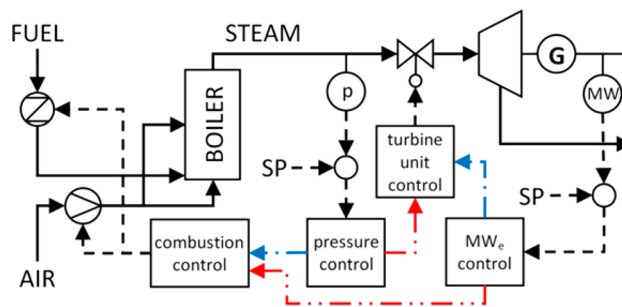
Figure 3. Unit master concepts: turbine-following (red) and boiler-following (blue) control.

In boiler-following control, the MW_e is controlled with the turbine throttle valve and the pressure with the combustion power (fuel and oxidant). A change in the load demand alters

the valve position, and the resulting pressure disturbance is compensated with the combustion power. In turbine-following control, the pressure is controlled with the turbine valve and the MW_e with the combustion power. The heat generation changes according to the load demand and the steam flow is altered to adjust the pressure, which results in an output MW_e change.

2.2.2. Feedwater Control. Feedwater flow rate control is required in order to make up for formed steam. In drum boilers, this largely translates into drum water level control. In OTU boilers, feedwater affects the steam generation directly, which is why mildly superheated steam properties are usually controlled.

2.2.3. Steam Temperature Control. Superheating takes place in a block of superheater (SH) heat exchangers. The main steam (live steam) temperature is regulated between these stages with water sprays from the feedwater line (desuperheaters, DSH), usually with cascade control structures (temperature before and after the spray). The spray water also appears as a steam flow disturbance.

2.2.4. Main Steam Pressure Control. The main steam pressure before the turbine valve is regulated. The pressure can be modified either by changing the turbine valve position or by increasing the steam generation (heat and feedwater). One design factor is whether the pressure is controlled to be constant (constant pressure mode) or whether it is allowed to change with the load level (sliding-pressure mode).

2.2.5. Combustion Control. Combustion control concerns the regulation of the fuel and the oxidant gas, with set points coming from the unit master control. Flue gas O_2 control is included to ensure a sufficient O_2 supply. In CFB boilers, a major requirement is also to maintain the fluidization of the solids. The combustion presents many sources for disturbances, which may require state estimation.[34]

2.2.6. Turbine-Generator Unit Control. Turbogenerator control consists of power, voltage, and frequency control. The generated MW_e depends on the combustion heat and the feedwater, but momentary changes can be made with the turbine valve. Frequency control can be achieved as a cascade structure with the MW_e control.

The OTU boiler is challenging to control. Flow conditions are complex, as water and steam are not separated at a fixed boundary. Thus, there is a direct connection between the evaporation and superheating stages, which leads to strong interactions between steam pressure, steam temperature, and feedwater control. The small OTU storage capacity reduces the possibilities for load disturbance rejection, and combustion disturbances are easily carried over to the steam properties. The high pressures and temperatures in supercritical boilers also lead to small control tolerance limits. All of these factors call for tight control and improved feedforward action.

3. PLANTWIDE CONTROL AND CONTROL PERFORMANCE

Plantwide control provides a control solution for the entire process with good performance and stability, when considering plant dynamics, constraints, disturbances, and control law.[8,18,35] Plantwide design typically employs decentralized control with conventional controllers, such as PID or low-dimensional MIMO (multiple input–multiple output) controllers. Plantwide methods provide the manipulated (MV) and controlled variables (CV) and their pairing into control loops.

3.1. Variable Selections and Performance Evaluation. Process degrees of freedom (DOF) analysis is conducted to determine the amount of MVs for managing CVs. The control degrees of freedom (CDOF)[7,36] should especially be considered, for example, by analyzing the flowsheet one process unit at a time and comparing the total amount of streams (material and energy) to the number of streams that are restrained (e.g., one stream in a mixer) or redundant from being manipulated (e.g., pressures of process units in series), eq 1.[37]

$$CDOF = N_{total} - \sum_{units} (N_{restrained} + N_{redundant}) \qquad (1)$$

where N_{total}, $N_{restrained}$, and $N_{redundant}$ are the amounts of total, restrained, and redundant streams.

MVs, CVs, and measurements are selected systematically based on the DOF, constraints, and steady-state economic optimization.[18] Active constraints and process stabilization should be considered when selecting CVs, and MVs should have favorable static and dynamic qualities. One MV can be designated as the throughput manipulator (TPM), that is, the DOF used to regulate the throughput in the primary process path, from the feed streams to the products.[38,39] The TPM sets the overall production rate, and inventory control should radiate outward from the TPM.

A central question of plantwide control and ICPD is the selection of criteria for describing desirable system behavior.[7] One such criterion is controllability, that is, the ability of the process to achieve and maintain a desired equilibrium. Controllability can be defined in various ways,[10,40,41] such as integral controllability with integrity (ICI).[15,16] A system is ICI controllable if it remains stable, when control loops with integral action are arbitrarily opened and closed or when all loop gains are detuned by the same factor (0–1). Decentralized integral controllability (DIC) is similar to the ICI, but it also demands that the loop gains can be detuned by individual factors.

3.2. Relative Gain Analysis. Relative gain analysis can be used for examining loop interactions, controllability, robustness, and open-loop stability[10] in the OTU-CFB flowsheet. All relative gain methods are variations of the basic relative gain array (RGA).[12] RGA modifications include the performance-RGA (control performance and one-way coupling),[10] the block relative gain (connections between blocks of MVs and CVs),[16,25] the effective RGA (combines RGA with bandwidth or crossover frequencies),[42] and the partial relative gain (PRG),[14] which is discussed in section 3.2.2.

3.2.1. RGA and DRGA. The RGA is calculated with eq 2 from the open-loop steady-state process gain matrix **G**.

$$RGA(\mathbf{G}) = \mathbf{G} \times (\mathbf{G}^{-1})^T = \begin{bmatrix} \lambda_{11} & \cdots & \lambda_{1n} \\ \vdots & \ddots & \vdots \\ \lambda_{m1} & \cdots & \lambda_{mn} \end{bmatrix} \qquad (2)$$

where **G** is the gain matrix, λ_{mn} are relative gains, and "$\times$" is element-by-element multiplication.

Equation 2 applies to square matrices with an equal amount of MVs and CVs, but it has also been modified for nonsquare ones.[43] The RGA contains interaction terms for all single input–single output (SISO) pairings in the system, it is scaling invariant and forms row/column sums of ones. An RGA element signifies the ratio of the open-loop gain for a variable

pairing when all other control loops are open ($g_{OL,OL}$) to the gain when the other loops are closed ($g_{OL,CL}$), eq 3.

$$\lambda_{mn} = \frac{g_{OL,OL}}{g_{OL,CL}} = \frac{(\partial y_m / \partial u_n)_{OL,OL}}{(\partial y_m / \partial u_n)_{OL,CL}} \tag{3}$$

where g is a gain, y is an output, u is an input, n are input indices, and m are output indices.

The RGA can be used for selecting control MV−CV pairings so that interacting effects from other loops on $g_{OL,OL}$ are small. Thus, pairings with λ_{mn} close to 1 are good, and negative λ_{mn} are to be avoided due to instability caused by gain sign change. However, $\lambda_{mn} = 0$ is not conclusive in itself.[14] Small positive λ_{mn} values, usually below 0.5 or even 0.67, are poor (gain increase when closing loops).[9,44] For λ_{mn} larger than 1, interactions dampen the open-loop gain, which requires attention during control (gain increase when opening loops). Very large λ_{mn} values, commonly above 10, require large controller gains and may signify an ill-conditioned system.[44−46]

The dynamic RGA (DRGA), eq 4, extends the (zero frequency) RGA by applying eq 2 to the MV−CV frequency response matrix,[10,11,13] for example, eq 5.[47] The complex DRGA elements are commonly presented as absolute values. Frequency domain investigations are important, as different frequencies might result in different preferred control variable pairings.[42,48]

$$\begin{aligned} \text{DRGA}(\mathbf{H}(j\omega)) &= \mathbf{H}(j\omega) \times (\mathbf{H}(j\omega)^{-1})^T \\ &= \begin{bmatrix} a_{\lambda 11} + b_{\lambda 11}j & \cdots & a_{\lambda 1n} + b_{\lambda 1n}j \\ \vdots & \ddots & \vdots \\ a_{\lambda m1} + b_{\lambda m1}j & \cdots & b_{\lambda mn} + b_{\lambda mn}j \end{bmatrix} \end{aligned} \tag{4}$$

$$\mathbf{H}(j\omega) = \mathbf{D} + \mathbf{C}(j\omega\mathbf{I} - \mathbf{A})^{-1}\mathbf{B} \tag{5}$$

where $\mathbf{H}(j\omega)$ is the frequency response at frequencies ω (rad/s), a and b are the real and complex terms of the DRGA elements λ_{mn}, and $\mathbf{A}$, $\mathbf{B}$, $\mathbf{C}$, and $\mathbf{D}$ are matrices in a standard state space format.

Control solution ranking can be simplified by using the RGA number,[10] which can also be applied to the DRGA, i.e. nDRGA in eq 6. In the nDRGA, the DRGA with chosen MV−CV pairs on the diagonal is compared to the identity matrix $\mathbf{I}$. As such, a small nDRGA is preferable.

$$\text{nDRGA}(\mathbf{H}(j\omega)) = \| \text{DRGA}(\mathbf{H}(j\omega)) - \mathbf{I} \|_N \tag{6}$$

where "N" is a norm, usually an absolute sum. In this work, "N" is the sum of diagonal elements.

The RGA is often used together with the Niederlinski index (NI), eq 7. The NI denotes the stability of variable pairings: a NI value below zero indicates an unstable system.[14,16] If the MV− CV pairings are located on the diagonal of $\mathbf{G}$, the denominator in eq 7 is simplified to $\prod_i g_{ii}$.

$$\text{NI} = \det(\mathbf{G}) / \det(\hat{\mathbf{G}}) \tag{7}$$

where $\hat{\mathbf{G}}$ is the matrix obtained by setting to zero all elements of gain matrix $\mathbf{G}$ that do not correspond to an input−output pairing in a given block-decentralized control structure.

3.2.2. Partial Relative Gain. A downside of the RGA is that it might be misleading for large MV−CV systems because of RGA element changes during partial control. In partially controlled systems, only certain outputs with objectives are controlled, for example, when control systems are designed hierarchically or when some outputs are only controlled indirectly.[10]

This can be remedied with the partial relative gain (PRG),[14] which is why it was chosen for the large OTU-CFB system matrices of this work.

The PRG of a partially controlled subsystem, eq 8, is calculated by applying eq 2 to the subsystem gain matrix $\bar{\mathbf{G}}_{mn}$. Gains $\bar{\mathbf{G}}_{mn}$ can be obtained with eq 9. When CV−MV pairings "c" are closed and perfect integral control is assumed, outputs y_c can be controlled to zero.

$$\text{PRG}_{mn}(\mathbf{G}) = \text{RGA}(\bar{\mathbf{G}}_{mn}) = \bar{\mathbf{G}}_{mn} \times (\bar{\mathbf{G}}_{mn}^{-1})^T \tag{8}$$

$$\bar{\mathbf{G}}_{mn} = \mathbf{G}(y_o, u_o) - \mathbf{G}(y_o, u_c) \cdot \mathbf{G}(y_c, u_c)^{-1} \cdot \mathbf{G}(y_c, u_o) \tag{9}$$

where PRG_{mn} is the subsystem PRG, $\bar{\mathbf{G}}_{mn}$ is the modified subsystem gain matrix with loops $y_c - u_c$ closed under integral control, and "o" denotes open loops (CV and MV indices "m" and "n").

The PRG is useful as a condition for ICI controllability.[14] A system $\mathbf{G}$ (size $k \times k$, MV−CV pairs on the diagonal) is ICI if and only if all diagonal RGA elements and the diagonal PRG elements of all partially controlled subsystems ($l \times l$, $l = 2, 3,..., k − 1$) are positive. If NI is also positive, 2×2 subsystems need not be checked. ICI controllability is a useful property for multiloop control, as it enables individual controller tuning without introducing instability in the plantwide system.

4. OTU-CFB RELATIVE GAIN ANALYSIS TEST SETUP

This section sets up the PRG and the DRGA analysis for an industrial OTU-CFB condensing power plant in the range of several hundred MW$_e$ (Figure 4). The ICI controllability criterion is specifically tested to determine, whether it offers any advantage for the OTU-CFB. The target of the design is to form feasible control structures between the main process inputs and outputs.

4.1. Model. The investigated large scale OTU-CFB uses a supercritical Benson cycle consisting of an economizer preheater, evaporator water-walls, a four-stage superheating block, three DSH sprays and a reheater. The CFB has a standard hotloop configuration and includes Intrex solid material heat exchangers. The boiler utilizes one coal fuel fraction. Since the focus of the investigation is on the product steam, the condenser is not included in the study.

The power plant was simulated with an extensively validated dynamic model of Sumitomo SHI FW.[29] The simulator is implemented in APROS[49] and consists of standard process unit submodels that are arranged to form the boiler flowsheet. Flowsheet and component dimensions, boundary conditions, and model state values are obtained from steady-state in-house design data.

The thermal hydraulics modeling considers the conservation of mass, momentum, and energy for the supercritical water-steam phase.[50] Heat transfer and wall friction correlations are selected based on wall temperature, saturation temperature, critical heat flux, and minimum film boiling temperature. The solution is based on a staggered grid discretization, where mass and energy equations are solved in the middle of the mesh and momentum equations at the control volume borders. Process units contain control volumes for inlet, outlet, and relevant bulk regions.

The CFB hotloop is modeled using a 1-D Matlab/Simulink CFB block, and this submodel is interfaced with the steam and flue gas path model in APROS. The model utilizes both physical first-principles modeling and empirical correlations.[4,33] The furnace, separator, and Intrex heat exchanger are modeled as units with ideally mixed calculation elements.

4.2. Process Inputs and Outputs. The APROS model was used for the OTU-CFB relative gain analysis. The control degrees
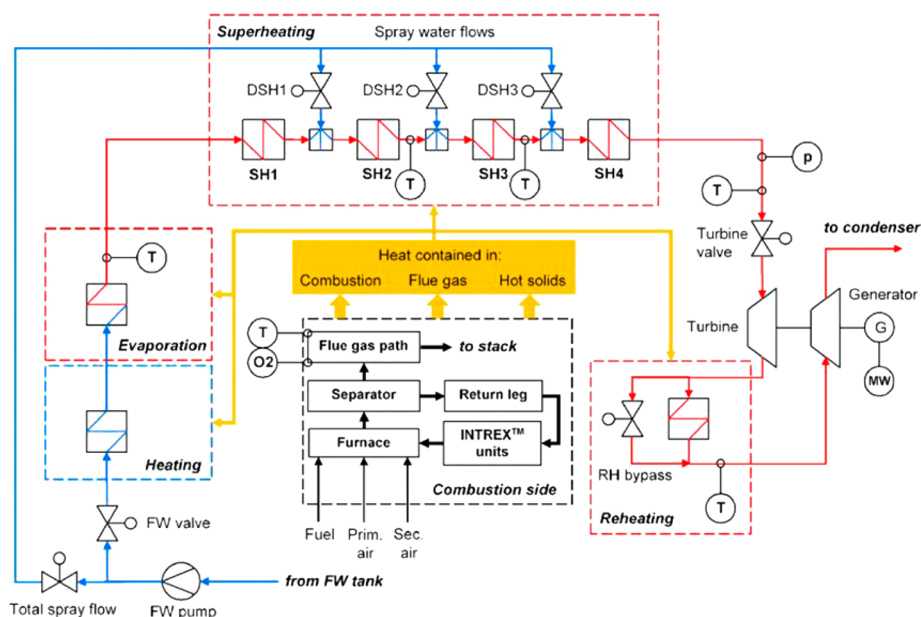
Figure 4. Flowsheet of the OTU-CFB boiler. Feedwater (FW) is marked in blue, steam flows in red, heat transfer in yellow. SH = superheater, DSH = desuperheater, RH = reheater.

of freedom (CDOF) were determined, and open-loop step tests were conducted. Step response data for selected CVs was used to form steady-state gain matrix and transfer function models.

4.2.1. Degrees of Freedom and TPM Considerations. The CFB combustion side (Figure 4) contains five adjustable flows: the fuel, the primary air, the secondary air, the solid material circulation rate, and the flue gas flow. The flue gas flow and circulation rate MVs are limited by furnace pressure and bed inventory safety constraints. The inputs to the steam channel are the feedwater flow to the evaporator and the total DSH flow, which both come from the feedwater line. The steam flow can be adjusted with the feedwater or the turbine valve. The total spray water is split between the three DSH nozzles. A further control possibility is to regulate the steam flow in the reheater, using a bypass with a control valve.

The CDOF is calculated with eq 1 by analyzing each process unit and combining the results into the total CDOF. Considering safety constraints, 42 mass/energy streams can be counted in total, 29 in the steam path, and 13 on the combustion/flue gas side. On the basis of the amount of mass balances without inventories, the steam side has 18 restrained streams (valves, turbines, mixers, feedwater pump, preheater) and the combustion side has 5 (heat exchangers). Pressure control results in redundancy in the steam path and the flue gas duct, and the system heat exchangers thus contain 10 redundant streams. This results in a CDOF of $(29 + 13) - (18 + 5) - 10 = 9$. The independent inputs of the boiler can be selected for example, according to Table 1.

The electrical power at the turbine depends both on the steam flow and the energy content of the steam. The overall MW_e control target thus translates into a steady-state set point for the heat generation through combustion. Three process inputs can be used to adjust the MW_e output, and one of these MVs is available as the boiler throughput manipulator.

- turbine valve: steam volume flow change, transient mass flow change.
- feedwater flow: steam mass flow change, change in energy content (constant fuel firing).

Table 1. Independent MVs of the OTU-CFB Boiler[a]

variable (steam side)	abbreviation	variable (combustion side)	abbreviation
feedwater flow to evaporator	FW	fuel flow to furnace	Fuel
turbine valve position	T.valve	secondary air to furnace	Sec air
desuperheater 1 spray flow	DSH1	primary air to furnace	Prim air
desuperheater 2 spray flow	DSH2		
desuperheater 3 spray flow	DSH3		
reheater bypass valve position	RHvalve		

[a]The primary air flow can basically be treated as a CDOF, although it is also partly bounded by the need to maintain the fluidization.

- fuel and air flows: steam energy content change, no mass flow change (constant FW flow).

In boiler-following control, the TPM is located at the product stream, as the valve can alter the MW_e output quickly. In turbine-following control, the MW_e is modified by the steam generation, that is, the TPM is at the process feed. Steam generation is altered slowly with the fuel firing power, but in theory, the feedwater flow could also be used. No CDOF was specifically designated as the TPM in this work, as the analysis was not limited to any predetermined unit master setup. The OTU cycle also does not directly translate into a traditional inventory control problem.

Twelve MVs were selected for the study, consisting of all MVs from Table 1 and three "combined" MVs (several inputs altered with the same percentage): "total DSH flow" (DSH1, DSH2, and DSH3), "firing power" (fuel and air) and "boiler load" (fuel, air, and feedwater). CVs were selected based on control goals and constraints: main steam pressure and temperature, steam temperature after the evaporator, steam temperatures after superheaters 2−3, steam temperature after the reheater, flue gas (FG) O_2 percentage and temperature, and total output MW_e.

4.2.2. Test Setup and RGA Modeling. On the basis of the CDOF, four square system case studies were constructed to

Table 2. Case Studies 1−4, MV−CV Groups That Are Considered for the OTU-CFB Analysis

var.	inputs	outputs	var.	inputs	outputs
	Case 1			Case 2	
1	T.valve	steam pressure	1	T.valve	steam pressure
2	total DSH	steam temp	2	DSH1 flow	steam temp
3	boiler load	total MW$_e$	3	DSH2 flow	temp SH2
			4	DSH3 flow	temp SH3
			5	boiler load	total MW$_e$
	Case 3			Case 4	
1	T.valve	steam pressure	1	T.valve	steam pressure
2	FW flow	steam temp	2	FW flow	steam temp
3	fuel flow	evap. temp	3	Sec air flow	evap. temp
4	Prim air flow	flue gas O$_2$	4	DSH1 flow	flue gas O$_2$
5	Sec air flow	flue gas temp	5	DSH2 flow	temp SH2
6	total DSH	total MW$_e$	6	DSH3 flow	temp SH3
			7	RHvalve	RH temp
			8	firing power	total MW$_e$

highlight different control tasks in the boiler. The MVs and CVs of these cases 1−4 are shown in Table 2.

Case 1 focuses on the main steam parameters and the MW$_e$ output, that is, the unit master control setup. Case 2 expands on the main steam temperature control task by also considering intermediate SH temperatures together with the unit master control. Case 3 centers on steam generation and combustion control by separating the "boiler load" MV into its individual flows. Case 4 combines all cases into a full plantwide boiler controllability and interaction analysis.

The power plant model was simulated for cases 1−4 in the open-loop around a 95% load level operating point. Stepwise ±5−10% changes were made to the chosen process inputs one at a time, with other inputs remaining constant. The open-loop gain matrix **G** (Table S1) between the MVs and CVs of the OTU-CFB could be determined from the settled output variable responses.

To outline ICI control structures with the PRG method, all possible MV−CV structures for a particular case were first analyzed with the steady-state RGA, Equation 2, and structures with negative RGA elements were discarded. The remaining solutions were screened by excluding candidates with negative NI values, eq 7. All possible PRG matrices were then calculated by closing loops down to 2 × 2 subsystems, eq 9, and applying eq 8. Structures with negative PRG elements were discarded. The remaining structures represented the ICI solutions, which were ranked based on their PRG elements (λ) in a similar way to the RGA (c.f. section 3.2.1):

$0 < \lambda \leq 0.1$	Bad: poor robustness and controllability, risk of singularity/negative PRG.
$0.1 < \lambda \leq 0.5$	Problematic: control issues, uncertainty with nonlinear PRG scale.
$0.5 < \lambda \leq 0.85$	Neutral: attention required during design, loops close → gains increase.
$0.85 < \lambda \leq 1.2$	Good: preferable, close to ideal PRG value with few interactions.
$1.2 < \lambda \leq 5$	Neutral: attention required during control, loops open → gains increase.
$5 < \lambda \leq 10$	Problematic: control issues, but not excessively large PRG.
$\lambda > 10$	Bad: poor performance with ill-conditioning or similar MV effects.

The steady-state PRG results were extended for multiple frequencies with the DRGA. The step test time series data was used to identify SISO transfer functions for all MV−CV pairs, using "tfest" in Matlab (least-squares minimization of weighted quadratic error, instrumental variable initialization). In most cases, second order models with delay were sufficient to capture the MV−CV dynamics (e.g., Figure 5). The frequency
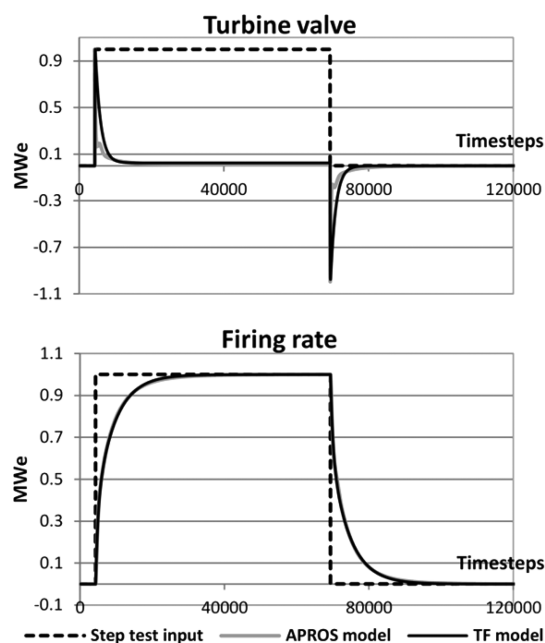
Figure 5. APROS simulator and 2nd order transfer function (TF) MW$_e$ outputs (normalized) as a function of time for a positive and negative step test in the turbine valve and firing rate inputs.

responses of cases 1−4 were obtained using the transfer functions and eq 5 ("freqresp" in Matlab). The DRGA was then calculated for each frequency, eq 4. The focus was on both ICI and non-ICI structures in the 0−0.5 rad/s frequency range (e.g., Garrido et al.[24]), considering common boiler disturbance speeds (e.g., ≈ 3 s/MW$_e$ load ramps).

In total, the OTU-CFB control structure selection procedure can be summarized as follows:

1. Select MVs and CVs, determine all possible MV−CV control structure candidates.
2. Make MV step tests, obtain process gain matrix **G** and MV−CV transfer functions.
3. Calculate RGA from **G** → discard structures with negative RGA elements.
4. Calculate NI index from **G** → discard structures with negative NI values.
5. Determine gain matrices $\overline{\mathbf{G}}_{mn}$ for all possible partially controlled subsystems.
6. Calculate PRG matrices for all partially controlled subsystems → Discard structures that have negative PRG elements in at least one subsystem.
7. Rank resulting ICI controllable structures based on their PRG element distribution (amounts of good and poor PRG elements in all partially controlled subsystems).
8. Calculate DRGA in desired ω range from transfer function frequency responses $\mathbf{H}(j\omega)$.
9. Rank preferred plantwide structures based on nDRGA at each frequency, compare to PRG.

5. OTU-CFB CONTROL STRUCTURE SELECTION

The outcomes of the relative gain analysis are explored here, the steady-state ICI PRG results in subsection 5.1 and the frequency domain DRGA results in subsection 5.2. The focus is on the conclusiveness of the steady-state analysis and the ICI criterion compared to the DRGA results.

5.1. Steady-State Analysis. All ICI control structures from the PRG analysis are displayed for cases 1−4 in sections 5.1.1−5.1.4. The RGA is also shown separately for case 1, while the RGAs of cases 2−4 are provided in the Supporting Information. Structures are annotated as vectors [a b c ...], where "a, b, c, ..." are the MV indices for controlling the respective CVs (Table 2), that is, the position in the vector is the CV and the number in that position is the MV. The structures with the largest amount of good (0.85−1.2) and smallest amount of poor PRG elements (<0.1 and >10) are ranked as the best.

5.1.1. Case 1: Main Control Loops. Case 1 examines the unit master control setup between the steam pressure and output MW_e, and how the loops interact with steam temperature control. In this 3 × 3 system, MVs and CVs can be paired into six possible control structures. Two MV−CV connections have negative RGA elements (Table 3), and three

Table 3. Steady-State RGA Matrix of the Case 1 System, 3 Input MVs and 3 Output CVs

RGA	MV →	T.valve	Tot DSH	Boiler load
CV ↓	INDEX	1	2	3
steam p	1	0.993	0.007	−0.0004
steam T	2	0.004	0.995	0.002
total MW_e	3	0.003	−0.002	0.999

structures thus remain: [1 2 3], [2 3 1], [2 1 3]. Notably, one of the negative RGA elements is "boiler load−steam pressure" (boiler-following control).

Control structures [1 2 3], [2 3 1], and [2 1 3] all have three partially controlled 2 × 2 subsystems [**1 2 3**] → [((1)) 2 3], [1 ((2)) 3], [1 2 ((3))]; [**2 3 1**]→ [((2)) 3 1], [2 ((3)) 1], [2 3 ((1))]; [**2 1 3**] → [((2)) 1 3], [2 ((1)) 3], [2 1 ((3))], closed loop marked with "(())". Each structure thus has six PRG elements from the remaining MV−CV connections (Table 4).

The three structures all have positive NI values, which directly make them ICI controllable (section 3.2.2). The ICI criterion thus provides no extra screening of structures compared to the RGA. The smallest degree of loop interactions (all PRG elements close to 1) is obtained with structure I, where the steam pressure is controlled with the turbine valve, the temperature is controlled with the spray water, and the generated MW_e is controlled with the boiler load. In the ICI structures ranked second and third, the pressure is controlled with the DSH flow, which is infeasible in practice. This is also

visible as poor RGA and NI values. Structure III is clearly the worst in terms of the PRG.

Structure I represents basic turbine-following control. On the basis of the ICI criterion, this setup thus enables individual control loop tuning. This is understandable, as the output MW_e is ultimately determined by the generated heat, and the steam pressure can be directly adjusted with the turbine valve. In the basic boiler-following structure [3 2 1], the negative "boiler load−steam pressure" RGA element makes ICI controllability impossible. However, when this loop is closed to form a partially controlled system, the remaining control connections [((3)) 2 1] have excellent PRGs, meaning that this MV−CV connection is responsible for the poor controllability.

5.1.2. Case 2: Spray Water Flows. Superheater stage temperature control is considered by dividing the total DSH flow into its individual components DSH1, DSH2, and DSH3; 120 possible control connections exist for this 5 × 5 system. Only seven structures have positive RGA elements (Table S2), and one of these has a negative NI index. Three structures are ICI controllable based on the PRG (Table 5).

In structure I, the turbine valve is used for the steam pressure and each SH temperature is controlled with the preceding spray (DSH3 for main steam). The PRG distribution of structure I is clearly superior compared to structures II and III. The nine larger elements in structure I are all smaller than 1.9 and are generated in those subsystems, where the steam pressure and output MW_e loops are closed. In general, for all control structures the closing of these loops results in larger PRGs for the spray flow MVs. This points toward the similar effects of DSH1, DSH2, and DSH3 on the remaining process CVs, that is, the steam temperatures in the superheater line.

Structures II and III suggest that DSH1 should be used for steam pressure control and the turbine valve for the respective superheater temperature. A similar switch is suggested in structure III for DSH3 and the boiler load. These structures are impractical, and coincidentally these connections are also responsible for the poor PRG distributions of structures II and III.

5.1.3. Case 3: Combustion/Flue Gas Side. Analysis on the steam generation is provided by examining the fuel, primary/secondary air, and feedwater flows separately: 720 control structures can be generated in the resulting 6 × 6 system. Out of these, 28 have positive RGA elements (Table S3) and 19 have positive NI values.

Two ICI structures are obtained through the PRG analysis (Table 6). Both solutions are feasible in practice, but structure I is clearly superior in terms of its PRG distribution. Structure I corresponds to existing control practices: the fuel determines the heat generation, the feedwater has a direct effect on the evaporator, the secondary air is used for flue gas O_2 trim, and the primary oxidant has the largest cooling effect in the furnace. Structure II has a similar setup, but the roles of the feedwater and fuel MVs are reversed. The results thus highlight the

Table 4. Case 1 ICI Control Structures, Ranked by Their PRG distributions: Total Average (avg) PRG, Amounts of PRG Elements Belonging to Different Ranges, and NI Index

			no. of PRG elements in range							
rank	structure	NI	0−0.1	0.1−0.5	0.5−0.85	0.85−1.2	1.2−5	5−10	>10	avg. PRG
1	I: [1 2 3]	1.0089	0	0	0	6	0	0	0	1.00
2	II: [2 3 1]	82600	0	0	2	2	2	0	0	1.23
3	III: [2 1 3]	136	2	2	0	2	0	0	0	0.50

Table 5. Case 2 ICI Control Structures, Ranked by Their PRG Distributions: Total Average (avg) PRG, Amounts of PRG Elements Belonging to Different Ranges, and NI Index

rank	structure	NI	no. of PRG elements in range							avg. PRG
			0−0.1	0.1−0.5	0.5−0.85	0.85−1.2	1.2−5	5−10	>10	
1	I: [1 4 2 3 5]	0.340	0	0	0	61	9	0	0	1.11
2	II: [2 4 1 3 5]	18.7	14	3	12	33	8	0	0	0.77
3	III: [2 5 1 3 4]	11300	29	5	6	20	6	4	0	0.97

Table 6. Case 3 ICI Control Structures, Ranked by Their PRG Distributions: Total Average (avg) PRG, Amounts of PRG Elements Belonging to Different Ranges, and NI Index

rank	structure	NI	no. of PRG elements in range							avg. PRG
			0−0.1	0.1−0.5	0.5−0.85	0.85−1.2	1.2−5	5−10	>10	
1	I: [1 6 2 5 4 3]	0.231	0	0	1	117	62	0	0	1.33
2	II: [1 6 3 5 4 2]	1.60	30	26	21	65	38	0	0	0.95
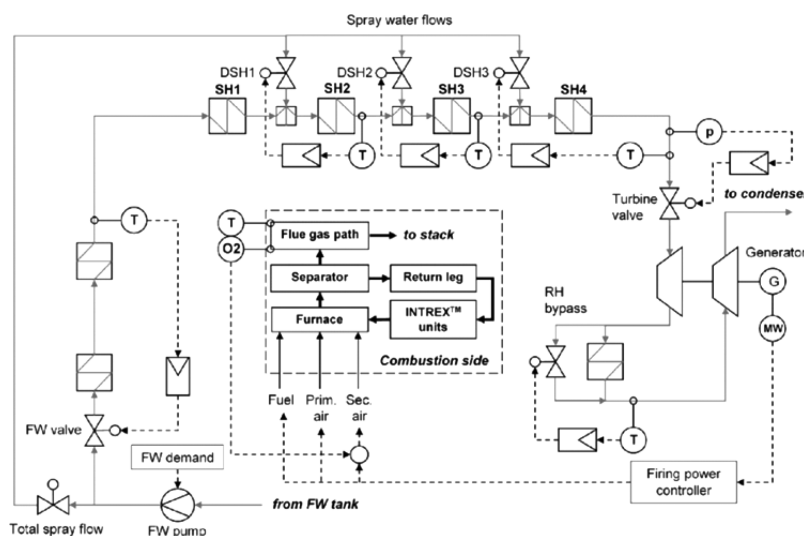
Figure 6. Conceptual plantwide control solution for the best ICI structure I of the PRG analysis. Dashed lines are control signals, exact controller or connection types are not considered.

Table 7. Case 4 ICI Control Structures, Ranked by Their PRG Distributions: Total Average (avg) PRG, Amounts of PRG Elements Belonging to Different Ranges, and NI Index

rank	structure	NI	no. of PRG elements in range							avg. PRG
			0−0.1	0.1−0.5	0.5−0.85	0.85−1.2	1.2−5	5−10	>10	
1	I: [1 6 2 3 4 5 7 8]	0.321	0	4	7	919	76	2	0	1.12
2	II: [1 6 7 3 4 5 2 8]	0.358	117	47	116	643	85	0	0	0.87
3	III: [1 6 8 3 4 5 7 2]	2.32	122	60	99	632	95	0	0	0.88

connection between the fuel and the feedwater as the main components for steam formation.

There are some larger PRG elements in structure I (>2, but not ill-conditioned), mostly related to the primary and secondary air flow control loops. The similar effects of the air flows on the flue gas O_2 and temperature CVs can thus be inferred from the analysis. Almost all of the 30 small (<0.1) PRG elements of structure II are related to the feedwater and fuel MV connections. The PRG thus highlights a preference between the two feasible ICI control structures: using the feedwater for MW_e control results in reduced controllability compared to the reverse solution.

5.1.4. Case 4: Overall OTU-CFB Control Structure. Case 4 examines the 8 × 8 plantwide problem. The primary air is assumed to be fixed to ensure fluidization; 40320 control

structures exist between the MVs and CVs; 180 structures have no negative RGA elements (Table S4); and 94 solutions are left after the NI screening. The PRG analysis only produces three ICI structures and suggests that structure I (Figure 6) is clearly preferable, as it has a significant amount of excellent PRG values (Table 7). The two inferior structures II and III both have a large number of small PRG elements (over 100 elements below 0.1) that are mainly caused by pairings that are different from structure I. For each structure, 1008 PRG elements in 738 partially controlled systems were examined.

Structures I−III all contain some large PRG elements (>2) which are always observed for the DSH and feedwater flow control connections. This observation is similar to that in case 2, and the PRG thus suggests potential control performance issues caused by the similar effects of the DSH and feedwater flows on

superheater stage temperatures. The small PRG elements of the ICI structures (<0.5 for I and <0.1 for II and III) also show a surprising connection between feedwater flow and reheater control. The explanation might be that the chosen MV is the reheater bypass valve position, meaning that the bypass steam flow is also affected by feedwater flow changes.

The highest ranked plantwide structure I (Figure 6) corresponds to design experience for turbine-following control, meaning that the existing control practices can be validated as ICI, and controllers can be tuned individually without instability within this structure. This can be verified through simulations (Figure 7) by tuning each of the controllers of
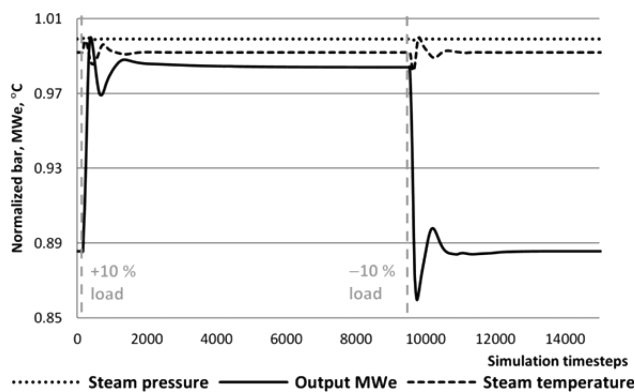
Figure 7. PID controlled constant pressure load step simulations with the original APROS boiler model (normalized), utilizing ICI control scheme I from Table 7 and Figure 6.

Figure 6 separately with all other control loops open, and then closing all loops to form the plantwide control system. On the basis of the simulations, the plantwide system remains stable as long as the individual loops are stable.

All in all, case 4 demonstrates that the PRG analysis can be used to synthesize ICI control structures for the full OTU-CFB flowsheet. The PRG provides a much more effective screening of control alternatives (3 solutions) in the large 8×8 system compared to the open-loop RGA (180 solutions), although the RGA suggests the same primary solution as the PRG. The RGA is more flexible than the PRG for enabling "unorthodox" control structures, but many of these would also be infeasible in practice (e.g., flue gas temperature control with steam side sprays).

5.2. Dynamic Analysis. All of the plantwide control structures that were suggested by the ICI analysis have a turbine-following unit master setup. Boiler-following MW_e control is enabled by the RGA and the NI in the 8×8 system (e.g., structure [2 6 8 3 4 5 7 1]), but not with the "firing power—steam pressure" control connection due to its negative RGA element. Adjusting the MW_e with the turbine valve is advantageous in real life for fast load transients, as having the TPM close to the product is better for control (cf. section 4.2.1). Transient speeds of the main MVs are listed in Table S5.

The unit master control findings from the ICI analysis can be explained by the small turbine valve static gain on the output MW_e (Figure 5), and by the conclusion that the boiler-following control loops are not independent in the ICI sense (no integrity). A change in the MW_e set point without compensating the firing power would require the valve position to change constantly, which would similarly decrease the

steam pressure. This interaction becomes apparent when the boiler-following control structure [8 6 2 3 4 5 7 1] is analyzed further with the PRG. While the open-loop process has 143 PRGs below 0, closing the "firing power—steam pressure" loop (negative RGA) yields a subsystem that would fulfill all necessary ICI criteria (positive RGA, NI, and PRGs), even with a good PRG distribution. Therefore, as long as steam pressure control remains active, controllability could also be obtained for the boiler-following setup.

Hence, the ICI PRG analysis provides incomplete information about preferred OTU-CFB plantwide control structures. The process dynamic behavior also needs to be considered, as new loop interactions might be revealed, and MVs might have large transient effects compared to their steady-state gains. This is the motivation for the frequency-dependent DRGA investigations in sections 5.2.1–5.2.4. For simplicity, results are shown as DRGA numbers, nDRGA in eq 6.

5.2.1. Case 1: Main Control Loops. The DRGA numbers of ICI structures I–III (Table 4) and the basic boiler-following structure IV are shown in Figure 8. The turbine-following ICI structure I with the highest PRG element ranking also has the lowest nDRGA values for the whole frequency region. On the basis of the results, the DRGA validates the ICI structure I as the best option for the 3×3 system.

Boiler-following structure IV with its one negative RGA element at zero frequency has a lower nDRGA in the entire frequency region (excluding zero) than both of the ICI structures II and III. The degree of loop interactions also increases for the turbine-following structure I at higher frequencies, mainly due to the slowness of the "firing power—MW_e" control. The controllability of boiler-following structure IV similarly improves above zero, but its nDRGA starts to increase again above 0.15 rad/s because of the "turbine valve—steam pressure" DRGA, as the valve has an immediate effect on the steam pressure. Clearly the increased MW_e control performance of structure IV is overshadowed by the increased loop decoupling of structure I.

5.2.2. Case 2: Spray Water Flows. The DRGA (Figure 9) mostly suggests the same structure as the ICI analysis (Table 5). Structure I has the lowest DRGA number for almost the entire frequency range except for 0.05–0.1 rad/s, where boiler-following structure IV is momentarily preferred. In general, structure IV has the second lowest nDRGA at most frequencies, but it is infeasible at zero frequency.

The dynamic analysis thus does not emphasize boiler-following control, most likely since the "boiler load" MV includes both the fuel+air and feedwater flows. While the fuel and air affect the MW_e and steam pressure slowly, the feedwater alters the steam flow quickly (Table S5). This makes basic turbine-following control feasible even at higher frequencies.

On the basis of the individual DRGA elements, the temperatures at the turbine and after SH2 are clearly the best CV selections for DSH3 and DSH1. The preferred connection is less clear for DSH2 due to significant loop interactions. Interestingly, all structures show increased nDRGAs between 0.05–0.1 rad/s, which could indicate a problematic region for temperature disturbances.

5.2.3. Case 3: Combustion/Flue Gas Side. Several control structures beside ICI structures I–II (Table 6) can be considered in practice. The fuel, feedwater, air flow, and turbine valve MVs can, in principle, be used for controlling the steam pressure. Similarly, the evaporator temperature can be adjusted with the feedwater, air, or fuel flows. Either the fuel or the
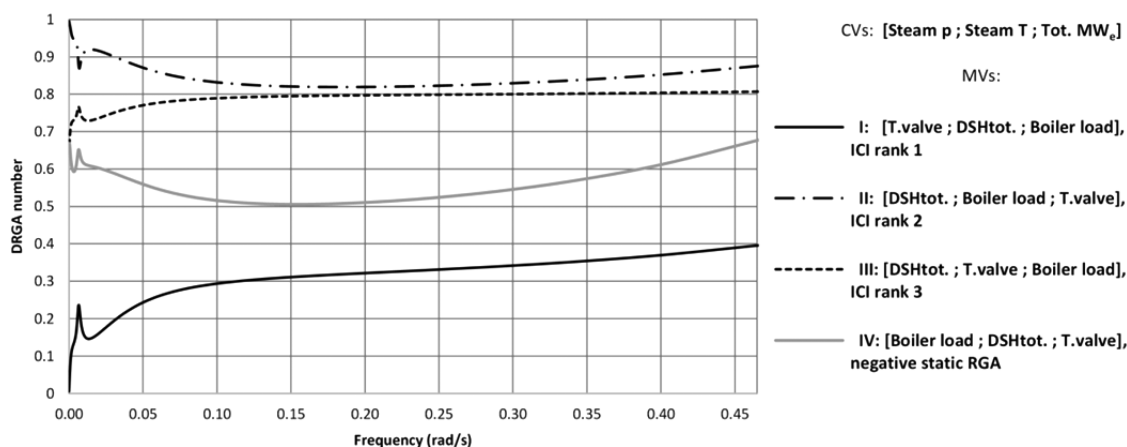
Figure 8. DRGA numbers as a function of frequency for case 1 control CV−MV connections: ICI structures I−III and boiler-following structure IV with negative zero frequency RGA.
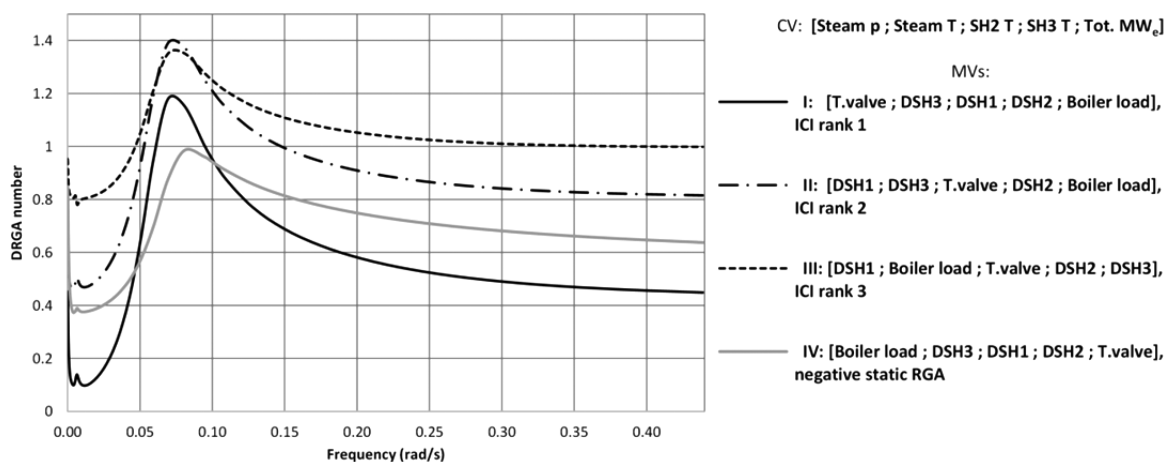
Figure 9. DRGA numbers as a function of frequency for case 2 control CV−MV connections: ICI structures I−III and boiler-following structure IV with negative zero frequency RGA.
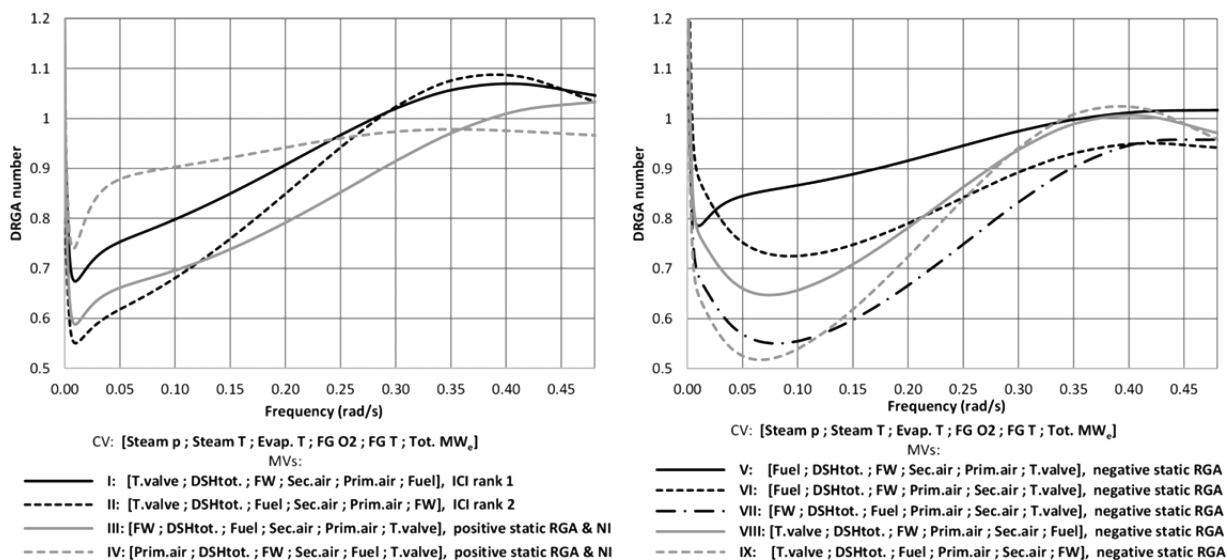
Figure 10. DRGA numbers as a function of frequency for case 3 control CV−MV connections: ICI structures I−II, structures III−IV with positive zero frequency RGA and NI, as well as boiler-following V−VII and turbine-following VIII−IX structures (negative zero frequency RGA).

primary air could be feasible for flue gas temperature control. Because of this, relevant non-ICI structures III−IX were included in the analysis (Figure 10).

Unlike the previous cases, there is a clear difference between the case 3 DRGA and ICI PRG results. ICI structure II immediately becomes better than the best ICI structure I beyond

zero frequency, and turbine-following structure IX has the lowest nDRGA between 0.02−0.12 rad/s. Above this range, boiler-following control (VI and VII) is preferable. These transitions between control structures take place because higher frequency disturbances favor connections that result in increased decoupling between the evaporator, the steam flow, and the turbine (Table 8). However, additional experiments

Table 8. Control Structures with the Lowest DRGA Numbers at Each Frequency Range in Case 3

freq (rad/s)	best structure	unit master setup	control structure change to decrease loop interactions
0−0.01	I	turbine-follow	ICI structure with independent loop tuning
0.01−0.02	II	turbine-follow	turbine−evaporator decoupling improved with "feedwater− MW_e" and "fuel−evaporator T" connections
0.02−0.12	IX	turbine-follow	primary and secondary air connections switched
0.12−0.4	VII	boiler-follow	boiler-follow control, MW_e controlled with feedwater
0.4−0.5	VI	boiler-follow	steam pressure and MW_e decoupling increased with "fuel− steam pressure", "feedwater−evaporator T" connections

also showed that the turbine-following setup IX became preferable again between 0.5−1 rad/s. For such fast disturbances, controlling the steam pressure with the MV that has the shortest settling time (Table S5) might indeed be preferable.

A second observation is that the best control structures mostly apply a reversed oxidant control setup than what is used by ICI structures I and II, that is, the flue gas O_2 is controlled with the primary air and the flue gas temperature with the secondary air. This control structure change is interesting, especially when considering the negative values of these elements in Table S3.

5.2.4. Case 4: Plantwide Boiler Control. The control structures with the best DRGA numbers are given in Figure 11, including ICI structures I−III (Table 7) and relevant non-ICI structures IV−VI. Again, the best ICI structure I only has the lowest nDRGA at zero frequency. Above that, other structures are preferred.

Below 0.2 rad/s the lowest nDRGA is obtained with turbine-following ICI structure III, in which the feedwater is used for MW_e control and the firing power for the evaporator temperature. The boiler-following structure IV (steam pressure−feedwater control) also generates good nDRGA values. The basic boiler-following structure VI is clearly superior above 0.2 rad/s, and structure V also has low nDRGA values in this region. In V, the evaporator temperature is adjusted with DSH3 (infeasible), mainly due to the effect of the spray on the hotloop superheaters (Table S1).

The individual DRGA elements of the 8 × 8 system (Figure 12) show that DSH1 (d), DSH3 (f), and the reheater bypass valve (g) all have clear loop pairings (elements close to 1), as does the secondary air (c) below 0.25 rad/s. Inputs a, b, e, and h are more complex. The firing power (h) is mainly connected to the evaporation and combustion (flue gas O_2). Although the steam pressure was always selected as the CV for the turbine valve (a) by the steady-state ICI criterion, at 0.2−0.35 rad/s the valve is more suitable for MW_e control. The output MW_e is a good pairing for the feedwater (b), as is the steam pressure (low frequencies) and temperature (high frequencies). As in case 2, selecting a control pairing for DSH2 (e) is clearly challenging.

To conclude, no structure can be selected as superior in the entire frequency range based on the DRGA alone. An "optimal" solution would be a combination of turbine-following control for slow disturbances and boiler-following control for faster ones. These results can be verified through closed-loop simulations (PID control) for the "best" structures III and VI (Figure 13). The boiler-following structure VI can achieve an almost instantaneous MW_e response, but there is a significant interacting effect on the main steam pressure that can only be corrected slowly with the firing power, as indicated by the ICI analysis. Aggressive tuning for the pressure controller easily resulted in system instability, and the controllers had to be tuned together. Turbine-following ICI structure III on the other hand gives a slower MW_e response, but the related fluctuation in the steam pressure is small. The structure III loops are clearly less dependent on each other than in structure VI, and the control loops were easier to tune.

6. CONCLUSIONS

A once-through circulating fluidized bed boiler (OTU-CFB) was examined using relative gain analysis in order to form
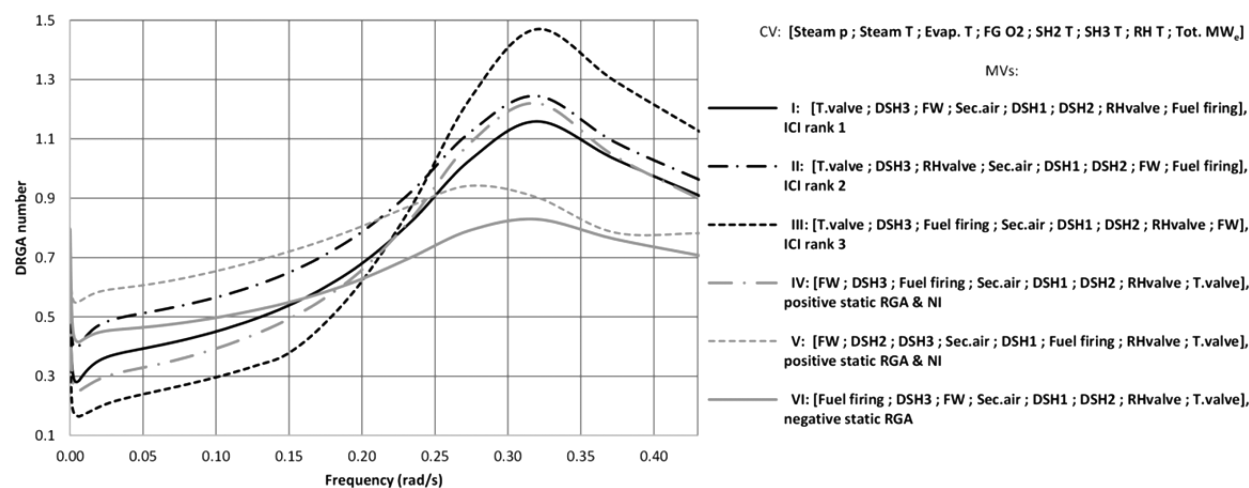
Figure 11. DRGA numbers as a function of frequency for case 4 control CV−MV connections: ICI structures I−III, structures IV−V with positive zero frequency RGA and NI, and the basic boiler-following structure VI with negative zero frequency RGA.
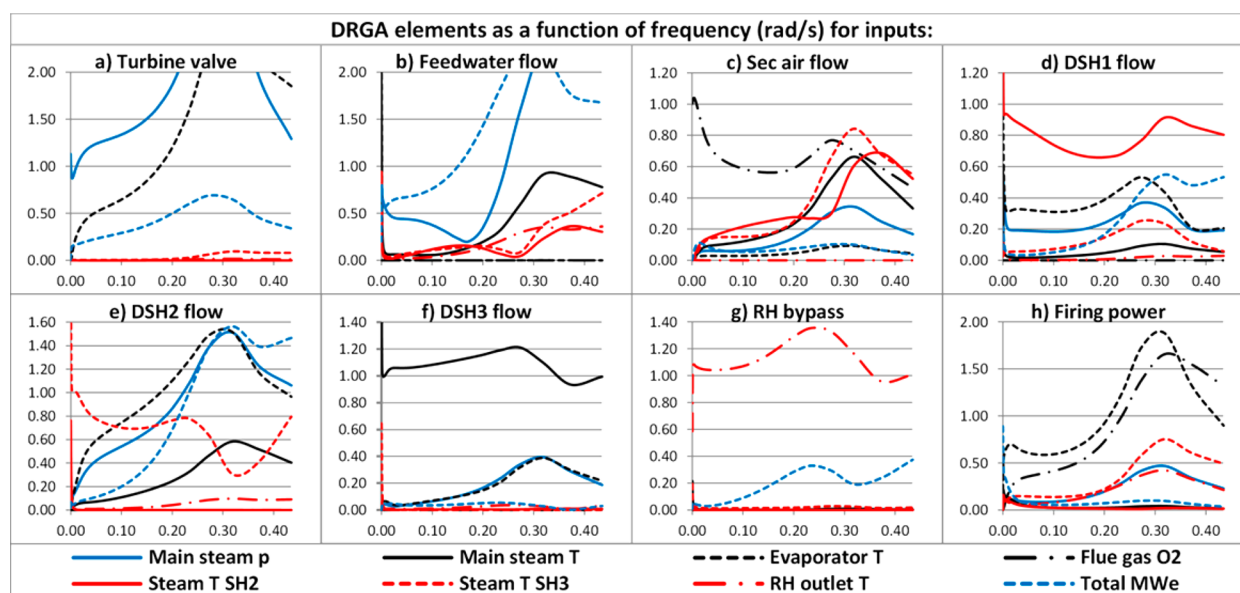
Figure 12. DRGA elements as a function of frequency for case 4; separate figures for each MV.
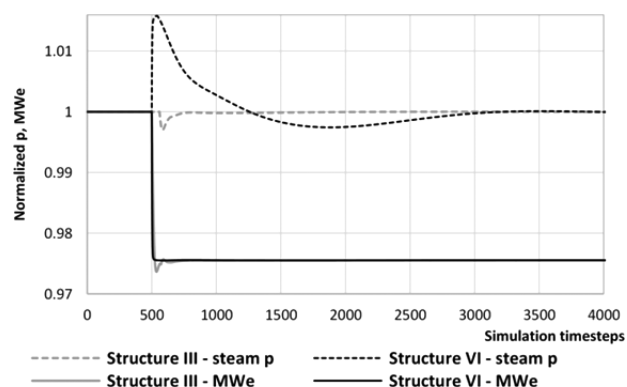
Figure 13. Normalized output MW_e set point step (constant pressure mode) for control structures III (turbine-following) and VI (boiler-following). PID controllers with tight tunings were used.

decentralized control structures for the power plant. The relative gain array (RGA) was applied to the steady-state gain matrix of an OTU-CFB simulator, as well as for higher frequencies (DRGA). Input−output sets ranging from 3×3 to 8×8 MIMO systems were investigated. Partial relative gain (PRG) was used to generate control structures with integral controllability with integrity (ICI). ICI is a useful property in the power plant, as it enables an independent tuning of its control loops. The PRG is only featured in a few publications.

The PRG ICI analysis provided a more rigorous screening of control structures than the RGA, especially for large OTU-CFB systems. The results were in line with existing control practices, using a basic turbine-following setup. However, the steady-state ICI criterion was also somewhat limited, as it labeled boiler-following control as infeasible despite its good real-life performance.

In contrast, control structures that were deemed to be poor at zero frequency often became favorable in the DRGA analysis, including boiler-following structures. Indeed, highly ranked ICI control structures commonly suffered from loop interactions above zero frequency. The findings are understandable for the turbine-following ICI structures, where fast output power disturbances are difficult to compensate. However,

it should be noted that the chosen manipulated and controlled variable sets, as well as the frequency range, also influence the analysis outcomes.

The PRG and DRGA analysis highlighted the direct effect of the feedwater on the OTU steam path and the resulting interactions between steam pressure/temperature and output power control in the plantwide framework. The separate feedwater and spray flow inputs also cause slight ill-conditioning in the system. The DRGA indicated that turbine-following control would benefit from adjusting the output MW_e with the faster feedwater flow instead of the firing power.

Future work with OTU-CFB relative gain analysis will concern its broader application to the plantwide problem, considering multiple load levels, various disturbances and different process structures. Combustion power plants are facing major challenges in the near future, as they need to manage increasing response requirements in terms of speed and flexibility. It is likely that the layouts of future plants will differ from existing ones. The design of high-performing control structures thus requires that robust tools be available for plantwide control design.

■ ASSOCIATED CONTENT

Ⓢ Supporting Information

The Supporting Information is available free of charge on the ACS Publications website at DOI: 10.1021/acs.iecr.7b03259.

> Table data: Open-loop gain matrix of the OTU-CFB process, RGA matrices of boiler test cases 2−4, time domain behavior of the main boiler manipulated variables (PDF)

■ AUTHOR INFORMATION

Corresponding Author
*Tel: +358443434979. E-mail: hultgrenmatias@gmail.com.

ORCID ⓘ

Matias Hultgren: 0000-0001-8782-3808

Present Address
‡Outotec, Kuparitie 10, PO Box 69, FI-28101 Pori, Finland, matias.hultgren@outotec.com.

Notes

The authors declare no competing financial interest.

■ NOMENCLATURE

a = real term of CV−MV frequency response
b = imaginary term of CV−MV frequency response
CDOF = control degrees of freedom, −
DOF = degrees of freedom, −
DRGA = dynamic relative gain array, −
$\mathbf{G}$ = open-loop steady-state gain matrix between CVs and MVs
$\hat{\mathbf{G}}$ = modified $\mathbf{G}$, elements not used in control connections set to zero
$\bar{\mathbf{G}}_{mn}$ = partially controlled system $\mathbf{G}$, loops between m and n open (rest closed)
g = gain between CV and MV
$\mathbf{H}$ = open-loop frequency response matrix between CVs and MVs
$\mathbf{I}$ = identity matrix, −
m = controlled output variable (CV) index, −
n = manipulated input variable (MV) index, −
MW_e = output electrical megawatts, MW
N_X = amount of streams in DOF, X = "total"/"restrained"/"redundant", −
nDRGA = dynamic relative gain array number, −
NI = Niederlinski index, −
p = pressure, bar
PRG_{mn} = partial relative gain matrix, loops between m and n open (rest closed), −
RGA = relative gain array, −
T = temperature, °C
u = process input variable
y = process output variable
λ_{mn} = relative gain between CV m and MV n, −
ω = frequency, rad/s

■ REFERENCES

(1) Joronen, T.; Kovács, J.; Majanne, Y. *Voimalaitosautomaatio*; Suomen Automaatioseura ry: Helsinki, Finland, 2007.
(2) Klefenz, G. *Automatic Control of Steam Power Plants*; B.I.-Wissenschaftsverlag: Mannheim/Wien/Zürich, Germany/Austria/Switzerland, 1986.
(3) Sarkar, D. K. *Thermal Power Plant Design and Operation*; Elsevier: Amsterdam, Netherlands, 2015.
(4) Hultgren, M.; Ikonen, E.; Kovács, J. Oxidant control and air-oxy switching concepts for CFB furnace operation. *Comput. Chem. Eng.* **2014**, *61*, 203−219.
(5) Stanger, R.; Wall, T.; Spörl, R.; Paneru, M.; Grathwohl, S.; Weidmann, M.; Scheffknecht, G.; McDonald, D.; Myöhänen, K.; Ritvanen, J.; Rahiala, S.; Hyppänen, T.; Mletzko, J.; Kather, A.; Santos, S. Oxyfuel combustion for CO_2 capture in power plants. *Int. J. Greenhouse Gas Control* **2015**, *40*, 55−125.
(6) Leckner, B.; Gómez-Barea, A. Oxy-fuel combustion in circulating fluidized bed boilers. *Appl. Energy* **2014**, *125*, 308−318.
(7) Sharifzadeh, M. Integration of process design and control: A review. *Chem. Eng. Res. Des.* **2013**, *91* (12), 2515−2549.
(8) Luyben, W. L.; Tyréus, B. D.; Luyben, M. L. *Plantwide Process Control*; McGraw-Hill: New York, NY, 1999.
(9) Ogunnaike, B. A.; Ray, W. H. *Process Dynamics, Modeling, and Control*; Oxford University Press: New York, NY, Oxford, U.K., 1994.
(10) Skogestad, S.; Postlethwaite, I. *Multivariable Feedback Control, Analysis and Design*; Wiley: Chichester, U.K., 1996.
(11) McAvoy, T. J. Some Results on Dynamic Interaction Analysis of Complex Control Systems. *Ind. Eng. Chem. Process Des. Dev.* **1983**, *22* (1), 42−49.
(12) Bristol, E. H. On a new measure of interaction for multivariable process control. *IEEE Trans. Autom. Control* **1966**, *11* (1), 133−134.
(13) Witcher, M.; McAvoy, T. J. Interacting control systems: steady state and dynamic measurement of interaction. *ISA Trans.* **1977**, *16*, 35−41.
(14) Häggblom, K. E. In *Partial Relative Gain: A New Tool for Control Structure Selection*. Proceedings of the 1997 AIChE Annual Meeting, Los Angeles, CA, Nov 16−21, 1997; Los Angeles, 1997.
(15) Campo, P. J.; Morari, M. Achievable Closed-Loop Properties of Systems Under Decentralized Control: Conditions Involving the Steady-State Gain. *IEEE Trans. Autom. Control* **1994**, *39* (5), 932−943.
(16) Chiu, M.-S.; Arkun, Y. Decentralized Control Structure Selection Based on Integrity Considerations. *Ind. Eng. Chem. Res.* **1990**, *29* (3), 369−373.
(17) Niva, L.; Ikonen, E.; Kovács, J. Self-optimizing control structure design in oxy-fuel circulating fluidized bed combustion. *Int. J. Greenhouse Gas Control* **2015**, *43*, 93−107.
(18) Skogestad, S. Control structure design for complete chemical plants. *Comput. Chem. Eng.* **2004**, *28* (1−2), 219−234.
(19) Prasad, G.; Irwin, G. W.; Swidenbank, E.; Hogg, B. W. Plant-wide predictive control for a thermal power plant based on a physical plant model. *IEE Proc.: Control Theory Appl.* **2000**, *147* (5), 523−537.
(20) Garduno-Ramirez, R.; Lee, K. Y. Compensation of control-loop interaction for power plant wide-range operation. *Control Eng. Pract.* **2005**, *13* (12), 1475−1487.
(21) Aurora, C.; Magni, L.; Scattolini, R.; Colombo, P.; Pretolani, F.; Villa, G. Predictive control of thermal Power Plants. *Int. J. Robust Nonlin. Control* **2004**, *14* (4), 415−433.
(22) Biyanto, T. R.; Prasetya, H. E. G.; Bayuaji, R.; Nugroho, G.; Soehartanto, T. Design Plant-wide Control to Waste Heat Recovery Generation on Cement Industry Based HYSYS. *Procedia Comput. Sci.* **2015**, *72*, 170−177.
(23) Rambalee, P.; Gous, G.; de Villiers, P. G. R.; McCulloch, N.; Humphries, G. In *Control and Stabilization of a Multiple Boiler Plant: An APC Approach*. Proceedings of the 13th IFAC Symposium on Automation in Mining, Mineral and Metal Processing, Cape Town, South Africa, Aug 2−4, 2010; Jemwa, G. T., Aldrich, C., Eds.; IFAC: Cape Town, 2010; pp 109−114.
(24) Garrido, J.; Morilla, F.; Vázquez, F. In *Centralized PID control by decoupling of a boiler-turbine unit*. Proceedings of the 2009 European Control Conference, Budapest, Hungary, Aug 23−26, 2009; Budapest, 2009; pp 4007−4012.
(25) Manousiouthakis, V.; Savage, R.; Arkun, Y. Synthesis of Decentralized Process Control Structures Using the Concept of Block Relative Gain. *AIChE J.* **1986**, *32* (6), 991−1003.
(26) Basu, P. *Combustion and Gasification in Fluidized Beds*; Taylor & Francis: Boca Raton, FL, 2006.
(27) Blaszczuk, A.; Nowak, W.; Krzywanski, J. Effect of bed particle size on heat transfer between fluidized bed of group b particles and vertical rifled tubes. *Powder Technol.* **2017**, *316*, 111−122.
(28) Kovács, J.; Kettunen, A.; Ojala, J. In *Modelling and control design of once-through boilers*. Proceedings of the 8th Power Plant and Power System Control Symposium, Toulouse, France, Sept 2−5, 2012; Fadel, M., Caux, S., Eds.; IFAC: Toulouse, 2012; pp 196−200.
(29) Paloranta, M.; Kettunen, A.; Kovács, J. In *Dynamic simulations of the World's first supercritical CFB-OTU boiler*. Proceedings of the 9th International Conference on Circulating Fluidized Beds, Hamburg, Germany, May 13−16, 2008; Hamburg, 2008.

(30) Blaszczuk, A.; Nowak, W.; Jagodzik, S. Effects of operating conditions on $deNO_x$ system efficiency in supercritical circulating fluidized bed boiler. *J. Power Technol.* **2013**, *93* (1), 1−8.

(31) Duan, L.; Zhao, C.; Zhou, W.; Qu, C.; Chen, X. O_2/CO_2 coal combustion characteristics in a 50 kW_{th} circulating fluidized bed. *Int. J. Greenhouse Gas Control* **2011**, *5* (4), 770−776.

(32) Krzywanski, J.; Czakiert, T.; Blaszczuk, A.; Rajczyk, R.; Muskala, W.; Nowak, W. A generalized model of SO_2 emissions from large- and small-scale CFB boilers by artificial neural network approach: Part 1. The mathematical model of SO_2 emissions in air-firing, oxygen-enriched and oxycombustion CFB conditions. *Fuel Process. Technol.* **2015**, *137*, 66−74.

(33) Ritvanen, J.; Kovács, J.; Salo, M.; Hultgren, M.; Tourunen, A.; Hyppänen, T. In *1-D Dynamic Simulation Study of Oxygen Fired Coal Combustion in Pilot and Large Scale CFB Boilers*. Proceedings of the 21st International Conference on Fluidized Bed Combustion, Vol. 1, Naples, Italy, June 3−6, 2012; EnzoAlbanoEd.e: Naples, 2012; pp 72−79.

(34) Hultgren, M.; Ikonen, E.; Kovács, J. In *Circulating Fluidized Bed Boiler State Estimation with an Unscented Kalman Filter Tool*. Proceedings of the 23rd IEEE International Conference on Control Applications, Antibes, France, Oct 8−10, 2014; pp 310−315.

(35) Stephanopoulos, G.; Ng, C. Perspectives on the synthesis of plant-wide control structures. *J. Process Control* **2000**, *10* (2−3), 97−111.

(36) Luyben, W. L. Design and Control Degrees of Freedom. *Ind. Eng. Chem. Res.* **1996**, *35* (7), 2204−2214.

(37) Konda, N. V. S. N. M.; Rangaiah, G. P.; Krishnaswamy, P. R. A simple and effective procedure for control degrees of freedom. *Chem. Eng. Sci.* **2006**, *61* (4), 1184−1194.

(38) Price, R. M.; Georgakis, C. Plantwide regulatory control design procedure using a tiered framework. *Ind. Eng. Chem. Res.* **1993**, *32* (11), 2693−2705.

(39) Price, R. M.; Lyman, P. R.; Georgakis, C. Throughput Manipulation in Plantwide Control Structures. *Ind. Eng. Chem. Res.* **1994**, *33* (5), 1197−1207.

(40) Ogata, K. *Modern Control Engineering*, 5th ed.; Prentice Hall: New Jersey, NJ, 2010.

(41) Shields, R. W.; Pearson, J. B. Structural Controllability of Multiinput Linear Systems. *IEEE Trans. Autom. Control* **1976**, *21* (2), 203−212.

(42) Xiong, Q.; Cai, W.-J.; He, M.-J. A practical loop pairing criterion for multivariable processes. *J. Process Control* **2005**, *15* (7), 741−747.

(43) Chang, J.-W.; Yu, C.-C. The relative gain for non-square multivariable systems. *Chem. Eng. Sci.* **1990**, *45* (5), 1309−1323.

(44) Alhammadi, H. Y.; Romagnoli, J. A. Process design and operation: Incorporating environmental, profitability, heat integration and controllability considerations. In *The Integration of Process Design and Control*; Seferlis, P., Georgiadis, M. C., Eds.; Elsevier: Amsterdam, Netherlands, 2004; pp 264−305.

(45) Skogestad, S.; Morari, M. Implications of Large RGA Elements on Control Performance. *Ind. Eng. Chem. Res.* **1987**, *26* (11), 2323−2330.

(46) Skogestad, S. Dynamics and Control of Distillation Columns: A Tutorial Introduction. *Chem. Eng. Res. Des.* **1997**, *75* (6), 539−562.

(47) Laub, A. J. Efficient Multivariable Frequency Response Computations. *IEEE Trans. Autom. Control* **1981**, *26* (2), 407−408.

(48) Engell, S.; Trierweiler, J. O.; Völker, M.; Pegel, S. Tools and indices for dynamic I/O- controllability assessment and control structure selection. In *The Integration of Process Design and Control*; Seferlis, P., Georgiadis, M. C., Eds.; Elsevier: Amsterdam, Netherlands, 2004; pp 430−463.

(49) Apros Process Simulation Software, Nuclear and Thermal Power Plant Applications. Fortum Power and Heat Oy & VTT Technical Research Centre of Finland Ltd. http://www.apros.fi (accessed Sept 19, 2017).

(50) Hänninen, M.; Ylijoki, J. *The one-dimensional separate two-phase flow model of APROS, VTT Tiedotteita—Research Notes 2443*; Technical Report, VTT Technical Research Centre of Finland; Edita Prima Oy: Helsinki, Finland, 2008.

OTU-CFB boiler control design with the dynamic relative gain array and partial relative gain

SUPPORTING INFORMATION

Matias Hultgren[,†,‡], Enso Ikonen[†], Jenő Kovács[†]*

[†]Systems Engineering, University of Oulu, POB 4300, FI-90014 Oulun yliopisto, Finland.

E-mail: [*,†]hultgrenmatias@gmail.com, [†]enso.ikonen@oulu.fi, [†]jeno.kovacs@oulu.fi.

Contents

[‡]Outotec, Kuparitie 10, PO Box 69, FI-28101 Pori, Finland, matias.hultgren@outotec.com.

Table S1. Steady-state gain effects in the OTU-CFB, normalized with the input maxima.

	T.valve	FW	Fuel	Prim air	Sec air	Tot DSH	DSH 1	DSH 2	DSH 3	RHvalve	Firing power	Boiler load
Steam p	−1.0	0.04	0.2	−0.1	−0.1	0.04	0.04	0.03	0.03	0.1	0.2	0.2
Steam T	−0.2	−1.0	1.0	−0.4	−0.4	−1.0	−1.0	−1.0	−1.0	0.8	1.0	0.02
Evap. T	−0.4	−0.2	0.3	−0.2	−0.1	−0.1	−0.1	−0.1	−0.1	0.3	0.3	0.1
FG O$_2$	0.0	0.0	−0.0002	0.001	0.002	0.0	0.0	0.0	0.0	0.0	0.0	0.0
FG T	−0.1	−0.3	0.6	−1.0	−1.0	−0.2	−0.2	−0.2	−0.2	0.1	0.4	0.1
SH2 T	−0.3	−0.8	0.8	−0.3	0.04	−0.5	−0.8	−0.4	−0.3	0.8	0.8	0.02
SH3 T	−0.2	−1.0	1.0	−0.6	−0.2	−0.8	−1.0	−1.0	−0.4	0.9	1.0	−0.02
RH T	−0.1	−0.7	0.8	0.002	−0.3	−0.7	−0.7	−0.7	−0.6	−1.0	0.8	0.1
Tot MW$_e$	0.01	0.1	1.0	−0.2	−0.4	0.1	0.1	0.1	0.1	−0.3	1.0	1.0

Table S2. The steady-state RGA matrix of the case 2 system, 5 input MVs and 5 output CVs.

RGA	MV →	T.valve	DSH1	DSH2	DSH3	Boiler load
CV ↓	INDEX	1	2	3	4	5
Steam p	1	0.989	0.025	−0.011	−0.002	−0.002
Steam T	2	0.0006	−0.661	0.008	1.651	0.001
SH2 T	3	0.005	1.797	−0.796	−0.007	0.0007
SH3 T	4	0.002	−0.153	1.800	−0.649	−0.0001
Tot MW$_e$	5	0.003	−0.008	−0.001	0.006	1.000

Table S3. The steady-state RGA matrix of the case 3 system, 6 input MVs and 6 output CVs.

RGA	MV →	T.valve	FW	Fuel	Prim air	Sec air	Tot DSH
CV ↓	INDEX	1	2	3	4	5	6
Steam p	1	0.983	0.127	–0.012	0.025	–0.014	–0.109
Steam T	2	0.008	–0.643	0.055	–0.210	0.119	1.671
Evap T	3	0.017	1.806	0.040	–0.186	0.078	–0.756
FG O$_2$	4	0.000	0.000	–0.058	–1.205	2.263	0.000
FG T	5	–0.012	–0.349	0.028	2.664	–1.507	0.176
Tot MW$_e$	6	0.003	0.059	0.947	–0.088	0.062	0.018

Table S4. The steady-state RGA matrix of the case 4 system, 8 input MVs and 8 output CVs.

RGA	MV →	T.valve	FW	Sec air	DSH1	DSH2	DSH3	RHvalve	Firing
CV ↓	INDEX	1	2	3	4	5	6	7	8
Steam p	1	1.049	0.122	0.000	–0.118	–0.018	0.005	–0.025	–0.015
Steam T	2	–0.014	–1.102	–0.0002	–0.065	0.175	1.629	0.270	0.108
Evap T	3	–0.050	1.764	0.0002	–0.832	–0.052	0.051	0.077	0.042
FG O$_2$	4	0.000	0.000	1.001	0.0002	–0.0001	0.000	0.000	–0.001
SH2 T	5	0.001	–0.212	0.000	1.934	–0.785	–0.01	0.043	0.028
SH3 T	6	0.0005	–0.147	–0.0001	–0.053	1.819	–0.651	0.026	0.006
RH T	7	0.01	0.490	0.0001	0.130	–0.136	–0.031	0.629	–0.091
Tot MW$_e$	8	0.004	0.086	–0.001	0.004	–0.002	0.006	–0.020	0.924

Table S5. Time domain behavior of the main MVs from the APROS dynamic model. Results are normalized for each CV with respect to the largest MV (smaller percentage, shorter time).

Normalized times	Turbine valve			Firing power			Feedwater flow		
% of max time	Rise time	Settling time	Time delay	Rise time	Settling time	Time delay	Rise time	Settling time	Time delay
Main steam p	5	26	0	100	100	67	0.4	89	100
Total MW$_e$	0.01	33	0	100	100	0	0.1	90	0
Main steam T	100	100	0	74	82	60	83	94	100
Evaporator T	17	60	0	100	100	100	96	95	50
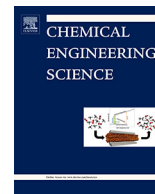
Integrated control and process design for improved load changes in fluidized bed boiler steam path

Matias Hultgren *, Enso Ikonen, Jenő Kovács

Systems Engineering, University of Oulu, Linnanmaa, POB 4300, FI-90014 Oulun yliopisto, Finland

HIGHLIGHTS

- Process and control design were integrated for a fluidized bed boiler steam path.
- The steam storage distribution and feedback controllers were optimized together.
- Boiler-following control was assessed and selected based on relative gain methods.
- Improved load transitions, controllability and disturbance rejection were reached.
- The design suggested a large total steam storage, preferably close to the turbine.

GRAPHICAL ABSTRACT
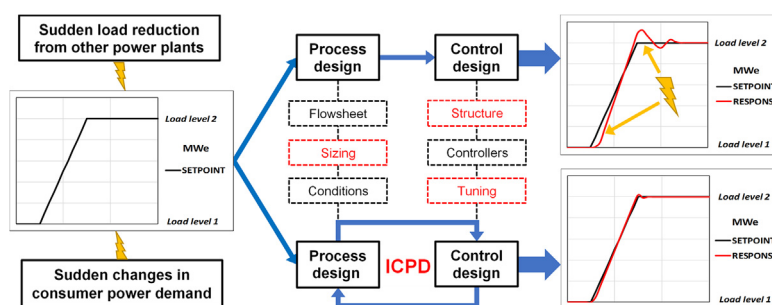
ABSTRACT

Integrated control and process design is considered for a power plant to obtain improved load changes in output electrical power (MW_e). Fast load transitions are increasingly needed in conventional power plants, which calls for a deeper integration between the boiler and its control system. An integrated design methodology is applied to an industrial boiler steam path in this paper; no past reports of such an application exist in the literature. The methodology utilizes dynamic optimization together with performance relative gain array and closed-loop disturbance gain controllability analysis. The aim is to optimize the boiler steam storage distribution, the turbine valve operation, and the electrical power and main steam pressure controllers during different MW_e ramp reference trajectories. The methodology was successful in defining closed-loop designs with excellent MW_e setpoint tracking, small steam pressure disturbances and minimal steam throttling. The results also highlighted the challenges related to integrated design in power plants.

© 2019 Elsevier Ltd. All rights reserved.

1. Introduction

In this paper, integrated control and process design is performed for a circulating fluidized bed (CFB) boiler. Dynamics and control are becoming increasingly important in the operation of thermal power plants due to demands from the power generation market (IEA, 2011). Most importantly, combustion power plants are increasingly operated in fast load transitions (Alobaid et al., 2016; Franzosi et al., 2006; Kovács et al., 2012; Wang et al., 2014) and less at maximum load with the best operational efficiency. Improving the load change performance is challenging due to the complex dynamics and interconnected nature of the boiler steam cycle. Increased emission requirements, challenging

Nomenclature

CFB	circulating fluidized bed
CV	controlled output variable
e_E	mass flow to turbine electrical power conversion factor, $MW \cdot s \cdot kg^{-1}$
d	process disturbance variable, –
DSH	desuperheater spray
D_p	derivative gain for pressure "p" PID controller, –
E	output electrical power at the turbine, MW
F	frequency range for relative gain analysis, rad/s
f	pipe friction factor, $1/m^4$
$\mathbf{G}$	open-loop process transfer function matrix between CVs and MVs
$\bar{\mathbf{G}}$	scaled open-loop process transfer function matrix
$\hat{\mathbf{G}}$	diagonal matrix of the control MV–CV connections
g	gain magnitude between CV and MV, –
$\mathbf{G}_d$	open-loop disturbance transfer function matrix between CVs and disturbances
$\bar{\mathbf{G}}_d$	scaled open-loop disturbance transfer function matrix
$\hat{\mathbf{G}}_d$	closed-loop disturbance gain (CLDG) matrix in the frequency domain
$\mathbf{I}$	identity matrix
I_i	integral gain for output "i" PID controller ("p" or "E"), –
ICPD	integrated control and process design
J	integrated control and process design objective function, –
j	individual design objective, –
m_W	steam mass flow, subscripts "in" and "out" for input and output, kg/s
$\bar{m}_W$	nominal steam mass flow, kg/s
L	firing power, kg/s
MV	manipulated input variable
N_p	derivative filter for pressure "p" PID controller, –
p	main steam pressure, bar
p_i	steam pressure in a section "i", subscript "n" denotes pressure after the section, bar
$\bar{p}$	nominal steam pressure, bar
P_i	proportional gain for output "i" PID controller ("p" or "E"), –
q_E	evaporator storage percentage parameter, %
q_{S1}	parameter for percentage of superheater storage before DSH cooling, %
r	valve coefficient, $m \cdot s$
RGA	relative gain array
SP	setpoint
s	Laplace s-plane operator, rad/s
T	time range of dynamic testing, s
t	time, s
t_I	boiler thermal inertia time delay, s
u	process input variable, subscript "c" denotes control of a specific output, –
v	turbine valve position, –
$\bar{v}$	nominal turbine valve position, –
x_{HP}	portion of the electrical power that is generated at the turbine high-pressure section, –
y	process output variable, –
Γ	performance relative gain array (PRGA) matrix in the frequency domain, –
Γ_n	PRGA number in the frequency domain, –
ρ_W	steam density, kg/m^3
τ_E	evaporator steam storage coefficient, $m \cdot s^2$
τ_S	superheater (SH) steam storage coefficient, $m \cdot s^2$
τ_{S1}	superheater steam storage coefficient before DSH spray cooling, $m \cdot s^2$
τ_{S2}	superheater steam storage coefficient after DSH spray cooling, $m \cdot s^2$
τ_{HP}	turbine high-pressure section time constant, s
τ_I	boiler thermal inertia time constant, s
τ_{LP}	turbine low-pressure section time constant, s
τ_{TOT}	normalized total steam storage parameter, $m \cdot s^2$
ω	radial frequency, rad/s

new fuels and new technologies like oxy-firing introduce additional challenges for boiler operation.

The new requirements call for advanced control and effective control design methods. Centralized model predictive control (MPC) has been a major driving force in this work (Aurora et al., 2004; Chan et al., 2014; Franzosi et al., 2006; Klaučo and Kvasnica, 2017; Ławryńczuk, 2017; Prasad et al., 2000; Prasad et al., 2002; Rovnak and Corlis, 1991). The application of fuzzy and neural network MPC has been frequently reported for increasing the coordination between the boiler and the turbine, and for overcoming problems due to complex process dynamics (Kong et al., 2015; Liu et al., 2010; Ma et al., 2016; Zhang et al., 2017). In general, a plantwide design focus is essential for achieving an improved coordination of the power plant control tasks. Systematic plantwide control has mainly been deployed for specific boiler setups, such as oxy combustion (e.g. Niva et al., 2015; Niva et al., 2017; Jin et al., 2015). Hultgren et al. (2015, 2017b) examined plantwide control structure selection and interaction analysis based on relative gains for once-through and oxy-fired CFB boilers. Multiloop PID decoupling and tuning was investigated e.g. by Garduno-Ramirez and Lee (2005), Garrido et al. (2009) and Zhang et al. (2012). Moreover, established operational methods like condensate throttling (Long et al., 2017; Wang et al., 2017), steam extraction setups at the turbine (Kovács et al., 2012; Zhou and Wang, 2017), and condenser control adjustments (Wang et al., 2014; Wang et al., 2015) are still being investigated in order to reach improved performance.

Despite advances in load transition control, control design alone is not going to be enough to meet the performance challenges in thermal boiler design, as the restrictions to setpoint tracking and stability are ultimately determined by the process design. A deeper interaction between process and control design is needed to obtain improved output power responses, high efficiency, sufficient steam quality and good operational safety. In integrated control and process design (ICPD), the process and its control system are designed at the same time (Sharifzadeh, 2013; Vega et al., 2014), which enables the consideration of dynamic bottlenecks that limit achievable control performance. At the same time, process specific dynamics can be incorporated more thoroughly into the boiler control system design.

Integrated design can be carried out using a process knowledge oriented approach, or the problem can be formulated as a "closed" framework, where process and control parameters are optimized (Hultgren et al., 2017a). This paper investigates ICPD optimization (Sakizlis et al., 2004; Yuan et al., 2012) for conventional power plant load change performance. The optimization formulation depends on the design scope and current status (greenfield or existing plant) of the target boiler (Fig. 1).

This paper considers fully simultaneous ICPD design for the steam path of an industrial-scale CFB drum boiler. The aim is to
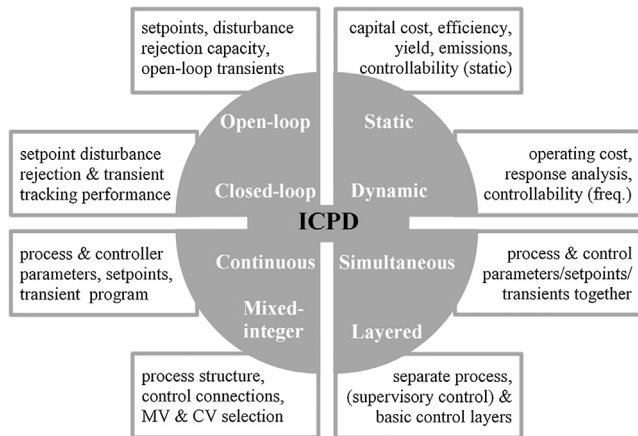
Fig. 1. Algorithm structures and features of ICPD optimization. Design applications and variables are listed in the accompanying text boxes. MV/CV = manipulated/controlled variable, freq. = frequency.

determine how the steam storage capacity should be distributed in the boiler, and how the main control loops should be tuned to obtain faster load changes. Sufficient controllability should also be maintained in the steam path, measured with the performance relative gain (PRGA) and closed-loop disturbance gain (CLDG) arrays. The evaporator and superheater steam storage capacities, the turbine valve nominal position, and the main steam pressure and electrical power PID controller parameters are optimized using a systematic ICPD design methodology. The main contribution of the paper is to propose a method for deriving power plant steam cycle design guidelines and to demonstrate the benefits of an integrated ICPD approach for thermal power plants.

Currently there is little existing literature available concerning ICPD in combustion power plants. Diangelakis et al. utilized mixed-integer dynamic optimization for residential scale power plants (Diangelakis et al., 2017; Diangelakis and Pistikopoulos, 2016; Diangelakis and Pistikopoulos, 2017). Capra and Martelli (2015) carried out a joint process and part-load design for organic Rankine cycles, using continuous derivative-free optimization. Chen and Bollas (2017) optimized air preheating and steam temperature setpoints together with supervisory control for a chemical looping plant. Hultgren et al. (2017a) made a literature review about ICPD design in power plants, and specified possibilities for applying ICPD in CFB boilers. The work contained basic ICPD design examples for a CFB steam path, and in the present paper these initial simulations are extended into a full ICPD design case.

The paper is structured as follows. Section 2 outlines the operational principle of the CFB boiler and its steam cycle. Section 3 presents the storage capacity model that is used for investigating boiler load changes and discusses the relative gain design tools and optimization methods that are utilized in the ICPD framework. Section 4 presents the CFB steam path ICPD design setup, followed by assessment of the performance of the design via simulations in Section 5. Finally, Section 6 concludes the paper.

2. Boiler process and control

The combustion power plant is divided into the combustion side and water-steam cycle subsystems (Alobaid et al., 2016; Joronen et al., 2007; Sarkar, 2015). Fuel is combusted in the furnace, and heat is transferred to the water-steam side. Feedwater is pumped and evaporated in the furnace evaporator, and the saturated steam is heated further in the superheating block, which often consists of several superheater (SH) units and cooling desuperheater spray flows (DSH). The formed main steam expands

stage-wise in the turbine (high-pressure and low-pressure sections) to generate power.

Depending on the evaporator setup, boilers are classified into drum or once-through boilers. In drum boilers, water and steam are separated in a drum after the evaporation and recirculated to the evaporator. In once-through boilers, evaporation and superheating take place in a once-through path with no set separation stage. Another defining feature of the boiler is whether it is used in constant- or sliding-pressure mode. In constant-pressure mode, a constant main steam pressure is maintained at the turbine on different boiler load levels. While this enables the use of stored steam as a fast control reserve on part-loads, throttling the steam flow with the turbine valve contributes heavily to exergy destruction and leads to reduced operational efficiency. In sliding-pressure mode, the main steam pressure is altered together with the boiler load level, which enables a high efficiency. However, when operating in pure sliding mode with the turbine valve fully open, no fast steam control reserves can be utilized for load changes.

The main controlled parameters of a condensing power plant (Joronen et al., 2007; Klefenz, 1986) are the generated power and the main steam properties, i.e. flow, temperature and pressure (Fig. 2). The output electrical power (MW_e) is controlled either with the fuel firing power or by modifying the steam flow to the turbine with the turbine throttling valve. The main steam pressure can similarly be modified either with the turbine valve or the firing power, which is regulated by combustion control. Feedwater is controlled to provide enough water for steam formation. The main steam temperature is typically adjusted with the DSH sprays in the superheating section.

Electrical power and main steam pressure control is coordinated with the unit master strategy (Fig. 2), the basic setups of which are boiler-following and turbine-following control (Joronen et al., 2007). In boiler-following control, the electrical power is controlled with the turbine valve and the pressure with the fuel firing power. The MW_e setpoint alters the steam flow, and the pressure disturbance is compensated with the firing power. In turbine-following control, the opposite connections are applied: The firing power is altered according to the MW_e setpoint, and the turbine valve position is changed to regulate the pressure.

Proper selection of the unit master control strategy is crucial for improving load change performance. Altering the steam flow to the turbine with the turbine valve results in immediate changes in the MW_e output, which enables fast and accurate load changes. However, this only provides a transient response to the electrical power, as the generated steam from the evaporation remains unchanged. Controlling the MW_e output with the firing power is slow, but at steady-state the generated steam and thus the electrical power mainly depend on the firing power. These effects can be observed from Fig. A1, where the electrical power was controlled with the fuel + air flows or the turbine valve only. When the constraints of the manipulated variables were disregarded, the turbine valve opening had to be increased constantly to maintain the new electrical power setpoint, while using the fuel + air flows for MW_e control slowly settled on a new steady-state. On the other hand, tight control was easily achieved during the ramp with the turbine valve, whereas the combustion power required almost instantaneous, practically infeasible changes in order to achieve a comparable MW_e response.

The target process of this paper is the steam path of an industrial condensing drum boiler in the range of >100 MW_e with steam superheating and a two-stage turbine expansion. The power plant uses the CFB combustion technology, where fuel and bed material particles are fluidized with the oxidant gas flows and circulated in the furnace hotloop (Kovács et al., 2012; Sarkar, 2015). The dynamic behavior of the combustion side is simplified as a thermal inertia term.

Fig. 2. Control of main steam properties and output MW$_e$, schematic figure. Dashed lines are control connections, boiler-following (BF) and turbine-following (TF) control schemes are highlighted.

3. Model and methods

The modeling and design tools of this paper are described here. Section 3.1 describes the boiler model, Section 3.2 the controllability analysis tools, and Section 3.3 the ICPD optimization. The goal of the ICPD design was to optimize the steam storages and electrical power/steam pressure controllers to obtain accurate MW$_e$ set-point tracking, small steam pressure disturbances and good controllability. The ICPD modeling aimed at describing the process as a series of interconnected dynamic elements, where the effect of design parameters could be separated from the overall input–output responses. The individual process stages were thus modeled using simple linear dynamics, which together resulted in a higher-order transfer function matrix in the Laplace "s" domain. This approach is admissible in the region surrounding the nominal operating point, when considering the steam path mass storage dynamics.

3.1. Steam path model

The industrial power plant model is a generic dynamic steam path model that is used at the Sumitomo SHI FW company for load transition control design. It consists of transfer function elements for the boiler, evaporator, superheater, turbine and turbine valve. The model describes the relation between steam pressure and flow at different stages of the steam path, as well as the relation to the output electrical power at the turbine (Doležal and Varcop, 1970).

The evaporation and superheating sections are considered as lumped mass storages for steam, i.e. "mass storage coefficients" τ_E and τ_S, Eq. (1), which translate into time constants. The superheating storage coefficient is divided into two terms (τ_{S1} and τ_{S2}) in order to investigate DSH spray disturbances. The driving force for the steam flow is the pressure difference over the section, Eq. (2).

$$p_i(s) = \frac{1}{C \cdot s} \left[m_{W,in}(s) - m_{W,out}(s) \right] \tag{1}$$

$$p_i(s) - p_{i,n}(s) = \frac{2 \cdot f \cdot \bar{m}_{W,out}}{\rho_W} m_{W,out}(s) \tag{2}$$

where C is the mass storage coefficient of the evaporator (τ_E) or superheater (τ_S), p_i is steam pressure in section "i", $p_{i,n}$ is steam pressure after section "i", $m_{W,in}$ and $m_{W,out}$ are input and output steam mass flows ($\bar{m}_{W,out}$ is nominal flow), ρ_W is steam density, and f is a pipe friction factor that depends on the pressure and load levels in the boiler.

The thermal inertia of the boiler is a first-order block (3) that describes the steam generation dynamics between the combustion side input flows (fuel and air) and the formed steam on the water-steam side.

$$\frac{m_{W,out}(s)}{L(s)} = e^{-t_I \cdot s} \frac{1}{\tau_I \cdot s + 1} \tag{3}$$

where τ_I is thermal inertia, t_I is load change delay and L is firing power (combustion side load).

The turbine is modeled using first-order transfer functions (4) that describe the dynamics between the incoming steam and the generated power (Joronen et al., 2007; Kundur, 1994). The turbine consists of a high-pressure and low-pressure section. The turbine valve is modeled as the product of the main steam pressure, the valve position and a valve coefficient "r", linearizing the bilinear term in Eq. (5).

$$\frac{E(s)}{m_{W,in}(s)} = e_E \left(\frac{x_{HP}}{\tau_{HP} \cdot s + 1} + \frac{1 - x_{HP}}{\tau_{LP} \cdot s + 1} \right) \tag{4}$$

$$m_{W,out}(s) = rp(s)v(s) = r\bar{p}v(s) + r\bar{v}p(s) \tag{5}$$

where x_{HP} is the portion of power generated in the high-pressure turbine, τ_{HP} and τ_{LP} are high- and low-pressure turbine time constants, E is electrical power, e_E is a conversion factor, r is valve coefficient, and v is turbine valve position; $\bar{p}$ and $\bar{v}$ are nominal pressure and valve position values.

The steam path model can be constructed from Eqs. (1)–(5) according to Fig. A.2, Appendix A. The nominal model parameters

are obtained from steam tables and in-house design data. Linearizing, an open-loop 2×2 transfer function matrix (6) between the investigated inputs and outputs of the boiler can be constructed. The manipulated variables (MV) are the firing power L and the turbine valve position v. The controlled variables (CV) are the main steam pressure p and electrical megawatts E.

3.2. Controllability & interaction analysis

The boiler control structure is selected based on the performance relative gain array (PRGA) and the closed-loop disturbance gain (CLDG). Controllability often refers to "state controllability" in control theory and is evaluated e.g. by considering

$$\mathbf{G}(s) = \begin{bmatrix} \frac{p(s)}{L(s)} & \frac{p(s)}{v(s)} \\ \frac{E(s)}{L(s)} & \frac{E(s)}{v(s)} \end{bmatrix} = \begin{bmatrix} e^{-t_l \cdot s} \dfrac{\alpha_{11}}{s^4 + \beta_{11} \cdot s^3 + \gamma_{11} \cdot s^2 + \delta_{11} \cdot s + \varepsilon_{11}} & \dfrac{-\alpha_{12} \cdot s^2 - \beta_{12} \cdot s - \gamma_{12}}{s^3 + \delta_{12} \cdot s^2 + \varepsilon_{12} \cdot s + \zeta_{12}} \\ e^{-t_l \cdot s} \dfrac{\alpha_{21} \cdot s + \beta_{21}}{s^6 + \gamma_{21} \cdot s^5 + \delta_{21} \cdot s^4 + \varepsilon_{21} \cdot s^3 + \zeta_{21} \cdot s^2 + \eta_{21} \cdot s + \theta_{21}} & \dfrac{\alpha_{22} \cdot s^4 + \beta_{22} \cdot s^3 + \gamma_{22} \cdot s^2 + \delta_{22} \cdot s}{s^5 + \varepsilon_{22} \cdot s^4 + \zeta_{22} \cdot s^3 + \eta_{22} \cdot s^2 + \theta_{22} \cdot s + \kappa_{22}} \end{bmatrix} \quad (6)$$

where $\mathbf{G}$ is the input-output process transfer function matrix, and α, β, γ, δ, ε, ζ, η, θ, κ are positive coefficients provided in Eqs. (B.1)–(B.4), Appendix B.

The main steam temperature is assumed to be perfectly controlled with a DSH spray between superheater storages τ_{S1} and τ_{S2}. This means that active steam temperature control with the DSH flow will generate steam mass flow disturbances to superheating section 2 at a specified operating point, while superheating section 1 will be unaffected by these disturbances. The DSH spray disturbance transfer function is derived as Eq. (7) from the block diagram in Fig. A.2.

$$\mathbf{G}_d(s) = \begin{bmatrix} \frac{p(s)}{d(s)} \\ \frac{E(s)}{d(s)} \end{bmatrix} = \begin{bmatrix} \dfrac{\alpha_{d1} \cdot s^2 + \beta_{d1} \cdot s + \gamma_{d1}}{s^3 + \delta_{d1} \cdot s^2 + \varepsilon_{d1} \cdot s + \zeta_{d1}} \\ \dfrac{\alpha_{d2} \cdot s^3 + \beta_{d2} \cdot s^2 + \gamma_{d2} \cdot s + \delta_{d2}}{s^5 + \varepsilon_{d2} \cdot s^4 + \zeta_{d2} \cdot s^3 + \eta_{d2} \cdot s^2 + \theta_{d2} \cdot s + \kappa_{d2}} \end{bmatrix} \quad (7)$$

where d is a disturbance, $\mathbf{G}_d$ is the disturbance transfer function matrix between p and E and the DSH spray disturbance d, and α_d, β_d, γ_d, δ_d, ε_d, ζ_d, η_d, θ_d, κ_d are positive coefficients provided in Appendix B, Eqs. (B.5)–(B.6).

In total, the overall 2×2 steam path model can be illustrated in Fig. 3. The figure also shows how p and E can be controlled by L and v through unit master control.

the controllability matrix rank (Kalman criterion). In this paper, the "input–output controllability" definition is used, as it is relevant for industrial control design (Skogestad and Postlethwaite, 2005). Input–output controllability ensures that outputs can be kept within a set band from their references despite unknown bounded variations (disturbances or process changes), and it can be analyzed e.g. with relative gain methods like the PRGA and CLDG.

The PRGA and CLDG are based on the relative gain array (RGA) (Bristol, 1966), modified for the frequency domain (Witcher and McAvoy, 1977; McAvoy, 1983). The RGA consists of input–output interaction measures that signify how process open-loop gains change when other loops are closed (Ogunnaike and Ray, 1994). Control connections with elements close to 1 are ideal; negative values result in a gain sign change and should be avoided; small positive values result in gain amplification when loops are closed; and large elements signify gain amplification when loops are opened.

The PRGA is calculated as a scaled inverse of the plant at zero frequency (gains) or higher frequencies (frequency responses). A general definition for a 2×2 MV–CV system PRGA is shown in Eq. (8).
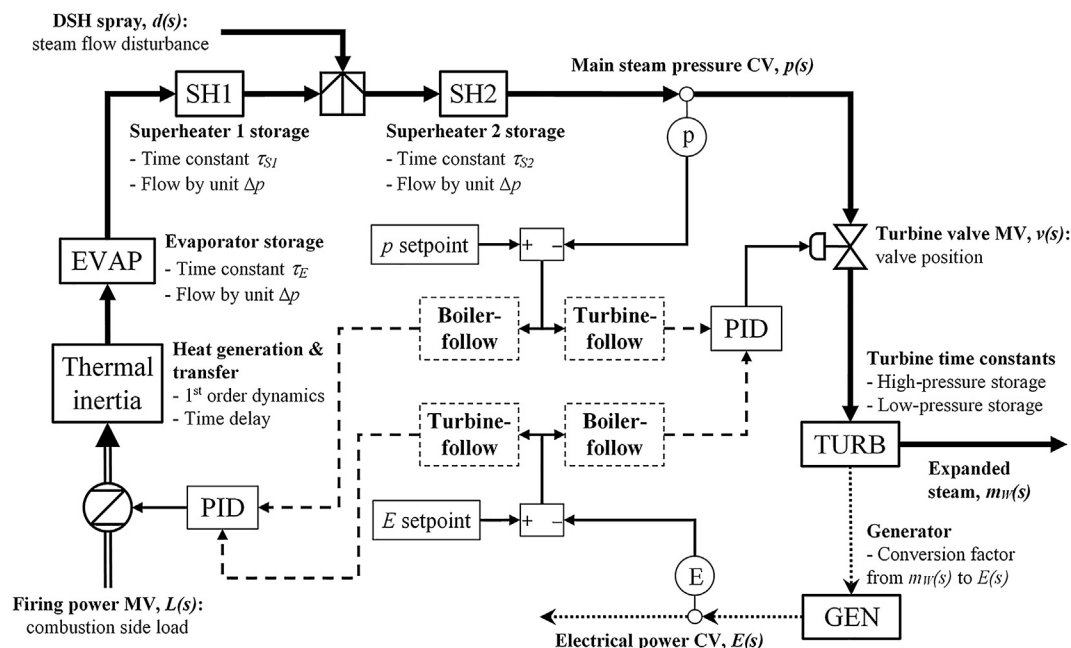

Fig. 3. Conceptual diagram of the process model between MVs and CVs. The alternative boiler-following and turbine-following unit master control connections are illustrated.

$$\Gamma(s) = \hat{\mathbf{G}}(s) \cdot \bar{\mathbf{G}}(s)^{-1} = \begin{bmatrix} \frac{y_1(s)}{u_{c1}(s)} & 0 \\ 0 & \frac{y_2(s)}{u_{c2}(s)} \end{bmatrix} \cdot \begin{bmatrix} \frac{y_1(s)}{u_1(s)} & \frac{y_1(s)}{u_2(s)} \\ \frac{y_2(s)}{u_1(s)} & \frac{y_2(s)}{u_2(s)} \end{bmatrix}^{-1} \qquad (8)$$

where Γ is the PRGA, $\hat{\mathbf{G}}$ is a scaled diagonal transfer function matrix of the control MV–CV connections, $\bar{\mathbf{G}}$ is a scaled process transfer function matrix, u denotes scaled input MVs (L and v), y denotes scaled output CVs (p and E), and u_{cn} is the input used for controlling output "n".

Among the relative gain methods, the PRGA is well-suited for highlighting controllability related feedback control limitations for the MV–CV connections of a chosen control system. Diagonal PRGA elements are the same as in the RGA and should ideally be close to 1. Off-diagonal elements signify interactions that have a detrimental effect on control performance and should be as small as possible. Control structures can conveniently be ranked in a specified frequency range ω with the PRGA number, Eq. (9), comparing the PRGA to the ideal case, i.e. an identity matrix $\mathbf{I}$.

$$\Gamma_n(s) = ||\Gamma(s) - \mathbf{I}||_N \qquad (9)$$

where Γ_n is the PRGA number and N denotes a chosen norm. The absolute sum norm is used in this paper, similarly to Skogestad and Postlethwaite (2005). Notably, the PRGA is more applicable for examining one-way interactions than the basic RGA, which always gives an identity matrix for a triangular process system. This feature is especially useful for the negligible steady-state electrical power gain of the turbine valve (c.f. Section 2), which is also visible in the process model equations, as the $E(s)/v(s)$ transfer function has a zero in the origin in Eq. (6).

The DSH spray flow effects are analyzed at different frequencies with the CLDG, general definition for a 2×2 MV–CV system with one disturbance in Eq. (10). A CLDG matrix element represents the apparent open-loop gain from a disturbance to an output when all control loops are closed in the system. As disturbances should influence controlled outputs as little as possible, all CLDG elements should preferably be small, especially smaller than the control connection frequency response magnitudes "g" of the respective outputs. Unlike the basic RGA, Eqs. (8)–(10) depend on variable scaling and the chosen control connections.

$$\hat{\mathbf{G}}_d(s) = \Gamma(s) \cdot \bar{\mathbf{G}}_d(s) \qquad (10)$$

where $\bar{\mathbf{G}}_d$ is the scaled disturbance transfer function matrix and $\hat{\mathbf{G}}_d$ is the CLDG.

3.3. ICPD optimization

The generic ICPD process optimization problem has been defined in the time domain e.g. by Kookos and Perkins (2004) or Sakizlis et al. (2004). Considering the scope of the CFB steam path optimization problem, these basic formulations can be summarized with Eqs. (11)–(12), which can then be applied to the open-loop steam path model in the Laplace "s" domain.

$$\min_{X,U} J(y(t), u(t), X, U) \qquad (11)$$

subject to the process, control and controllability constraints:

$$\begin{cases} m(x'(t), x(t), u(t), X) = 0 \\ m_0(x(0), u(0), X) = 0 \\ \mu(y(t), x(t), u(t)) = 0 \\ n(u'(t), u(t), X, U) \leq 0 \\ \varphi(y(t), u(t), U) = 0 \\ \sigma(y(j\omega), u(j\omega), X) = 0 \\ t \epsilon [0, T] \\ \omega \epsilon [0, F] \end{cases} \qquad (12)$$

where J is the optimization objective, t is time, T is time range, ω is frequency, F is frequency range, x are process states, u are control variables, X are process parameters, U are controller parameters, m are process equations with initial conditions m_0, n are system inequality constraints, φ are controller equations, y are measurements, μ are measurement equations and σ are controllability equations.

In the steam path ICPD problem, the differential state equations $m(t)$ can be outlined as the state-space representation (Åström and Hägglund, 2006) of the open-loop transfer function models $\mathbf{G}(s)$ and $\mathbf{G}_d(s)$, Eqs. (6)–(7). The states $x(t)$ are the intermediate steam flows and pressures in the steam path (c.f. Fig. A.2). The measurement equations $\mu(t)$ describe how $y(t)$ are obtained from the states, i.e. the main steam pressure $p(t)$ and the turbine steam flow, which is converted by e_E to the electrical power $E(t)$. The inequality constraints $n(t)$ contain gain and rate constraints for $u(t)$ (i.e. $L(t)$ and $v(t)$), as well as bounds for the parameters X and U that are to be optimized. The controller equations comprise the steam pressure and electrical power feedback controllers (PID in this work, Eq. (B.7) transformed to the time domain). Finally, the controllability equations consist of the PRGA and CLDG matrix evaluation in the chosen frequency domain, Eqs. (8)–(10).

The boiler ICPD design must be carried out for the closed-loop steam path in the dynamic domain, where the load-following MW$_e$ setpoint tracking is optimized directly. As can be seen from the process model Eqs. (6)–(7) and (B.1)–(B.6), optimizing any of the process design parameters will directly influence the open-loop system dynamics, as well as the PRGA and CLDG matrices of the system. The process and its controllers also need to be tuned simultaneously within the same framework, as controller tunings would otherwise affect the optimality of process structure alternatives. Moreover, the design requires a large search space especially for the controller parameters.

The ICPD problem can be solved by implementing a hybrid two-level optimization approach. On the upper level, feasible solution regions are first located using a random search algorithm in a wide search space, specified through initial simulations with feasible controller tunings. The regions with the best ICPD objective values are then refined on the lower level, using simplex search optimization. As such, the optimal solution is located in two consecutive stages with two different optimization algorithms, where the closed-loop process response is evaluated for each candidate solution.

As a random search algorithm, the genetic algorithm "ga" of Matlab 2017 (Goldberg, 1989; Conn et al., 1991; Conn et al., 1997) was considered, using a solution population of 500 and 50 maximum generations. In the considered approach, the initial population is randomized, solutions are ranked based on the ICPD objective, and fitness values are obtained as the inverse square root of the rank. 25 solutions with the best fitness values are passed on directly to the next generation as elites, and the remaining generation is formed through crossover and mutation. Parent solutions are selected by organizing the population into segments according to the fitness values and performing the selection at uniform intervals ("stochastic uniform"). Crossover takes place by selecting elements randomly from each parent with a 0.8 crossover fraction. Mutations are calculated by adding a random zero-mean Gaussian vector to a parent ("mutation uniform"), with a mutation probability of 0.15.

The Nelder-Mead simplex search (Lagarias et al., 1998), "fminsearch" in Matlab 2017, was used for the lower level. A simplex of $n + 1$ points (n equals the number of parameters) is moved towards the optimum through reflection, expansion, contraction and shrink operations. A constraint modification is used for the design parameters (D'Errico, 2012), utilizing a sinusoid transform

to the unconstrained space. The search is periodically reinitialized by offsetting the optimization parameters one at a time.

In total, the ICPD algorithm can be summarized in the procedure below. While the individual design methods of the boiler ICPD procedure are established in literature, the procedure itself was devised for this paper. Notably, the ICPD optimization is fully simultaneous (Hultgren et al., 2017a) for all continuous parameters of the problem despite its two-level structure: both the upper level random search and lower level simplex search stages optimize the same process and controller parameters, and they use the same objective function to evaluate the results. As the control structure is selected beforehand based on controllability analysis and the process structure is based on design requirements, the discrete design decisions of the boiler steam path were carried out sequentially.

(1) Select the ICPD design parameters and specify the design objective.
(2) Select the 2×2 unit master control structure between MVs and CVs (boiler-following or turbine-following) through a PRGA & CLDG analysis in the frequency domain, favoring:
   - control pairings with PRGA elements close to 1
   - small off-diagonal PRGA elements
   - small CLDG elements to minimize the effect of disturbances
(3) Apply the controller equations with feedback (Åström and Hägglund, 2006) to $\mathbf{G}(s)$, Eq. (6): $p(s)/L(s)$ and $E(s)/v(s)$ for boiler-follow or $p(s)/v(s)$ and $E(s)/L(s)$ for turbine-follow.
(4) Perform initial controller tuning at process parameter limits to locate an approximate feasible region of operation and set it as the ICPD search space.
(5) Perform genetic algorithm optimization for process and controller parameters in the full search space with a limited number of generations.
(6) Construct smaller search space(s) around candidate solution (s) from the genetic algorithm.
(7) Refine solution(s) through simplex search, apply constraints if necessary.
(8) Obtain the ICPD result from the simplex optimization and validate it against a reference case.

4. CFB boiler steam path ICPD

The integrated design setup for the industrial CFB boiler steam path storage capacity, turbine valve throttling trajectory and boiler unit master control structure is discussed here. The control connections between the system CVs (steam pressure, electrical power) and MVs (firing power, turbine valve position) were

selected prior to the ICPD optimization in Section 4.1, using PRGA and CLDG analysis. The ICPD algorithm was then implemented to the steam path model in Section 4.2.

4.1. Control structure selection

The PRGA and CLDG were evaluated at $\omega = 0$–0.5 rad/s for Eqs. (6)–(7), using boiler-following and turbine-following control connections. The firing power, turbine valve and DSH disturbance variables were scaled by the distance between their upper and lower saturation limits. For the DSH spray, this was 25% of the main steam flowrate. The main steam pressure and electrical power were scaled by the largest allowed setpoint error: 10% for the power and 20% for the pressure.

The results are displayed in Figs. 4 and 5. At zero frequency, boiler-following diagonal PRGA elements were inferior to turbine-following control because of the small steady-state MW_e gain of the turbine valve. However, boiler-following control became superior already above 0.01 rad/s. In terms of loop interactions, boiler-following control thus provides better load change performance if the firing power is compensated sufficiently at steady-state, which was also discovered by Hultgren et al. (2017b) for plantwide CFB boiler control. The PRGA indicated that at zero frequency, there was a minor off-diagonal interacting effect from the steam pressure control connection. However, it was largely overshadowed by the off-diagonal PRGA element of the electrical power, which increased rapidly above zero frequency, peaked at 0.02 rad/s and diminished slowly after this. The peak is derived from the combined effect of the L and v gains on E. These control performance limiting interactions are thus present for both turbine-following and boiler-following control. Notably, the off-diagonal effects wouldn't have been visible with the dynamic RGA.

The CLDG showed that DSH disturbances will not present control performance issues for the output that is controlled with the turbine valve (output E for boiler-follow mode, steam p for turbine-follow mode), as the corresponding CLDG values were negligible for the entire frequency region. The gain magnitudes of the firing power, on the other hand, were surpassed by their CLDG elements already at 0.02 rad/s, as the firing power response is slow at the turbine. Moreover, below 0.15 rad/s the turbine-following CLDG between E and the DSH spray was much larger than the CLDG between the DSH and p in boiler-follow mode. Thus, steam temperature control action will result in performance problems for the firing power control loop especially in turbine-follow mode.

All in all, the boiler-following structure could be selected for the 2×2 boiler system. As this result is supported by design experience for fast load transitions, the boiler-following ICPD results were not benchmarked against similar turbine-following results
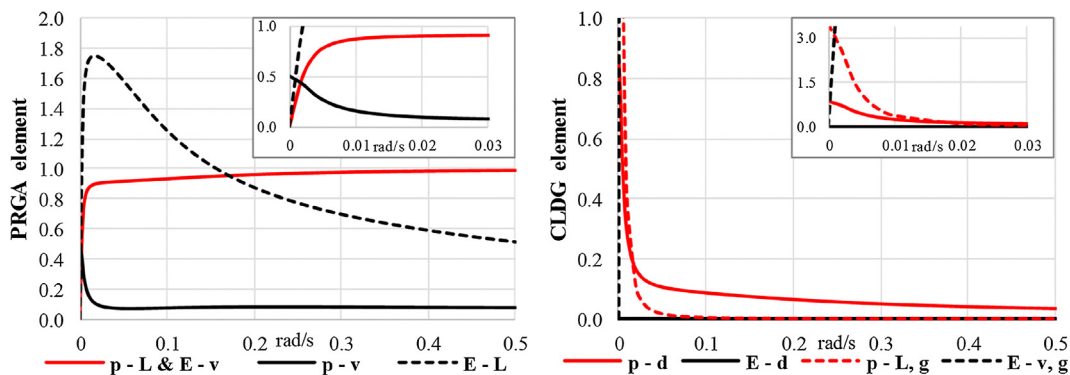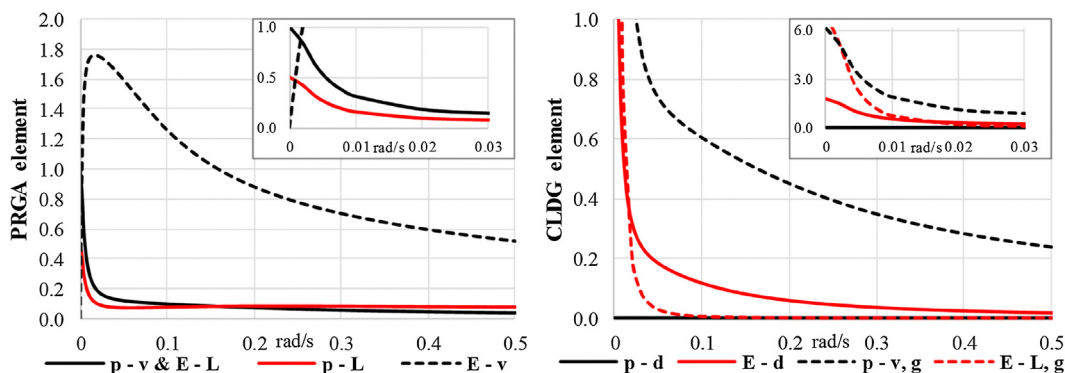

Fig. 4. PRGA magnitudes (left), CLDG and open-loop gain magnitudes (right), for boiler-following control (p control with L, E control with v); steam pressure p, electrical power E, firing power L, turbine valve v, open-loop gain magnitude g. The frequency range 0–0.03 rad/s is magnified.

Fig. 5. PRGA magnitudes (left), CLDG and open-loop gain magnitudes (right), for turbine-following control (p control with v, E control with L); steam pressure p, electrical power E, firing power L, turbine valve v, open-loop gain magnitude g. The frequency range 0–0.03 rad/s is magnified.

in this paper. While unit master control is typically implemented using higher-level strategies, multi-loop single-input–single-out put PID control was utilized in this work. The boiler-following closed-loop process model for the optimization was formed from Eq. (6) by applying the PID controller transfer functions, Eq. (B.7), with feedback. Nominal starting values for the PID parameters were obtained through crude tuning with the Matlab 2017 PID tuner (Åström and Hägglund, 2006). These simulations showcased that the derivative action was not necessary for the electrical power PID, and it was thus omitted from further analysis. Challenges in obtaining stable tunings for the boiler-following setup were clearly observed.

4.2. ICPD design setup

Next, the ICPD optimization was performed for the closed-loop boiler model, using boiler-following control. Since the aim was to improve MW$_e$ setpoint tracking during load changes, the optimization was carried out directly in the dynamic domain with different MW$_e$ setpoint ramps. The obtained dynamic responses were assessed based on setpoint tracking and controllability criteria.

4.2.1. Design test matrix

The ICPD optimization was performed separately for four load change scenarios (Table 1). Moderate load change magnitudes of $\leq 15\%$ MW$_e$ were considered in order to remain within a feasible operating region of the linear CFB steam path model. The main focus of the ICPD design was on constant pressure operation, where the electrical power output was ramped to a new load level, while maintaining a constant main steam pressure. Therefore, the main scenarios I and II considered constant pressure operation. Scenario I consisted of a small and fast load change, corresponding to a sudden change in the network load demand. Scenario II was a larger and slower ramp, representing a planned load transition. For comparative purposes, ICPD was also carried out for the same MW$_e$ ramps in sliding-pressure mode in scenarios III and IV: the main steam pressure was ramped together with the electrical power, using the same ramp speed and starting time for both outputs. In a more realistic case, sliding-pressure transitions would require

individual ramp programs for the pressure and the output power, but for simplicity this was not considered in this study.

All scenarios were simulated from a stable operating point of 80% output power. The initial load level was chosen in order to investigate turbine valve saturation: Since steam throttling contributes to exergy destruction and should be avoided at nominal loads, the possibility to open the valve enough when load demand increases is limited. For this reason, the ICPD optimization was only carried out for positive load changes. The new setpoint was maintained for 3750 timesteps after each ramp to eliminate the effect of possible oscillations in the analysis.

4.2.2. Target parameters

The parameters to be optimized by the ICPD algorithm are shown in Table 2. The main process parameters were the steam storage capacities of the evaporator (τ_E) and superheating sections 1 (τ_{S1}) and 2 (τ_{S2}), implemented as the total storage τ_{TOT}, the evaporator percentage q_E of this storage, and the percentage q_{S1} of the superheater storage that is placed in τ_{S1}. The turbine valve opening at the 80% load level was included to balance disturbance rejection and exergy destruction. The controller parameters were P, I, D and N for the main steam pressure p, and P and I for the electrical power E.

All process and controller parameters were scaled by dividing them with their nominal starting values. The minimum evaporator storage was limited rather tightly around the design value due to the need to produce a required amount of steam for all process designs. The superheater storage setup could be varied more freely, and a 50% τ_{S1}/τ_{S2} distribution was assumed as the nominal starting value. The turbine valve opening is technically limited between 0 and 100%, but a larger minimum valve opening (0.73 of nominal) was chosen in order to reduce steam throttling. PID parameter boundaries were determined based on the initial controller tuning, observing stability limits and active disturbance rejection, while maintaining the search space as large as possible. While this approach was deemed sufficient for this work, closed-loop stability criteria could be included as a pre-analysis step or as an optimization constraint in a fully systematic boiler ICPD design procedure in the future.

Table 1
Load change test program for the boiler steam path ICPD optimization.

Load change scenario	E setpoint (%)	Ramp time (timesteps)	Ramp speed (% MW/step)	Main steam p setpoint (%)
I: Fast small load ramp at constant p	+5	13	0.385	0
II: Slow large load ramp at constant p	+15	210	0.07	0
III: Fast small load ramp at sliding p	+5	13	0.385	+5
IV: Slow large load ramp at sliding p	+15	210	0.07	+15

Table 2
Parameters to be designed through ICPD. Minimum and maximum constraints reported as multipliers to the nominal starting values of the parameters, i.e. they are normalized.

Process parameter	Name	Min	Max	Controller parameter	Name	Min	Max
Total steam storages	τ_{TOT}	0.42	1.69	Steam p gain, P	P_p	0.00	5.20
Evaporator storage percentage of τ_{TOT}	q_E	0.97	1.25	Steam p integrator, I	I_p	0.01	36944.30
SH storage percentage before DSH of τ_S	q_{S1}	0.20	1.80	Steam p derivator, D	D_p	0.00	12.17
Turbine valve nominal position	$\bar{v}$	0.73	1.22	Steam p D filter, N	N_p	0.00	1991.49
				Output E gain, P	P_E	0.02	114.04
				Output E integrator, I	I_E	0.00	3873.03

4.2.3. Optimization objective

The ICPD optimization objective was constructed as a combination of desirable qualities for the closed-loop load change response, resulting in the weighted sum (13)–(19). The individual terms were scaled by dividing them with their values for the nominal boiler design and control parameters. This approach enabled a direct comparison of conflicting design goals, especially as the starting point for the design was a validated closed-loop process setup. As such, J doesn't have a direct physical significance in the steam path, but rather represents the tradeoff between desirable conflicting design objectives. Weighting factors were selected for the terms j_1–j_6 based on how the cost function terms changed due to typical process parameter modifications.

$$J = j_1 + j_2 + j_3 + j_4 + j_5 + j_6 \tag{13}$$

$$j_1 = \int_0^T (p(t) - p_{SP}(t))^2 dt \tag{14}$$

$$j_2 = 10 \cdot \int_0^T (E(t) - E_{SP}(t))^2 dt \tag{15}$$

$$j_3 = -2 \cdot v(0) \cdot \int_0^T v(t) dt \tag{16}$$

$$j_4 = \int_0^T |v(t) - \max(v(t), v_{min})| dt$$
$$+ \int_0^T |v(t) - \min(v(t), v_{max})| dt \tag{17}$$

$$j_5 = \int_0^F \Gamma_n(j\omega) d\omega \tag{18}$$

$$j_6 = 2 \cdot \int_0^F \sum \left| \hat{\mathbf{G}}_d(j\omega) \right| d\omega \tag{19}$$

where J is the ICPD objective, j is an individual design objective, p is pressure, E is electrical power, SP is setpoint, v_{min} and v_{max} are the minimum and maximum boundaries of the turbine valve control signal v, T is the dynamic ramp test duration, F is the investigated frequency range for the relative gain analysis, Γ_n is the PRGA number and $\hat{\mathbf{G}}_d$ is the CLDG.

Terms j_1 and j_2 account for the main steam pressure and electrical power tracking performance. The performance was evaluated directly by integral square errors for the entire timespan of the load change tests. An equal weight was placed on the load ramp duration and the steady-state period after it. Due to the heavy focus on load change performance, the MW$_e$ error j_2 was given a large weight.

Term j_3 is the turbine valve exergy penalty, which was evaluated by integrating the valve control signal over the test timespan, with an aim to keep the valve open as much as possible. The integral sum was multiplied with the nominal valve position to highlight the initial steady-state. Term j_4 is the valve saturation, calculated by comparing the saturated signal to the unsaturated signal and integrating the difference over time. The purpose of j_4 was to maintain an adequate control reserve for electrical power disturbances.

The effect of input–output controllability was included in terms j_5–j_6, evaluated with the PRGA and the CLDG, which were calculated at $\omega = 0$–0.5 rad/s using the "freqresp" function in Matlab 2017 (Laub, 1981). The goal for controllability j_5 was to minimize the PRGA number, Eq. (9), integrated over frequency range F. The disturbance controllability objective j_6 was to minimize all DSH spray CLDG elements, utilizing a similar absolute sum formulation to Eq. (9). As the CLDG decreased quickly compared to the PRGA at higher frequencies, it was given a slightly larger weight.

5. Results

The outcomes of the boiler steam path ICPD design were analyzed in this section. The design results were compared against load ramps where only the parameters of the main steam pressure and electrical power PID controllers were optimized (all process parameters remained at their original values).

The responses for the constant pressure scenarios can be viewed in Figs. 6–8; the fast 5% ramps (scenario I) in Fig. 6, the slow 15% ramp (scenario II) in Fig. 7. The control signals L and v for both scenarios are depicted in Fig. 8. Process outputs and manipulated variables were normalized with the respective nominal 80% load starting values. The optimized process and controller parameters and the improvements in the ICPD objective are shown in Table 3.

The ICPD algorithm maximized the total steam storage capacity for both ramp scenarios I and II in constant pressure mode. The evaporator storage was minimized, the superheater storage maximized, and the superheater storage was preferably distributed to the section after the DSH spray. The PID parameters were always successfully tuned together with the modified process structure.

The results indicated that adding storage capacity in the whole steam path improved the constant pressure load change performance and controllability. The capacity should be placed close to the turbine to improve the boiler–turbine decoupling and decrease the effect of DSH spray disturbances on the power output. The results thus set a guideline especially for superheater design, as a superheater with a large thermal storage capacity, such as the CFB Intrex™ heat exchanger, should preferably be placed close to the turbine. The results similarly suggested that boilers with small evaporator steam storages, such as once-through boilers, might actually be useful for constant pressure operation.

Results similar to the constant pressure tests were obtained for sliding-pressure load changes (Figs. 9–11). Again, the overall storage capacity was maximized, the evaporator storage was minimized, and the main superheating storage was placed at τ_{S2} (Table 4). The controller parameters were adequately tuned for each modified process.
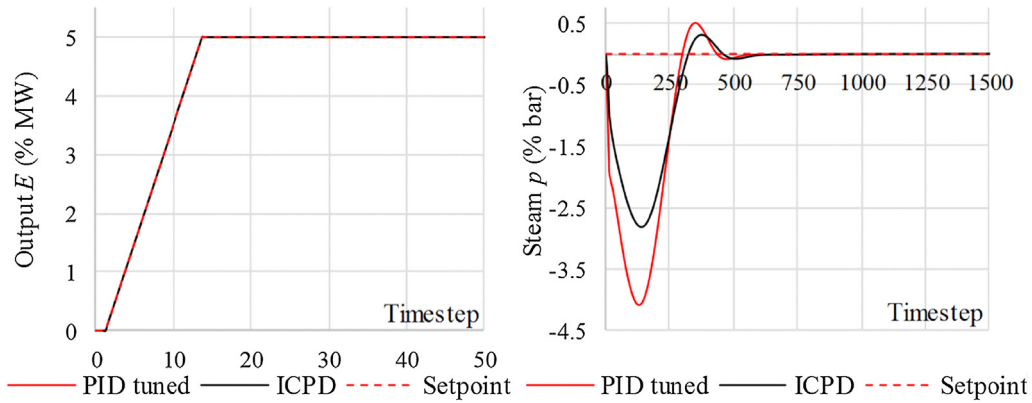
Fig. 6. Normalized electrical power E and main steam pressure p responses during fast 5% constant pressure load ramp (scenario I). Zero level is the nominal starting load.
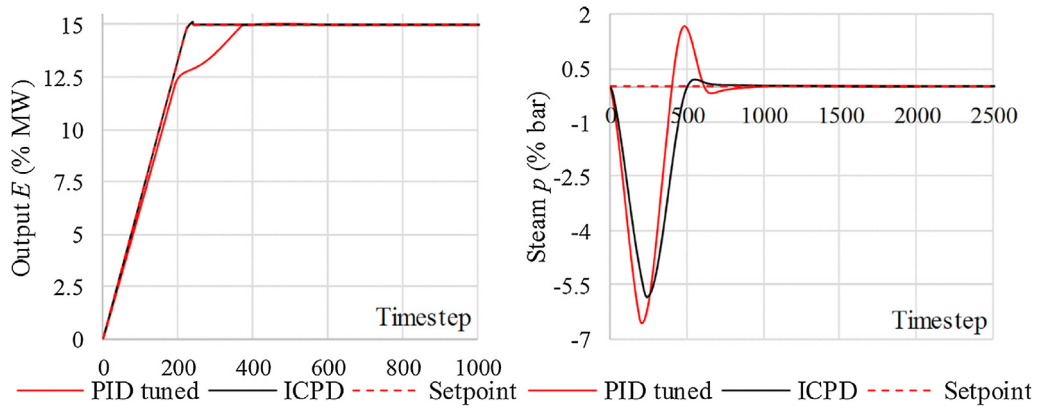
Fig. 7. Normalized electrical power E and main steam pressure p responses during slow 15% constant pressure load ramp (scenario II). Zero level is the nominal starting load.
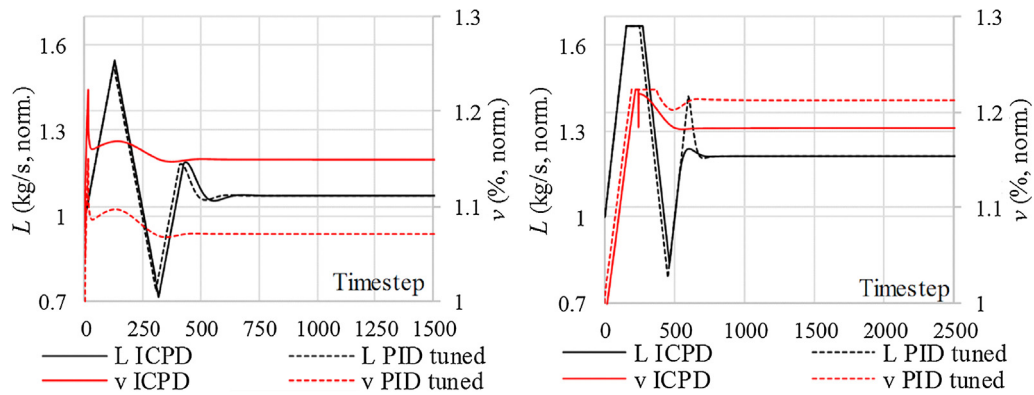
Fig. 8. Firing power (L) and turbine valve (v) during scenarios I (left) and II (right). Both MVs are normalized with their respective starting values, 1 is the nominal MV value.

Table 3
Scenario I and II optimized parameters and objective function values, ICPD and reference PID tuning design cases. Values reported as multipliers to the nominal starting parameters/objectives.

Constant pressure	Parameter, % of nominal value										Objective % of nominal
	τ_{TOT}	q_E	q_{S1}	$\bar{v}$	P_p	I_p	D_p	N_p	P_E	I_E	
ICPD, ramp I	1.69	0.97	0.20	1.08	2.91	2.23	5.09	727.26	2.71	118.88	0.095
PID, ramp I	1	1	1	1	1.85	1.66	3.00	7.41	12.85	3464.13	0.215
ICPD, ramp II	1.69	0.97	0.20	0.97	1.44	2.48	3.70	55.06	2.31	35.58	0.049
PID, ramp II	1	1	1	1	2.00	2.93	3.13	1973.62	0.19	0.002	0.419
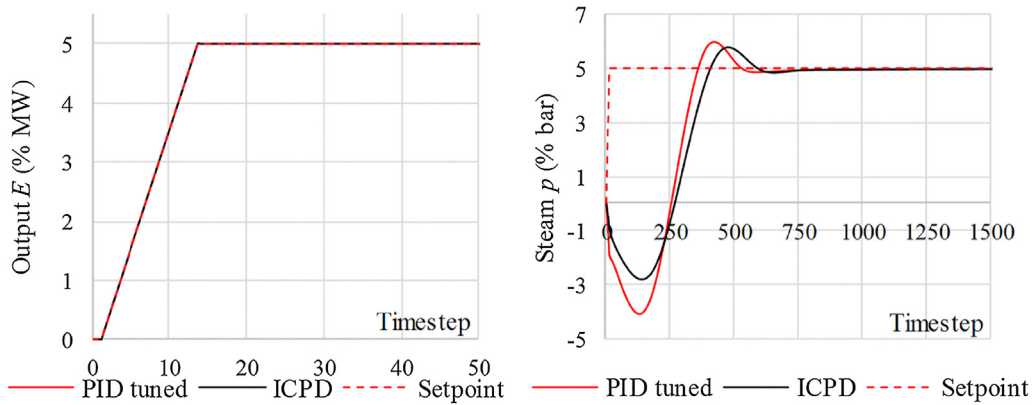
Fig. 9. Normalized electrical power E and main steam pressure p responses during fast 5% sliding-pressure load ramp (scenario III). Zero level is the nominal starting load.
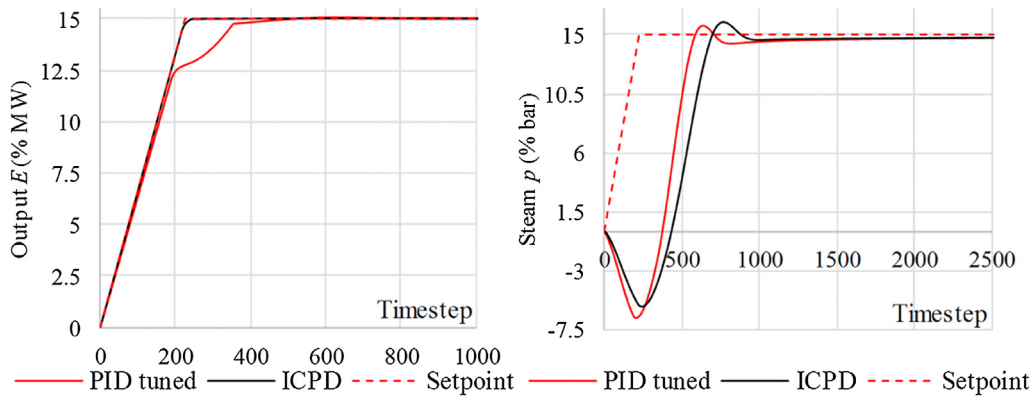
Fig. 10. Normalized electrical power E and main steam pressure p responses during slow 15% sliding-pressure load ramp (scenario IV). Zero level is the nominal starting load.
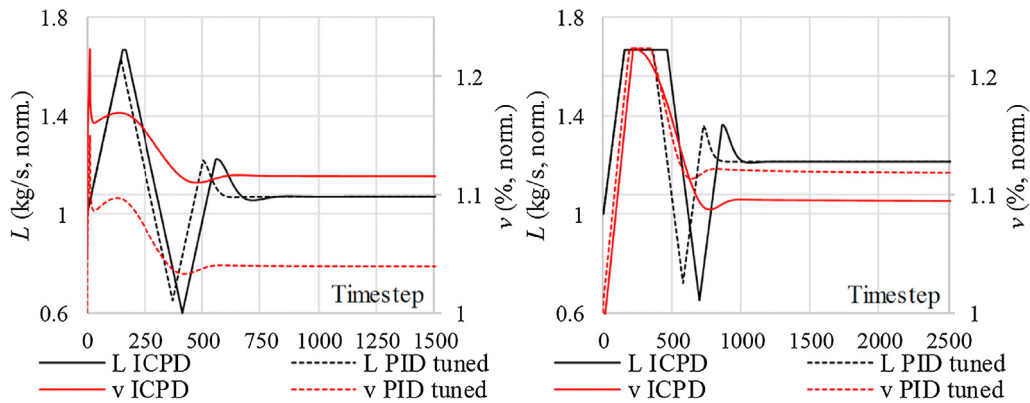
Fig. 11. Firing power (L) and turbine valve (v) during scenarios III (left) and IV (right). Both MVs are normalized with their respective starting values, 1 is the nominal MV value.

Table 4
Scenario III and IV optimized parameters and objective function values, ICPD and reference PID tuning design cases. Values reported as multipliers to the nominal starting parameters/objectives.

| Sliding-pressure | Parameter, % of nominal value | | | | | | | | | | Objective |
	τ_{TOT}	q_E	q_{S1}	$\bar{v}$	P_p	I_p	D_p	N_p	P_E	I_E	% of nominal
ICPD, ramp III	1.69	0.97	0.20	1.08	1.99	0.56	3.78	11.94	2.87	133.01	0.125
PID, ramp III	1	1	1	1	1.59	0.57	2.80	741.39	12.79	3432.46	0.227
ICPD, ramp IV	1.69	0.97	0.20	0.97	1.64	0.41	3.33	782.93	1.99	0.08	0.088
PID, ramp IV	1	1	1	1	1.31	0.47	2.42	1045.56	0.265	0.001	0.439

Interestingly, the present sliding-pressure results contrasted with the earlier findings of Hultgren et al. (2017a), where only the lumped superheater storage "τ_S" was optimized in sliding-pressure mode together with the boiler-following main steam pressure controller parameters. In that study, the best control performance was obtained with a small superheater storage, and the optimization resulted in improvements in both steam pressure and electrical power control performance.

The differences between the present findings and the previous results can be explained by the nature of boiler-following control. Reaching a new steam pressure setpoint is faster with a small steam storage, while electrical power control benefits from a large storage due to the turbine valve throttle reserve. At the same time, turbine valve MW_e control generates a pressure disturbance, the magnitude of which depends on the steam storage. A large storage thus also has a positive impact on steam pressure control. This tradeoff was confirmed by testing different weighting factors for the objective J. The PRGA and CLDG also favored a large storage, which ultimately lead to the present results.

The turbine valve nominal position was adjusted by the ICPD design for all load scenarios in such a way that load ramps only resulted in short controller saturation periods during the ramp (Figs. 8 and 11). The valve could thus be used effectively for improving load change performance with a minimum exergy penalty. Naturally this behavior depends on the chosen objective function weighting factors. Moreover, similar PID controller parameters were repeated for the different load scenarios, especially for the main steam pressure controller. The largest variations between the ICPD results of different scenarios were seen in the electrical power PID integrator I_E.

All in all, the ICPD design was clearly able to improve the boiler load change performance with simultaneous controller and process design parameter alterations. The hybrid two-level optimization framework was proven to be a robust approach, and the design results could be reproduced reliably during consecutive runs. The objective function breakdown in Table A.1 for the ICPD and optimal PID tuning cases showed that the ICPD results were superior compared to the PID optimization for most individual objectives j_1–j_6. For the fast ramping scenarios I and III, significant improvements in steam pressure tracking and process controllability were obtained at the cost of a negligible electrical power control penalty compared to the optimally tuned PID. For the slow ramps II and IV, the nominal turbine valve position was not enough to obtain the desired setpoint ramp (c.f. Figs. 7 and 10), and the ICPD algorithm thus slightly increased the steam throttling at the 80% starting load.

Despite the successful ICPD implementation, the steam path design case highlighted the challenges of a fully simultaneous dynamic optimization for the entire power plant. Even though the examined boiler and its control structure were simplified (linear mass storage model without other control loops or complex dynamics like the drum water-steam balance), the optimization objective had many local minima especially close to the discovered optima. This problem can be attributed to several reasons. Firstly, a fully simultaneous ICPD approach is inherently multi-optimum in nature, as each set of evaporator and superheater storages essentially has at least one set of preferred controller tunings. Secondly, the ICPD objective was constructed from several conflicting normalized terms. For future work, different objective functions and a more systematic testing of objective weightings could be considered. Thirdly, some of the individual objectives could give similar values for different process and control setups, especially the integral square error terms. This effect was emphasized for the turbine valve–electrical power control loop, as the valve has an immediate MW_e response.

6. Conclusions

Modern power plant design criteria increasingly focus not only on efficiency but also on fast load changes, which requires novel and robust design approaches. Integrated control and process design (ICPD) aims at finding improved plantwide closed-loop process designs through simultaneous optimization of the process and its control system. This work reported, for the first time, the application of an ICPD methodology for the steam path of an industrial circulating fluidized bed boiler in order to obtain improved load change performance.

The goals of the boiler ICPD were to minimize the electrical power (MW_e) tracking error during load changes, maintain adequate main steam pressure control, adjust the turbine valve operation to maintain a sufficient steam control reserve and minimize exergy destruction, and generate process structures with good controllability. To achieve this, an ICPD framework was formulated for a steam storage model of the industrial boiler, utilizing boiler-following control for the electrical power and the main steam pressure. The methodology combines a two-stage dynamic closed-loop optimization with performance relative gain array (PRGA) and closed-loop disturbance gain (CLDG) analysis.

The ICPD design successfully improved the MW_e load changes and the other design goals. For constant pressure mode, the total storage in the steam path was maximized, a maximum storage was placed in the last superheating section, and the evaporator storage was minimized. Tuning of the steam pressure and electrical power controller parameters was provided for the modified process structure. Different load transition scenarios provided similar design outcomes for the process and controller parameters. A large total steam storage was favored by the ICPD algorithm for both constant pressure and sliding-pressure mode, as it enabled quick MW_e changes, good controllability and small pressure disturbances. This is interesting, as boilers with small storage capacities are generally used in sliding-pressure mode.

All in all, the results established an ICPD procedure that can readily be employed for load-following CFB boiler design. The procedure was validated with a linear mass storage modeling approach, describing the steam path as a series of simple dynamic elements. The challenging nature of the optimization problem justified this approach, but more comprehensive results would require detailed modeling, including e.g. combustion side, heat transfer and evaporation dynamics. Economic aspects were not considered at this stage, but they should be included in future work, especially as a large steam storage is a major capital cost for the plant. This could be achieved with an additional economic ICPD design goal or by converting all optimization objectives to their economic counterparts.

The control structure design of this paper considered the performance limiting interactions of main steam pressure and electrical power control, as well as steam temperature control disturbances through the CLDG. In future work, more disturbance scenarios and plantwide control performance will also be evaluated. PID control was exclusively utilized due to its prevalence in power plant control, but future work should also consider advanced model-based control, which has been a growing trend in ICPD literature. This way, the boiler control system could be more closely integrated with the process structure, as the control action would be calculated directly from process modifications, bypassing the need to adjust controller parameters through ICPD. Alternatively, ICPD could employ a two-level embedded approach for process and controller parameters. In any case, the results of this paper stress the importance of a systematic analysis of the power plant control structure and loop interactions in the ICPD design formulation.

Declaration of interests

Acknowledgments

Appendix A

Appendix A contains additional figures and ICPD design results. Fig. A.1 shows example simulations, where the boiler electrical power (controlled variable, CV) is only controlled with the combustion power (fuel + air flows) or the turbine valve (manipulated variables, MV). The results were generated using a transfer function model identified from a full once-through CFB industrial simulator. Rate and gain constraints of the MVs were disregarded in order to highlight the theoretical MV demands during a tightly controlled load change in the electrical power CV.

Fig. A.2 shows the block diagram of the open-loop CFB steam path process model of this paper, complete with transfer function equations for the process blocks.

Table A.1 shows a more detailed objective function evaluation for the ICPD optimization than was given in Tables 3–4, including the values of individual objectives j_1–j_6.
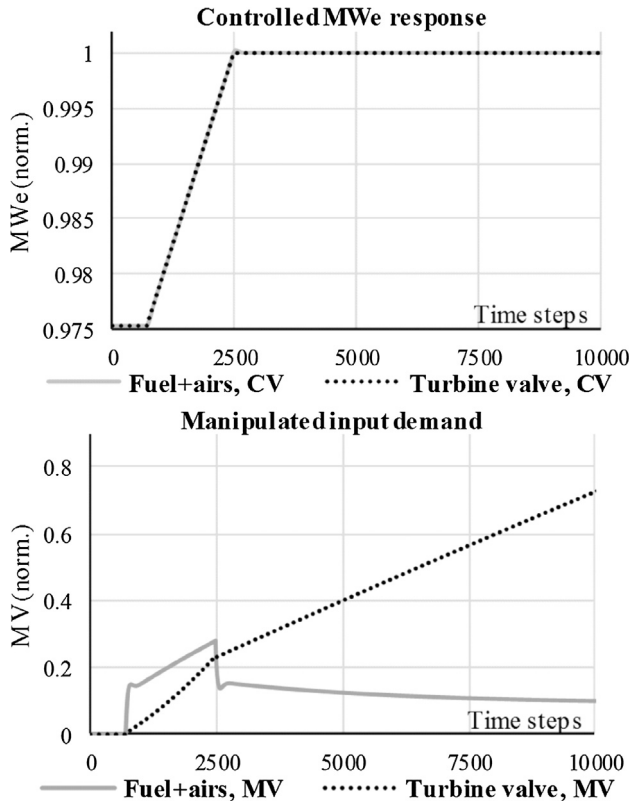
Fig. A1. Manipulated variable demands during a simulated MW$_e$ setpoint ramp, when the output electrical power is only controlled with the turbine valve (dotted) or the fuel + air flows (grey): tight single input–single output PI control, no variable constraints or other control loops active.

Appendix B

Appendix B provides equations for the CFB steam path model transfer function parameters, α, β, γ, δ, ε, ζ, η, θ, κ: The parameters for the process transfer function matrix $\mathbf{G}(s)$, Eq. (6), are given in equation groups (B.1)–(B.4). The parameters for the disturbance transfer function matrix $\mathbf{G}_d(s)$, Eq. (7), are given in equation groups (B.5)–(B.6).

$$
\begin{cases}
\alpha_{11} = \dfrac{\rho_W^2}{4f^2 \bar{m}_{W,out}^2 \tau_I \tau_E \tau_{S1} \tau_{S2}} \\[2ex]
\beta_{11} = \dfrac{\rho_W(2\tau_E+\tau_{S1})}{2f\bar{m}_{W,out}\tau_E\tau_{S1}} + \dfrac{\rho_W}{2f\bar{m}_{W,out}\tau_{S2}} + \dfrac{r\bar{v}}{\tau_{S2}} + \dfrac{1}{\tau_I} \\[2ex]
\gamma_{11} = \dfrac{\rho_W^2(\tau_E+\tau_{S1}+\tau_{S2})}{4f^2\bar{m}_{W,out}^2\tau_E\tau_{S1}\tau_{S2}} + \dfrac{r\bar{v}\rho_W(2\tau_E+\tau_{S1})}{2f\bar{m}_{W,out}\tau_E\tau_{S1}\tau_{S2}} + \dfrac{\rho_W(2\tau_E+\tau_{S1})}{2f\bar{m}_{W,out}\tau_I\tau_E\tau_{S1}} + \dfrac{\rho_W}{2f\bar{m}_{W,out}\tau_I\tau_{S2}} + \dfrac{r\bar{v}}{\tau_I\tau_{S2}} \\[2ex]
\delta_{11} = \dfrac{\rho_W^2(r\bar{v}\tau_I+\tau_E+\tau_{S1}+\tau_{S2})}{4f^2\bar{m}_{W,out}^2\tau_I\tau_E\tau_{S1}\tau_{S2}} + \dfrac{r\bar{v}\rho_W(2\tau_E+\tau_{S1})}{2f\bar{m}_{W,out}\tau_I\tau_E\tau_{S1}\tau_{S2}} \\[2ex]
\varepsilon_{11} = \dfrac{r\bar{v}\rho_W^2}{4f^2\bar{m}_{W,out}^2\tau_I\tau_E\tau_{S1}\tau_{S2}}
\end{cases}
\tag{B.1}
$$

$$
\begin{cases}
\alpha_{12} = \dfrac{\bar{p}r}{\tau_{S2}} \\[2ex]
\beta_{12} = \dfrac{\bar{p}r\rho_W(2\tau_E+\tau_{S1})}{2f\bar{m}_{W,out}\tau_E\tau_{S1}\tau_{S2}} \\[2ex]
\gamma_{12} = \dfrac{\bar{p}r\rho_W^2}{4f^2\bar{m}_{W,out}^2\tau_E\tau_{S1}\tau_{S2}} \\[2ex]
\delta_{12} = \dfrac{\rho_W(2\tau_E+\tau_{S1})}{2f\bar{m}_{W,out}\tau_E\tau_{S1}} + \dfrac{\rho_W}{2f\bar{m}_{W,out}\tau_{S2}} + \dfrac{r\bar{v}}{\tau_{S2}} \\[2ex]
\varepsilon_{12} = \dfrac{\rho_W^2(\tau_E+\tau_{S1}+\tau_{S2})}{4f^2\bar{m}_{W,out}^2\tau_E\tau_{S1}\tau_{S2}} + \dfrac{\rho_W r\bar{v}(2\tau_E+\tau_{S1})}{2f\bar{m}_{W,out}\tau_E\tau_{S1}\tau_{S2}} \\[2ex]
\zeta_{12} = \dfrac{r\bar{v}\rho_W^2}{4f^2\bar{m}_{W,out}^2\tau_E\tau_{S1}\tau_{S2}}
\end{cases}
\tag{B.2}
$$

$$
\begin{cases}
\alpha_{21} = \dfrac{e_E r\bar{v}\rho_W^2(\tau_{HP}+x_{HP}\tau_{LP}-x_{HP}\tau_{HP})}{4f^2\bar{m}_{W,out}^2\tau_I\tau_E\tau_{S1}\tau_{S2}\tau_{HP}\tau_{LP}} \\[2ex]
\beta_{21} = \dfrac{e_E r\bar{v}\rho_W^2}{4f^2\bar{m}_{W,out}^2\tau_I\tau_E\tau_{S1}\tau_{S2}\tau_{HP}\tau_{LP}} \\[2ex]
\gamma_{21} = \beta_{11} + \dfrac{(\tau_{HP}+\tau_{LP})}{\tau_{HP}\tau_{LP}} \\[2ex]
\delta_{21} = \gamma_{11} + \dfrac{(\tau_{HP}+\tau_{LP})}{\tau_{HP}\tau_{LP}}\beta_{11} + \dfrac{1}{\tau_{HP}\tau_{LP}} \\[2ex]
\varepsilon_{21} = \delta_{11} + \dfrac{(\tau_{HP}+\tau_{LP})}{\tau_{HP}\tau_{LP}}\gamma_{11} + \dfrac{1}{\tau_{HP}\tau_{LP}}\beta_{11} \\[2ex]
\zeta_{21} = \varepsilon_{11} + \dfrac{(\tau_{HP}+\tau_{LP})}{\tau_{HP}\tau_{LP}}\delta_{11} + \dfrac{1}{\tau_{HP}\tau_{LP}}\gamma_{11} \\[2ex]
\eta_{21} = \dfrac{(\tau_{HP}+\tau_{LP})}{\tau_{HP}\tau_{LP}}\varepsilon_{11} + \dfrac{1}{\tau_{HP}\tau_{LP}}\delta_{11} \\[2ex]
\theta_{21} = \dfrac{1}{\tau_{HP}\tau_{LP}}\varepsilon_{11}
\end{cases}
\tag{B.3}
$$

$$
\begin{cases}
\alpha_{22} = \dfrac{e_E\bar{p}r(\tau_{HP}+x_{HP}\tau_{LP}-x_{HP}\tau_{HP})}{\tau_{HP}\tau_{LP}} \\[2ex]
\beta_{22} = \dfrac{e_E\bar{p}r}{\tau_{HP}\tau_{LP}}\cdot\left(\dfrac{\rho_W(2\tau_E+\tau_{S1})(x_{HP}\tau_{LP}-x_{HP}\tau_{HP}+\tau_{HP})}{2f\bar{m}_{W,out}\tau_E\tau_{S1}} + \dfrac{\rho_W(x_{HP}\tau_{LP}-x_{HP}\tau_{HP}+\tau_{HP})}{2f\bar{m}_{W,out}\tau_{S2}} + 1\right) \\[2ex]
\gamma_{22} = \dfrac{e_E\bar{p}r}{\tau_{HP}\tau_{LP}}\cdot\left(\dfrac{\rho_W^2(\tau_E+\tau_{S1}+\tau_{S2})(x_{HP}\tau_{LP}-x_{HP}\tau_{HP}+\tau_{HP})}{4f^2\bar{m}_{W,out}^2\tau_E\tau_{S1}\tau_{S2}} + \dfrac{\rho_W(2\tau_E+\tau_{S1})}{2f\bar{m}_{W,out}\tau_E\tau_{S1}} + \dfrac{\rho_W}{2f\bar{m}_{W,out}\tau_{S2}}\right) \\[2ex]
\delta_{22} = \dfrac{e_E\bar{p}r}{\tau_{HP}\tau_{LP}}\cdot\dfrac{\rho_W^2(\tau_E+\tau_{S1}+\tau_{S2})}{4f^2\bar{m}_{W,out}^2\tau_E\tau_{S1}\tau_{S2}} \\[2ex]
\varepsilon_{22} = \delta_{12} + \dfrac{(\tau_{HP}+\tau_{LP})}{\tau_{HP}\tau_{LP}} \\[2ex]
\zeta_{22} = \varepsilon_{12} + \dfrac{(\tau_{HP}+\tau_{LP})}{\tau_{HP}\tau_{LP}}\delta_{12} + \dfrac{1}{\tau_{HP}\tau_{LP}} \\[2ex]
\eta_{22} = \zeta_{12} + \dfrac{(\tau_{HP}+\tau_{LP})}{\tau_{HP}\tau_{LP}}\varepsilon_{12} + \dfrac{1}{\tau_{HP}\tau_{LP}}\delta_{12} \\[2ex]
\theta_{22} = \dfrac{(\tau_{HP}+\tau_{LP})}{\tau_{HP}\tau_{LP}}\zeta_{12} + \dfrac{1}{\tau_{HP}\tau_{LP}}\varepsilon_{12} \\[2ex]
\kappa_{22} = \dfrac{1}{\tau_{HP}\tau_{LP}}\zeta_{12}
\end{cases}
\tag{B.4}
$$

Fig. A2. Transfer function block diagram of the open-loop boiler steam storage capacity model.

Table A.1
Objective function terms j_1–j_6 for all ICPD optimization and PID parameter optimization cases. Results are normalized with the nominal starting objective values (values below 1 signify improvement).

Objective % of nominal	ICPD ramp I	PID ramp I	ICPD ramp II	PID ramp II	ICPD ramp III	PID ramp III	ICPD ramp IV	PID ramp IV
j_1	0.3995	0.7866	0.4686	0.5271	0.8080	0.9536	0.9986	0.8480
j_2	0.0013	0.0000	0.0001	0.3912	0.0012	0.0000	0.0007	0.3865
j_3	1.1563	0.9992	0.9441	0.9956	1.1596	1.0015	0.9602	1.0050
j_4	1.0001	1.00	0.0005	0.0003	1.0001	1.0000	0.0006	0.0041
j_5	0.9978	1	0.9054	1	0.9980	1	0.9082	1
j_6	0.5662	1	0.5730	1	0.5662	1	0.5728	1

$$
\begin{cases}
\alpha_{d1} = \frac{1}{\tau_{S2}} \\
\beta_{d1} = \frac{\rho_W(2\tau_E + \tau_{S1})}{2f\bar{m}_{W,out}\tau_E\tau_{S1}\tau_{S2}} \\
\gamma_{d1} = \frac{\rho_W^2}{4f^2\bar{m}_{W,out}^2\tau_E\tau_{S1}\tau_{S2}} \\
\delta_{d1} = \delta_{12} \\
\varepsilon_{d1} = \varepsilon_{12} \\
\zeta_{d1} = \zeta_{12}
\end{cases}
\tag{B.5}
$$

$$
\begin{cases}
\alpha_{d2} = \frac{e_E r\bar{v}(\tau_{HP} + x_{HP}\tau_{LP} - x_{HP}\tau_{HP})}{\tau_{HP}\tau_{LP}\tau_{S2}} \\
\beta_{d2} = \frac{e_E r\bar{v}}{\tau_{HP}\tau_{LP}} \cdot \left(\frac{\rho_W(2\tau_E + \tau_{S1})(\tau_{HP} + x_{HP}\tau_{LP} - x_{HP}\tau_{HP})}{2f\bar{m}_{W,out}\tau_E\tau_{S1}\tau_{S2}} + \frac{1}{\tau_{S2}} \right) \\
\gamma_{d2} = \frac{e_E r\bar{v}}{\tau_{HP}\tau_{LP}} \cdot \left(\frac{\rho_W^2(\tau_{HP} + x_{HP}\tau_{LP} - x_{HP}\tau_{HP})}{4f^2\bar{m}_{W,out}^2\tau_E\tau_{S1}\tau_{S2}} + \frac{\rho_W(2\tau_E + \tau_{S1})}{2f\bar{m}_{W,out}\tau_E\tau_{S1}\tau_{S2}} \right) \\
\delta_{d2} = \frac{e_E r\bar{v}}{\tau_{HP}\tau_{LP}} \cdot \frac{\rho_W^2}{4f^2\bar{m}_{W,out}^2\tau_E\tau_{S1}\tau_{S2}} \\
\varepsilon_{d2} = \varepsilon_{22} \\
\zeta_{d2} = \zeta_{22} \\
\eta_{d2} = \eta_{22} \\
\theta_{d2} = \theta_{22} \\
\kappa_{d2} = \kappa_{22}
\end{cases}
\tag{B.6}
$$

Additionally, Eq. (B.7) shows the standard form of the PID controller with derivative filtering, modified from Åström and Hägglund (2006). The *P*, *I* and *D* parameters are referred to for the pressure and electrical power feedback controllers in Table 2.

$$
C(s) = P + I \cdot \frac{1}{s} + D \cdot \frac{N}{s + N}
\tag{B.7}
$$

References

Alobaid, F., Mertens, N., Starkloff, R., Lanz, T., Heinze, C., Epple, B., 2016. Progress in dynamic simulation of thermal power plants. Prog. Energy Combust. Sci. 59, 79–162.

Aurora, C., Magni, L., Scattolini, R., Colombo, P., Pretolani, F., Villa, G., 2004. Predictive control of thermal Power Plants. Int. J. Robust Nonlin. Control. 14 (4), 415–433.

Bristol, E.H., 1966. On a new measure of interaction for multivariable process control. IEEE Trans. Autom. Control. 11 (1), 133–134.

Capra, F., Martelli, E., 2015. Numerical optimization of combined heat and power Organic Rankine Cycles – Part B: Simultaneous design & part-load optimization. Energy 90 (1), 329–343.

Chan, K.H., Dozal-Mejorada, E.J., Cheng, X., Kephart, R., Ydstie, B.E., 2014. Predictive control with adaptive model maintenance: Application to power plants. Comput. Chem. Eng. 70, 91–103.

Chen, C., Bollas, G.M., 2017. Semi-batch chemical-looping reactors integrated with combined cycle power plants operating at transient electricity demand. In: Proceedings of the FOCAPO/CPC 2017 Conference, Tucson, January 8–12, 2017. FOCAPO/CPC, Tucson, AR, 6 p.

Conn, A.R., Gould, N.I.M., Toint, P.L., 1991. A globally convergent augmented lagrangian algorithm for optimization with general constraints and simple bounds. SIAM J. Numer. Anal. 28 (2), 545–572.

Conn, A.R., Gould, N.I.M., Toint, P.L., 1997. A globally convergent augmented lagrangian barrier algorithm for optimization with general inequality constraints and simple bounds. Math. Comput. 66 (217), 261–288.

D'Errico, J., 2012. fminsearchbnd, fminsearchcon, Mathworks, Mathworks File Exchange. Online: https://www.mathworks.com/matlabcentral/fileexchange/8277-fminsearchbnd–fminsearchcon (accessed 12.05.18).

Diangelakis, N.A., Burnak, B., Pistikopoulos, E.N., 2017. A multi-parametric programming approach for the simultaneous process scheduling and control – Application to a domestic cogeneration unit. In: Proceedings of the FOCAPO/CPC 2017 Conference, Tucson, January 8–12, 2017. FOCAPO/CPC, Tucson, AR, 6 p.

Diangelakis, N.A., Pistikopoulos, E.N., 2016. Modelling, design and control optimization of a residential scale CHP system. In: Kopanos, G.M., Liu, P., Georgiadis, M.C. (Eds.), Advances in Energy Systems Engineering. Springer, Cham, Switzerland, pp. 475–506.

Diangelakis, N.A., Pistikopoulos, E.N., 2017. A multi-scale energy systems engineering approach to residential combined heat and power systems. Comput. Chem. Eng. 102, 128–138.

Doležal, R., Varcop, L., 1970. Process Dynamics, Automatic Control of Steam Generation Plant. Elsevier, Amsterdam, Netherlands.

Franzosi, R., Miotti, A., Pretolani, F., Scattolini, R., 2006. Traditional and advanced control of coal power plants: a comparative study. In: Proceedings of the American Control Conference, Minneapolis, June 14–16, 2006. IEEE, Minneapolis, MN, pp. 3451–3456.

Garduno-Ramirez, R., Lee, K.Y., 2005. Compensation of control-loop interaction for power plant wide-range operation. Control Eng. Pract. 13 (12), 1475–1487.

Garrido, J., Morilla, F., Vázquez, F., 2009. Centralized PID control by decoupling of a boiler-turbine unit. In: Proceedings of the European Control Conference, Budapest, August 23–26, 2009. EUCA, Budapest, Hungary, pp. 4007–4012.

Goldberg, D.E., 1989. Genetic Algorithms in Search, Optimization & Machine Learning. Addison-Wesley, Boston, MA.

Hultgren, M., Ikonen, E., Kovács, J., 2017a. Integrated control and process design in CFB boiler design and control – application possibilities. In: Dochain, D., Henrion, D., Peaucelle, D. (Eds.), Proceedings of the 20th IFAC World Congress, Toulouse, July 9–14, 2017. IFAC, Toulouse, France, pp. 1997–2004.

Hultgren, M., Ikonen, E., Kovács, J., 2017b. Once-through circulating fluidized bed boiler control design with the dynamic relative gain array and partial relative gain. Ind. Eng. Chem. Res. 56 (48), 14290–14303.

Hultgren, M., Kovács, J., Ikonen, E., 2015. Combustion control in oxy-fired circulating fluidized bed combustion. In: Proceedings of the 22nd International Conference on Fluidized Bed Conversion, Turku, June 14–17, 2015. FBC, Turku, Finland, pp. 1195–1205.

IEA, 2011. Harnessing Variable Renewables, A Guide to the Balancing Challenge. International Energy Agency, Paris, France.

Jin, B., Su, M., Zhao, H., Zheng, C., 2015. Plantwide control and operating strategy for air separation unit in oxy-combustion power plants. Energy Conv. Manage. 106, 782–792.

Joronen, T., Kovács, J., Majanne, Y., 2007. Voimalaitosautomaatio. Suomen Automaatioseura ry, Helsinki, Finland.

Klaučo, M., Kvasnica, M., 2017. Control of a boiler-turbine unit using MPC-based reference governors. Appl. Therm. Eng. 110, 1437–1447.

Klefenz, G., 1986. Automatic Control of Steam Power Plants. B.I.-Wissenschaftsverlag, Mannheim/Wien/Zürich, Germany/Austria/Switzerland.

Kong, X., Liu, X., Lee, K.Y., 2015. Nonlinear multivariable hierarchical model predictive control for boiler-turbine system. Energy 93 (1), 309–322.

Kookos, I.K., Perkins, J.D., 2004. The back-off approach to simultaneous design and control. In: Seferlis, P., Georgiadis, M.C. (Eds.), The Integration of Process Design and Control. Elsevier, Amsterdam, Netherlands, pp. 216–238.

Kovács, J., Kettunen, A., Ojala, J., 2012. Modelling and control design of once-through boilers. In: Fadel, M., Caux, S. (Eds.), Proceedings of the 8th Power Plant & Power System Control Symposium, Toulouse, September 2–5, 2012. IFAC, Toulouse, France, pp. 196–200.

Kundur, P., 1994. Power System Stability and Control. McGraw-Hill, USA.

Lagarias, J.C., Reeds, J.A., Wright, M.H., Wright, P.E., 1998. Convergence properties of the Nelder-mead simplex method in low dimensions. SIAM J. Optim. 9 (1), 112–147.

Laub, A.J., 1981. Efficient multivariable frequency response computations. IEEE Trans. Autom. Control. 26 (2), 407–408.

Ławryńczuk, M., 2017. Nonlinear predictive control of a boiler-turbine unit: A state-space approach with successive on-line model linearisation and quadratic optimisation. ISA Trans. 67, 476–495.

Liu, X., Guan, P., Chan, C.W., 2010. Nonlinear multivariable power plant coordinate control by constrained predictive scheme. IEEE Trans. Control Syst. Tech. 18 (5), 1116–1125.

Long, D., Wang, W., Yao, C., Liu, J., 2017. An experiment-based model of condensate throttling and its utilization in load control of 1000 MW power units. Energy 133, 941–954.

Ma, L., Lee, K.Y., Wang, Z., 2016. Intelligent coordinated controller design for a 600 MW supercritical boiler unit based on expanded-structure neural network inverse models. Control Eng. Pract. 53, 194–201.

McAvoy, T.J., 1983. Some results on dynamic interaction analysis of complex control systems. Ind. Eng. Chem. Proc. Des. Dev. 22 (1), 42–49.

Niva, L., Hultgren, M., Ikonen, E., Kovács, J., 2017. Control structure design for oxy-fired circulating fluidized bed boilers using self-optimizing control and partial relative gain analyses. In: Dochain, D., Henrion, D., Peaucelle, D. (Eds.), Proceedings of the 20th IFAC World Congress, Toulouse, July 9–14, 2017. IFAC, Toulouse, France, pp. 2023–2030.

Niva, L., Ikonen, E., Kovács, J., 2015. Self-optimizing control structure design in oxy-fuel circulating fluidized bed combustion. Int. J. Greenhouse Gas Control 43, 93–107.

Ogunnaike, B.A., Ray, W.H., 1994. Process Dynamics, Modeling, and Control. Oxford University Press, New York, NY.

Prasad, G., Irwin, G.W., Swidenbank, E., Hogg, B.W., 2000. Plant-wide predictive control for a thermal power plant based on a physical plant model. IEE Proc. Control Theory Appl. 147 (5), 523–537.

Prasad, G., Irwin, G.W., Swidenbank, E., Hogg, B.W., 2002. A hierarchical physical model-based approach to predictive control of a thermal power plant for efficient plant-wide disturbance rejection. Trans. Inst. Meas. Control 24 (2), 107–128.

Rovnak, J.A., Corlis, R., 1991. Dynamic matrix based control of fossil power plants. IEEE Trans. Energy Conv. 6 (2), 320–326.

Sakizlis, V., Perkins, J.D., Pistikopoulos, E.N., 2004. Recent advances in optimization-based simultaneous process and control design. Comput. Chem. Eng. 28 (10), 2069–2086.

Sarkar, D.K., 2015. Thermal Power Plant Design and Operation. Elsevier, Amsterdam, Netherlands.

Sharifzadeh, M., 2013. Integration of process design and control: A review. Chem. Eng. Res. Des. 91 (12), 2515–2549.

Skogestad, S., Postlethwaite, I., 2005. Multivariable Feedback Control, Analysis and Design. Wiley, Chichester, U.K.

Vega, P., Lamanna de Rocco, R., Revollar, S., Francisco, M., 2014. Integrated design and control of chemical processes – Part I: Revision and classification. Comput. Chem. Eng. 71, 602–617.

Wang, W., Li, L., Long, D., Liu, J., Zeng, D., Cui, C., 2017. Improved boiler-turbine coordinated control of 1000 MW power units by introducing condensate throttling. J. Proc. Control. 50, 11–18.

Wang, W., Liu, J., Zeng, D., Niu, Y., Cui, C., 2015. An improved coordinated control strategy for boiler-turbine units supplemented by cold source flow adjustment. Energy 88, 927–934.

Wang, W., Zeng, D., Liu, J., Niu, Y., Cui, C., 2014. Feasibility analysis of changing turbine load in power plants using continuous condenser pressure adjustment. Energy 64, 533–540.

Witcher, M.F., McAvoy, T.J., 1977. Interacting control systems: Steady state and dynamic measurement of interaction. ISA Trans. 16, 35–41.

Yuan, Z., Chen, B., Sin, G., Gani, R., 2012. State-of-the-art and progress in the optimization-based simultaneous design and control for chemical processes. AIChE J. 58 (6), 1640–1659.

Zhang, S., Taft, C.W., Bentsman, J., Hussey, A., Petrus, B., 2012. Simultaneous gains tuning in boiler/turbine PID-based controller clusters using iterative feedback tuning methodology. ISA Trans. 51 (5), 609–621.

Zhang, F., Wu, X., Shen, J., 2017. Extended state observer based fuzzy model predictive control for ultra-supercritical boiler-turbine unit. Appl. Therm. Eng. 118, 90–100.

Zhou, Y., Wang, D., 2017. An improved coordinated control technology for coal-fired boiler-turbine plant based on flexible steam extraction system. Appl. Therm. Eng. 125, 1047–1060.

Åström, K.J., Hägglund, T., 2006. Advanced PID Control. ISA – Instrumentation, Systems, and Automation Society. Research Triangle Park, NC.